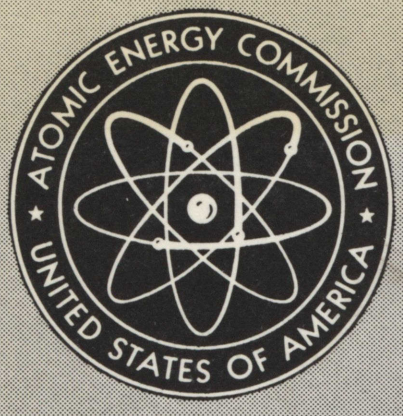

IDO-24467

ADVANCED TEST REACTOR

Final Shielding Design Report

By
J. O. Howard
G. M. Jacks

December 1963

Ebasco Services, Inc.
New York, New York

Atomic Energy Division
Babcock & Wilcox Company
Lynchburg, Virginia

UNITED STATES ATOMIC ENERGY COMMISSION • DIVISION OF TECHNICAL INFORMATION

LEGAL NOTICE

Printed in USA. Price $6.00. Available from the Clearinghouse for Federal Scientific and Technical Information, National Bureau of Standards, U. S. Department of Commerce, Springfield, Va.

USAEC Division of Technical Information Extension, Oak Ridge, Tennessee

IDO - 24467
REACTOR TECHNOLOGY
(TID - 4500, 35th. Ed.)

ADVANCED TEST REACTOR

Final Shielding Design Report

December 1963

By
J. O. Howard
G. M. Jacks
Engineering Department

Reviewed by: R. A. Webb, Chief
Nuclear Analysis Section

Approved by: A. H. Lazar
ATR Project Engineer

AEC Contract No. AT(10-1)-1075
B&W Contract No. 59-3063

Prepared for
EBASCO SERVICES, INC.
and Submitted to
THE UNITED STATES ATOMIC ENERGY COMMISSION
Idaho Operations Office
by
THE BABCOCK & WILCOX COMPANY
Atomic Energy Division
Lynchburg, Virginia

ACKNOWLEDGMENT

The authors thank Mr. W. R. Smith for his guidance and assistance throughout the course of this work.

FOREWORD

This report is the second and final report of shield design engineering and radiation analysis work for the Advanced Test Reactor (ATR). The first volume was the Interim Shielding Design Report, SR-88, published in September, 1961, which contained all Title I and a portion of the Title II design results. All of the information included in the interim report has been updated as necessary and is included herein. Additionally, the later Title II design work is described. Of particular importance are the results of the heat generation rate calculations for the core and internals. These heating rates are expected to be severe in the high power density ATR, and the difficult shielding geometries encountered made necessary the development of special methods for their accurate prediction.

This report should serve as a reference document describing the calculation methods used and design results obtained during work on the ATR contract. It has been written for the use and review of the reactor prime contractor, EBASCO SERVICES, INC., the reactor builder, THE UNITED STATES ATOMIC ENERGY COMMISSION, and the future operator, THE PHILLIPS PETROLEUM COMPANY.

W. R. Smith, Supervisor
Shielding Analysis Group

ABSTRACT

This report has been prepared as a design reference document describing the calculation methods and engineering results for shielding analysis work done during the design of the Advanced Test Reactor. All calculations that are significant in the plant shield design are described. Also included are sections on heat generation rates, materials activation, and spent fuel and test element transfer.

The calculation descriptions are divided into two parts: The methods used to obtain the activity of the source are described in Section 3, and the geometry and the attenuation equations from source to dose point are described in the remaining sections.

CONTENTS

CONTENTS (Cont'd)

List of Tables

List of Figures

Page

Figure

Figures (Cont'd)

1. INTRODUCTION

1.1. General Description

The ATR is a high-flux, beryllium reflected, water cooled and moderated test reactor incorporating advanced design features. One such feature is a flux trap core configuration affording neutron fluxes of greater than 10^{15} neut/cm^2-sec to nine experimental loops. From a shielding viewpoint, the reactor presents several particularly interesting aspects. The core materials for the fuel region are aluminum and uranium dioxide plates and water. The core configuration can be roughly visualized as four equal-radius hollow cylinders of fuel arranged symmetrically around a similar central cylinder. This configuration shown in Figure 1-1, causes difficult geometry problems in treating dose rates and heating rates at intermediate distances from the core where two or more lobes contribute significantly to the flux.

Another feature of interest is the high fast-neutron flux in the core, which produces high values for N-16 water activation in the primary coolant. The 17-day core lifetime and the resulting frequent refueling operations require particular attention to transient dose rates and personnel exposure environment during refueling operations. Experience gained by Phillips Petroleum Company in MTR and ETR operation indicated a definite possibility of test loop fuel specimen failure and subsequent fission product distribution throughout the loop. This possibility was considered in test loop cubicle shielding designs.

The reactor vessel contains the core and reflector assembly and provides space and access, shown in Figure 1-2, for various experimental facilities. The coolant is pressurized light water, which also provides shielding during refueling and experiment-handling operations.

In addition to the experimental loop facilities and capsule test facilities in the beryllium reflector, there are two outer capsule irradiation facilities consisting of aluminum blocks 4 inches by 4 inches by 5 feet

long attached to the outer wall of the core reflector tank. An internal fuel element storage facility is also provided in the vessel to reduce the shutdown time for certain operations. Two storage racks, each accommodating 12 fuel elements, are located in diametrically opposed positions in the water space between the core reflector tank and the inlet flow baffle. Shielding inside the vessel consists of two annular stainless steel thermal shields used to reduce the gamma heating in the vessel and in the concrete surrounding the vessel.

The reactor building encloses an area approximately 200 feet by 200 feet extending 60 feet above and 60 feet below grade. The first floor is located at grade and includes the following areas: reactor area, storage canal area, utility area, general storage and laydown area, critical facility area, control rooms, and offices. The first and second mezzanine floors include office areas and heating and ventilating equipment rooms. The first and second basements are devoted to experiment cubicles and equipment, heat exchangers, demineralizers, and heating, ventilating and electrical equipment. (See Figures 1-3, 1-4, and 1-5.)

1.2. Design Parameters

The general reactor design parameters used as basic data for the shielding calculations are shown in Table 1-1.

1.3. Dose Rate Summary

A general summary of the calculated dose rates throughout the plant is shown in Table 1-2.

1.4. Radiation Control Areas

In an experimental reactor such as the ATR, it is impractical and uneconomical during the design of the reactor to attempt to specify a complete shield arrangement that anticipates all operating eventualities. Instead, precautions to limit radiation exposure during these operations can best be achieved through administrative control by supervisory and health physics personnel as the occasions arise. In most cases this control can be accomplished by using access limitations or local shielding. Table 1-3 is a general listing of those areas, operations, and conditions requiring radiation control procedures.

Table 1-1. ATR Design Parameters

Parameter	Quantity or description
Reactor rated thermal power	250 MW
Average power density	0.954 MW/liter
Maximum power density	2.8 MW/liter
Axial maximum-to-average power ratio	1.40
Radial maximum-to-average power ratio	1.63
Local maximum-to-average power ratio	1.15
Combined maximum-to-average power ratio	2.61
Primary system design pressure	390 psig
Primary system operating pressure	300 psia
Primary system design temperature	240 F
Primary system inlet temperature	130 F
Total coolant flow through reactor vessel	21.6×10^6 lb/hr
Average coolant velocity through fuel element	42.5 fps
Average coolant flow through fuel element	3.11×10^5 lb/hr
Leakage coolant flow	9.2×10^6 lb/hr
Reflector	6.7×10^6 lb/hr
Flux trap region	1.5×10^6 lb/hr
Thermal shields	1.0×10^6 lb/hr
Coolant inlet temperature	130 F
Coolant exit temperature at rated power	169 F
Core dimensions:	
Active fuel length	48 in.
Fuel spacing (℄ to ℄)	2.5 in.
Number of elements in core	40
Number of test positions	9
Fuel element:	
Metal-to-water ratio	0.8
Type	Plate
Shape of fuel region	Cored cylinder
Clad material	X8001 Al
Form of uranium	Fully enriched U-235
Number of plates per element	19
Experiment region:	
Pressure tube ID	2.125 in.
Pressure tube OD	2.530 in.
Insulation tube ID	2.635 in.
Insulation tube OD	2.875 in.
Flux trap H_2O volume fraction, A-3, A-5, A-1	0.3, 0.4, 1.00
Flux trap Al volume fraction, A-3, A-5, A-1	0.7, 0.6, 0.0
Nuclear data:	
Total fuel loading, U-235	33 kg
Effective lifetime	17 EFPD
Average U-235 burnup in 17 days	5.4 kg

Table 1-2. Summary of Calculated Dose Rates

Location	Maximum calculated dose rate during full power operation, mrem/hr	Maximum calculated dose rate after shutdown, mrem/hr
Outside reactor concrete shield	6.0	<1.0
Outside experiment H_2O loop cubicles (N-16 activity only)	2.5	<1.0
Inside experiment H_2O loop cubicles	5.0 from adjacent operating cubicles (N-16 only), 6.0 from reactor and primary piping	<1.0
Subpile room	No access	1.0 from core through vessel bottom head (does not include streaming through bottom head penetrations)
Rod access room	10.0	<2.5
Floor above heat exchangers	1.5	<1.0
Reactor area, first floor	1.0	<1.0 except during specimen and loop component transfer
Reactor vessel top head	1.0	<1.0 except during specimen and loop component transfer
Above storage canal and at floor level near parapet	1.0	1.0
Above storage canal during spent fuel transfer	50.0 transient	50.0 transient
Below storage canal	1.0	1.0
Outside walls of storage canal	1.0	1.0
Surface of water above ATRC	6.0 with ATRC operating at 5 kw	- -

Table 1-2. (Cont'd)

Location	Maximum calculated dose rate during full power operation, mrem/hr	Maximum calculated dose rate after shutdown, mrem/hr
Below ATRC canal	1.0 with ATRC at 5 kw	- -
Outside walls of ATRC canal	1.0 with ATRC at 5 kw	- -
Outside pipe tunnel	6.0	<1.0
Motor area outside pump cubicles	7.0	<1.0
Inside pump cubicles	4.0 from heat exchangers and piping, 7.0 from adjacent pump cubicle	- -
Nozzle access trench	No access	12.0 from core and stored fuel (does not include streaming through vessel penetrations)
Office areas	<0.25	<0.25 except during specimen and loop component transfer

Table 1-3. Radiation Control Areas

Location	Operation	Radiation sources
Nozzle access trench	Removal of instruments and irradiated capsules	Streaming through instrument wells, activated capsules
Subpile room	Experiment loop removal, general maintenance	Contaminated experiment loops; streaming through inpile loop penetrations; spent fuel elements passing through transfer chute
Pipe corridor	Maintenance of rod drive mechanisms	Contaminated experiment loops, spent fuel passing through transfer chute
Experiment loop test cubicles	Maintenance of test loop equipment	Contaminated test loops
Reactor area, first floor	Removal of activated loop components	Streaming out of top and bottom of transfer cask
Reactor top head area, vessel top head shield removed	Spent fuel removal, general maintenance	Contaminated experiment loops, raised fuel elements
Top head shield, and cask transfer station	Transfer of test specimen	Test specimen

Figure 1-1. Reactor Cross Section,
Sheet No. 1
(Dwg. No. 670-M-428)

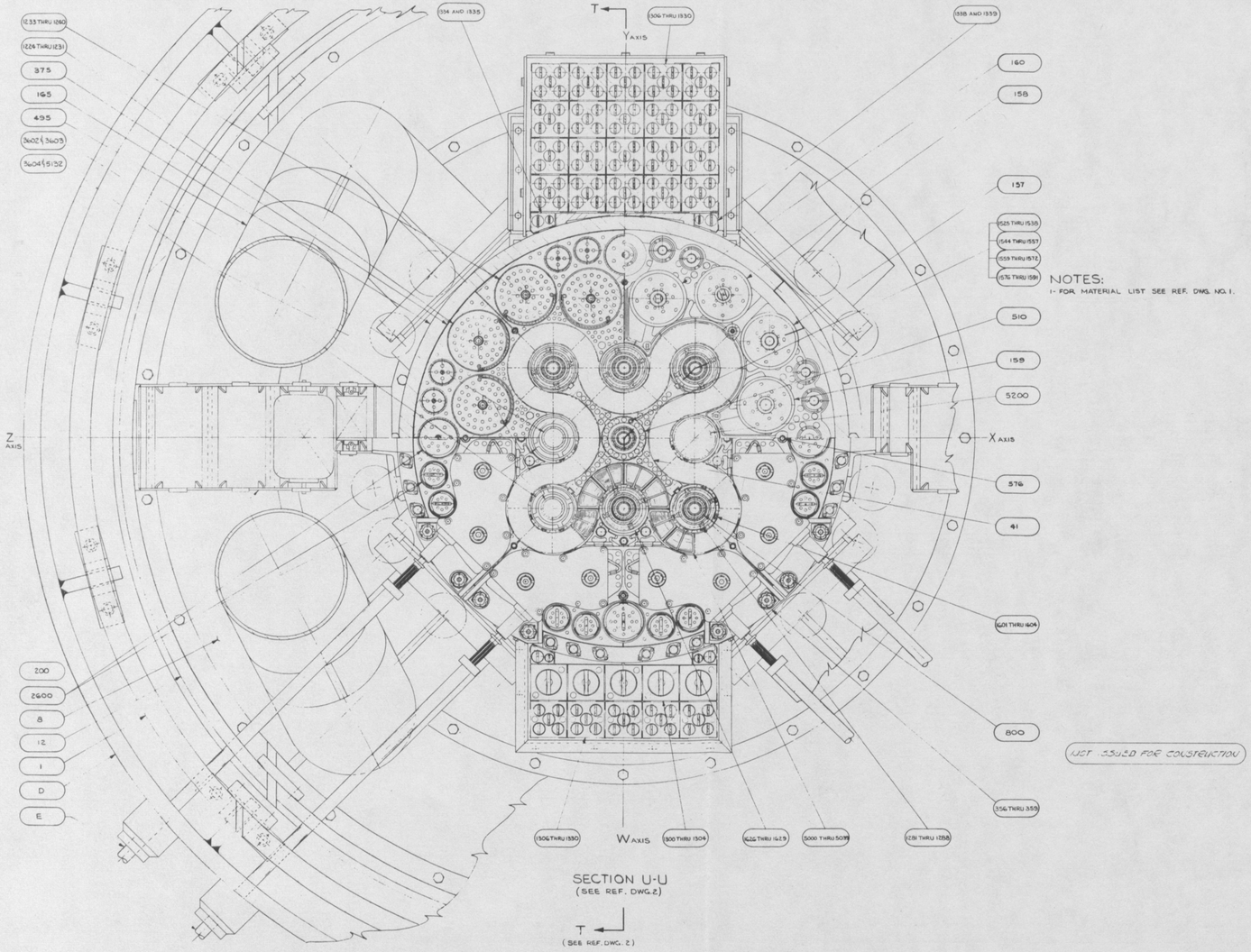

Figure 1-2. Reactor and Internals Assembly Vertical Section (Dwg. No. 670-M-426)

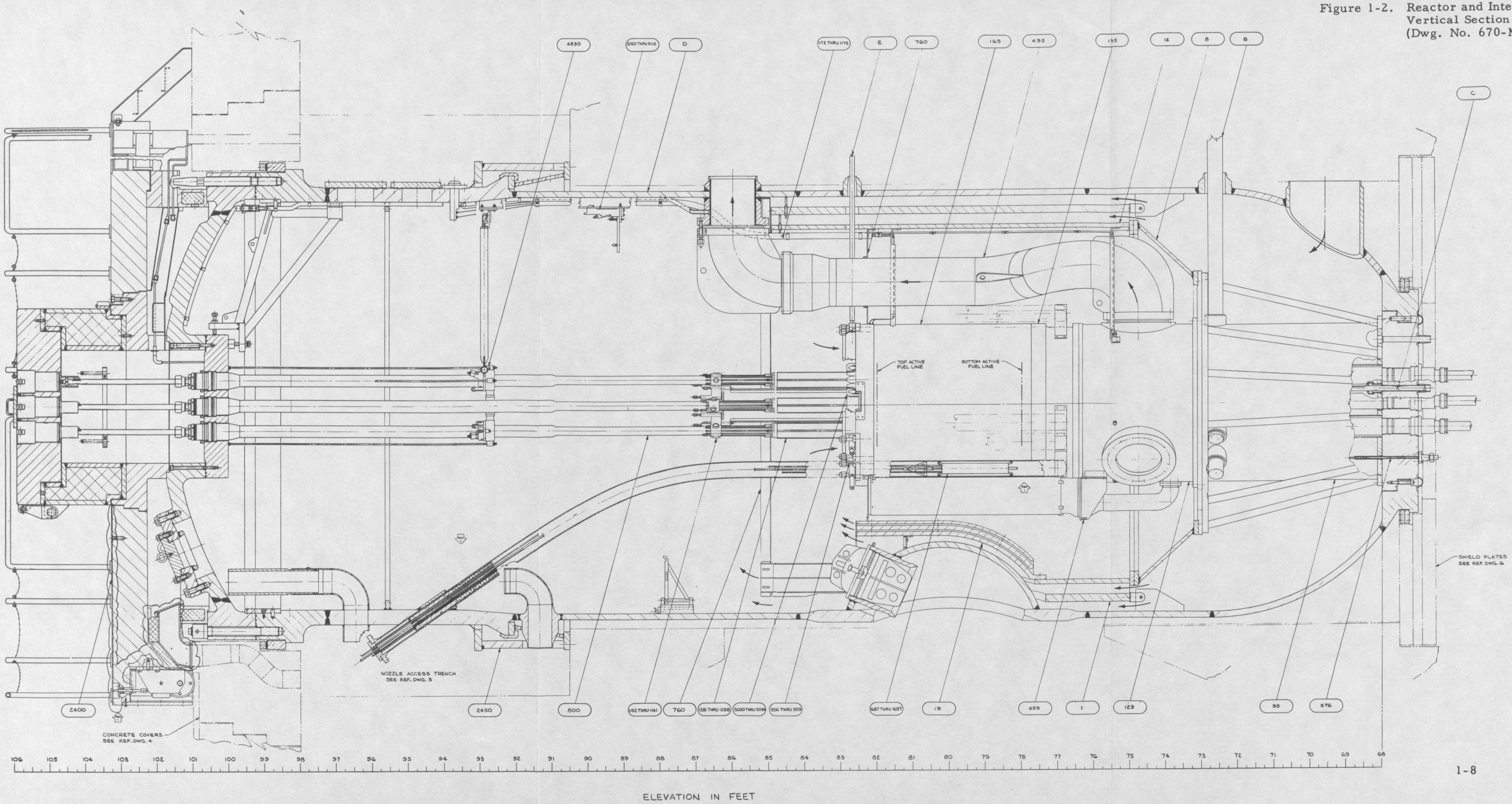

670-MR PART NO.	MATERIAL LIST NAME
A	NECK SHIM ROD DRIVE HOUSING TRANSITION BY UNITED SHOE MACH. CO.
B	SAFETY ROD DRIVE ASSEMBLY BY AMF
C	NECK SHIM ROD DRIVE HOUSING BY UNITED SHOE MACH. CO.
D	REACTOR VESSEL ASSEMBLY BY BALDWIN LIMA HAMILTON
E	OUTER SHIM CONTROL DRIVE MECHANISM BY BENDIX CORP.
1	THERMAL SHIELD ASS'Y.
8	INLET FLOW BAFFLE LOWER HEAD
12	INLET FLOW BAFFLE UPPER CYLINDER
19	TRANSITION FILLER ASS'Y.
41	NECK SHIM ROD HOUSING ASSEMBLY
95	CORE SUPPORT TANK FINAL MACH.
129	FLOW DISTRIBUTION TANK FINAL MACH.
135	REFLECTOR SUPPORT TANK ASS'Y.
157	Be ALIGNING CUP WELDMENT R.H. TYPE 1
158	Be ALIGNING CUP WELDMENT L.H. TYPE 1
159	Be ALIGNING CUP WELDMENT R.H. TYPE 2
160	Be ALIGNING CUP WELDMENT L.H. TYPE 2
165	CORE REFLECTOR TANK ASS'Y.
200	SPENT FUEL STORAGE RACK ARRG'T.
356 THRU 359	GEAR BOX SUPPORT BEAM ASS'Y.
375	REFLECTOR BLOCKS ASS'Y.
455	CAPSULE IRRADIATION TANKS ARRG'T.
495	OUTLET FLOW PIPES ARRG'T.
510	CENTER FLUX TRAP & N-16 ASS'Y.
576	N-16 SAMPLE TUBE AND PENETRATION BODY ASSEMBLY
760	PROTECTIVE COVER ASS'Y.
800	NR & PW LOOP FACILITIES INPILE COMPONENT ASSEMBLY
1132 THRU 1141	PRESSURE TUBE LOCATER TIES
1172 THRU 1175	PRESSURE TAPS & INDICATOR LINES ASS'Y.
1224 THRU 1231	OUTER SHIM CONTROL CYLINDER ASS'Y. R.H.
1233 THRU 1240	OUTER SHIM CONTROL CYLINDER ASS'Y. L.H.
1242 THRU 1261	NECK SHIM ROD ASSEMBLY
1266 THRU 1269	NECK REGULATING ROD
1281 THRU 1288	SAFETY ROD ASSEMBLY
1300 THRU 1304	REFLECTOR BLOCK ASS'Y. "A"
1306 THRU 1330	REFLECTOR BLOCK ASS'Y. "B"
1334 AND 1335	REFLECTOR BLOCK ASS'Y. "C"
1338 AND 1339	REFLECTOR BLOCK ASS'Y. "D"
1525 THRU 1538	POISON INSERT SLEEVE ASS'Y.
1544 THRU 1557	CENTER FLUX TRAP POISON INSERT ROD ASSEMBLY
1559 THRU 1572	FLUX TRAP FILLER ROD ASSEMBLY LONG
1576 THRU 1591	FLUX TRAP FILLER ROD ASSEMBLY SHORT
1601 THRU 1604	INNER FLUX TRAP BAFFLE ASS'Y.
1626 THRU 1629	OUTER FLUX TRAP BAFFLE
1687 THRU 1697	CARRIAGE ASSEMBLY FOR ION AND FISSION CHAMBERS
2400	REACTOR TOP HEAD SHIELDING GEN. ARRG'T.
2450	CAPSULE TRENCH SHIELDING ASS'Y.
2600	CAPSULE FACILITY ASSEMBLY
4550	PRESSURE TUBE VIBRATION TIE ASS'Y.
5000 THRU 5039	FUEL ELEMENT ASSEMBLY
5065 THRU 5112	ADJUSTABLE BRACKET ASS'Y.
3602 & 3603	LOOP DUMMY PRESSURE TUBE ASS'Y.
3604 & 5192	LOOP DUMMY FLUX TRAP FILLER ASS'Y.
5200	GAS COOLED LOOP FACILITIES INPILE COMPONENT ASSEMBLY

Figure 1-3. Reactor Building First-Floor Plan (Dwg. No. 670-A-5)

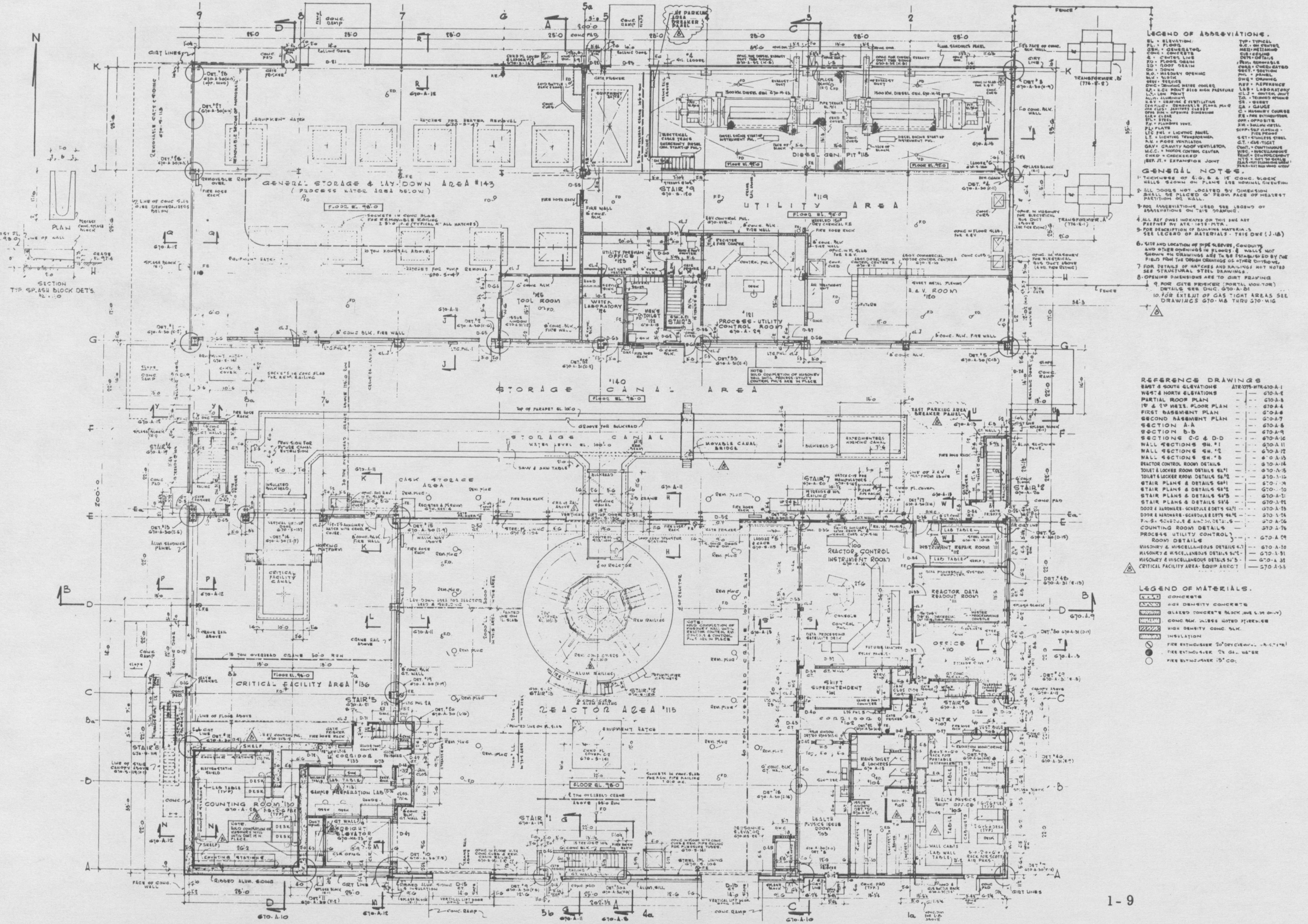

Figure 1-4. Reactor Building First-Basement Plan (Dwg. No. 670-A-6)

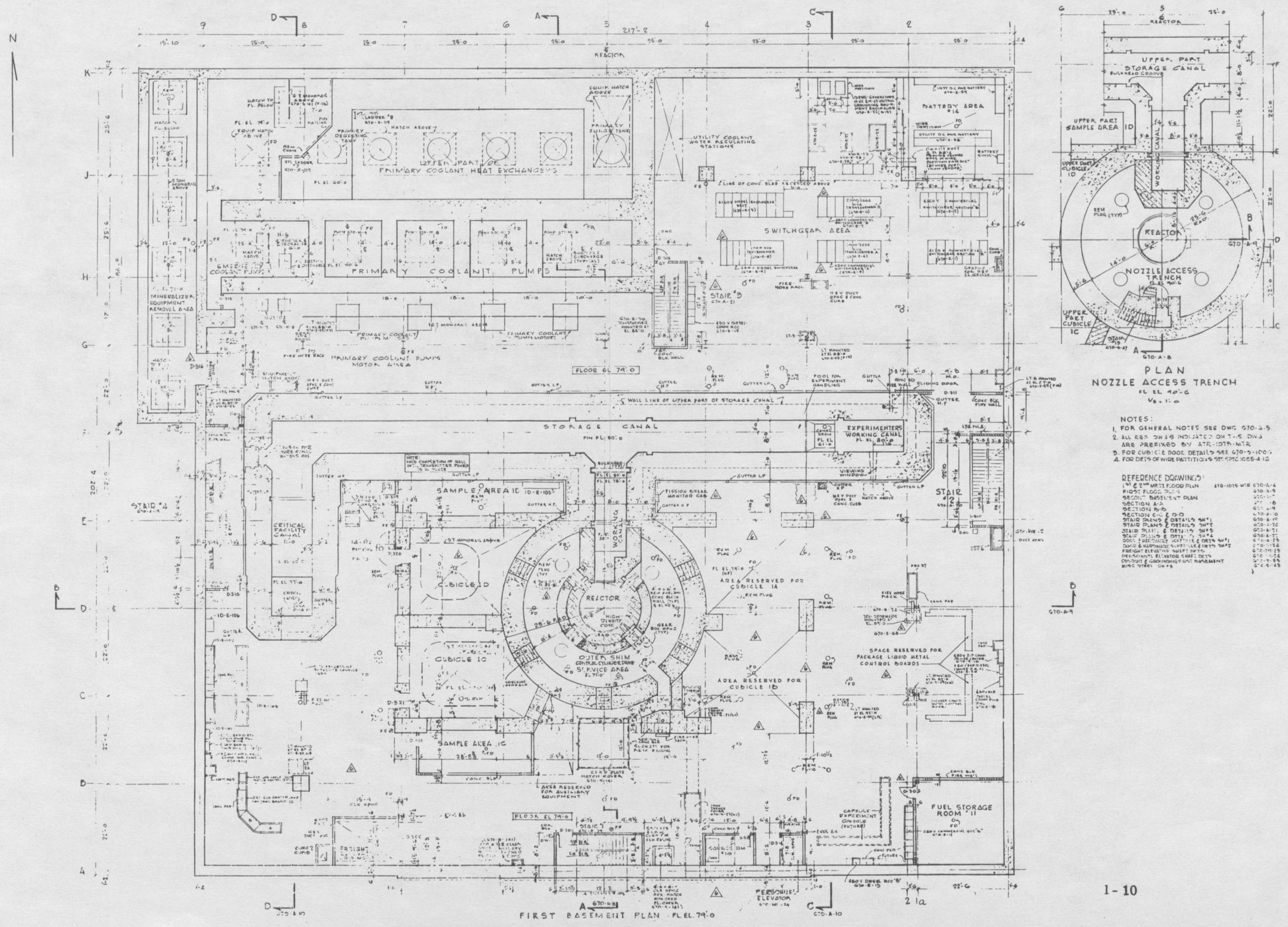

PLAN
NOZZLE ACCESS TRENCH
EL EL 40'-6
$V_8 = 1:0$

NOTES:
1. FOR GENERAL NOTES SEE DWG G70-A-5.
2. ALL REF DWGS INDICATED ON THIS DWG ARE PREFIXED BY ATR-1015-M7R.
3. FOR CUBICLE DOOR DETAILS SEE G70-A-100(S).
4. FOR DETS OF WIRE PARTITIONS SEE SPEC 1055-A-1(S).

REFERENCE DRAWINGS:

1ST & 2ND MEZZ FLOOR PLAN	ATR-1015-M7R G70-A-4
FIRST FLOOR PLAN	G70-A-5
SECOND BASEMENT PLAN	G70-A-7
SECTION A-A	G70-A-8
SECTION B-B	G70-A-9
SECTION C-C & D-D	G70-A-10
STAIR PLANS & DETAILS SH#1	G70-A-10
STAIR PLANS & DETAILS SH#2	G70-A-11
STAIR PLANS & DETAILS SH#3	G70-A-12
STAIR PLANS & DETAILS SH#4	G70-A-13
DOORS & ELECTRICAL SCHEDULE & DETS SH#1	G70-A-25
DOOR & HARDWARE SCHEDULE & DETS SH#2	G70-A-14
FREIGHT ELEVATOR SHAFT DETS	G70-A-15
PERSONNEL ELEVATOR SHAFT DETS	G70-A-16
CONDUIT & GROUNDING FIRST BASEMENT	G70-E-65
MISC STEEL SH #3	G70-S-43

Figure 1-5. Reactor Building Second-Basement Plan (Dwg. No. 670-A-7)

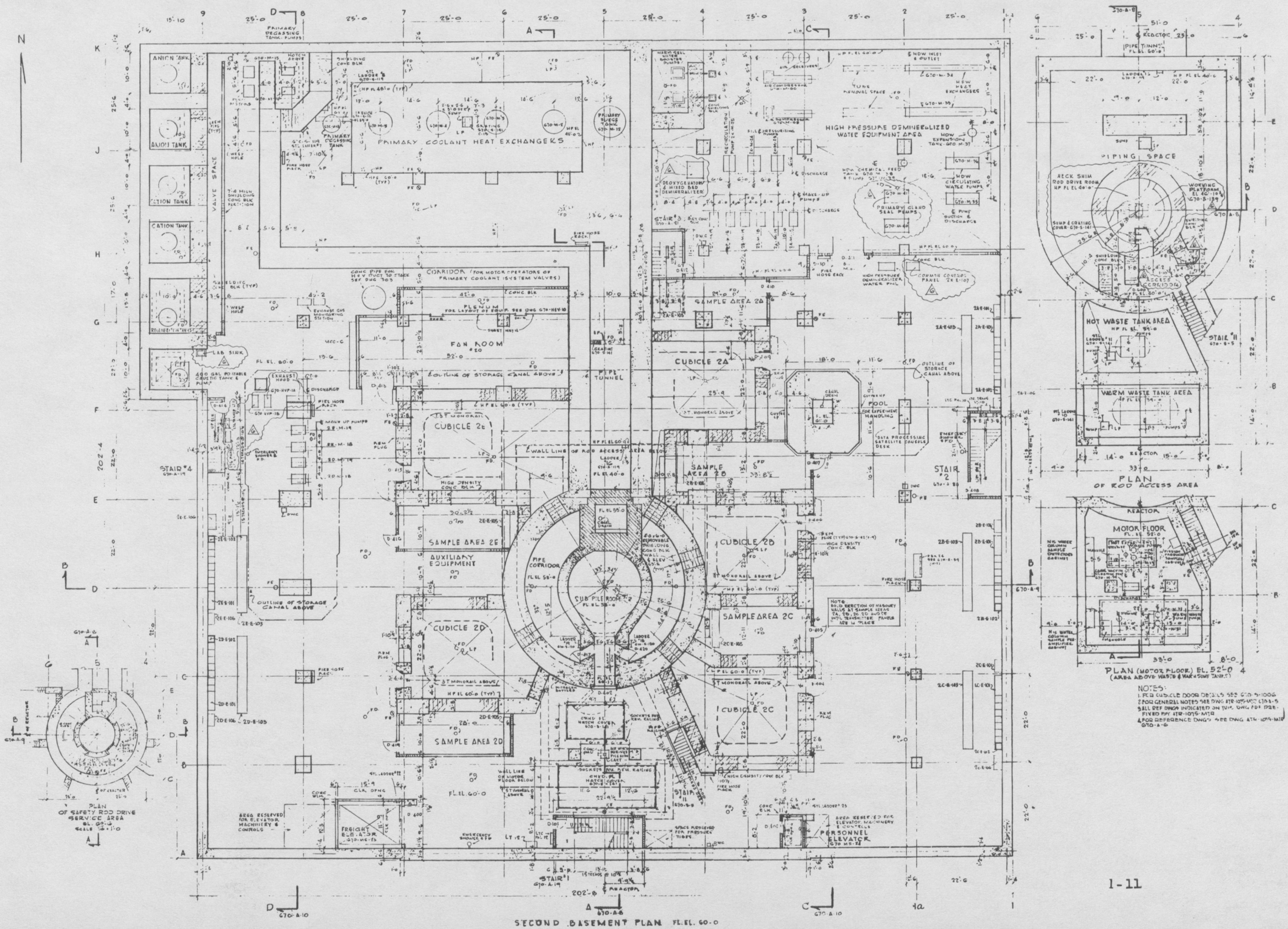

2. CALCULATION METHODS

Shielding design calculations for the ATR are based on techniques and procedures in general use in the industry. The equations for the flux from regular geometric sources were compiled at an early date by Sievert[1] and have been extended and widely repeated in other References 2, 3, 4. The simpler geometric source flux calculations (point, line, disc, slab, truncated cone, cylinder) have been programmed for the digital computer and are available for use on standard Babcock & Wilcox Company computer codes (see Appendix B). Appendix A describes a coded method of computing the secondary gamma ray flux through a laminated semi-infinite shield region. For the more crucial calculations, such as the inpile heat generation rates, the primary and secondary gamma fluxes were computed using a point-source summation program (see Appendix D). Methods used in computing source activities are described in the next section and in the appendixes or are referred to where standard procedures are described in the literature.

Neutron flux values, described in Section 3.1, were generated using a Babcock & Wilcox Company 20-group diffusion code. In the region outside the core, where the thermal neutron flux is important in secondary gamma calculations, the fluxes were checked with good agreement by scaling up Lid Tank Shield Facility data. The fluxes have not been compared with removal theory fluxes at the exterior of the shield since all neutron fluxes become completely insignificant outside the concrete surrounding the reactor.

All gamma ray source strength and attenuation calculations had unit energy intervals and the appropriate form of buildup for dose rate or heat generation rate. NDA infinite-medium buildup values[5], generated by moments method solutions of the time-independent Boltzmann equation for the flux, were used. In most cases, the Taylor sum-of-exponentials form of the buildup[6] was used.

3. SOURCE ACTIVITIES

3.1. Neutron Fluxes

As previously noted, fast and thermal neutron fluxes in the core and inside the reactor vessel were generated by the 20-group diffusion equations programmed for the Electrodata digital computer. This one-dimensional multiregion calculation gives the flux as a function of space and lethargy, approximating the continuous neutron spectrum by 20 discrete lethargy groups. The basic diffusion equation employed is shown below:

$$\nabla D(r,u)\nabla\phi(r,u) - [\Sigma^A(r,j) + \Sigma^I(r,u) + \Sigma^S(r,u)]\phi(r,u) + S(r,u) = 0 \quad (3\text{-}1)$$

where $\nabla D\nabla\phi$ = leakage rate

$\Sigma^A\phi$ = absorption rate

$\Sigma^I\phi$ = inelastic scattering rate

$\Sigma^S\phi$ = elastic scattering rate

S = source term, which is a summation of terms representing the fission source, elastic scattering sources from hydrogen and from elements other than hydrogen, and inelastic scattering

The flux is calculated in the program for each lethargy group, i, at some position, r, in the region by:

$$\phi_i(r) = \int_{u_i}^{u_{i+1}} \phi(u,r)\,du \quad (3\text{-}2)$$

Total flux in each region, j, is computed in the program by:

$$\phi_{ij}^{T} = \int_{R_{j-1}}^{R_j} \phi_i r^{\gamma} dr \qquad (3-3)$$

where R_{j-1} and R_j are region boundaries and γ refers to the geometry chosen.

The total fast and thermal fluxes resulting from the 20-group program are shown in Section 5 (Figure 5-2) for the core midplane through the primary shield. Although it is probable that the fluxes shown far out in the shield are somewhat overestimated by the use of diffusion theory, removal theory fluxes were not calculated because additional (structural) concrete exists between the magnetite and the pipe tunnel resulting in the flux being insignificant at the shield exterior. In the region where the thermal flux is important in the calculation of secondary gamma ray sources, the fast flux predicted by diffusion theory was independently checked by scaling up ORNL Lid Tank Shield Facility (LTSF) fluxes. The comparison is shown in Figure 3-1. The neutron spectra predicted by the 20-group equations for the fuel, flux trap, and reflector regions are shown in Section 3.4.

The neutron flux and spectrum predictions are important from a shielding viewpoint because the ATR thermal flux outside the fuel-reflector region enters into the secondary gamma and thermal activation calculations as a source term and because the fast flux in and near the core is the source of coolant activation N-16 gamma rays as well as Na-24 and Mg-27 recoil product activities in the coolant. Both fast and thermal flux, of course, affect operating core gamma source strengths. The neutrons alone pose no direct shielding problem since they are attenuated to insignificance inside the primary shield as previously noted.

3.2. Operating Core Gamma Sources

Gamma rays produced in the reactor core during power operation are normally referred to as primary gamma rays. The significant sources of primary gamma rays are prompt photons emitted during the fission process, capture gamma rays emitted almost instantaneously

by excited nuclei after capture of thermal neutrons, fission product gamma rays given off in decay, and inelastic scattering gamma rays emitted by the nucleus in an inelastic scattering event. All of these sources, with one exception, are of significance in the calculation of ATR primary gamma source strengths. Inelastic scattering gamma rays are negligible in the ATR core since only a small amount of heavy material is present.

At energies of 1 mev and above, the prompt and fission product gamma sources were obtained from the expression proposed by Goldstein[7]:

$$N(E) = 14.0\, e^{-1.1E} \text{ per mev per fission}$$

Multiplying the solution of this equation in each energy interval by the fission density in the core gives the full-power source strengths. Below 1 mev, the prompt gamma sources were computed independently from the data reported by Maienschien et al[8]. The fission product decay gamma rays in the energy range below 1 mev were estimated so that the total fission product decay energy was 5.5 mev per fission. These low energy sources were significant in analyzing core heat generation. Capture gamma source strengths in the core were obtained by using capture rates in core materials obtained directly from the 20-group diffusion program solutions. Core materials considered were water, aluminum, iron, nickel, zirconium, and U-235. The capture gamma yield spectra for each material were taken from Deloume[9], and the data were modified in the lower energies to match the energy spectra to the binding energy of the excited nucleus. The average gamma ray source strengths in the fuel region at a power level of 250 MW are shown in Table 3-1.

Table 3-1. Gamma Ray Source Strengths in Fuel Region

Energy interval, mev	Average energy, mev	Source strength, photons/cc-sec
0.3 - 0.5	0.4	1.2×10^{14}
0.5 - 1.5	1.0	1.7×10^{14}
1.5 - 2.5	2.0	5.3×10^{13}
2.5 - 3.5	3.0	1.9×10^{13}
3.5 - 4.5	4.0	7.6×10^{12}
4.5 - 5.5	5.0	6.0×10^{12}
5.5 - 6.5	6.0	3.1×10^{12}
6.5 - 7.5	7.0	7.2×10^{11}
7.5 - 8.5	8.0	1.0×10^{12}

In calculations involving the homogenized core, source strengths were obtained from the fuel region sources by means of a volume ratio.

Linear absorption coefficients for the core were calculated for each energy interval by volume weighting the coefficients of the various core materials. Absorption coefficients for the individual elements were taken from Reference 10. A plot of the linear absorption coefficient in the fuel region is shown in Figure 3-2 as a function of energy.

3.3. Secondary Gamma Rays

Secondary gamma rays are capture gamma rays born outside the core as a result of thermal neutron capture in reflector and shield materials and internals. Consequently, the source activity for secondary gamma rays is a function of the thermal neutron flux level at the specific location being considered. In the ATR design, secondary gamma dose rates and heat generation rates contribute significantly to the total dose and heating rates even at locations inside the pressure vessel near the reflector. This is because very high fluxes, which cause high secondary gamma production, exist in and near the reflector region.

The secondary gamma production rate is given by the expression:

$$S_{vi} = \Sigma_a \gamma_i \phi_{th} \text{ photons/cc-sec-mev} \quad (3\text{-}4)$$

where

Σ_a = thermal neutron macroscopic absorption coefficient per centimeter

γ_i = gamma ray yield in the ith energy group, photons/capture-mev

ϕ_{th} = thermal neutron flux, neut/cm^2-sec

The gamma ray yields were taken from Deloume[9], and the thermal neutron flux profile was obtained from the 20-group diffusion program.

Resonance neutron capture in the shield region contributes no more than 10-20% to the secondary gamma sources and was not included in the calculations.

Two methods were employed to calculate the secondary gamma flux. Some of the earlier calculations were done analytically by using modifications to the equation for the uncollided secondary gamma flux at the plane surface of an infinite slab shield. Since this equation refers to a single infinite homogeneous slab source, the equation was revised for use with a series of slab sources of different materials to accomplish the following objectives:

1. Individual unit energy intervals could be followed for gamma radiation.
2. The contribution of any individual source slab could be determined at any location in the shield.
3. Buildup could be applied from each source to any interface so that a builtup flux could be obtained from the entire source array at any point.

The revisions to the single slab equation to accomplish these objectives consisted of: (1) a substitution of "relaxation length" distance for real distance to facilitate programming, (2) a difference method whereby the entire shield array was assumed to have a flux of the same slope as the source slab and whereby the flux was assumed to be attenuated exponentially from the source slab. This difference method gave the separate contributions from each source slab at each dose point chosen. The equations used in the secondary gamma calculation were programmed for the digital computer and are shown in the discussion in Appendix A of this report.

The second method for determining the secondary gamma flux uses a computer code for summing point sources over an annular source region (see Appendix D). Provisions are made in the program for axial and radial variations in the source strength. Actual shield sizes, i.e., height and thickness, are specified as inputs to the program as opposed to the semi-infinite shield that must be assumed for the analytical solution. The size of the source mesh volume is chosen by the programmer, and the incremental variations in the source strength, both radial and axial, can be made to correspond to the thermal neutron flux profile in the source shield.

For relatively large shield heights having exponential neutron radial fluxes and no axial variation in the thermal flux, agreement of point source and analytical solution programs is good. However, the ATR seldom has this condition, and most of the final secondary gamma design calculations were done with the point source program.

3.4. Primary Coolant Activation

The activity of the primary coolant during operation of a water-cooled reactor is due chiefly to three reactions involving the oxygen atom in H_2O. Activation of impurities in the coolant and leakage of fission products from the fuel will contribute to the total activation. The reactions which occur for oxygen are:

1. ${}_8O^{16}(n,p)\ {}_7N^{16}$
2. ${}_8O^{17}(n,p)\ {}_7N^{17}$
3. ${}_8O^{18}(n,\gamma)\ {}_8O^{19}$

Of these reactions, the major contributor to the activity is the N-16, which decays with a 7.35-second half-life. The emitted gamma ray energies are 6.1 mev and 7.1 mev, which yield 75 and 7 per 100 captures respectively. The effective energy considered for calculations was 6.3 mev, which yields 82%.

The N-16 reaction, which has a threshold energy of about 10 mev, is dependent on the high energy region of the fast neutron spectrum. Therefore, the prediction of the fast neutron core spectrum is of prime importance in the calculation of this activity. The high energy spectrum in the region of interest in the ATR was obtained from a multigroup

diffusion theory program. The program has a cutoff energy of 10 mev, which is based on the assumption that all neutrons having higher energies are included in the last group. Figures 3-3, 3-4, and 3-5 present the histograms of the neutron flux in the high energy groups for the fuel region, flux trap, and reflector respectively. The following equation provided an estimate of the continuous spectrum of neutrons from these histograms.

$$\frac{\phi_{avg}(E_m)\,\Delta E_n}{2} = \int_{E_n}^{E_n+\epsilon_n} \phi(E)\,dE = \frac{1}{2}\int_{E_n}^{E_n+\Delta E_n} \phi(E)\,dE \qquad (3\text{-}5)$$

where

$\epsilon_n \approx 0.4\,\Delta E_n$

$\phi_{avg}(E_m)$ = average neutron flux in energy group E_n to E_{n+1} with average energy E_m

$\Delta E_n = E_{n+1} - E_n$

E_n = lower energy boundary of neutron group n.

$E_n + \epsilon_n = E_m$

The calculated continuous spectrum below the cutoff energy of 10 mev and the extrapolation of this spectrum above 10 mev (dashed line) is shown in Figures 3-3, 3-4, and 3-5.

An independent check on the high energy spectrum used a method presented in Reference 11. This method assumes Watt's fission spectrum source of high energy neutrons. A correction is made to the spectrum to account for neutron removal from the high energy (> 10 mev) groups. The method is described by the equation:

$$\phi_{avg}(E) = \frac{\nu F_{avg} N(E)}{\Sigma_R(E)} \qquad (3\text{-}6)$$

where

ν = neutrons per fission for U-235 (2.43)

F_{avg} = average fission rate in fuel region (7.47×10^{13} fissions/cc-sec)

$N(E)$ = fractional number of neutrons in the energy group from E - 0.5 mev to E + 0.5 mev from Watt's fission spectrum

$\Sigma_R(E)$ = cross section for removal of a high energy neutron from energy group E to below the threshold energy of the reaction

The cross section for removal of a neutron from the energy groups above the threshold energy of the reaction was computed from the following assumptions.

1. That an elastic scattering reaction of a neutron having energy E_n with an atom of mass A has the probability of removal to below the threshold energy E_T of:

$$P_S = 1/4A \frac{E_T}{E_n} \left[(A + 1)^2 - (A - 1)^2 \right] \qquad (3\text{-}7)$$

2. That an inelastic scattering reaction of a neutron with a low mass atom ($A < 30$) does not degrade the impinging neutron to below the threshold energy of the N-16 reaction.

3. That an inelastic scattering reaction of a neutron with a high mass atom ($A > 30$) degrades the impinging neutron to below the threshold energy of the N-16 reaction with a probability of one.

From these assumptions and the fuel region volume fractions of materials, the macroscopic differential cross section for removal of a neutron from the high energy groups was computed. The results are presented in Table 3-2 and are plotted on Figure 3-3 (solid line).

Table 3-2. Parameters for Calculation of the High Energy Neutron Spectrum

E, mev	Σ_R	N(E)	$\phi_{avg}(E)$
10	0.065	9.53×10^{-4}	1.39×10^{12}
11	0.038	4.38×10^{-4}	1.07×10^{12}
12	0.029	1.99×10^{-4}	6.27×10^{11}
13	0.023	8.95×10^{-5}	3.60×10^{11}
14	0.019	4.01×10^{-5}	1.91×10^{11}
15	0.018	1.77×10^{-5}	8.90×10^{10}
16	0.017	6.07×10^{-6}	4.12×10^{10}
17	0.016	2.6×10^{-6}	1.95×10^{10}
18	0.015	1.1×10^{-6}	9.24×10^{9}

The results obtained from the independent check substantiate the use of a continuation of the multigroup spectrum slope as an approximation of a continuous neutron spectrum above 10 mev. The extrapolated neutron spectrum was used in all calculations, and the spectrum above 10 mev used in each of the activating regions is shown in Figures 3-3, 3-4, and 3-5.

The cross section for the O-16 (n, p) N-16 reaction as a function of neutron energy has been measured by Martin[12] and is shown in Figure 3-6. The average of this curve over a fission spectrum of neutrons is 20 μb ± 6 μb, which has a ±30% uncertainty in the absolute values of the experimental measurements. The value of the average cross section agrees favorably with the value of 16 μb given by Rockwell[2], however, it is a factor of about two higher than recent measurements made by Shure[13].

The activation of primary coolant during exposure to neutron flux is based on the differential equation,

$$dN/dt = \Sigma\phi - \lambda N \qquad (3\text{-}8)$$

where
- N = number density of active nuclide, atoms/cc
- t = time, sec
- Σ = macroscopic activation cross section, cm^{-1}
- ϕ = neutron flux, neut/cm^2-sec
- λ = active nuclide decay constant, sec^{-1}

Consider the single pass core described by the following diagram:

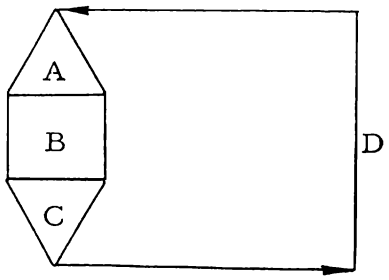

where
- A = plenum region
- B = incore region
- C = plenum region
- D = exterior primary coolant loop

Similarly, let t_A, t_B, t_C, t_D be the transit times in each of the regions during a single pass of coolant through the system. Equation 3-4 can be solved as a function of time if the neutron flux in each region can be described. Assuming that the neutron flux in region B is constant and that the flux is attenuated exponentially in the plenum regions A and C, the fluxes in the regions are as follows:

$$\phi_A = A'e^{ax} \tag{3-9}$$

$$\phi_B = B' \tag{3-10}$$

$$\phi_C = C'e^{-cx} \tag{3-11}$$

where x is chosen as some distance where activation is negligible, A' and C' represent the neutron flux at x = 0, and B' is the flux value in the incore region.

By writing the distance (x) as velocity times time (vt), Equations 3-8 and 3-9 are applied to the upper plenum as follows:

$$dN/dt = \Sigma A'e^{avt} - \lambda N \tag{3-12}$$

The solution is

$$Ne^{\lambda t} = \frac{\Sigma A'}{av + \lambda} e^{(av + \lambda)t} + K \tag{3-13}$$

when $t = 0$, $N = N_0$

Then,

$$N = \frac{\Sigma A'}{av + \lambda} (e^{avt} - e^{-\lambda t}) + N_0 e^{-\lambda t} \tag{3-14}$$

Solution of this time-dependent equation provides the activation in the upper plenum. Similar solutions are evident for the core region and lower plenum. Letting α equal the number density of the nuclide existing in region C after a single pass,

$$\alpha = \frac{\Sigma A'}{av + \lambda} \left(e^{av_A t_A} - e^{-\lambda t_A} \right) e^{-\lambda(t_B + t_C)}$$

$$+ \frac{\Sigma B'}{\lambda} \left(1 - e^{-\lambda t_B} \right) e^{-\lambda t_C} + \frac{\Sigma C'}{cv_C - \lambda} \left(e^{-\lambda t_C} - e^{-cv_C t_C} \right) \tag{3-15}$$

Since t_D is the transient time in the exterior loop, the total number density of the active nuclide entering the activation region for the second pass is

$$N = a e^{-\lambda t_D} \tag{3-16}$$

Letting $T = t_A + t_B + t_C + t_D$, after the nth pass, the saturation number density is

$$N = a \sum_{n=1}^{\infty} e^{-(n-1)\lambda T} = \frac{a}{1 - e^{-\lambda T}} \tag{3-17}$$

Therefore, the saturation activity leaving a single pass core is

$$\lambda N = \frac{\lambda a}{1 - e^{-\lambda T}} \tag{3-18}$$

The coolant activity of N-16 was calculated assuming a series of single-pass activating regions of different flow velocities and, therefore, different core lag times. The total equilibrium activity is then the sum of the individual contributions.

$$A_{total} = \sum_{all\ regions} f_i A_i \tag{3-19}$$

where f_i = fraction of flow through activating region i

A_i = activity induced in region i

The regions calculated, as well as transient times and calculation parameters, are shown in Table 3-3. The assumption was made that all plenum activation occurs within 10 inches above and 10 inches below the active core region.

Total loop transient time, including exterior loop time t_D not shown in Table 3-3, is taken to be 37 seconds.

Table 3-3. Parameters for Calculation of N-16 Activity

Region	Flow rate, gpm	Flow ratio, f_i	Velocity, fps	Time, sec		
				t_A	t_B	t_C
Fuel plates	25,300	0.532	44	0.034	0.091	0.034
Side plates	1,230	.026	44	.034	.091	.034
Reflector body	2,530	.053	30	.36	.133	.36
Rotating drums	7,520	.159	30	.36	.133	.36
Outside annulus	650	.014	5	.36	.802	.36
Flux trap	6,110	.129	20	.41	.2	.41
Neck region	200	.004	20	0.41	0.2	0.41
Outside reactor tank	2, 000	.042	0.08	10.4	51	10.4
Aluminum capsule holders	1, 875	0.041	15	0.054	0.027	0.054
Totals	47,415	1.000				

The resulting equilibrium coolant activation obtained from the preceding equations and parameters is 2.2×10^7 disintegrations/cm^3-sec at 10 inches below the active core region. The decay of this activity with time is shown in Figure 3-7.

The O-17 (n,p) N-17 reaction has a threshold energy of about 10 mev. The product nucleus, N-17, decays with a 4.14-second half-life to O-17 by beta emission. The excitation energy of the residual O-17 nucleus is released by the emission of a neutron of about 1 mev.

The procedure for computing the N-17 activity in the test loop coolant is the same as that used in determining the N-16 activity. The cross section for the reaction was taken from Reference 2. Activities in coolant leaving the pressure vessel as a function of flow rate are as follows:

20 gpm	2.0×10^4 dis/cc-sec
60 gpm	1.2×10^4 dis/cc-sec
120 gpm	7.8×10^3 dis/cc-sec

3.5. Fission Products

The decay of long-lived (i.e., half-life longer than 1 minute) fission products constitutes the major radiation source from the reactor core after shutdown. Decay of these fission products creates a gamma ray spectrum over an energy range up to 5.4 mev. For shielding analysis the high energy portion of the spectrum is important. Until recently, fission product decay curves lumped the high energy gamma rays into groups that had a high energy group of 2.6 mev. Goldstein[7] tabulates J. F. Scoles's data[14] of fission product decay. This data divides the spectrum into 1 mev intervals up to the highest energy of 5.4 mev. The tabulation gives the gamma ray energy emission in mev/sec for each of six energy groups at various times after shutdown. The basis of the data is an initially clean reactor which operates at 1 watt for periods ranging from 10^{-4} hour to 10^6 hours.

For the ATR parameters of 250 MW power and total fuel region volume of 262 liters, the volumetric source strengths as a function of time after reactor shutdown for each of five fission product gamma energy groups are presented in Figure 3-8. The energy grouping used in Figure 3-8 is as follows:

Energy group	Energy limits, mev	Average energy, mev
1	0 - 0.99	0.5
2	1.0 - 1.99	1.5
3	2.0 - 2.99	2.5
4	3.0 - 3.99	3.5
5	4.0 - 4.99	4.5

A compilation of the fission product gamma energy release has also been made by Perkins and King[10]. This agrees well with the Scoles data down to about 1000 seconds after fission. However, for shorter decay times the Perkins and King data show a higher energy release rate and, for this reason, were used to obtain fission product gamma sources for calculations involving times after shutdown of 1000 seconds or less.

In conjunction with the use of the data described above, the buildup and decay of individual fission product isotopes in the ATR core have also been studied. The computer program DER-006A, which is described in Appendix C, was used. The fission product inventory predicted by this program is shown in Table 3-4. The activity of the individual isotopes is shown for various times after shutdown following 17 days of operation at 250 MW. For times after shutdown greater than 1000 seconds, the beta and gamma decay power predicted by the program is in good agreement with Scoles's data and with the work of Perkins and King. Between 100 and 1000 seconds after shutdown, the program results follow the Perkins and King data.

Table 3-4. ATR Fission Product Inventory After 17 Days of Operation at 250 MW Using 33 kg of Fuel

Shown in Disintegrations per Second per Gram of Uranium

Isotope	Time after shutdown					
	1/2 hr	1 hr	12 hr	24 hr	3 days	90 days
Se-83m	5.86×10^{3}	--	--	--	--	--
Se-83	2.17×10^{11}	9.48×10^{10}	1.07×10^{3}	--	--	--
Br-83	1.028×10^{12}	9.04×10^{11}	3.36×10^{10}	9.05×10^{8}	4.73×10^{2}	--
Kr-83m	1.127×10^{12}	1.100×10^{12}	1.170×10^{11}	4.24×10^{9}	2.70×10^{3}	--
Se-84	7.96×10^{7}	2.43×10^{3}	--	--	--	--
Br-84	1.39×10^{12}	6.97×10^{11}	1.66×10^{5}	--	--	--
Br-85	3.47×10^{9}	--	--	--	--	--
Kr-85m	3.31×10^{12}	3.06×10^{12}	5.33×10^{11}	7.92×10^{10}	3.84×10^{7}	--
Kr-85	2.14×10^{9}	2.14×10^{9}	2.16×10^{9}	2.17×10^{9}	2.17×10^{9}	2.13×10^{9}
Br-87	9.03×10^{2}	--	--	--	--	--
Kr-87	4.95×10^{12}	3.79×10^{12}	1.08×10^{10}	1.80×10^{7}	--	--
Br-88	--	--	--	--	--	--
Kr-88	7.73×10^{12}	6.82×10^{12}	4.35×10^{11}	2.16×10^{10}	1.32×10^{5}	--
Rb-88	8.33×10^{12}	7.54×10^{12}	4.88×10^{11}	2.42×10^{10}	1.47×10^{5}	--
Br-89	--	--	--	--	--	--
Kr-89	1.61×10^{10}	2.33×10^{7}	--	--	--	--
Rb-89	3.69×10^{12}	9.58×10^{11}	--	--	--	--
Sr-89	2.26×10^{12}	2.26×10^{12}	2.25×10^{12}	2.23×10^{12}	2.17×10^{12}	6.98×10^{11}
Kr-90	--	--	--	--	--	--
Rb-90	8.64×10^{9}	4.38×10^{6}	--	--	--	--
Sr-90	1.61×10^{10}	1.61×10^{10}	1.61×10^{10}	1.61×10^{10}	1.61×10^{10}	1.60×10^{10}
Y-90	1.25×10^{10}	1.25×10^{10}	1.29×10^{10}	1.33×10^{10}	1.44×10^{10}	1.60×10^{10}
Kr-91	--	--	--	--	--	--
Rb-91	3.07×10^{12}	6.97×10^{11}	--	--	--	--
Sr-91	1.37×10^{13}	1.32×10^{13}	6.06×10^{12}	2.57×10^{12}	8.33×10^{10}	--
Y-91m	5.57×10^{12}	5.51×10^{12}	2.66×10^{12}	1.12×10^{12}	3.65×10^{10}	--
Y-91	2.47×10^{12}	2.47×10^{12}	2.50×10^{12}	2.52×10^{12}	2.49×10^{12}	8.81×10^{11}
Kr-92	--	--	--	--	--	--
Rb-92	2.24×10^{6}	--	--	--	--	--
Sr-92	1.27×10^{13}	1.11×10^{13}	5.94×10^{11}	2.42×10^{10}	6.73×10^{4}	--
Y-92	1.43×10^{13}	1.41×10^{13}	3.64×10^{12}	4.52×10^{11}	4.98×10^{7}	--
Kr-93	--	--	--	--	--	--
Rb-93	--	--	--	--	--	--
Sr-93	7.78×10^{11}	3.99×10^{10}	--	--	--	--
Y-93	1.50×10^{13}	1.45×10^{13}	6.77×10^{12}	2.95×10^{12}	1.06×10^{11}	--
Kr-94	--	--	--	--	--	--
Rb-94	--	--	--	--	--	--
Sr-94	4.21×10^{8}	1.28×10^{4}	--	--	--	--
Y-94	4.90×10^{12}	1.39×10^{12}	1.27×10^{0}	--	--	--
Y-95	2.09×10^{12}	2.88×10^{11}	--	--	--	--
Zr-95	2.51×10^{12}	2.51×10^{12}	2.49×10^{12}	2.48×10^{12}	2.43×10^{12}	9.62×10^{11}
Nb-95m	2.49×10^{10}	2.49×10^{10}	2.57×10^{10}	2.65×10^{10}	2.89×10^{10}	1.42×10^{10}
Nb-95	3.87×10^{11}	3.88×10^{11}	4.07×10^{11}	4.27×10^{11}	5.06×10^{11}	1.22×10^{12}
Zr-97	1.43×10^{13}	1.40×10^{13}	9.00×10^{12}	5.51×10^{12}	7.80×10^{11}	--
Nb-97m	1.36×10^{13}	1.34×10^{13}	8.55×10^{12}	5.24×10^{12}	7.42×10^{11}	--
Nb-97	1.46×10^{13}	1.45×10^{13}	9.68×10^{12}	5.94×10^{12}	8.39×10^{11}	--
Nb-99	6.08×10^{10}	2.56×10^{8}	--	--	--	--
Mo-99	1.41×10^{13}	1.40×10^{13}	1.25×10^{13}	1.11×10^{13}	6.83×10^{12}	3.94×10^{3}

Table 3-4. (Cont'd)

Isotope	Time after shutdown					
	1/2 hr	1 hr	12 hr	24 hr	3 days	90 days
Tc-99m	1.41×10^{12}	1.41×10^{12}	1.34×10^{12}	1.21×10^{12}	7.49×10^{11}	4.32×10^{2}
Mo-101	2.85×10^{12}	6.86×10^{11}	--	--	--	--
Tc-101	6.78×10^{12}	2.52×10^{12}	--	--	--	--
Mo-102	1.75×10^{12}	3.10×10^{11}	--	--	--	--
Tc-102	1.82×10^{12}	3.22×10^{11}	--	--	--	--
Ru-103	1.75×10^{12}	1.75×10^{12}	1.74×10^{12}	1.72×10^{12}	1.67×10^{12}	3.67×10^{11}
Rh-103m	1.67×10^{12}	1.67×10^{12}	1.65×10^{12}	1.64×10^{12}	1.58×10^{12}	3.49×10^{11}
Mo-105	2.22×10^{10}	3.47×10^{8}	--	--	--	--
Tc-105	2.22×10^{10}	3.84×10^{8}	--	--	--	--
Ru-105	1.99×10^{12}	1.84×10^{12}	3.39×10^{11}	5.35×10^{10}	3.29×10^{7}	--
Rh-105m	2.00×10^{12}	1.85×10^{12}	3.40×10^{11}	5.36×10^{10}	3.30×10^{7}	--
Rh-105	2.12×10^{12}	2.12×10^{12}	1.89×10^{12}	1.53×10^{12}	6.20×10^{11}	--
Ru-106	2.86×10^{10}	2.86×10^{10}	2.86×10^{10}	2.86×10^{10}	2.85×10^{10}	2.41×10^{10}
Rh-106	2.86×10^{10}	2.86×10^{10}	2.86×10^{10}	2.86×10^{10}	2.85×10^{10}	2.41×10^{10}
Tc-107	3.62×10^{5}	--	--	--	--	--
Ru-107	3.87×10^{9}	2.13×10^{7}	--	--	--	--
Rh-107	2.63×10^{11}	1.19×10^{11}	2.98×10^{3}	--	--	--
Ru-108	1.04×10^{9}	5.80×10^{6}	--	--	--	--
Rh-108	1.13×10^{9}	6.27×10^{6}	--	--	--	--
Rh-109	4.68×10^{10}	3.31×10^{10}	1.62×10^{7}	3.96×10^{3}	--	--
Pd-109	6.60×10^{10}	6.53×10^{10}	3.88×10^{10}	2.10×10^{10}	1.82×10^{9}	--
Ag-109m	6.60×10^{10}	6.53×10^{10}	3.88×10^{10}	2.10×10^{10}	1.82×10^{9}	--
Pd-111	1.65×10^{10}	6.43×10^{9}	6.02×10^{1}	--	--	--
Ag-111	3.37×10^{10}	3.36×10^{10}	3.22×10^{10}	3.08×10^{10}	2.56×10^{10}	8.29×10^{6}
Pd-112	2.56×10^{10}	2.51×10^{10}	1.75×10^{10}	1.17×10^{10}	2.42×10^{9}	--
Ag-112	2.60×10^{10}	2.59×10^{10}	2.03×10^{10}	1.38×10^{10}	2.85×10^{9}	--
Ag-113	2.21×10^{10}	2.07×10^{10}	4.93×10^{9}	1.02×10^{9}	1.93×10^{6}	--
Cd-113m	7.36×10^{5}	7.37×10^{5}	7.46×10^{5}	7.49×10^{5}	7.49×10^{5}	7.25×10^{5}
Ag-114	7.24×10^{5}	2.21×10^{1}	--	--	--	--
Ag-115	9.02×10^{9}	3.25×10^{9}	--	--	--	--
Cd-115	2.40×10^{10}	2.39×10^{10}	2.08×10^{10}	1.78×10^{10}	9.78×10^{9}	1.31×10^{8}
In-115m	2.35×10^{10}	2.35×10^{10}	2.17×10^{10}	1.88×10^{10}	1.01×10^{10}	--
Cd-117m	2.10×10^{10}	1.87×10^{10}	1.48×10^{9}	9.25×10^{7}	1.41×10^{3}	--
Cd-117	2.31×10^{10}	2.20×10^{10}	2.04×10^{9}	1.28×10^{8}	1.95×10^{3}	--
In-117m	2.36×10^{10}	2.35×10^{10}	5.50×10^{9}	4.61×10^{8}	8.34×10^{3}	--
In-117	6.62×10^{9}	6.62×10^{9}	2.13×10^{9}	1.95×10^{8}	3.68×10^{3}	--
Sn-117m	4.64×10^{7}	4.64×10^{7}	4.64×10^{7}	4.55×10^{7}	4.12×10^{7}	5.56×10^{5}
Cd-118	1.56×10^{10}	1.03×10^{10}	1.09×10^{6}	5.08×10^{1}	--	--
In-118	1.71×10^{10}	1.32×10^{10}	1.20×10^{6}	5.58×10^{1}	--	--
In-119	7.21×10^{9}	2.19×10^{9}	--	--	--	--
Sn-119m	1.08×10^{9}	1.08×10^{9}	1.08×10^{9}	1.08×10^{9}	1.08×10^{9}	8.49×10^{8}
Sn-121	3.27×10^{10}	3.23×10^{10}	2.44×10^{10}	1.81×10^{10}	5.40×10^{9}	--
Sn-123	2.09×10^{10}	1.23×10^{10}	1.16×10^{5}	--	--	--
Sn-123m	2.35×10^{8}	2.35×10^{8}	2.35×10^{8}	2.34×10^{8}	2.32×10^{8}	1.49×10^{8}
Sn-125m	3.11×10^{9}	3.73×10^{8}	--	--	--	--
Sn-125	2.02×10^{10}	2.02×10^{10}	1.95×10^{10}	1.88×10^{10}	1.62×10^{10}	2.66×10^{7}
Sb-125	6.15×10^{8}	6.15×10^{8}	6.24×10^{8}	6.33×10^{8}	6.65×10^{8}	8.08×10^{8}
Te-125m	9.69×10^{6}	9.72×10^{6}	1.02×10^{7}	1.08×10^{7}	1.33×10^{7}	9.95×10^{7}
Sn-126	1.56×10^{11}	1.03×10^{11}	1.09×10^{7}	5.08×10^{2}	--	--
Sb-126	2.35×10^{11}	2.31×10^{11}	1.03×10^{11}	4.11×10^{10}	1.02×10^{9}	--
Sn-127	4.51×10^{11}	3.58×10^{11}	2.22×10^{10}	8.71×10^{6}	--	--
Sb-127	5.62×10^{11}	5.62×10^{11}	5.23×10^{11}	4.78×10^{11}	3.34×10^{11}	5.89×10^{4}
Te-127m	6.63×10^{9}	6.64×10^{9}	6.89×10^{9}	7.15×10^{9}	7.99×10^{9}	5.78×10^{9}
Te-127	4.76×10^{11}	4.76×10^{11}	4.67×10^{11}	4.42×10^{11}	3.19×10^{11}	5.78×10^{9}
Sn-128	8.21×10^{11}	5.70×10^{11}	1.87×10^{8}	2.95×10^{4}	--	--

Table 3-4. (Cont'd)

Isotope	Time after shutdown					
	1/2 hr	1 hr	12 hr	24 hr	3 days	90 days
Sb-128	7.68×10^{11}	6.92×10^{11}	2.28×10^{8}	3.61×10^{4}	--	--
Sb-129	2.19×10^{12}	2.03×10^{12}	3.88×10^{11}	6.36×10^{10}	4.60×10^{7}	--
Te-129m	1.66×10^{11}	1.66×10^{11}	1.67×10^{11}	1.65×10^{11}	1.59×10^{11}	2.63×10^{10}
Te-129	1.79×10^{12}	1.89×10^{12}	5.69×10^{11}	2.31×10^{11}	1.59×10^{11}	2.63×10^{10}
Sn-130	1.59×10^{9}	5.37×10^{5}	--	--	--	--
Sb-130	1.06×10^{12}	1.89×10^{11}	--	--	--	--
Sb-131	2.79×10^{12}	1.13×10^{12}	2.85×10^{3}	--	--	--
Te-131m	1.02×10^{12}	1.01×10^{12}	7.90×10^{11}	5.99×10^{11}	1.97×10^{11}	--
Te-131	5.60×10^{12}	3.84×10^{12}	8.01×10^{11}	6.07×10^{11}	2.00×10^{11}	--
I-131	5.23×10^{12}	5.23×10^{12}	5.07×10^{12}	4.89×10^{12}	3.17×10^{12}	2.23×10^{9}
Xe-131m	2.08×10^{11}	2.08×10^{11}	2.04×10^{11}	1.99×10^{11}	1.82×10^{11}	1.70×10^{9}
Sn-132	6.33×10^{8}	4.98×10^{4}	--	--	--	--
Sb-132	4.50×10^{9}	4.72×10^{5}	--	--	--	--
Te-132	1.01×10^{13}	1.00×10^{13}	9.11×10^{12}	8.18×10^{12}	5.31×10^{12}	3.66×10^{4}
I-132	1.01×10^{13}	1.01×10^{13}	9.40×10^{12}	8.44×10^{12}	5.48×10^{12}	3.78×10^{4}
Te-133m	7.82×10^{12}	5.62×10^{12}	3.96×10^{9}	1.44×10^{6}	--	--
Te-133	8.08×10^{12}	5.81×10^{12}	4.09×10^{9}	1.48×10^{6}	--	--
I-133	1.52×10^{13}	1.51×10^{13}	1.06×10^{13}	7.10×10^{12}	1.40×10^{12}	--
Xe-133m	3.65×10^{11}	3.65×10^{11}	3.58×10^{11}	3.37×10^{11}	2.20×10^{11}	--
Xe-133	1.33×10^{13}	1.34×10^{13}	1.33×10^{13}	1.30×10^{13}	1.08×10^{13}	1.21×10^{8}
Sb-134	1.03×10^{2}	--	--	--	--	--
Te-134	4.12×10^{12}	1.04×10^{12}	--	--	--	--
I-134	1.48×10^{13}	1.07×10^{13}	1.83×10^{9}	1.36×10^{5}	--	--
Te-135	3.04×10^{8}	9.30×10^{3}	--	--	--	--
I-135	1.33×10^{13}	1.26×10^{13}	4.03×10^{12}	1.16×10^{12}	7.98×10^{9}	--
Xe-135m	4.10×10^{12}	3.93×10^{12}	1.25×10^{12}	3.62×10^{11}	2.49×10^{9}	--
Xe-135	1.52×10^{13}	1.52×10^{13}	1.06×10^{13}	5.56×10^{12}	2.12×10^{11}	--
I-136	7.48×10^{6}	3.76×10^{0}	--	--	--	--
Cs-136	8.77×10^{9}	8.76×10^{9}	8.55×10^{9}	8.32×10^{9}	7.48×10^{9}	6.98×10^{7}
I-137	--	--	--	--	--	--
Xe-137	6.96×10^{10}	3.36×10^{8}	--	--	--	--
Cs-137	1.59×10^{10}	1.59×10^{10}	1.59×10^{10}	1.59×10^{10}	1.59×10^{10}	1.58×10^{10}
Ba-137m	1.46×10^{10}	1.46×10^{10}	1.46×10^{10}	1.46×10^{10}	1.46×10^{10}	1.45×10^{10}
I-138	--	--	--	--	--	--
Xe-138	3.84×10^{12}	1.13×10^{12}	2.34×10^{10}	--	--	--
Cs-138	1.06×10^{13}	6.61×10^{12}	7.19×10^{6}	1.87×10^{9}	--	--
I-139	--	--	--	--	--	--
Xe-139	--	--	--	--	--	--
Cs-139	1.66×10^{12}	1.86×10^{11}	--	--	--	--
Ba-139	1.23×10^{13}	9.82×10^{12}	4.55×10^{10}	1.28×10^{8}	--	--
Xe-140	--	--	--	--	--	--
Cs-140	1.05×10^{5}	--	--	--	--	--
Ba-140	8.96×10^{12}	8.95×10^{12}	8.73×10^{12}	8.50×10^{12}	7.62×10^{12}	6.86×10^{10}
La-140	8.07×10^{12}	8.08×10^{12}	8.21×10^{12}	8.29×10^{12}	8.12×10^{12}	7.91×10^{10}
Xe-141	--	--	--	--	--	--
Cs-141	--	--	--	--	--	--
Ba-141	4.40×10^{12}	1.38×10^{12}	1.28×10^{11}	--	--	--
La-141	1.36×10^{13}	1.26×10^{13}	1.63×10^{12}	1.72×10^{11}	2.14×10^{7}	--
Ce-141	4.28×10^{12}	4.29×10^{12}	4.30×10^{12}	4.09×10^{12}	6.50×10^{11}	--
Cs-142	7.53×10^{3}	--	--	--	--	--
Ba-142	4.65×10^{11}	1.45×10^{10}	--	--	--	--
La-142	1.15×10^{13}	8.70×10^{12}	1.81×10^{10}	2.14×10^{7}	--	--
Ba-143	--	--	--	--	--	--
La-143	5.02×10^{12}	1.68×10^{12}	5.92×10^{1}	--	--	--
Ce-143	1.46×10^{13}	1.45×10^{13}	1.15×10^{13}	8.95×10^{12}	3.27×10^{12}	--

Table 3-4. (Cont'd)

Isotope	Time after shutdown					
	1/2 hr	1 hr	12 hr	24 hr	3 days	90 days
Pr-143	7.77×10^{12}	7.78×10^{12}	7.90×10^{12}	7.96×10^{12}	7.73×10^{12}	9.93×10^{10}
Ce-144	5.75×10^{11}	5.75×10^{11}	5.75×10^{11}	5.73×10^{11}	5.71×10^{11}	4.63×10^{11}
Pr-144	5.75×10^{11}	5.75×10^{11}	5.75×10^{11}	5.73×10^{11}	5.71×10^{11}	4.63×10^{11}
Ce-145	9.72×10^{9}	9.51×10^{6}	--	--	--	--
Pr-145	9.46×10^{12}	8.92×10^{12}	2.48×10^{12}	6.13×10^{11}	2.29×10^{9}	--
Ce-146	1.70×10^{12}	3.80×10^{11}	--	--	--	--
Pr-146	5.36×10^{12}	2.74×10^{12}	2.35×10^{4}	--	--	--
Nd-147	3.98×10^{12}	3.98×10^{12}	3.86×10^{12}	3.75×10^{12}	3.32×10^{12}	1.60×10^{10}
Pm-147	2.90×10^{10}	2.90×10^{10}	3.04×10^{10}	3.17×10^{10}	3.68×10^{10}	7.20×10^{10}
Nd-149	2.59×10^{12}	2.18×10^{12}	4.81×10^{10}	7.53×10^{8}	4.50×10^{1}	--
Pm-149	3.06×10^{12}	3.06×10^{12}	2.72×10^{12}	2.34×10^{12}	1.26×10^{12}	2.93
Nd-151	2.84×10^{11}	7.11×10^{10}	--	--	--	--
Pm-151	1.18×10^{12}	1.16×10^{12}	8.82×10^{11}	6.52×10^{11}	1.95×10^{11}	--
Sm-151	4.74×10^{8}	4.74×10^{8}	4.87×10^{8}	4.97×10^{8}	5.16×10^{8}	5.24×10^{8}
Sm-153	3.52×10^{11}	3.49×10^{11}	2.97×10^{11}	2.49×10^{11}	1.23×10^{11}	--
Sm-155	3.03×10^{10}	1.25×10^{10}	4.43×10^{1}	--	--	--
Eu-155	1.39×10^{9}	1.39×10^{9}	1.39×10^{9}	1.39×10^{9}	1.39×10^{9}	1.25×10^{9}
Sm-156	2.97×10^{10}	2.87×10^{10}	1.34×10^{10}	5.83×10^{9}	2.10×10^{8}	--
Eu-156	1.71×10^{10}	1.71×10^{10}	1.72×10^{10}	1.70×10^{10}	1.55×10^{10}	2.10×10^{8}

3.6. Recoil Coolant Activities

The recoil escape into the primary coolant of nuclides formed by fast neutron reactions with the aluminum clad plate type fuel elements constitutes a significant source of activity during operation and after shutdown. The most important fast neutron reactions are:

$$\text{Al-27 (n, a) Na-24}$$
$$\text{Al-27 (n, p) Mg-27}$$

The Na-24 recoil nucleus, being the more energetic gamma ray emitter, is the major contributor to dose rates through more than a few mean free paths of shielding. The Na-24 nuclide decays with a 15.1-hour half-life by the emission of two gamma rays per disintegration having energies of 2.75 and 1.37 mev. Mg-27 decays with a 9.5-minute half-life with the emission of 0.84 and 1.01 mev gamma rays having yields of 100% and 20% respectively.

The cross section for production of the Na-24 nuclide has been measured experimentally and is well known as a function of energy. The reaction has a threshold energy of 3.26 mev and a fission-spectrum-averaged cross section of 0.56 millibarns[10]. The cross section versus energy of the impinging neutron is shown in Figure 3-9 taken from Reference 16.

The Mg-27 cross section is not as well known. The calculation is based on information from Reference 15, which gives a fission-spectrum-averaged cross section of 3.1 millibarns.

The specific activity of the Na-24 nuclide in the primary coolant water of the ATR was calculated by two methods. One method was an empirical fit to operating research reactor experience, and the other method was a theoretical approach using the energy dependent cross section shown in Figure 3-9. The empirical fit is represented by the equation:

$$C = \frac{9.5\ NP}{F\ (a + \lambda t)} \qquad (3\text{-}20)$$

where

C = specific activity, dis/cm^3-min

9.5 = empirical constant

N = number of elements

P = reactor power, MW

F = primary coolant flow rate, gpm $\times 10^{-3}$

α = demineralizer-to-total flow rate ratio

λ = decay constant of Na-24, sec^{-1}

t = total loop time, sec

The theoretical calculation was performed on the basis of the following assumptions:

1. That the range of the recoil product is equal to the range of an alpha particle in aluminum. This assumption was checked with previous reported values of the range of the Na-24 nuclide, and agreement was indicated.

2. That 25% (from geometry considerations) of all recoil particles formed within the thickness of the recoil range are released to the coolant water.

From an estimation of the neutron spectrum (Figure 3-3) and the energy dependent cross section (Figure 3-9), the total equilibrium specific activity of Na-24 in the aluminum can be found.

$$N_A = \Sigma_a \phi = N_0 \int_{E_T}^{\infty} \sigma(E)\, \phi\,(E)\, dE \qquad (3\text{-}21)$$

where

N_A = specific activity in coolant exposed aluminum

Σ_a = macroscopic reaction cross section

ϕ = average fast flux in core

N_0 = number density of aluminum

$\sigma(E)$ = energy dependent macroscopic reaction cross section

$\phi(E)$ = neutron flux in reactor core

And from the aforementioned assumptions,

$$N_c = 0.25\, (R_1)\, (S)\, (N_A)/V \qquad (3\text{-}22)$$

where N_c = specific activity in coolant water, dis/cm^3-sec

R_1 = range of recoil product in aluminum, cm

S = exposed aluminum surface area in core, cm^2

V = total primary coolant volume, cm^3

The results obtained from the two methods with no demineralization were 1.32×10^5 dis/cm^3-sec for the empirical formula and 1.27×10^5 dis/cm^3-sec for the theoretical equation. With the demineralizer operating, the equilibrium activity in the coolant was calculated to be 2.41×10^4 dis/cm^3-sec using the empirical correlation.

The specific activity of the Mg-27 nuclide in the primary coolant water was calculated in the same manner as the Na-24 activity. Similar assumptions were used. The Mg-27 activity was found to be less important during operation and after shutdown of the reactor, due to the shorter half-life and less energetic emission of gamma rays.

Figure 3-1. Comparison of Fast Flux Computed by 20-Group Code to That Scaled From LTSF Data

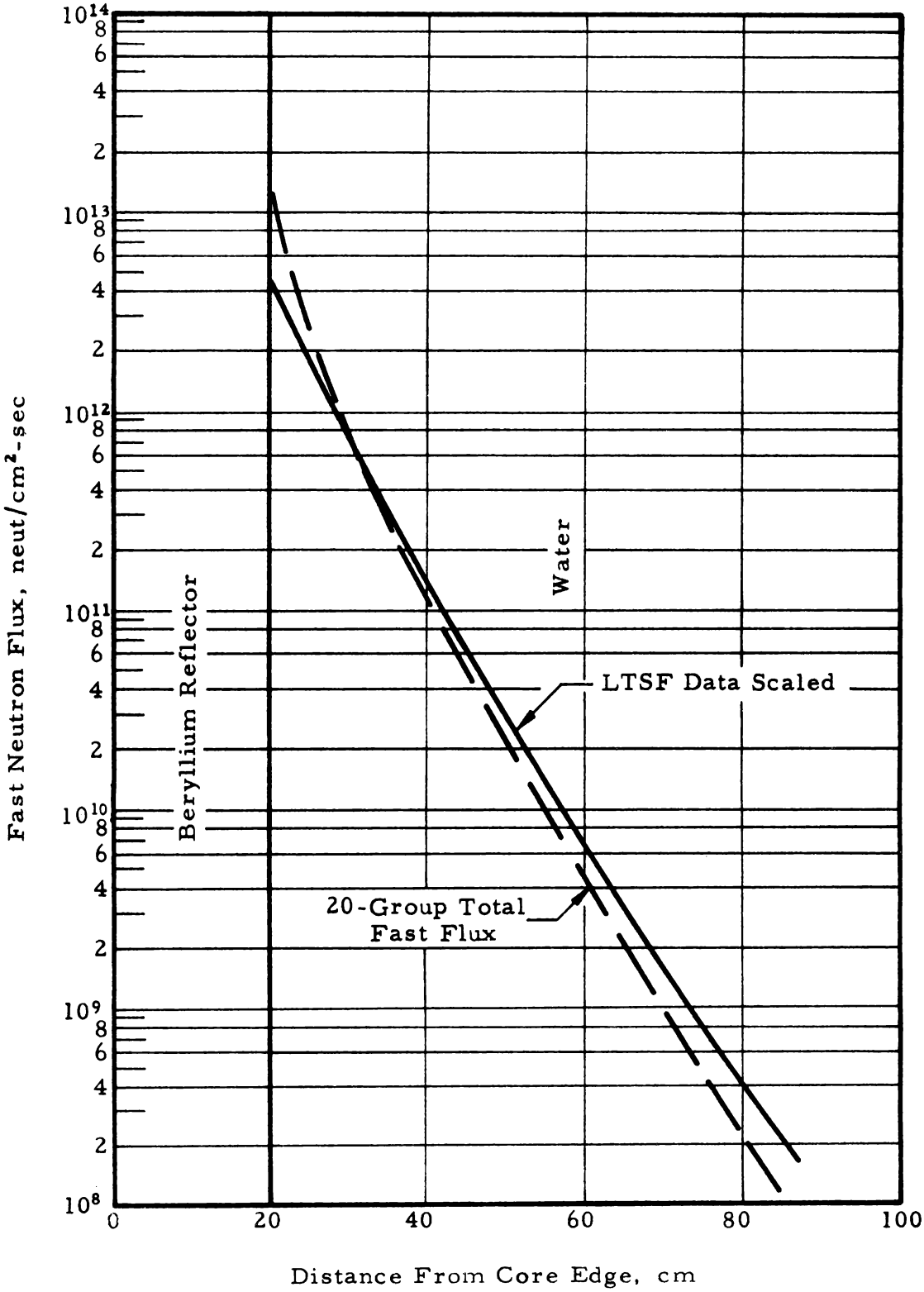

Figure 3-2. Linear Self-Absorption Coefficient for ATR Core Fuel Region

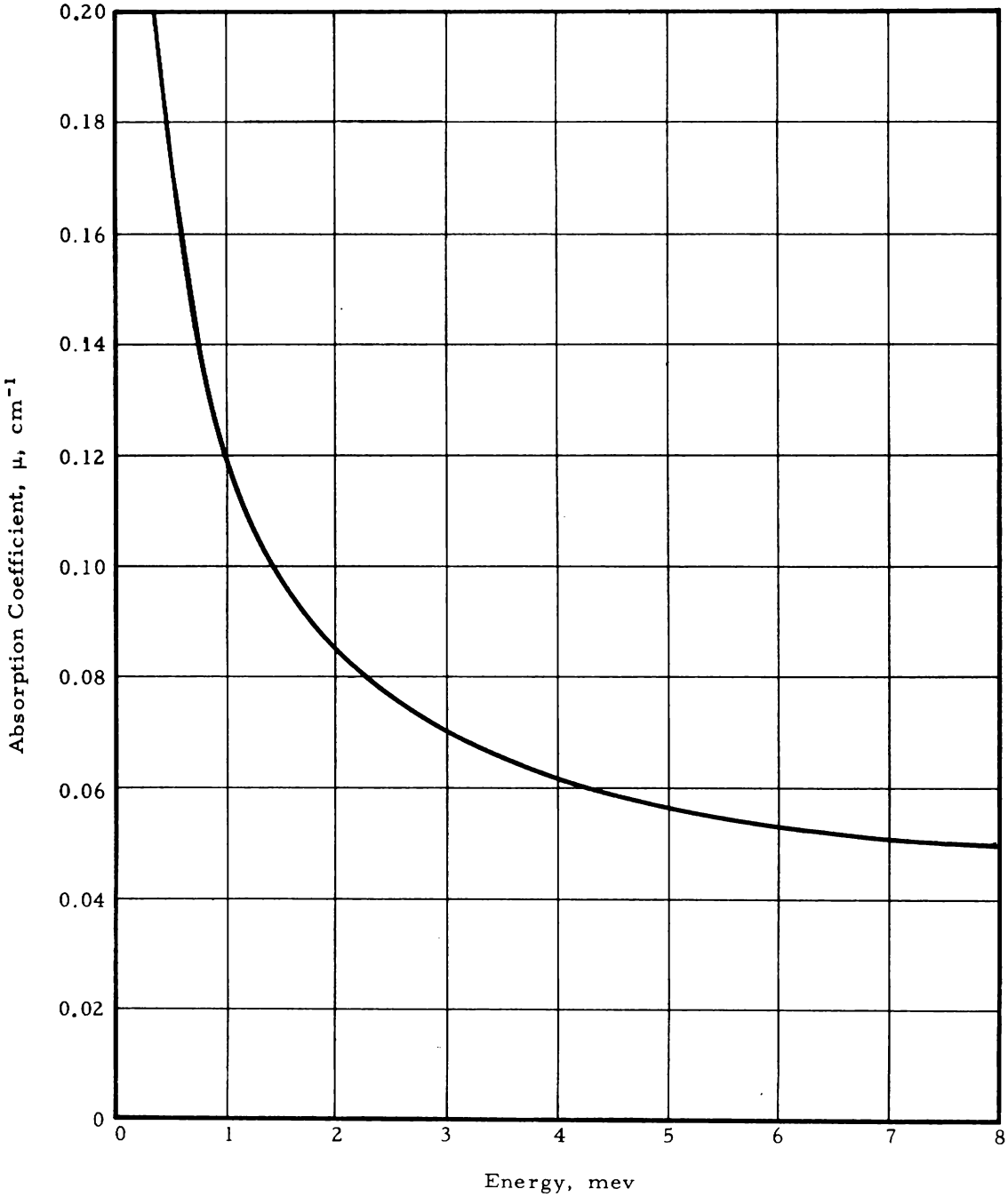

Figure 3-3. Fast Neutron Flux Spectrum in Fuel Region (Single Lobe Power = 50 MW)

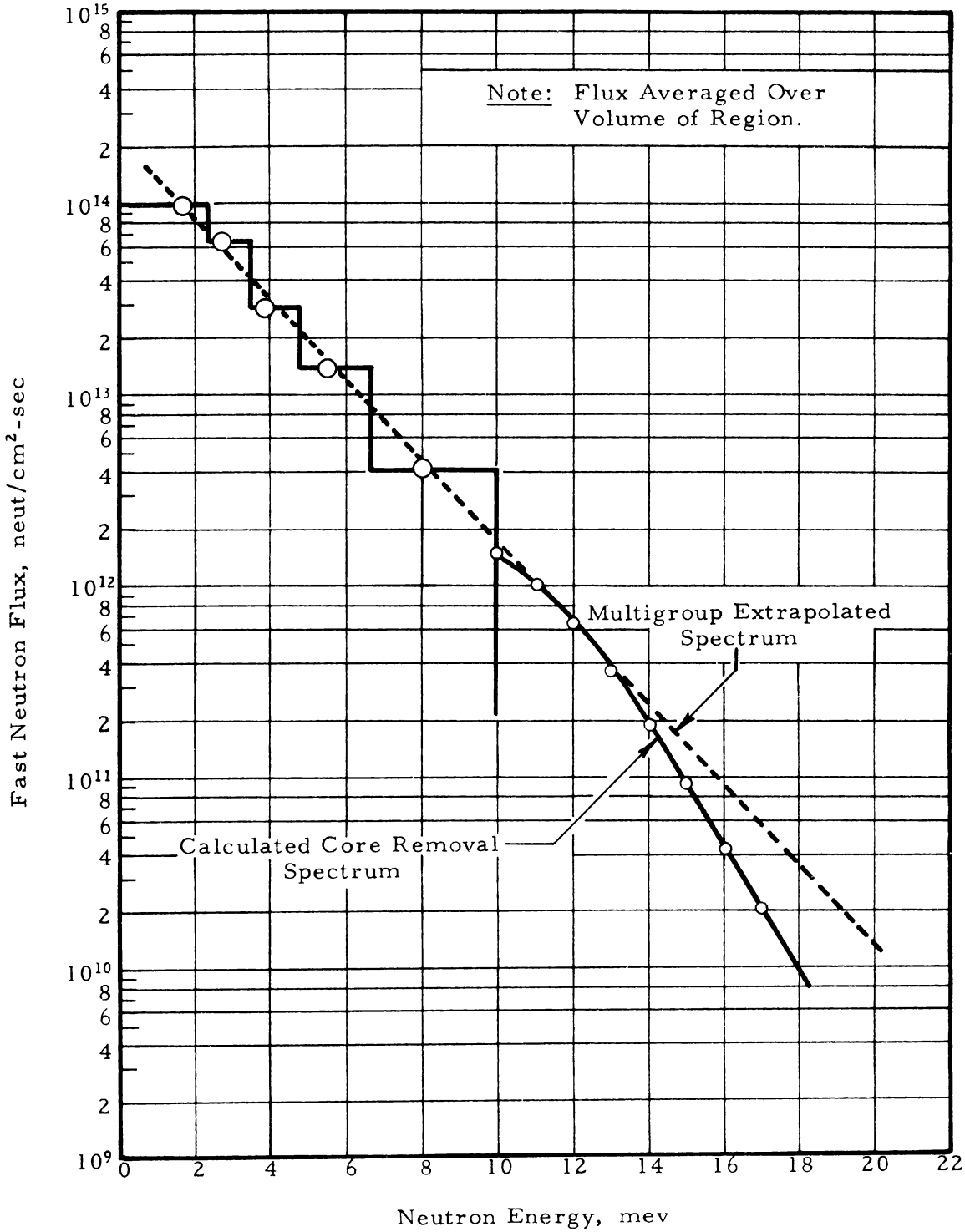

Figure 3-4. Fast Neutron Flux Spectrum in Flux Trap Region (Single Lobe Power = 50 MW)

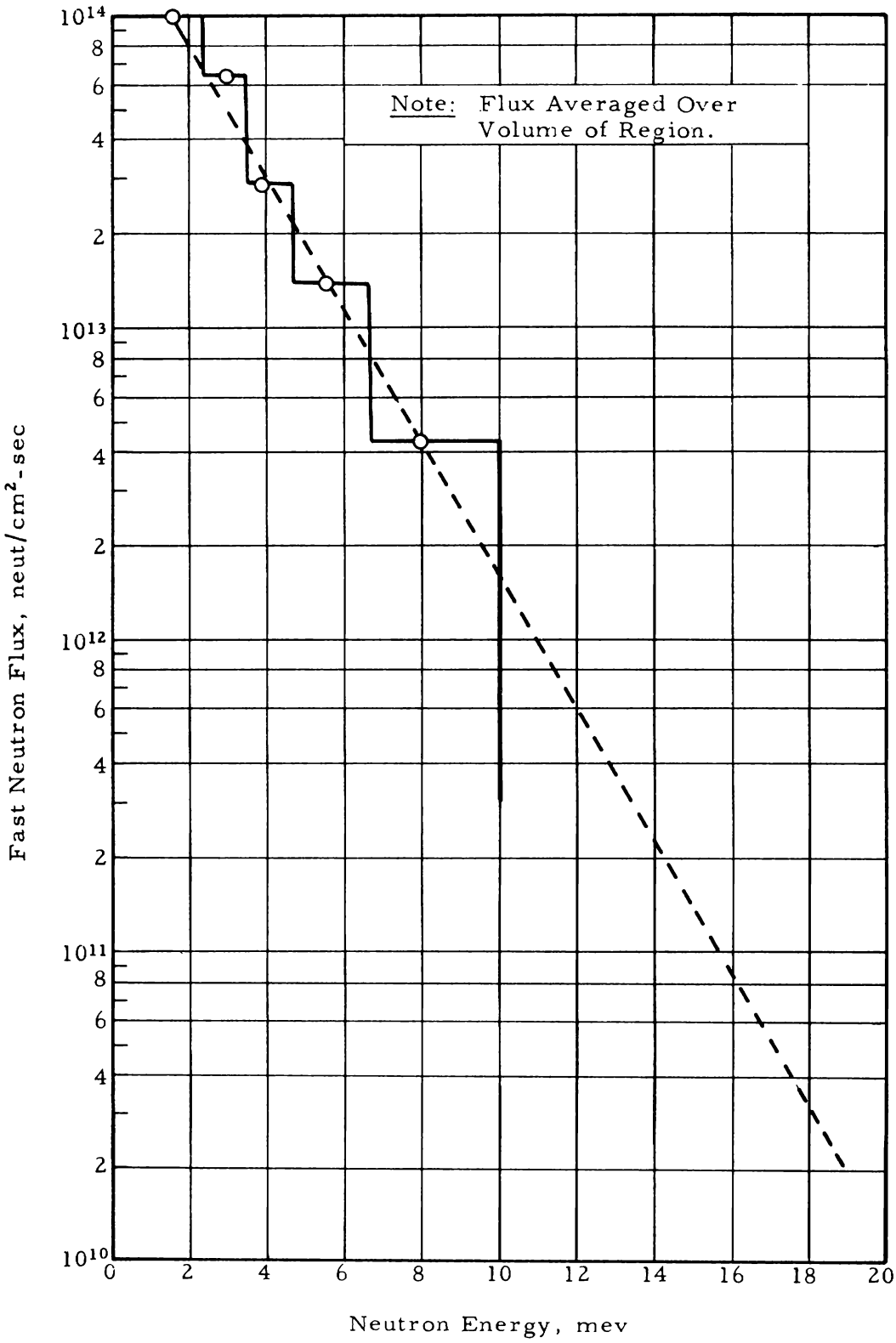

Figure 3-5. Fast Neutron Flux Spectrum in Reflector Region (Single Lobe Power = 50 MW)

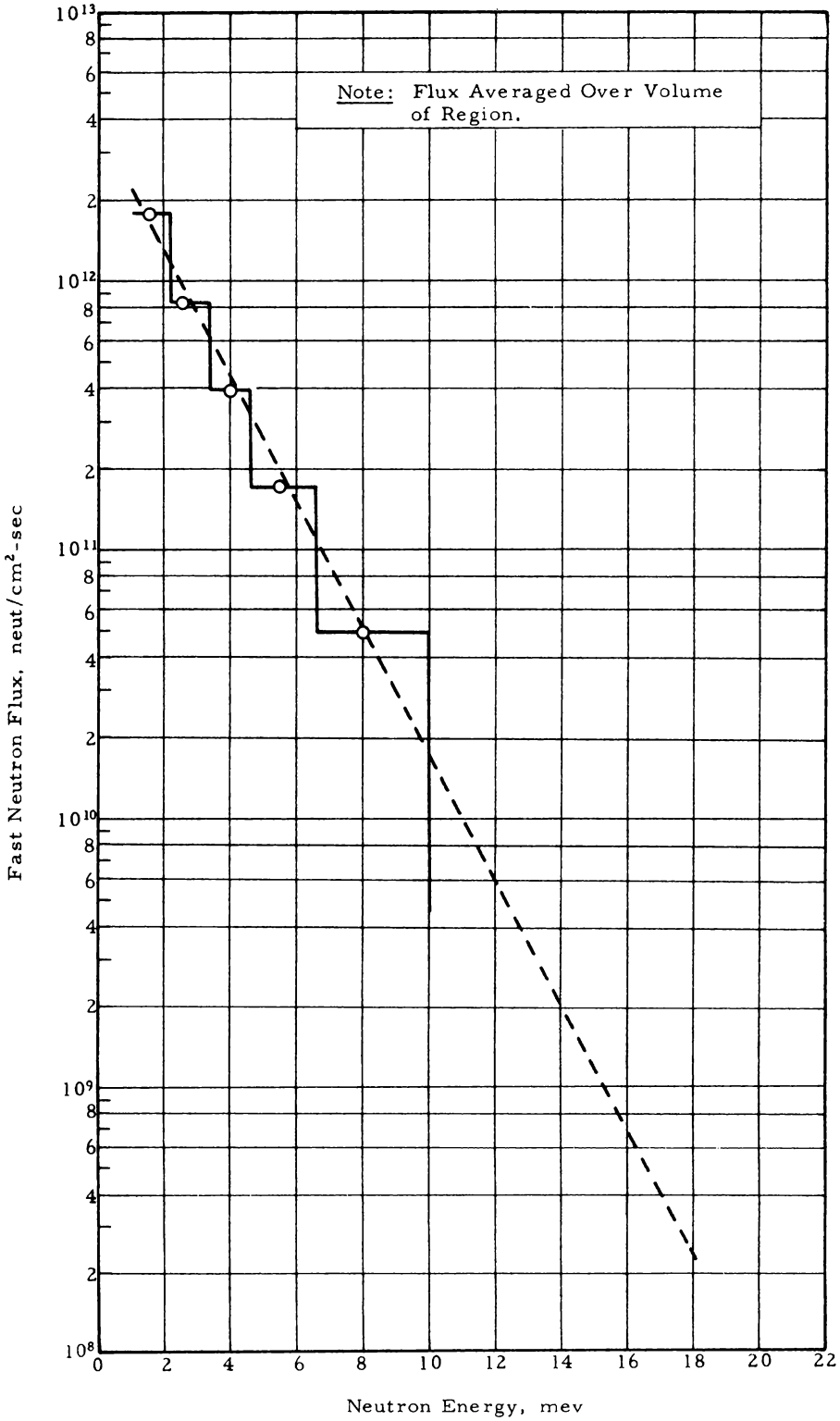

Figure 3-6. Cross Section for O-16 (n, p) N-16 Fast Neutron Reaction

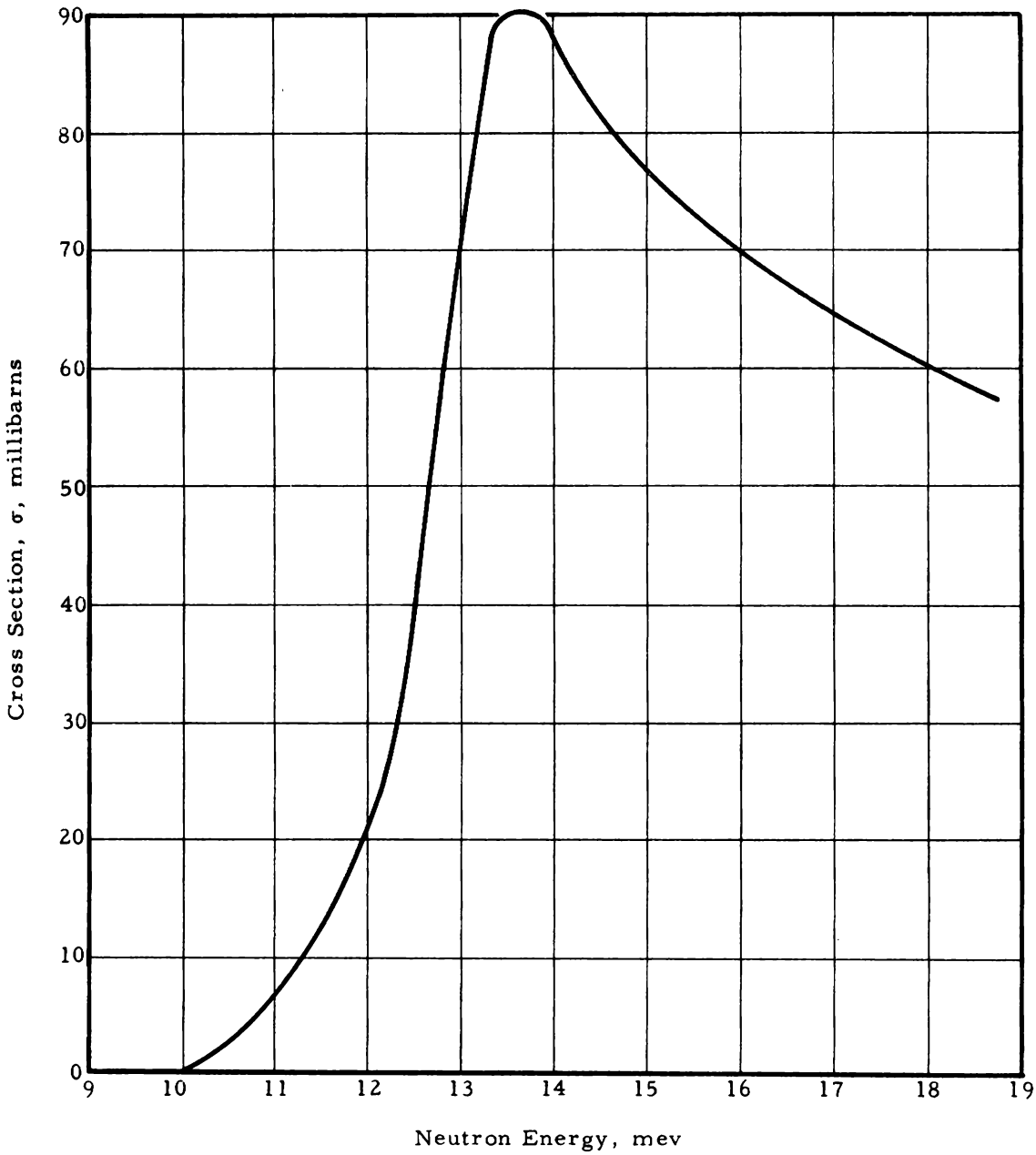

Figure 3-7. Equilibrium N-16 Activity Vs Delay Time After Leaving Bottom Plenum

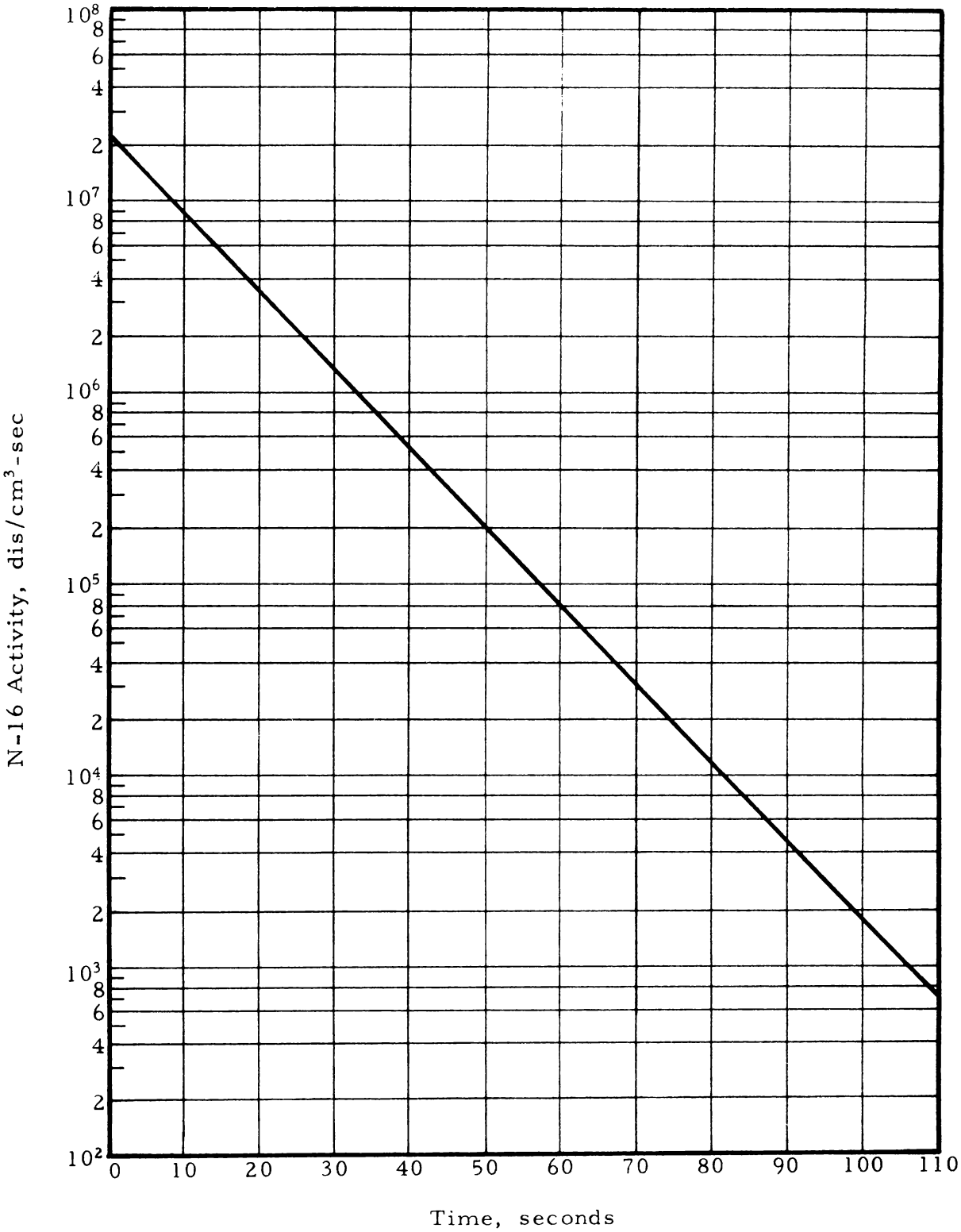

Figure 3-8. Fission Product Gamma Ray Source Strengths in Core Vs Time After Shutdown (Operating Time, 400 Hours)

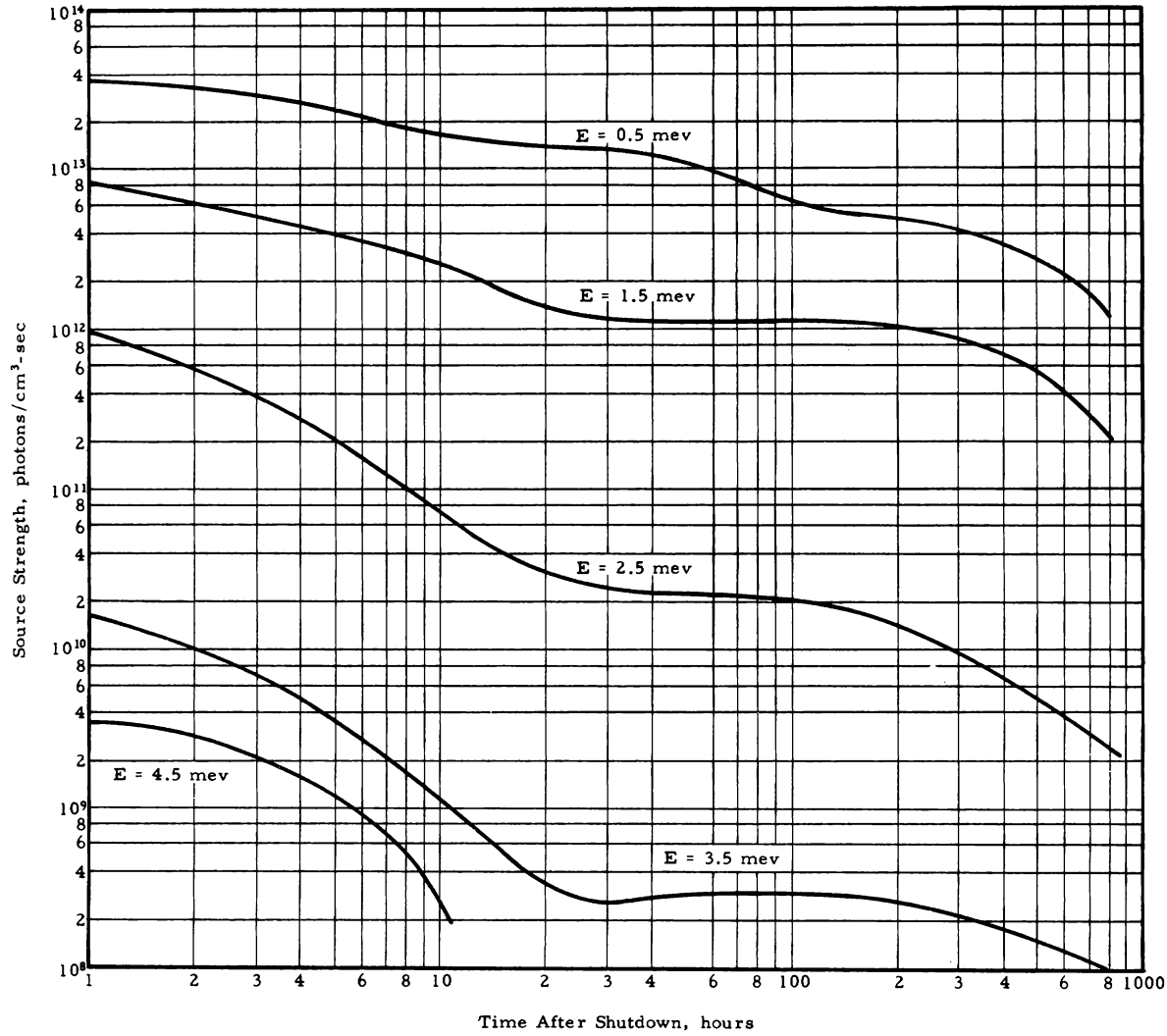

Figure 3-9. Cross Section for Al-27 (n, α) Na-24 Reaction[16]

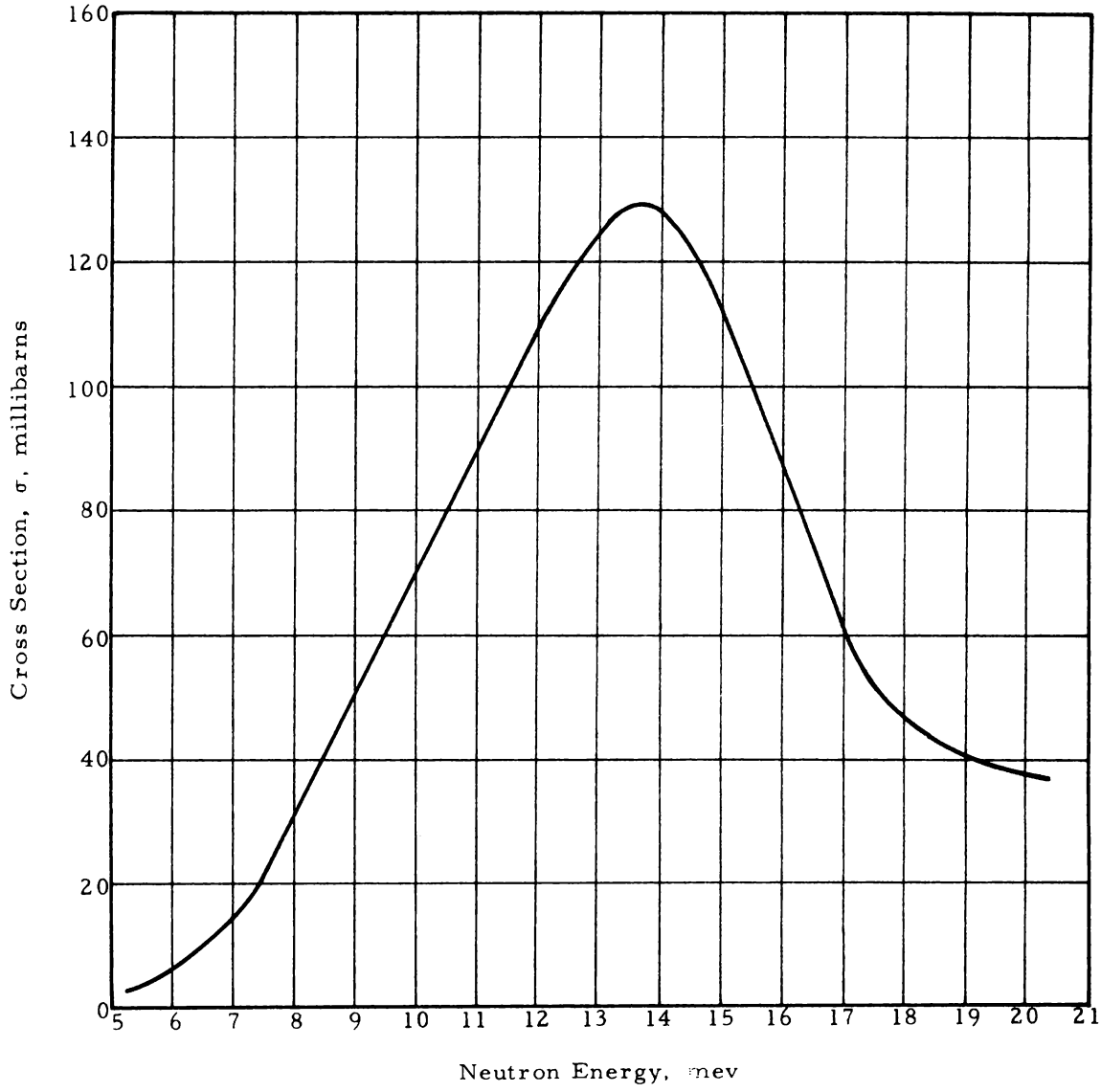

4. HEAT GENERATION RATES

4.1. General Description

When the gamma flux has been computed at a point, the gamma heat generation rate at that point is given by the formula:

$$\text{Heating Rate} = 1.6 \times 10^{-13} E\mu(E)\phi(E)/\rho, \text{ watts/gm} \qquad (4\text{-}1)$$

where:

1.6×10^{-13} = the conversion factor from mev/sec to watts

E = the initial gamma ray energy, mev

$\mu(E)$ = the energy absorption coefficient at energy E, cm^2/gm

$\phi(E)$ = the gamma flux at energy E, computed using energy absorption buildup factors, photons/cm^2-sec

ρ = the density of the material for which heating rates are being computed, gm/cc

The heating rate due to elastic scattering of neutrons is given by:

$$\text{Heating Rate} = 1.6 \times 10^{-13} \Sigma_S(E) E \overline{\Delta E}\, \phi(E)/\rho \qquad (4\text{-}2)$$

where:

$\Sigma_S(E)$ = the elastic scattering cross-section at energy E, cm^{-1}

E = the mean energy of the neutron group, mev

$\overline{\Delta E}$ = the average fractional energy lost per collision

$\phi(E)$ = the fast neutron flux at energy E, n/cm^2-sec

ρ = the density of the material for which heating rates are being computed

The bulk of the heating rates in the ATR is due to gamma rays. The rapid attenuation of the fast neutron flux outside the core region and the relatively small value of $\overline{\Delta E}$ for most materials minimize the importance of neutron heating due to elastic scattering. Only in the water and beryllium in and near the core is the neutron heating of any importance. An estimate of the heating rates due to inelastic scattering of fast neutrons showed that these heating rates were insignificant in comparison to those from elastic scattering and gamma ray absorption. Figures 1-1 and 1-2

show most of the core and vessel components that are mentioned in the following sections on heating rates.

4. 2. Inpile Heating Rates

A profile of the gamma heating rates across the core was computed with the use of computer code DER-013 (see Appendix D). A five-lobe model of the core was employed; i. e. , the fuel region was represented by five cylindrical annuli. The fuel region in each annulus was subdivided into 80-cc volume elements, and the gamma fluxes were calculated at various points at the core mid-plane along a line extending from the center of the core through an interior lobe. Fluxes were calculated at each dose point from the individual lobes for the nine energy groups shown in Table 3-1. The test regions in which the fluxes were calculated were assumed to be composed entirely of water, the energy absorption buildup factors for water were used exclusively in the calculations.

Figure 4-1 shows profiles of the gamma heating rates at the core mid-plane. Three cases were considered. Curve I shows the average heating rates obtained by assuming an average power distribution over the entire fuel region. Curve II shows the heating rates for an axial cosine power distribution ranging from 1.4 max/avg at the core mid-plane to 0.4 min/avg at the ends of the core. Curve III also shows the effect of a cosine power distribution and, in addition, shows the heating rate that would exist at each point if the nearest lobe to that point were operating at 75 MW.

The curves show the gamma heating rates in units of watts/gm of aluminum. A relatively small amount of fast neutron heating due to elastic scattering is also present in aluminum, and the neutron heating rates are listed below for each of the three cases described above. Only one value is given for each case, since the fast neutron flux is assumed to be constant radially across the core.

Case	Neutron heating rates in aluminum
I	0.6 watt/gm
II	0.85 watt/gm
III	1.1 watts/gm

4. 3. NR Loop Heating Rates

A calculation of the gamma heating rates in an NR test loop during operation and after shutdown was done for an interior lobe with a water-moderated flux trap. It was assumed that a test element, composed of 80% zirconium and 20% water, was operating at 800 kw in the loop. Heating rates were computed at three points: the outer surface of the insulating tube, the inner surface of the pressure tube, and at the center of the test specimen.

Gamma fluxes were calculated with computer code DER-013 (Appendix D) based on a five-lobe core model. The fluxes were calculated from the individual lobes and from the test element using energy absorption build-up factors for water. Operating core gamma sources were the same as those shown in Table 3-1. Volumetric source strengths for the operating test element were obtained from the core sources by using a power density ratio.

The gamma sources used in computing fission product heating after shutdown were taken from the data of Perkins and King as reported by Goldstein[6]. An operating time of 17 days at full power was assumed. Since the data for shutdown times of less than 100 seconds are not reported, the curves of Perkins and King were extrapolated to the operating fission product level (zero time shutdown) to obtain the fission-product gamma sources for shorter shutdown times.

Table 4-1 shows the gamma heating rates at the core mid-plane during full power operation with the following power distributions:

1. Uniform axial and radial power distribution.
2. Uniform radial power distribution and a cosine axial power distribution ranging from 1.4 max/avg at the core mid-plane to 0.4 min/avg at the core extremities.
3. Same as No. 2 except the heating was computed in a 75-MW lobe.

The fission product gamma heating rates are shown in Tables 4-2, 4-3, and 4-4 for various times following shutdown and for these same power distributions.

Table 4-1. Gamma Heating Rates During Operation (Interior Test Lobe)

Location	Average heating rates	Heating rates at core mid-plane	Heating rates at core mid-plane in a 75-MW lobe
Outside surface of the insulating tube	12 watts/gm of steel	16 watts/gm of steel	23 watts/gm of steel
Inside surface of the pressure tube	10 watts/gm of steel	13.3 watts/gm of steel	19 watts/gm of steel
Center of lobe	9.1 watts/gm of Zr	12.1 watts/gm of Zr	17.3 watts/gm of Zr

Table 4-2. Fission Product Gamma Heating Rates at the Outside Surface of the Insulating Tube (Interior Test Lobe)

Time after shutdown, sec	Average heating rates, watts/gm of steel	Heating rates at core mid-plane, watts/gm of steel	Heating rates at core mid-plane in a 75-MW lobe, watts/gm of steel
10^{-2}	3.86	5.13	7.34
10^{-1}	3.55	4.72	6.75
1	3.16	4.2	6.0
10	2.7	3.6	5.15
100	2.0	2.62	3.75
1000	0.95	1.26	1.8

Table 4-3. Fission Product Gamma Heating Rates at the Inside Surface of the Pressure Tube (Interior Test Lobe)

Time after shutdown, sec	Average heating rates, watts/gm of steel	Heating rates at core mid-plane, watts/gm of steel	Heating rates at core mid-plane in a 75-MW lobe, watts/gm of steel
10^{-2}	3.3	4.4	6.3
10^{-1}	3.0	4.0	5.72
1	2.65	3.52	5.03
10	2.2	2.93	4.2
100	1.6	2.13	3.05
1000	0.80	1.06	1.52

Table 4-4. Fission Product Gamma Heating Rates at the Center of the Interior Lobe

Time after shutdown, sec	Average heating rates, watts/gm of Zr	Heating rates at core mid-plane, watts/gm of Zr	Heating rates at core mid-plane in a 75-MW lobe, watts/gm of Zr
10^{-2}	2.82	3.75	5.36
10^{-1}	2.50	3.33	4.72
1	2.20	2.93	4.2
10	1.80	2.40	3.43
100	1.40	1.86	2.66
1000	0.65	0.865	1.24

4.4. Control Rod Heating

4.4.1. General Description

Essentially all of the heat generated in the hafnium control elements of the ATR is due to primary gamma rays originating in the core. In an element as heavy as hafnium the heating from elastic scattering of fast neutrons can be ignored. A conservative estimate of the volumetric gamma source strength due to thermal and resonance

neutron capture in hafnium showed this gamma flux to be negligible in comparison to gamma rays from core sources.

In hafnium both the total gamma and the energy absorption cross sections exhibit a sharp rise at the lower energies, i.e., below 1.5 mev. Since the heating rate is proportional to the energy absorption cross section, the low energy gamma rays, which are of little importance in other heating and shielding calculations, play an important role in hafnium heating. Consequently, more attention was devoted to the low energy end of the core gamma spectrum. Above 1.5 mev the gamma spectrum shown in Table 3-1 was used. From 0.3 to 1.5 mev the prompt gamma sources were computed from the data of Maienschien[8]. The equilibrium fission product activity in the range from 0.3 to 1.5 mev was estimated to match a total fission product energy release of 5.5 mev per fission. The resulting gamma ray sources used in calculating control rod heating rates are shown in Table 4-5.

Table 4-5. Gamma Ray Source Strengths in the Fuel Region at 250 MW

Energy interval, mev	Average energy, mev	Source strength, photons/cc-sec
0.3 - 0.5	0.4	1.2×10^{14}
0.5 - 0.75	0.625	7.1×10^{13}
0.75 - 1.0	0.875	4.8×10^{13}
1.0 - 1.5	1.25	5.4×10^{13}
1.5 - 2.5	2.0	5.3×10^{13}
2.5 - 3.5	3.0	1.9×10^{13}
3.5 - 4.5	4.0	7.6×10^{12}
4.5 - 5.5	5.0	6.0×10^{12}
5.5 - 6.5	6.0	3.1×10^{12}
6.5 - 8.5	7.5	1.7×10^{12}

Linear absorption coefficients for the fuel region, which were used in the calculations, are shown in Figure 3-2. To account for buildup, energy absorption buildup parameters for water were used.

4.4.2. Neck Shim Rods

Because of their location, the neck shim rods will experience the maximum heating rates occurring in the ATR core materials. Gamma fluxes incident on the rods were computed with program DER-013. The fuel region was homogenized and represented by segments of cylindrical annuli. A 20-cc mesh volume was chosen. Regions between the source region and the dose point were treated as cylindrical shields.

The expected "worst case" occurs in the center shim rod, since this rod is closest to the fuel region. Heating rates were thus computed at the core mid-plane in the center rod assuming the rod to be fully inserted. Although hafnium is a dense material, the neck shim rods are only 3/8 inch in diameter and are virtually surrounded by fuel. For these reasons attenuation by the rod itself is considered to be of little importance and was ignored in the calculations.

Average heating rates in the rod were obtained by assuming a uniform power distribution throughout the core. Actual heating rates at the core mid-plane were computed by assuming an axial cosine power distribution with all lobes operating at 50 MW. A maximum heating rate was also obtained by assuming an axial cosine power distribution with the center lobe at 75 MW and the other lobes at 50 MW. The resulting heating rates for the three cases are listed below.

Average heating rate, 39 watts/gm
Core mid-plane heating rate, 52 watts/gm
Maximum heating rate, 64 watts/gm

4.4.3. Hafnium Safety Rod

The total heat generation rates in a hafnium safety rod were calculated as a function of the distance from the end of the incore portion of the rod. It was assumed that the rod was withdrawn but immersed in water except for a 3-inch segment remaining inside the core. Curve 1 of Figure 4-2 shows the heating rate on the innermost portion of the safety rod, i.e., the part of the cylinder which is nearest the neck region, in a 75-MW lobe. Curve 2 is the same as Curve 1 except that the rod is in a 50-MW lobe. Curve 3 shows the heating rate along the rod at its outermost portion, radially opposite the neck region,

in a 50-MW lobe. The calculations were performed in the same manner as those for the neck shim rod heating rates.

4. 4. 4. Outer Shim Control Cylinders

The heating rate in the hafnium of the control cylinders is a function of the location of the cylinder with respect to the core and of the hafnium position due to cylinder rotation. The heating due to the primary gammas of the core and the secondary gammas of the beryllium reflector was calculated with computer program DER-013. Energy absorption buildup factors for water were utilized by the program.

The total heat generation rates from neutron and gamma radiation in the hafnium of the control drums are shown in Figure 4-3. These heating rates are shown at the core mid-plane as a function of the distance from the inner edge of the beryllium reflector. The two curves show the behavior of the heating rates in a hafnium medium in two radial directions, i. e. , along the core centerline through an inner lobe and along the centerline through an outer lobe. In the axial direction the heating rates follow the core power distribution.

4. 5. Heating Rates in the Storage Canal

The gamma heating rates in the walls of the storage canal were calculated based on 40 spent fuel elements stored in a 4-foot by 8-foot array. The array was treated as an infinite homogeneous slab source. Volumetric source strengths were obtained by volume weighting the fission product gamma sources in the core. Gamma fluxes were computed at various depths in the concrete, using the equation for an infinite slab source. At a given energy

$$\phi_\gamma = \frac{S_v}{2\mu_s}\left\{\frac{A_1}{1+a_1}E_2\left[(1+a_1)b\right] + \frac{(1-A_1)}{1+a_2}E_2[1+a_2]b\right\} \qquad (4\text{-}3)$$

where

ϕ_γ = gamma flux, photons/cm^2-sec

S_v = volumetric gamma source strength, photons/cc-sec

μ_s = linear absorption coefficient for the source region, cm^{-1}

A_1, a_1, a_2 = buildup parameters

b = total number of relaxation lengths in shield materials

The calculations were based on a uniform core power density, an operating time of 17 days at full power, and a shutdown time of 12 hours. The heating rates as functions of depth in the concrete are shown in Figure 4-4 for various thicknesses of the water slab between the row of spent elements and the concrete wall. The maximum heating rates, accounting for axial power peaking and a 75-MW lobe, would be about twice as great as those shown.

4.6. Heating Rates Below the Core

The region below the ATR core is mainly water extending down to 206 cm below the core mid-plane. At this elevation there is a 3-inch-thick steel grid plate. The gamma and neutron heating rates in this region below the core are shown in Figure 4-5 as functions of radial distance from the core axis for several elevations. The heating rates vary depending on the radial direction examined. Hence, the top four curves show the heating rates in two radial directions from the core, i.e., along a centerline through an interior lobe and along an outer lobe centerline. Beyond an elevation of 107 cm below the core mid-plane, however, the directional dependence of the heating rates is no longer significant.

The model employed for the calculations was a five-lobe core. DER-013 treated each of the lobes as a hollow cylindrical source having 50 MW of power with an axial cosine distribution and a uniform radial distribution. The water and the grid plate were handled as slab shields parallel to the core end. Energy absorption buildup factors for water were used for all points above the grid plate, but the buildup factors for iron were used for those points below the grid plate. The heating rates were calculated in watts/gram of aluminum.

4.7. Heating Rates in Concrete Surrounding the Pressure Vessel

Figures 4-6, 4-7, 4-8, and 4-9 show the heat generation rates in the magnetite concrete surrounding the pressure vessel. Rotational symmetry about the core axis was assumed in performing the calculations. There are three regions in which this is not valid, however. These three cases are discussed later. All heating rates are shown as a function of distance above the core mid-plane. However, because of

symmetry, the values are also applicable for elevations below the core mid-plane for the assumed axial power distribution.

Figure 4-6 is a radial plot of the heating rate as functions of concrete thickness for several elevations above the core mid-plane. It may be noted that the heating rates show an increase in magnitude at elevations above 6 feet as compared to those immediately below this elevation. This is attributed to the termination of the thermal shield, which effects a partial unshielding of the concrete to the core at these higher elevations.

Figures 4-7, 4-8, and 4-9 are plots of the heating rate as functions of distance above the core mid-plane at a constant depth of concrete. Both primary and secondary gamma heating rates are shown. The relative minima of the curves occur just below the top of the thermal shields, and the relative maxima are in a region just above the thermal shields.

The attenuation calculations were performed using DER-013 with the fuel, neck, and test regions represented by a homogeneous cylinder of 36 cm radius. An axial cosine power distribution, ranging from 1.4 max/avg at core mid-plane to 0.40 min/avg at the top and bottom of the core, and a uniform radial power distribution were assumed.

The three regions in which the heating rates depart from the generalized cases discussed above are the regions near the spent fuel, near the aluminum irradiation facility, and opposite the drop tube in the storage canal.

For the heating rates in the concrete opposite the stored fuel, the sources of importance were the core and the fission products of the stored fuel. The core was treated as a homogenized cylindrical source as described above. For the purpose of attenuating the primary (core) gammas, the stored fuel and fuel rack were treated as a homogenized slab. As a source, however, the homogenized stored fuel was assumed to be cylindrical and to possess a power distribution conforming to the cosine fit of the core. The heating rate in the concrete from primary gammas passing through the stored fuel is considerably lower than when water occupies the fuel rack location. At the core mid-plane in 1 inch of magnetite concrete, the primary gamma heating rate is 3.1×10^{-5} watt/cc. The heating rate from the spent fuel in a rack of 4-hour-shutdown elements at this point is 8.3×10^{-5} watt/cc. The beryllium

secondary gammas add only 4.3×10^{-6} watt/cc, making them rather insignificant as a contributor. The total heating rate from these three sources is 1.2×10^{-4} watt/cc. This is a factor of 2.6 lower than the heating rate shown in Figure 4-6 for the general case.

In the concrete region outside the 18-inch aluminum irradiation facility, the primary gamma heating rate in 1 inch of concrete at the core mid-plane is 2.3×10^{-5} watt/cc. The secondary gamma heating rate from the beryllium is 8.3×10^{-6} watt/cc, and the secondary gamma heating rate from the aluminum irradiation facility is 5.2×10^{-5} watt/cc. This gives a total of 8.4×10^{-5} watt/cc, which is a factor of 3.7 lower than the heating rate shown in Figure 4-6 for the general case.

In the concrete just outside the pressure vessel on the inner edge of the storage canal, the heating rate is somewhat higher than in the other regions around the pressure vessel. The small amount of water outside the 9-inch aluminum facility and the air volume within the drop tube bubble afford relatively little attenuation of the secondary gamma radiation. Thus, the aluminum assembly and the local shields are the main contributors to the heating rate. At the core mid-plane in the first inch of magnitite concrete in this region, the heating rates from the various sources are as follows:

Core	7.0×10^{-5} watt/cc
Secondary gamma from:	
Beryllium reflector	2.5×10^{-5}
2-inch S. S. bubble	1.5×10^{-5}
9-inch aluminum facility	2.5×10^{-4}
4-inch S. S. local shields	1.2×10^{-4}
Total	4.8×10^{-4} watt/cc

4.8. Heating Rates in the Aluminum Irradiation Facility

In the aluminum irradiation facility, there are three gamma sources responsible for the major portion of the heating. These sources are the primary gammas of the core, the secondary gammas of the beryllium reflector, and the secondary gammas from the aluminum facility itself. Using DER-013, the core was treated as a homogenized cylindrical source with a radius of 36 cm and a height of 4 feet. From

the inner edge of the aluminum facility out to about 17 cm in the aluminum, the core primary gammas dominate the heating. Beyond this point, however, the secondary gammas from the facility itself are the main source of the aluminum heating. As a source, the aluminum facility was treated as a 44° segment of a hollow cylinder with an inner radius of 65 cm, an outer radius of 115 cm, and a height of 4 feet. The heating from the secondary gammas of the beryllium reflector were the least important of the three sources. The heating from this source was a factor of 3.5 lower than that from the core primary gammas. The model used for the beryllium reflector was a hollow cylinder with an outer radius of 65 cm, an inner radius of 36 cm, and a height of 4 feet. The dose buildup factors for aluminum were used in all of the calculations. The power distribution for the secondary gamma sources was fitted to the multigroup thermal neutron flux profile. The core, however, was assumed to be operating at 250 MW with an axial cosine power distribution and a uniform radial power distribution.

Figure 4-10 shows the total heating rate in the aluminum irradiation facility at the core mid-plane as a function of aluminum thickness.

4.9. Heating Rates in the Beryllium Reflector

Figure 4-11 shows the total heat generation rate in the beryllium reflector at the core mid-plane as functions of the distance from the inner edge of the reflector. Since the heating rates vary with radial direction from the core, it is necessary to indicate these heating rates by two curves. The two curves show the behavior of the heating rate in two radial directions, i.e., along the core centerline through an interior lobe and along the centerline through an exterior lobe. In the axial direction the heating rates follow the core power distribution. All lobes were assumed to be operating at 50 MW.

The model employed for the calculations was a 5-lobe core of 250 MW with uniform radial power distribution and an axial distribution ranging from 1.4 max/avg at the core mid-plane to 0.4 min/avg at the top and bottom of the core. The heating from each of five lobes of the core was examined separately utilizing DER-013. The shielding of certain lobes by other lobes was simulated by homogenizing that part of the core providing the shielding. The heating from the secondary

gammas of the beryllium reflector itself, the core reflector tank, and the aluminum facility were examined using DER-013. Their contribution to the heating rates was small, but is included in the totals given in Figure 4-5. On the inner edge of the beryllium reflector, the neutron heating was found to contribute significantly to the total heating. This is especially true for the region of the reflector surrounding an inner lobe. Here the neutron heating is about 28% of the total. This percentage decreases rapidly, however, with increasing depth of beryllium.

4.10. Comparison of Heating Rate Calculations With ATRCE Measurements

The prediction of gamma heating rates during the ATR design has been based almost entirely on calculations. In an effort to provide experimental verification of the calculated heating rates, a number of film packet exposures were made in the ATR critical experiment.

The film packet exposures in the critical experiment yielded the integrated dose in units of roentgens. The calculated heating rates are in units of watts per gram of various materials. To provide a basis for comparison, the heating rates were transformed into dose rates. Since the heating rates per unit mass may vary significantly from one material to another, and since the gamma absorption properties of film are similar to those of water, the heating rates were converted to watts/gm of water. These numbers were then converted to dose rates using a value of 93 ergs/gm-hr equal to 1 rem/hr.

The contributions of the core and the test elements to the total dose rate were computed separately. The power level of the ATRCE during the run was approximately 0.35 watt. ATR calculations were based on a power level of 250 MW. This yields a power scaling factor for the core of 1.4×10^{-9}. The power levels for the test elements in the critical run were estimated to be 1×10^{-3} watt for the A-1 experiments and 1.8×10^{-3} watt for the A-5 experiments. The value used for all test elements in the ATR calculation was 800 kw. The resulting scaling factors are 1.25×10^{-9} for the A-1 experiments and 2.25×10^{-9} for the A-5 experiments.

A water-moderated flux trap was used in the ATR calculations, whereas a flux trap composed of about 65% water and 35% aluminum was used in the experiment. The contribution of thermal neutrons to

the film exposure was computed to be 8.6% of the total dose in the center experiment mockup and 9% in an interior experiment mockup. This contribution was subtracted from those dose measurements made in the core and experiments before comparing the measurements to the calculations. Since the relative value of thermal neutrons compared to gamma rays increases in the reflector and decreases outside the reflector by a varying amount, no correction was employed outside the core regions.

The test bundle in the critical experiment was composed of about 50% water and 50% aluminum with small amounts of fuel. The test bundle used in the ATR calculations was assumed to be 79% zirconium and 21% water. Since the gamma absorption properties of the two elements are quite different, a calculation was made to determine the dose rate at the center of an A-1 experiment with an element composed of 50% water and 50% aluminum. The results showed an increase of about 30% in the dose rate at this point, and this number was used in the comparison. It is not expected that the dose rates outside the pressure tube would increase by this percentage, since the relative effect of the test element on the total dose rate is reduced significantly in going from the center of the lobe to the outside of the pressure tube.

Figure 4-12 shows the results of the film packet exposures at the core mid-plane. The values shown are dose measurements in roentgen units.

Figure 4-13 shows a comparison between the dose rates measured in the ATRCE and those obtained from the ATR heating rate calculations. The curves show the radial profiles of the dose rates through the center of an A-1 experiment at the core mid-plane. As can be seen, there is reasonably good agreement between the two curves. The shape of the calculated curve follows the measurements closely. In general, the measured dose rates are 20-30% higher than the calculated values in the core region. It would be expected that the calculated values would be slightly higher than the measured values due to buildup of fission products. The calculations are based on a core that has been operating for 17 days, whereas the ATRCE was operated for 10 minutes to obtain the film exposure.

There are several possible sources of error. There is an uncertainty of ±12% in the processing and reading of the films. The contribution to the film exposure by intermediate and fast neutrons is not known;

however this effect is expected to be small. The most likely source of error is the fact that the response of the film is not linear with energy for gammas below 0.3 mev. The increase blackening of film by gammas below this energy tends to exaggerate their contribution to the total dose rate. In the calculations, errors can arise from uncertainties in source strengths, buildup factors, and geometrical approximations.

Figure 4-1. Inpile Gamma Heat Generation Rates

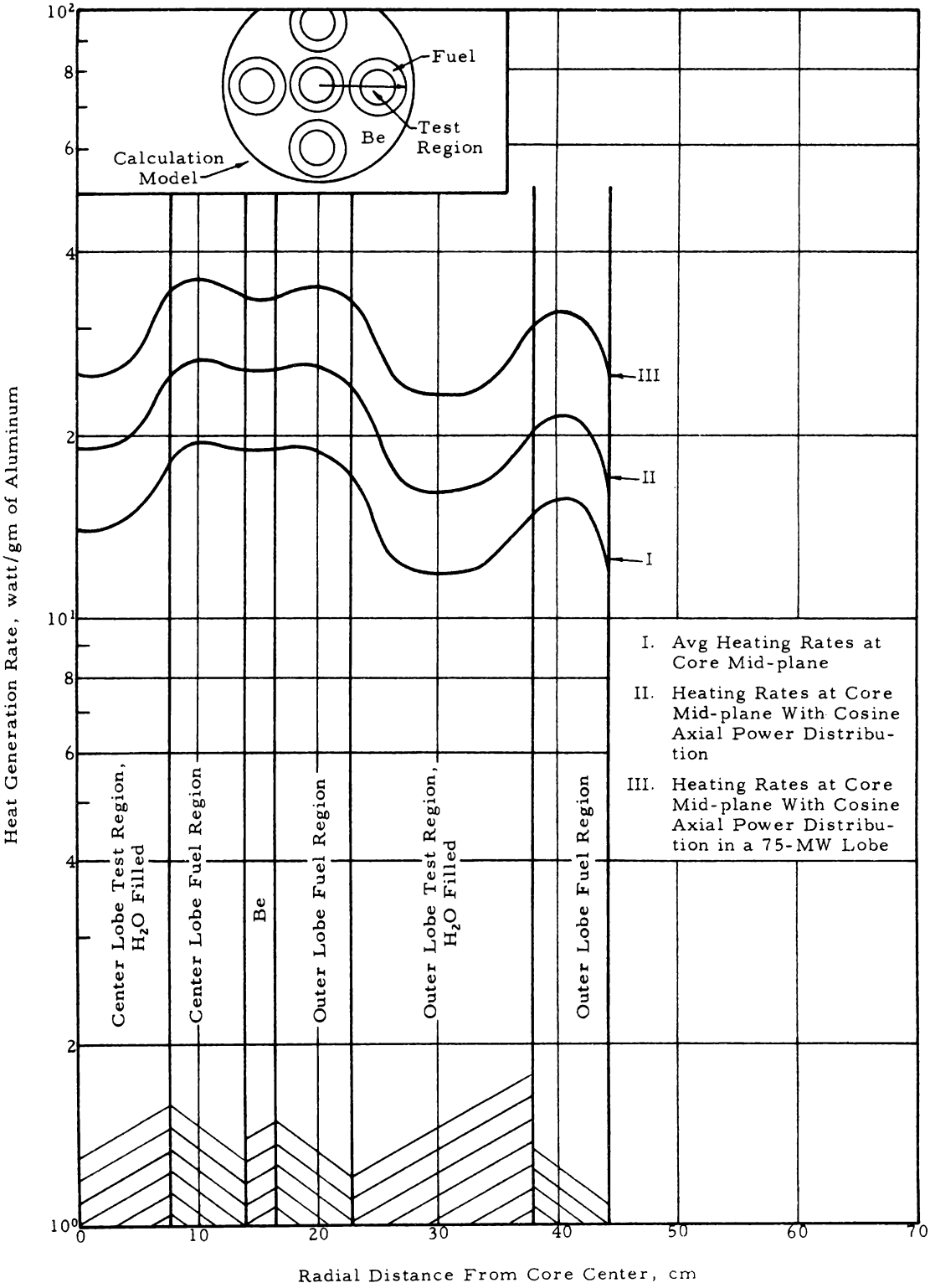

Figure 4-2. Heating Rates in a Hafnium Safety Rod Inserted 3 Inches (250-MW Core Power)

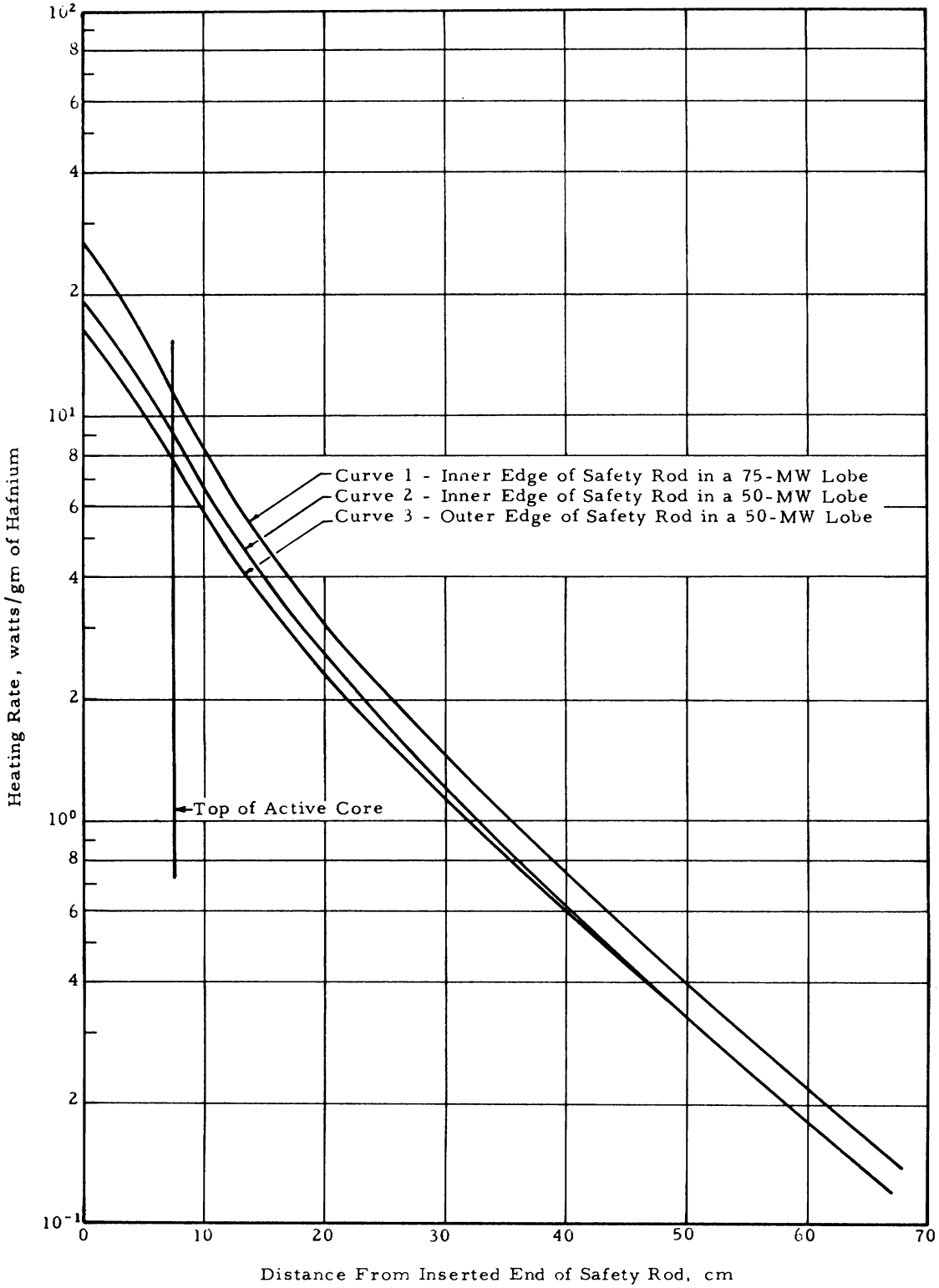

Figure 4-3. Heat Generation Rates in Hafnium Control Cylinder at Core Mid-Plane (Hafnium Density = 13.3 gm/cc)

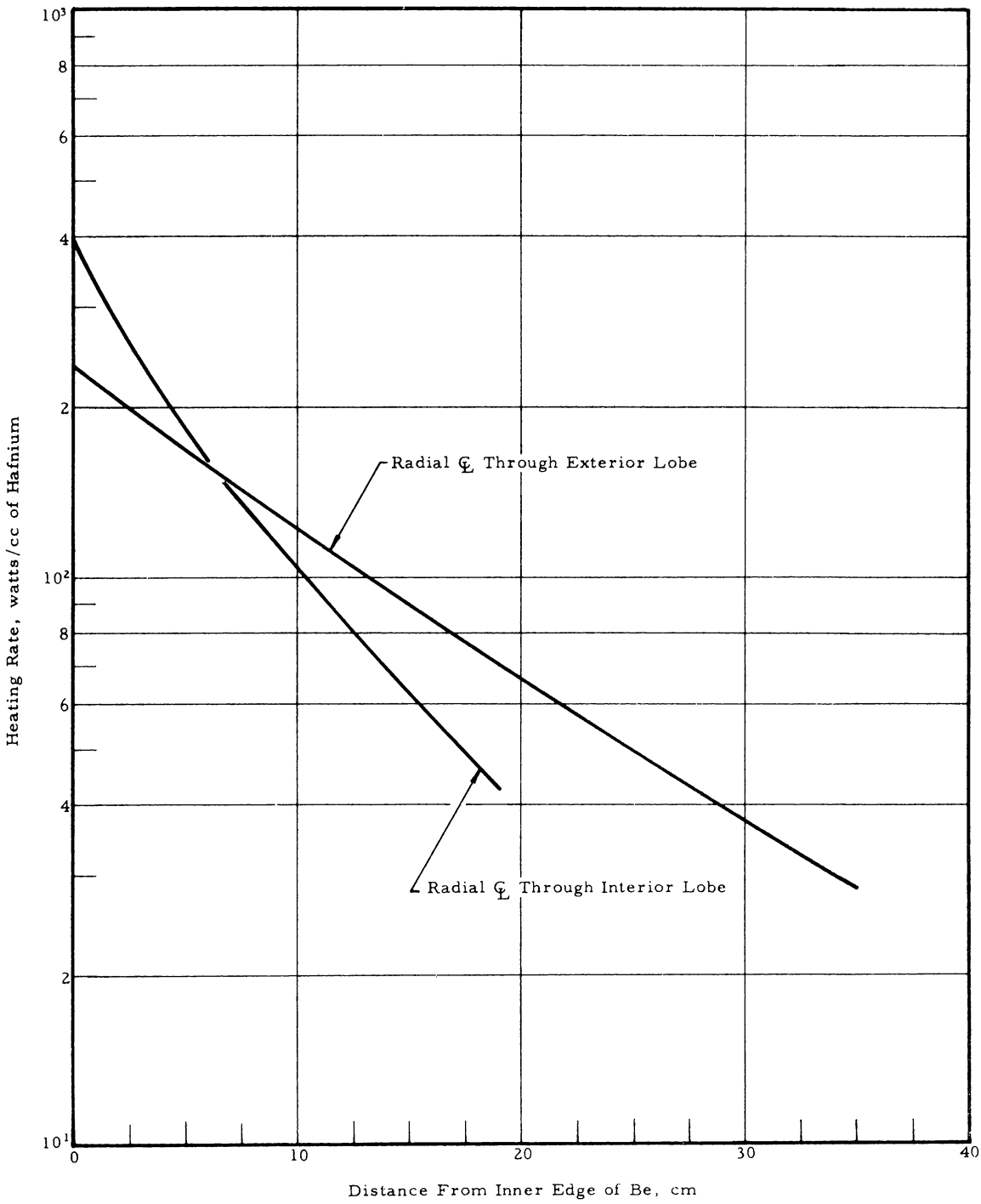

Figure 4-4. Average Gamma Heating Rates in Walls of Storage Canal From 40 Spent Elements 12 Hours After Shutdown

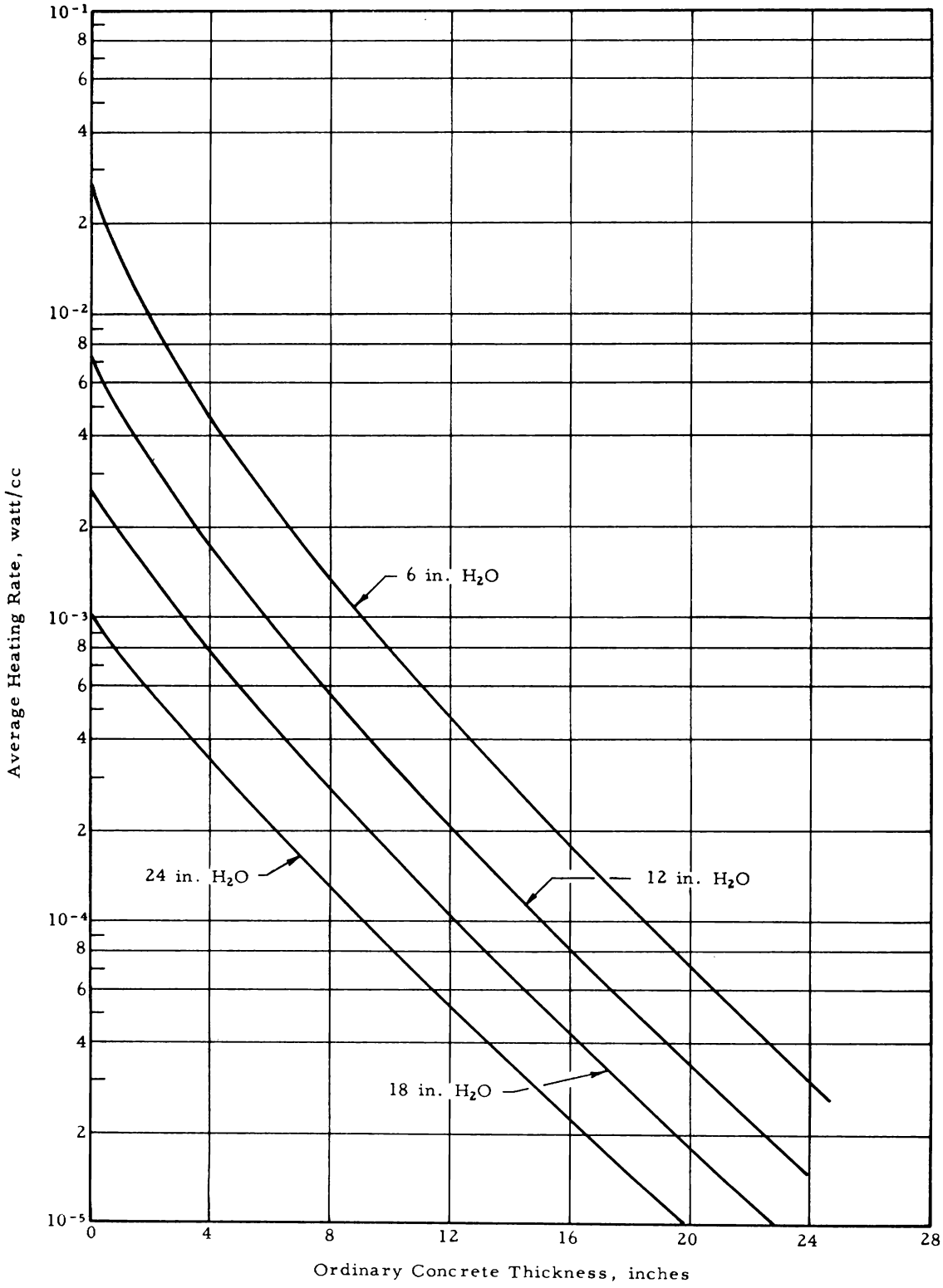

Figure 4-5. Total Heating Rates Below ATR Core

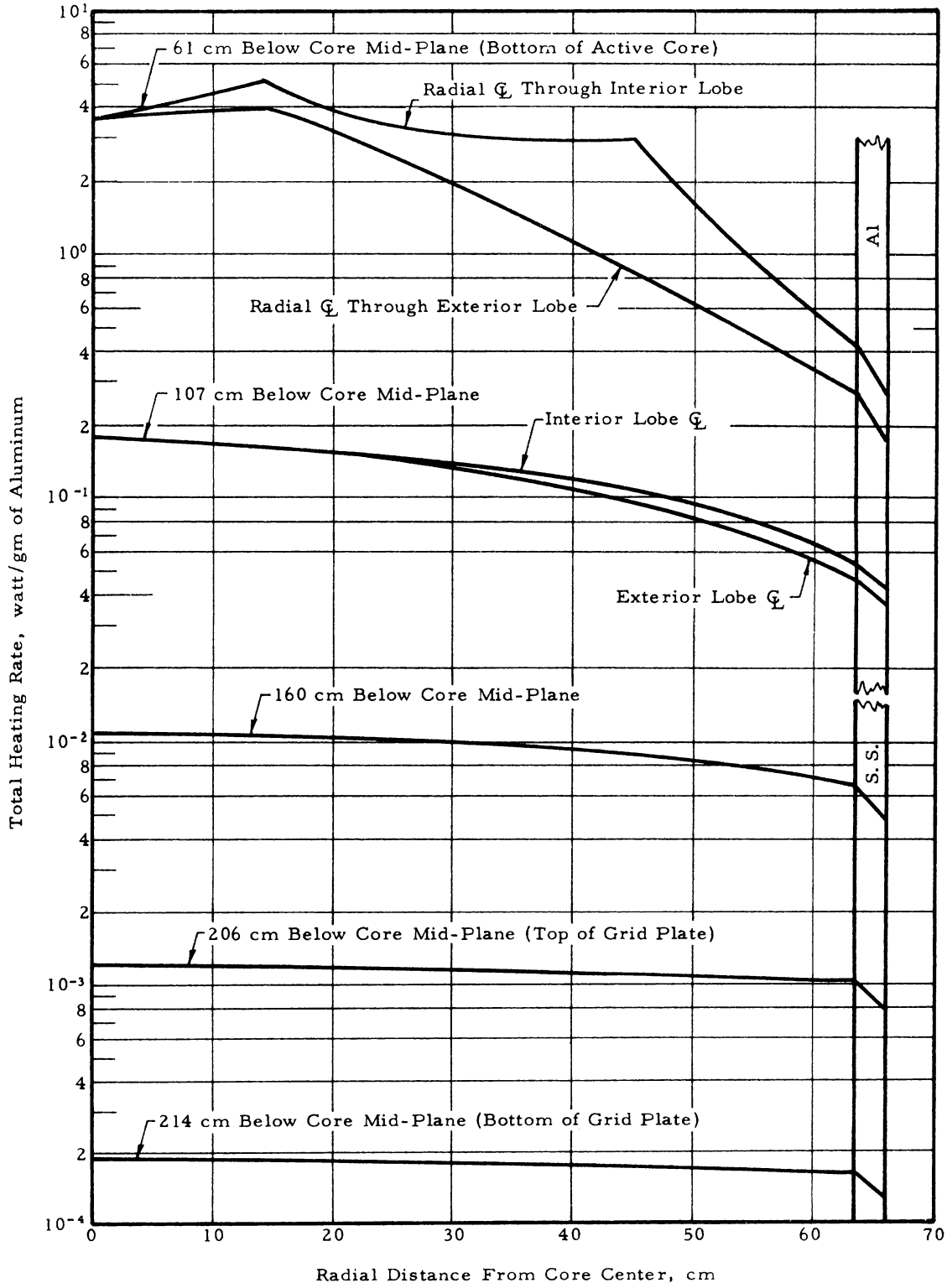

Figure 4-6. Heating Rates Through the Magnetite Concrete Around the Pressure Vessel

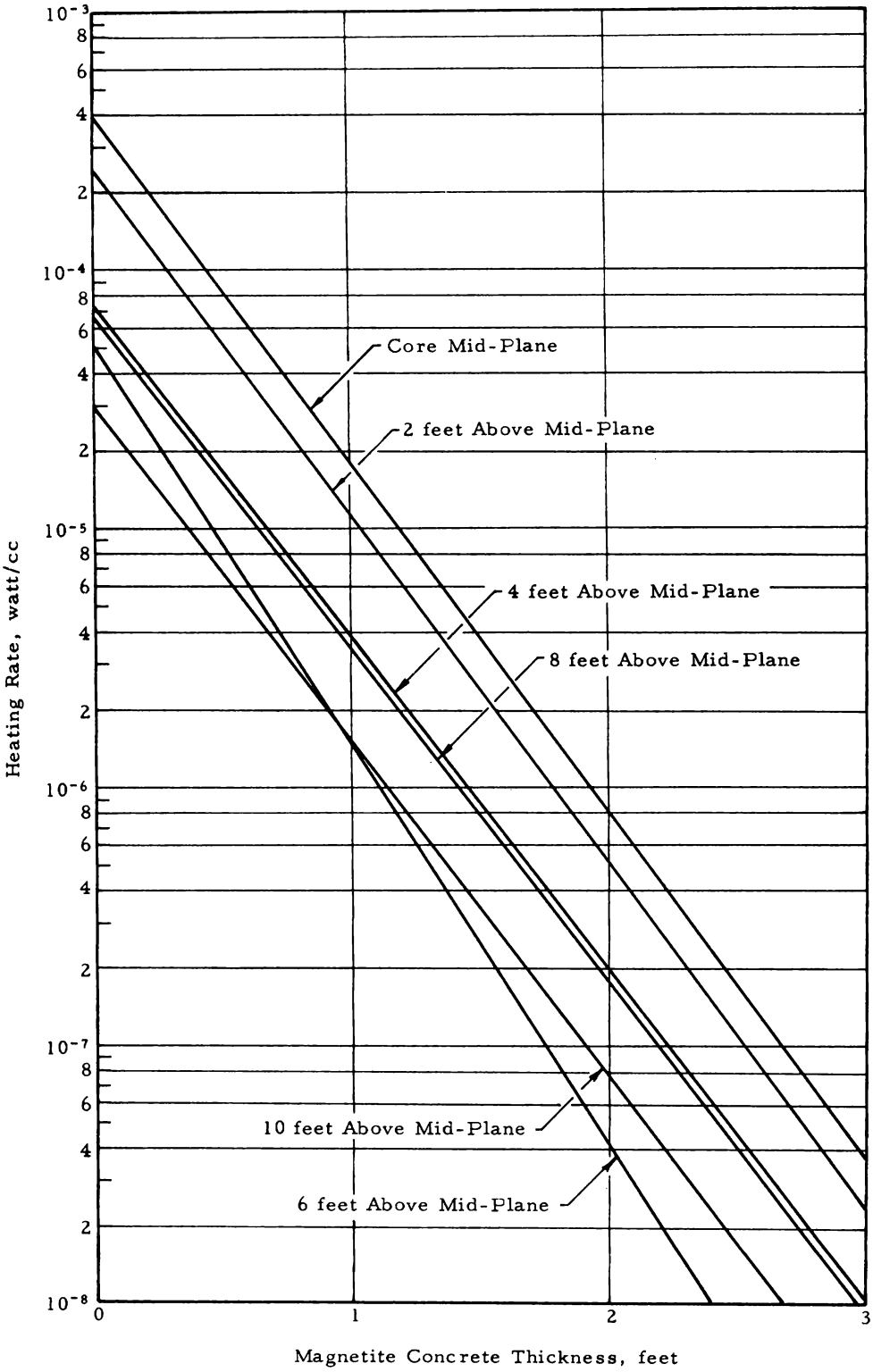

Figure 4-7. Heating Rates in Magnetite Concrete as Functions of Height Above Core Mid-Plane (1 Inch Inside Concrete)

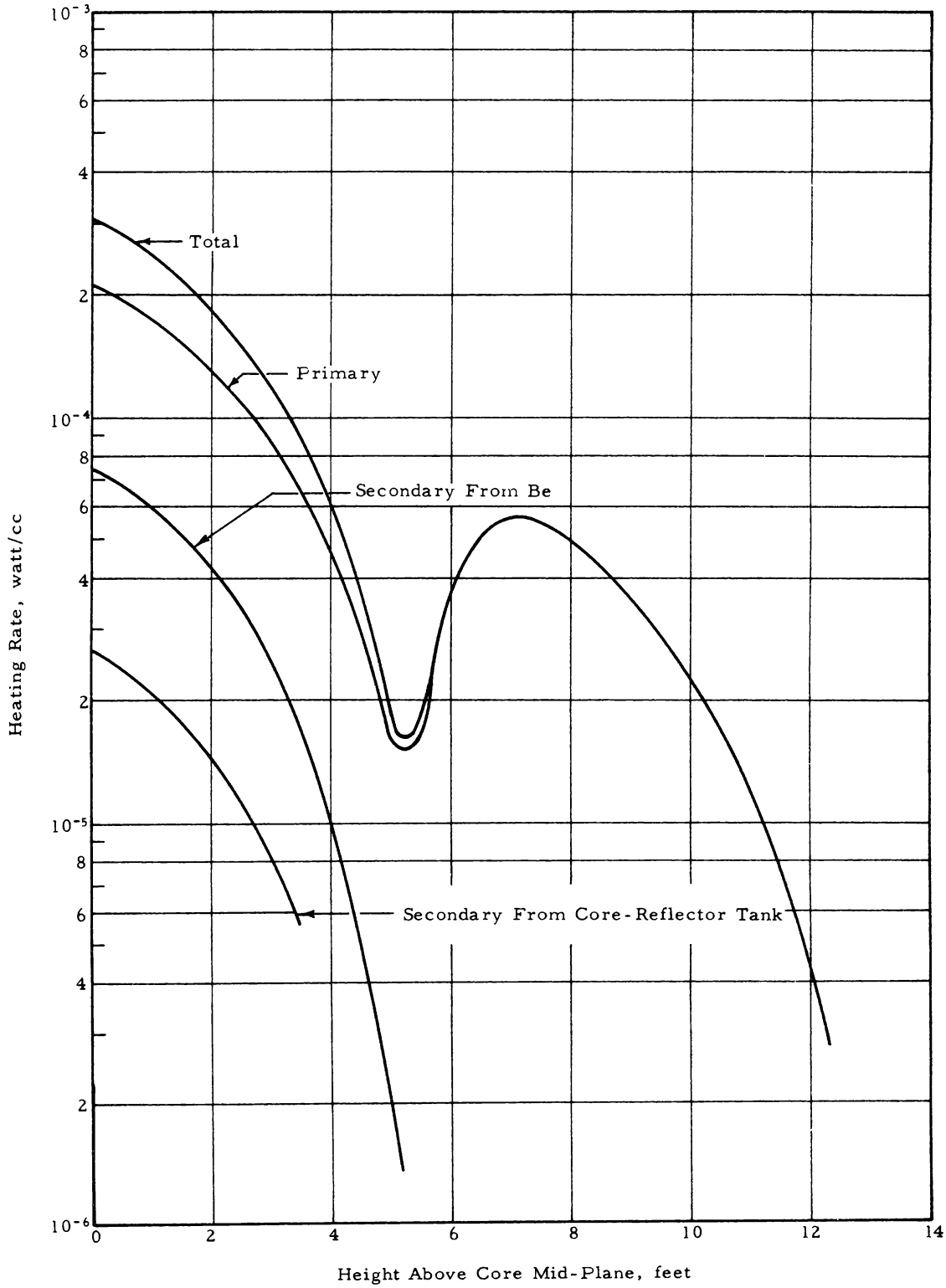

Figure 4-8. Heating Rates in Magnetite Concrete as Functions of Height Above Core Mid-Plane (1 Foot Inside Concrete)

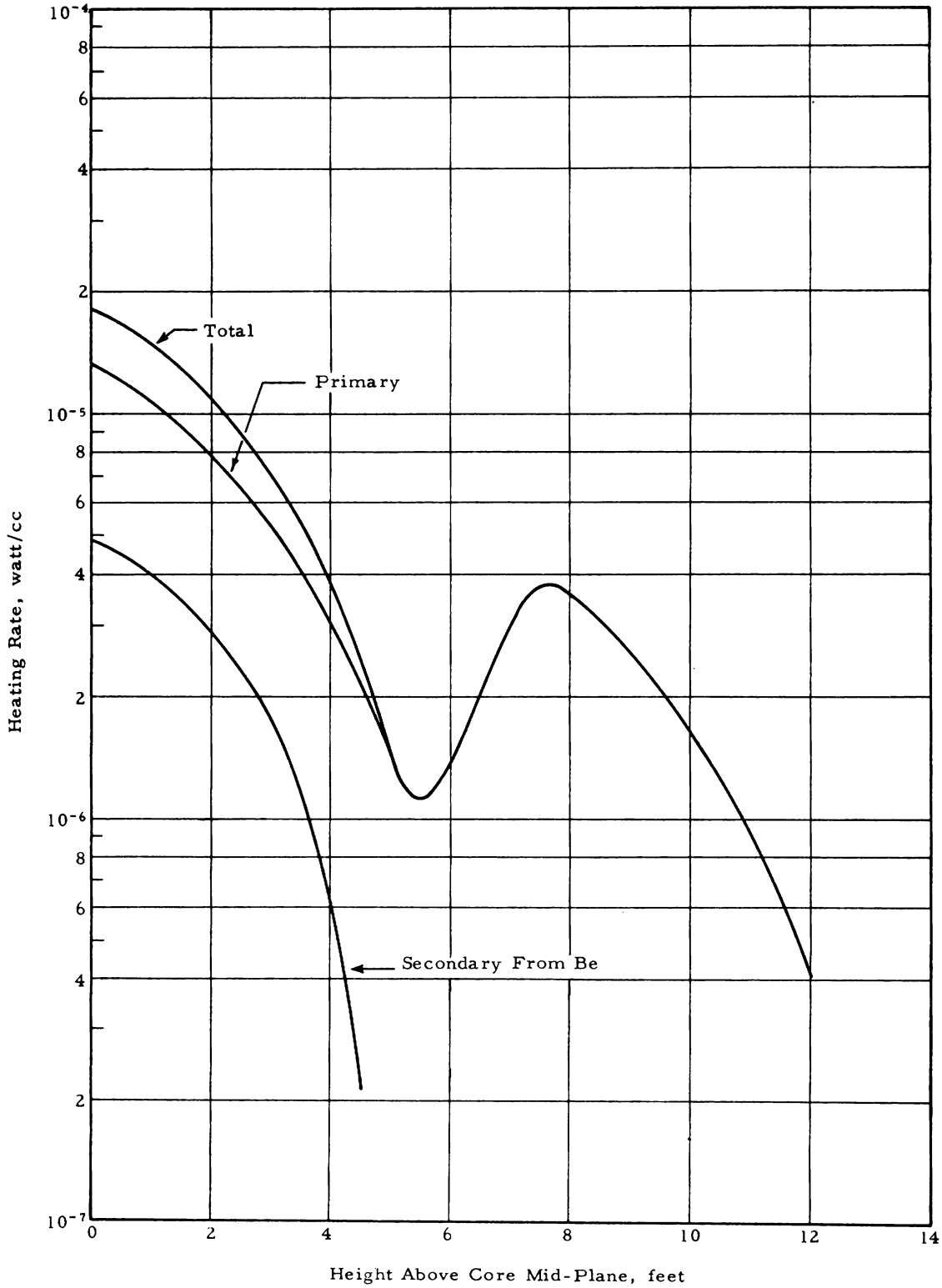

Figure 4-9. Heating Rates in Magnetite Concrete as Functions of Height Above Core Mid-Plane (2 Feet Inside Concrete)

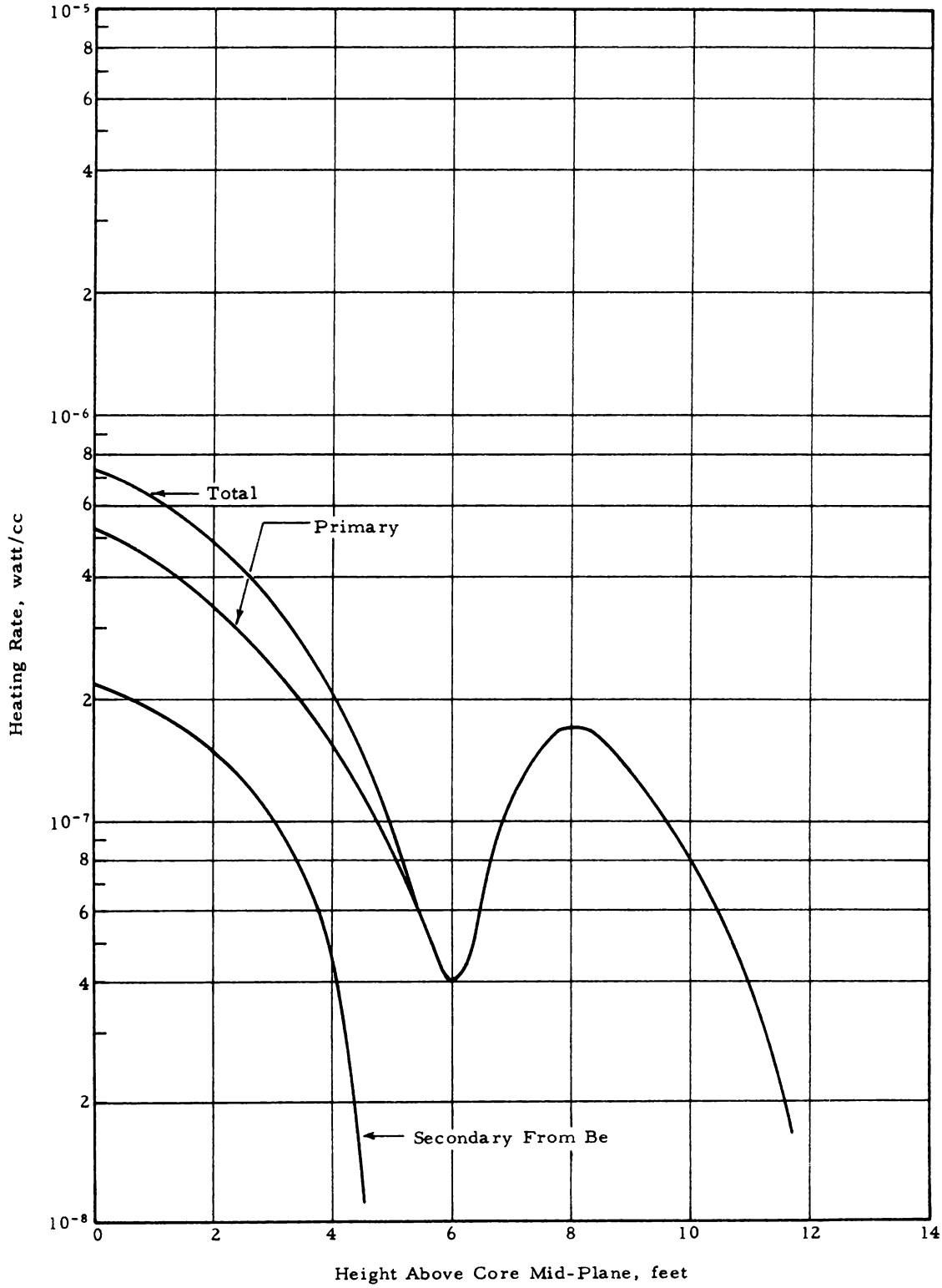

Figure 4-10. Total Heating Rate in the Aluminum Irradiation Facility at Core Mid-Plane

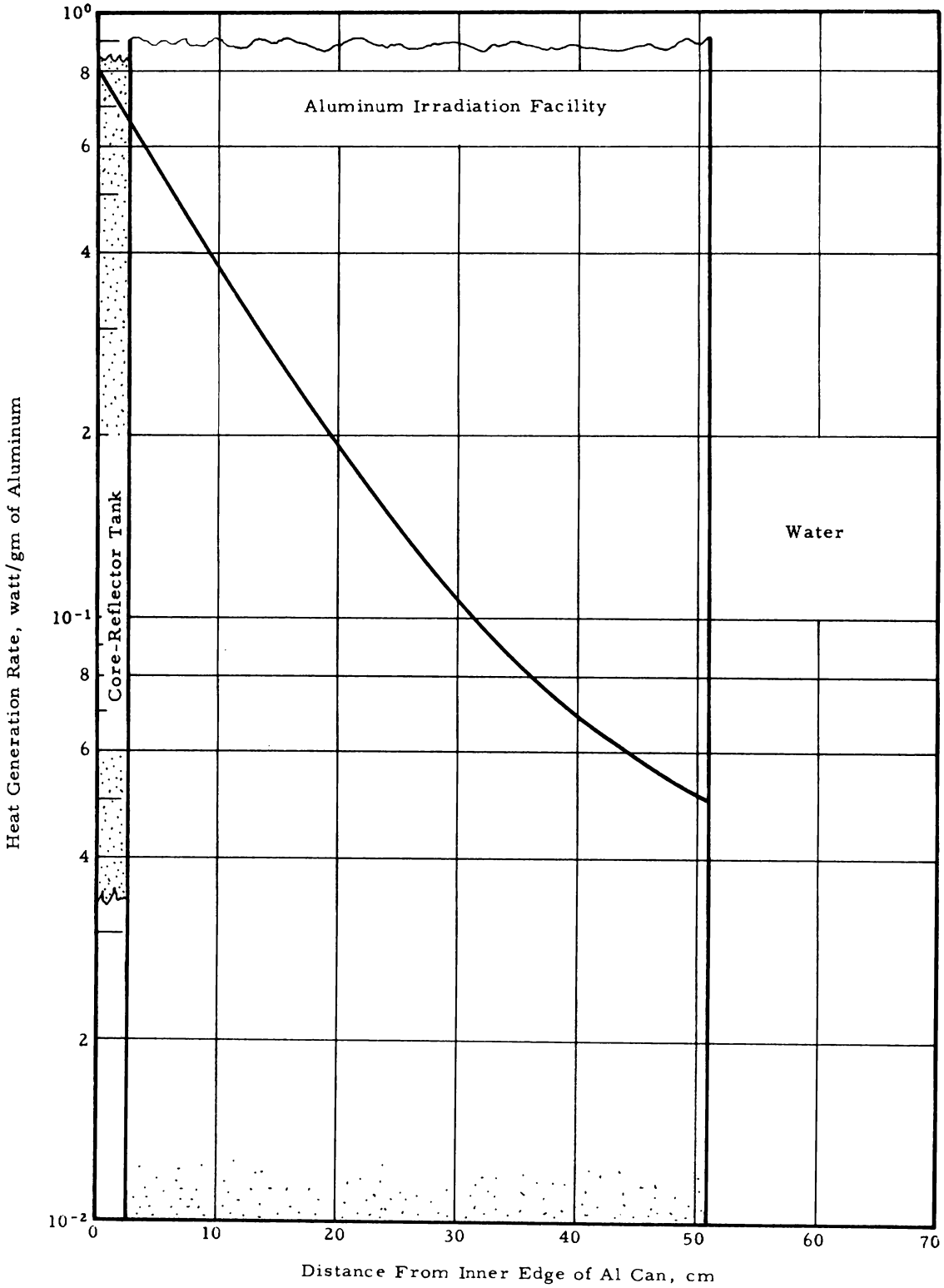

Figure 4-11. Total Heat Generation Rates in Beryllium Reflector at Core Mid-Plane (Density of Be = 1.84 gm/cc)

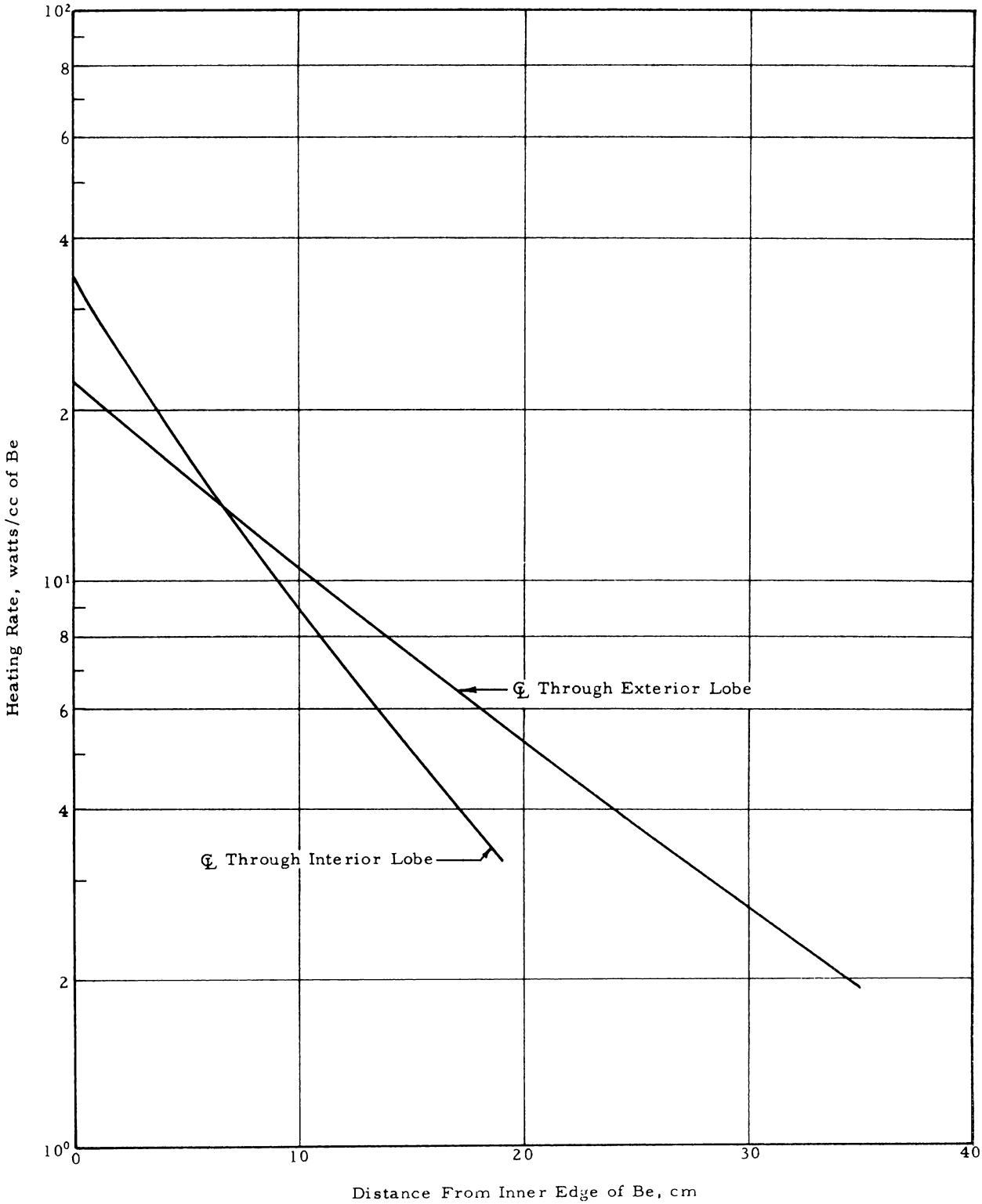

Figure 4-12. Mid-Plane Distribution of Film Packet Exposures

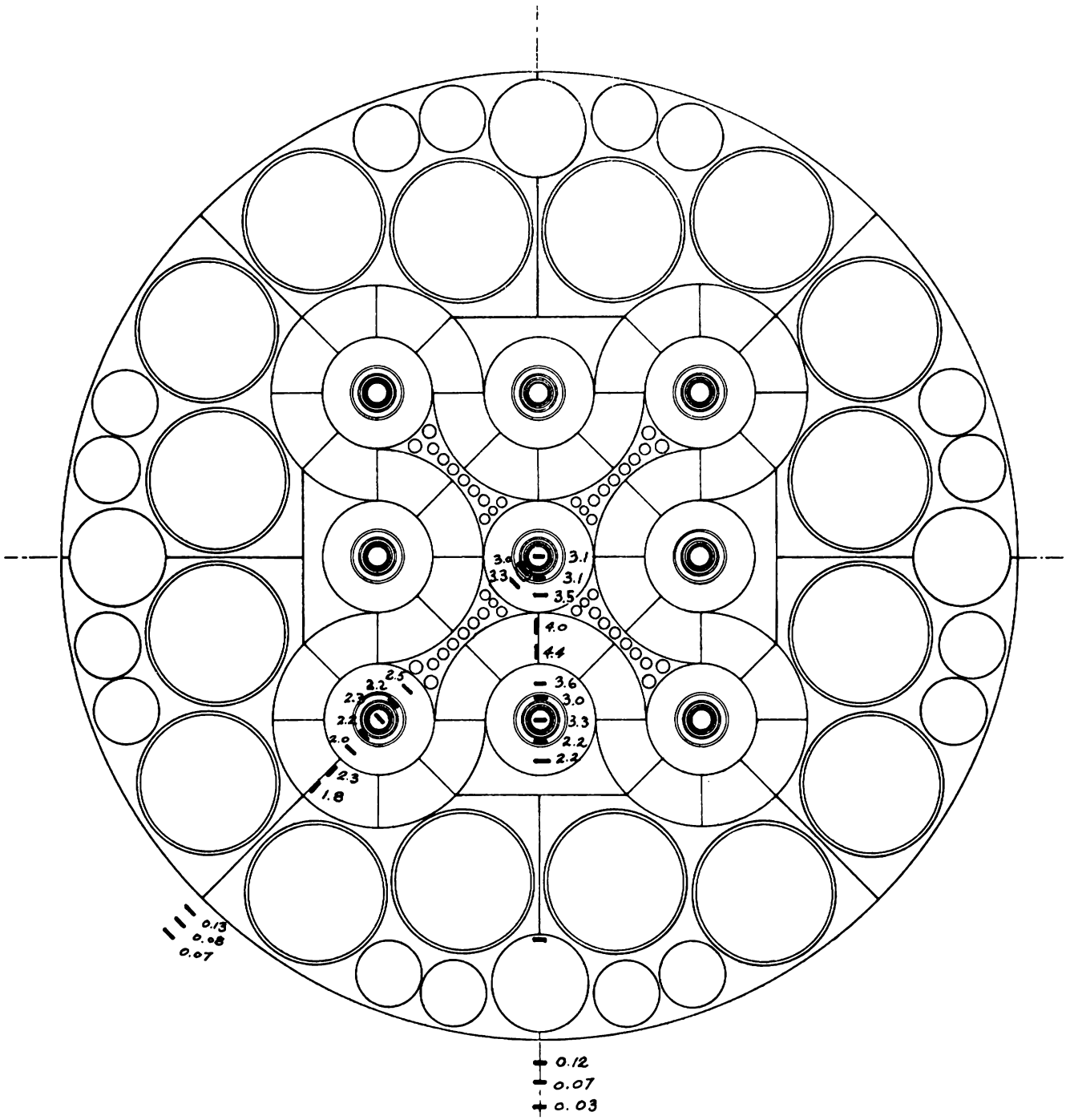

Figure 4-13. Comparison of ATR Calculations With ATRCE Measurements Through an A-1 Experiment at Core Mid-Plane

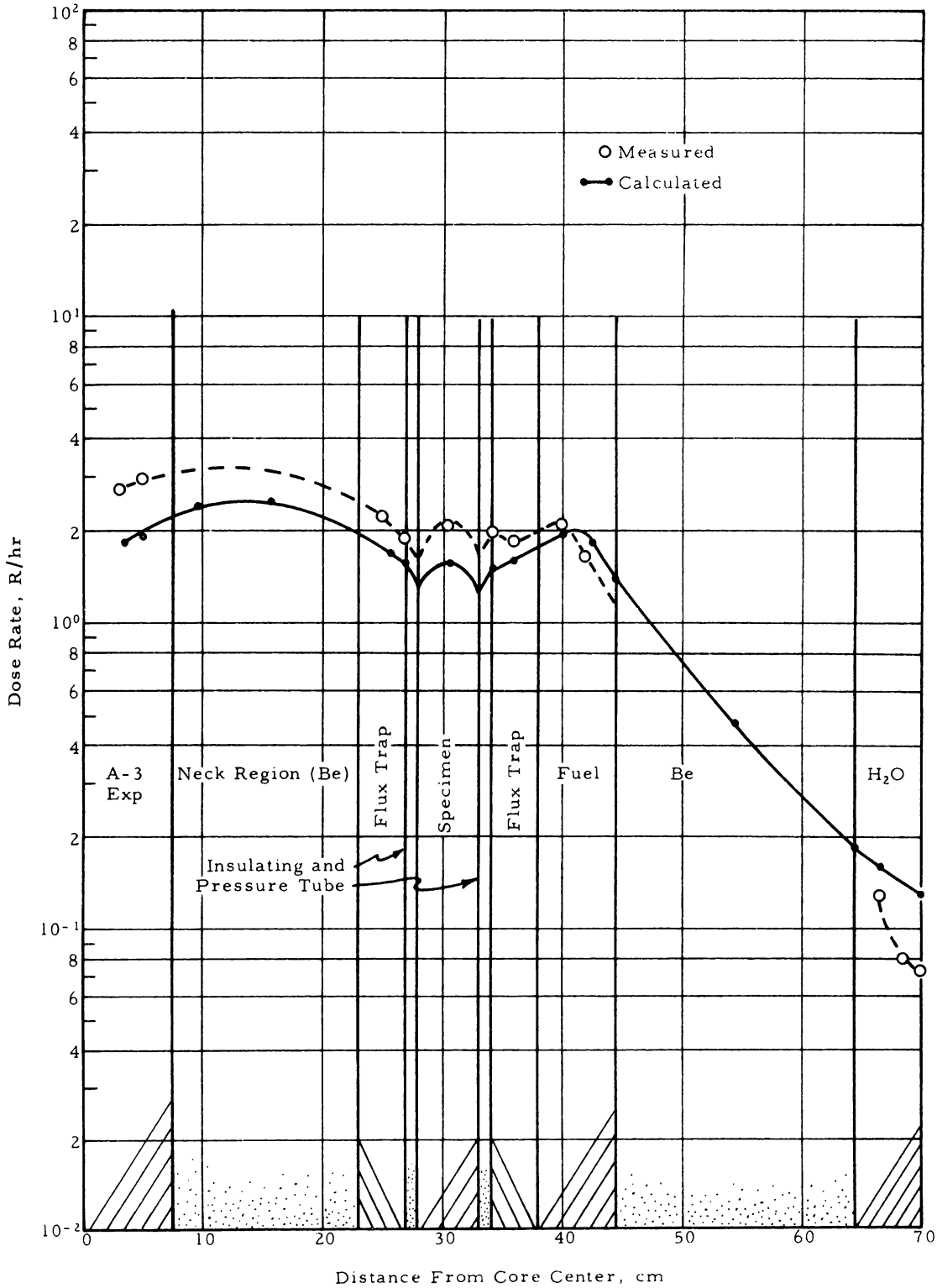

5. BUILDING SHIELDING

5.1. Primary Biological Shield

The primary biological shield is designed to attenuate radiation from the core and primary coolant to a level of 5 mrem/hr at the outer surface of the shield. The shield is composed of three sections. The first is a 3-foot-thick magnetite concrete shield surrounding the pressure vessel and extending 8-1/2 feet above and 12-1/2 feet below the core mid-plane. The second section is a 2-1/2-foot ordinary concrete shield adjacent to the magnetite shield. The ordinary concrete is sized primarily for structural requirements and must be relatively free from gamma heating and radiation damage. This protection is provided by the magnetite concrete. The third section is a 5-1/2-foot ordinary concrete shield surrounding the piping corridor. This shield is designed to reduce the level of radiation from N-16 in the primary coolant piping to 5 mrem/hr at the outer shield surface.

The calculation of primary and secondary gamma fluxes in the thermal shields and pressure vessel was made during the early stages of Title I and employed a somewhat conservative calculation model. However, since no design problems were encountered as a consequence of the results, it was deemed unnecessary to recompute these fluxes with more refined methods during Title II design.

For the gamma attenuation calculations, the core (including the test and neck regions) was homogenized and approximated by a cylinder of equivalent volume and height. This cylindrical core model was then positioned slightly off the vessel centerline so that its perimeter coincided with the perimeter of an external lobe. Volumetric gamma sources were obtained by volume weighting the gamma source strengths shown in Table 3-1. The gamma dose rates were computed along the core radial centerline with the aid of The Babcock & Wilcox computer program

DER-074 (Appendix B). Dose rate buildup factors for steel were used. The dose rate profile is shown in Figure 5-1.

The neutron flux profile was calculated using the methods outlined in Section 3.1. The flux was computed from a single lobe along a line from the core center through the center of the lobe. The lobe was approximated by a two region cylinder. The center region was considered as the homogenized test section. The outer region was the homogenized fuel section. Plots of the fast and thermal fluxes along the core radial centerline are given in Figure 5-2.

The secondary gamma fluxes and dose rates were computed from the above-mentioned thermal neutron flux profile. Details of the calculation are given in Section 3.3 and Appendix A. Figure 5-3 is a graph of the secondary gamma dose rates along the radial centerline of the core. The bulk of the secondary gamma flux is due to neutron capture in the beryllium reflector and the core-reflector tank. The relatively large thickness of water between the core and the thermal shield attenuates neutrons to such an extent that the secondary gammas produced in the thermal shields and pressure vessel make no significant contribution to the total gamma flux.

The 5-1/2-foot-thick ordinary concrete shield surrounding the piping corridor is sized for shielding the N-16 gammas from the primary coolant piping. The contribution from primary and secondary gammas to the total dose rate at the outer surface of this shield is negligible. Dose rate calculations are based on the primary coolant layout shown in Ebasco drawings ATR-1075-MTR-670 P-8 and P-10. The following transit times were used to obtain the N-16 activity at various locations:

Core exit to 18-inch-OD outlet pipe, 0.75 sec.
Core exit to 24-inch-OD outlet pipe, 3.0 sec.
Core exit to 36-inch-OD outlet pipe, 5.4 sec.

The pipes were represented by cylindrical sources, and dose rates through the concrete shield were calculated with computer program DER-074 (Appendix B). A pipe wall thickness of 3/8 inch was used. The dose rates from an 18-inch-OD and a 24-inch-OD pipe at the outer surface of the shield are shown in Figure 5-4 as a function of shield thickness.

5.2. Subpile and Rod Access Room Shielding

The shielding for the subpile room is designed to permit entry into the room one hour after reactor shutdown. No access is allowed during operation. The subpile room is shielded from the core by the 1-foot-thick vessel bottom head and by the 10-foot water depth between the core and bottom head. The dose rate from the core after 1 hour of shutdown was computed at the lower surface of the bottom head using the truncated cone geometry in computer program DER-074. Gamma sources were taken from Figure 3-8; dose buildup parameters used were those for steel. Assuming a solid steel bottom head, the dose rate was computed to be less than 1.0 mrem/hr. Higher radiation levels can be expected locally, however, as a result of radiation streaming through neck rod and inpile loop penetrations in the bottom head.

During the Title I phase of the ATR design, a procedure was devised whereby pressure tubes containing stuck test assemblies would be removed from the vessel through the drop tube. The pressure tube and element would then be stored temporarily in the deep end of the working canal adjacent to the subpile room. Consequently, the wall between the subpile room and the working canal was sized for this condition. It was assumed that an 800-kw test element, at 1 hour of shutdown following infinite operation, was positioned 1 foot from the wall. The element was represented by a line source of uniform strength, and the dose rate was computed along the mid-plane of the element through ordinary concrete. The dose rate as a function of concrete thickness is shown in Figure 5-5. To meet the design radiation level of 7.5 mrem/hr, a 6-foot-thick wall of ordinary concrete or an equivalent 4-foot thickness of magnetite is required. Although the procedure for removing stuck test assemblies was revised during Title II design, the shield wall was not changed, since nearly as much shielding is needed to reduce the transient dose rates to design level in the subpile room during spent fuel removal.

The failure of a test specimen and the subsequent release of fission products to the test loop coolant must also be considered in the shielding of the subpile and rod access rooms. Since it is impossible to predict the nature of such a failure, the analysis must be based on

a postulated test element failure. The following assumptions and parameters were used to determine the fission product source activity in the loop:

1. Bottom re-entrant loop with 200-gallon capacity.
2. 800-kw test specimen, infinite operation.
3. Release of 10% of the gross fission product gamma activity in the specimen to the coolant within 30 seconds.

The fission product gamma activity was taken from the tables in Appendix A of Reference 15. The total fission product gamma activity in the loop is shown in Table 5-1 as a function of energy and time after failure.

Table 5-1. Fission Product Gamma Activity in the Test Loop (Disintegrations/Second)

Energy interval, (mev)	Time after fission product release			
	0.6 Min	6 Min	1 Hr	10 Hr
0.5 - 1.5	1.3×10^{15}	1.3×10^{15}	8.0×10^{14}	3.0×10^{14}
1.5 - 2.5	1.6×10^{14}	1.5×10^{14}	7.7×10^{13}	8.3×10^{12}
2.5 - 3.5	1.0×10^{14}	4.3×10^{12}	1.4×10^{12}	1.4×10^{11}
3.5 - 4.5	3.3×10^{11}	3.3×10^{11}	2.8×10^{11}	3.0×10^{10}
4.5 - 5.5	2.5×10^{13}	4.4×10^{11}	- -	- -

Because it is assumed that the fission products are released to the test loop coolant in a few seconds, the dose rates will be significantly higher during the first few minutes after a failure than at some later time. Instead of increasing the shielding to lower these initial dose rates to the general design level, the shielding was sized for an integrated dose from fission products during the first hour after a failure. In this case the dose rates are of a transient nature rather than a continuous background, and a higher limit can be allowed.

The subpile room door is sized for a dose rate outside the door of 2.5 mrem/hr from N-16 in the test loops and an integrated dose of 12.5 mrem from loop fission products during the first hour following

a test failure. The dose rate from N-16 was calculated for nine loops operating at 20 gpm (worst condition). The loops were represented by line sources of uniform source strength. A mean distance of 24 feet between the source and the outer surface of the door was assumed. Figure 5-6 shows the calculated dose rate from a single loop versus steel thickness of the door. With nine loops, a steel door 10 inches thick is needed to limit the radiation level to 2.5 mrem/hr. The door thickness is governed by the N-16 activity. The first hour dose from fission product activity is approximately one-fourth of the design level dose for fission products.

The floor between the subpile and rod access rooms consists of 3 feet of magnetite concrete, 4 inches of steel, 6 inches of polyethylene, and local lead shielding. The concrete and steel are designed to shield the rod access room from core radiation and from N-16 in the test loop piping. Using the truncated cone geometry in computer program DER-074, the dose rate from the core during operation was computed to be less than 1 mrem/hr at the ceiling in the rod access room. The dose rate from the N-16 in the vertical section of the test loops was computed to be about 1.5 mrem/hr at the lower surface of the concrete, steel, and polyethylene shield complex. The loops were represented by line sources of uniform strength, and the dose rates were calculated by integrating along the length of the source. Self-absorption by the loop coolant water and piping was neglected. Buildup factors for concrete were used. The calculations were based on the 20-gpm flow rate, since this yields the maximum N-16 activity at this point.

Where the test loop traps and exit piping are embedded in the subpile room floor, lead replaces concrete as the shielding material. The dose rate from N-16 in a single loop, at a point 6 inches below the floor and directly beneath the loop, is shown in Figure 5-7 as a function of lead thickness. The effect of the 4-inch steel shield is also included. The calculation is based on a 20-gpm flow rate with the loop represented as a line source. A 6.5-inch lead shield was chosen, resulting in a dose rate of 2.5 mrem/hr in the rod access room. Because of slant penetrations through the shield, the contribution of adjacent loops to the dose rate at this point will be comparatively

insignificant. The 6-inch polyethylene shield is placed below the lead to insure adequate attenuation of the neutrons from the N-17 activity in the test loop coolant water.

In the rod access room, the design dose rate for a test specimen failure is a 25-mrem integrated dose during the first hour following the failure. The floor between the rod access and subpile rooms will provide sufficient shielding so that radiation levels in the rod access room from the postulated test element failure will be relatively insignificant. The only significant dose rates originate where the loops are embedded in the subpile room floor.

The computed dose rates in this area were based on the fission product gamma sources listed in Table 3-1. Two cases were considered. In one, the fission products were assumed to be uniformly dispersed throughout the loop. The portion of the loop pipe embedded in the floor was approximated by a uniform line source, and the dose rates were computed at the lower surface of the floor. With the 6.5-inch lead shield plus the steel and polyethylene, the resulting dose rates were negligible. In the second case it was assumed that 10% of the activity released to the loop was concentrated in the loop trap. It was further assumed that all of this activity was collected in the trap within 30 seconds after the test element failure. Using point source geometry, the dose rates were computed as a function of lead thickness for various times following test failure. The 4 inches of steel and the 6 inches of polyethylene were included in the calculations. Lead buildup factors were used. The resulting dose rates, at a point 1 foot below the shield surface, are shown in Figure 5-8.

The wall between the piping corridor and the rod access room is composed of 3 feet 8 inches of magnetite concrete. The dose rate at the wall surface is estimated to be about 6 mrem/hr based on the calculations for ordinary concrete. As seen in Figure 5-4, the dose rate from a 24-inch primary pipe through 5 feet 6 inches of ordinary concrete is 6 mrem/hr. The equivalent thickness of magnetite concrete required for shielding purposes was determined by applying a ratio of the linear absorption coefficient of magnetite concrete to that of ordinary concrete at 6.3 mev.

5.3. Coolant Canal and ATRC Shielding

The overall building height limits the depth of the storage canal to 20 feet. To meet the design radiation levels above the canal, fuel elements will be stored in the working canal until they have decayed sufficiently to permit transfer into the storage canal.

The condition that governs the length of the decay period is the transient dose rate that occurs when a spent fuel element is raised above the storage rack to be lowered into the rack. Figure 5-9 is a plot of water height required over a single ATR fuel element, following 17 days operation, to meet a 50 mrem/hr transient radiation level as a function of decay time. The overall water height in the canal is determined from the following dimensions starting from the canal floor:

1. Water circulation space, 6 in.
2. Fuel element height in storage rack, 5 ft 6 in.
3. Clearance above fuel element in raising element for storage, 6 in.
4. Fuel element raised above storage rack, 5 ft 6 in.
5. Water above raised element for a 50-mrem/hr transient dose rate after 10 days decay, 8 ft 0 in.
6. Total water height, 20 ft 0 in.

The 8-foot shield height was based on the dose rate at the surface of the water from an average fuel element with a uniform power distribution. Since most of the dose rate is due to the upper 1 foot of the element, this was considered to be as conservative as using the "hottest" element and accounting for end effects. The element was assumed to be a vertical line source, and the dose rate was calculated directly above the element in water by integrating point source attenuation kernels along the length of the element. The absorption coefficients of the element were assumed to be those of water.

The shielding calculations for the walls and floor of the storage canal are based on a row of 40 fuel elements, 4-inch center-to-center spacing, 15 days shutdown, and 6 inches from both the wall and floor. For sizing the wall, the row of elements was represented by a plane source expressed as:

$$S_A = \frac{S_V V}{A}$$

where

S_V = fission product gamma source strength per unit volume of fuel element

V = volume of 40 fuel elements

A = area of the plane formed by the row of elements

S_A = gamma source strength per unit area of plane

Dose rates were then calculated as a function of concrete thickness using the disk source case in program DER-074. It was assumed that there was 6 inches of water between the source and the canal wall. The curve of dose rate versus ordinary concrete thickness is shown in Figure 5-10. To meet a design dose rate of 1.0 mrem/hr outside the canal wall, 6 feet 6 inches of ordinary concrete is required. To facilitate construction around support beams, a wall thickness of 7 feet was used.

The dose rate through the canal floor was computed by dividing the above-mentioned plane source into a series of line sources 4 cm apart and parallel to the floor. Fluxes were then calculated from each line source. Figure 5-11 shows the total dose rate from all such line sources as a function of floor thickness. The canal floor forms the ceiling of cubicles 2A and 2E and a portion of the pipe tunnel. The floor thickness over these areas is sized for a 5.0-mrem/hr dose rate and is 5 feet 6 inches of ordinary concrete. Elsewhere, the floor is 7 feet thick with a resulting dose rate of less than 1.0 mrem/hr.

Shielding calculations for the ATR critical facility are based on a 5 kw core located to maintain 5 feet of water between the bottom of the active core and the canal floor and 5 feet of water between the center of the core and the canal wall. Dose rates were computed along the radial and axial centerlines of the core using computer program DER-074. Radially, the core was approximated by an equivalent radius homogeneous cylinder. Axially, a truncated cone approximation was used. In both cases a uniform power distribution was assumed. Core gamma source strengths were obtained from Table 3-1 using a power density ratio. Figure 5-12 shows the dose rate as a function of water height over the core. For a 22-foot canal the water height over the core is established as follows:

1. Provision for follower rod travel and snubber, 5 ft 0 in.
2. Length of active core, 4 ft 0 in.
3. Water height over core, 13 ft 0 in.
4. Total water depth, 22 ft 0 in.

As can be seen from Figure 5-12 the calculated dose rate through 13 feet of water is 6.5 mrem/hr.

The design transient dose rate for transferring irradiated fuel elements into the critical facility is 50 mrem/hr. Allowing 1 foot 6 inches for the end boxes and clearance and 4 feet for the active fuel length, the minimum shield water height available during transfer is 7.5 feet. As seen in Figure 5-9, a decay period of 20 days is necessary before irradiated fuel can be transferred into the critical facility.

The sides of the ATRC canal are sized for a dose rate of 1.0 mrem/hr at the shield surface. The calculations show that 6 feet of ordinary concrete are required to lower the dose rate to this level. The dose rate through the concrete wall is shown in Figure 5-13. The concrete floor below the critical experiment is also designed for a 1.0-mrem/hr dose rate at the shield surface, which results in a thickness of 5 feet. The dose rate is shown in Figure 5-14 as a function of floor thickness.

One end of the ATRC canal will be used for the storage of spent fuel elements and must be sized accordingly. The design for this end of the canal was based on a single ATR element stored 6 inches from both the canal wall and floor 12 hours after shutdown and a row of 40 ATR elements, 4-inch center-to-center spacing, stored 6 inches from the wall and floor 15 days after shutdown. In both cases an operating time of 17 days was assumed. The single element was represented by a line source for both the axial and radial dose rate calculations. Figure 5-15 is a plot of the dose rate through concrete along the radial centerline of the element. The calculations for the row of elements are the same as those for the storage canal. The dose rate profiles through the walls and floor are shown in Figures 5-13 and 5-14, respectively. The shield thicknesses are governed by the 40-element case. For a 1.0-mrem/hr dose rate, the required thicknesses are 6 feet 6 inches for the walls and 6 feet for the floor.

5.4. Coolant Loop Shielding

The coolant loop shielding was based on calculations of the dose rates from N-16 in the primary coolant. Using the calculated core exit equilibrium activity of 2.2×10^7 d/cm^3-sec and the transit times to the various loop pipes, the volumetric activities of coolant in various sections of piping were calculated. The N-16 activity was calculated for a half-life of 7.4 seconds and an 82% yield of 6.3-mev mean energy photons. All piping was assumed to have a uniform wall thickness of 3/8 inch of steel. The transit times used were those of the normal flow rate of 44,000 gpm. The times of transit for several of the loop regions are as follows:

1. Core to reactor outlet, 0.75 sec.
2. Reactor outlet to first 24-inch effluent pipe, 3.0 sec.
3. Reactor outlet to first 36-inch effluent pipe, 5.4 sec.
4. Reactor outlet to heat exchanger inlet, 1.8 sec.
5. Through heat exchanger, 10.5 sec.
6. Heat exchanger outlet to reactor inlet, 13.3 sec.
7. Total core to core time, 37.1 sec.

Computer program DER-074 was employed in the calculations in this section. A discussion of the methods of this program is found in Appendix B.

5.4.1. Piping Tunnel

The thickness of the walls of the piping tunnel was determined from the activity of the coolant in the 36-inch effluent pipe in the pipe tunnel. The N-16, having undergone decay of about four half-lives before returning to the pipe tunnel, makes the return pipe activity insignificant as a source in comparison with the outgoing pipe. The 36-inch effluent pipe was calculated to have a uniform volumetric source activity of 1.10×10^7 photons/cm^3-sec. This corresponds to the activity of this pipe at its entry into the piping tunnel on the reactor end. The pipe was treated as an infinitely long cylindrical source. The dose rates were calculated for the outside surface of the tunnel wall for a "straight through" geometry. Figure 5-16 shows a plot of dose rate versus

ordinary concrete thickness for the source discussed. The shield thickness is 5 feet 6 inches, which limits the average dose rate to about 6 mrem/hr at the outside surface of the tunnel wall.

5.4.2. Heat Exchanger Room Walls

The heat exchanger room walls were sized to allow a 2.5 mrem/hr dose rate at their outside surface. Each pipe in the primary coolant loop in the heat exchanger room was treated as a cylindrical source. Ordinary concrete shield thicknesses of 2 feet, 4 feet, and 6 feet were used in the calculations. The point of highest cumulative dose rate was found to be opposite the mid-section of Heat Exchanger 2. In this case, the dose point receives contributions from the adjacent heat exchangers as well as the two extra half-length portions of 36-inch pipe not found at the other end of the heat exchanger room. The dose point was assumed to be at distances of 20 feet, 30 feet, and 40 feet from Heat Exchanger 2 to assist in determining the exact location of the piping in the final layout. The distance to each of the pipes in the primary system was also calculated to correspond to these dose point locations. In order to simplify calculations, it was assumed that none of the pipes was shielded by other pipes. The heat exchangers were treated as homogenized cylindrical sources. The source strengths of some of the prime contributors to the dose rates in the heat exchanger rooms are listed below.

Source	S_v, photons/cm^3-sec
36-inch incoming pipe	5.77×10^6
24-inch distributor	5.77×10^6
20-inch heat exchanger inlet pipe	5.77×10^6
Heat exchanger (homogenized)	1.14×10^6
20-inch heat exchanger outlet pipe	2.30×10^6
30-inch collector pipe	2.30×10^6
24-inch and 20-inch pump pipes	2.30×10^6
24-inch return pipe	1.91×10^6
36-inch return pipe	1.91×10^6

Figures 5-17 and 5-18 show the plots of dose rates versus wall thickness due to the heat exchangers alone and due to the heat exchanger piping alone as a function of several dose point distances. The walls around the heat exchangers were sized for the worst case (a single concrete wall placed within 6 inches of the heat exchanger piping on the reactor side of the room). The wall thickness around the heat exchangers is 5 feet 6 inches, which limits the maximum dose rate to 6 mrem/hr at the outer surface of the shield wall.

5.4.3. Pump Cubicles

The walls and ceilings around the pump cubicles are constructed of ordinary concrete and are designed to allow personnel to work inside a particular pump cubicle with that pump shut down, but with adjacent pumps operating. In performing the dose rate calculations, the pumps were approximated by vertical cylindrical sources, 24 inches in diameter and 75 inches long, located in the center of the pump rooms. The dose rate through a concrete wall from a single pump, along the pump radial centerline, is shown in Figure 5-19. Figure 5-20 shows the dose rate from the heat exchangers and piping as a function of the cubicle wall thickness. This calculation involved the same sources and methods employed for the other heat exchanger walls.

The walls between the pump cubicles are 4 feet thick, and the resulting dose rate is about 6.5 mrem/hr at the wall surface in one cubicle from an adjacent operating cubicle. The wall between the pump cubicles and the heat exchanger area is 5 feet 6 inches thick and limits the dose rate in the cubicles from the heat exchanger and pipe sources to a maximum of 2.5 mrem/hr. The pump motor area is shielded from the pumps by a 4-foot wall thickness. As seen from Figure 5-19, the dose rate at the surface of the wall is about 6.5 mrem/hr. The floor above the pump cubicles is 5 feet 6 inches thick and is designed to limit the radiation level from the pumps to less than 1.0 mrem/hr at the surface of the floor.

5.4.4. Floor Above Heat Exchanger Room

The calculations of the dose rate on the surface of the floor above the heat exchanger room were made for three dose point distances of the "worst case", a point directly above Heat Exchanger 2.

The heat exchangers were approximated by homogenized truncated cones in these calculations, and each primary coolant pipe source was treated as an infinitely long cylinder. The shield thickness for a 1.0-mrem/hr dose rate on the floor surface was found to be 6 feet of ordinary concrete. Figure 5-21 is a plot of the total dose rate in this region as a function of ordinary concrete thickness at three dose point distances.

5.5. Cubicle Shielding

The exterior walls around the test cubicles are constructed of magnetite concrete and are designed to:

1. Attenuate radiation from N-16 in the test loops to 2.5 mrem/hr at the outer surface of the wall.

2. Restrict the integrated dose from fission products during the first hour following a test failure to 12.5 mrem at the outer surface of the wall.

The wall thicknesses between the cubicles are based on a dose rate of 7.5 mrem/hr inside a cubicle (with test loop shutdown) from adjacent operating cubicles and from the primary loop piping. The dose rate inside a cubicle from the primary loops is calculated to be about 5 mrem/hr. Since no cubicle is bounded by more than one other cubicle, the walls and floors between cubicles are sized for a 2.5-mrem/hr dose rate. The thicknesses of the cubicle ceilings in the first basement are governed by the 1.0-mrem/hr design dose rate on the reactor operating floor.

The shield thicknesses were determined by computing the dose rate at the outer surface of the shield from two adjacent 2.125-inch-ID loop pipes located at the inner surface of the shield. The pipes were represented by infinite line sources of uniform source strength.

Dose rates from the N-16 activity were calculated through magnetite concrete as a function of delay time from the reactor vessel for flow rates of 20, 60, and 120 gpm. The concrete thickness required for a 2.5-mrem/hr dose rate versus delay time is shown in Figure 5-22. The cubicle walls are constructed of magnetite concrete, and, based on the coolant flow rates, are required to be 32 inches thick to limit the N-16 dose rate to 2.5 mrem/hr. The cubicle floors and ceilings are constructed of ordinary concrete. The required thicknesses of the

ordinary concrete structures were obtained from a ratio of the linear absorption coefficient of magnetite concrete to that of ordinary concrete, evaluated at the mean energy of the N-16 gamma (6.3 mev). This ratio is about 1.7. Thus the cubicle floors and ceilings were determined to be 54 inches in thickness to meet the 2.5-mrem/hr design level. For the 1.0-mrem/hr design level on the reactor floor, the cubicle ceilings in the first basement are 5 feet in thickness.

The dose rate from fission products through the concrete was calculated assuming the activity to be uniformly distributed throughout the volume of a 200-gallon loop (see Section 5.2). The calculations were similar to those used in determining the N-16 dose rate except that a single 2.125-inch ID loop pipe was used as the source. The dose rate through the 3-foot shield is shown in Figure 5-23 as function of time after the test failure. As may be seen, the first-hour integrated dose is below the 12.5-mrem design level.

A point-source calculation was made to determine the dose rate outside the shield from a concentration of fission products inside the cubicle 1 foot from the shield wall. It was found that 4% of the fission products released to the coolant in the postulated accident could be concentrated at a point in the cubicle without exceeding the 12.5-mrem limit.

5.6. Nozzle Trench Shielding

The shielding for the nozzle access trench is designed to restrict the general radiation level in the trench (neglecting streaming through the nozzle penetrations) from elements in the core and temporary storage racks to 12.5 mrem/hr or less, 3 hours after shutdown. The shielding consists of a steel skirt, 2 inches thick, surrounding the pressure vessel and extending from the floor of the capsule trench to the 4-inch-thick vessel wall section.

Because of the orientation of the core with the nozzle trench shield, direct core radiation is forced to traverse a relatively large slant thickness of shield in a conventional line-of-sight shielding calculation. To account for the short-circuiting of radiation through the pressure vessel and nozzle trench shield, dose rates were computed by a two-step process. Both the total builtup energy flux and the unscattered energy flux

were calculated at the inside edge of the pressure vessel, at the elevation of the nozzle trench floor. These calculations were carried out with machine program DER-013 using a double exponential representation for the point-source energy buildup factors in water. The fluxes were computed for initial gamma energies of 1.5, 2.5, 3.5, and 4.5 mev. The differences between the total and the unscattered energy fluxes yielded the scattered energy fluxes.

The energy distribution of the scattered fluxes was determined for each initial energy from the moments method calculations of Goldstein and Wilkins (Reference 6). Given in the reference are the differential energy spectra in various media from point isotropic and plane monodirectional gamma ray sources. Data are shown for a number of initial gamma ray energies at various penetration distances. For the nozzle shield calculations, the point isotropic spectra in water were used. A penetration distance equal to the distance from the center of the core to the field point was chosen. Although the penetration distance varies from point to point in the core, the percentage change is relatively small, and the energy spectra are fairly insensitive to small percentage changes in penetration distances.

The scattered and unscattered energy fluxes were grouped into 1-mev energy intervals ranging from 0.5 to 4.5 mev. The scattered energy flux below 0.5 mev was ignored, since the energy spectra curves dip sharply and the absorption cross sections rise rapidly below 0.5 mev. The gamma rays incident on the pressure vessel were assumed to be monodirectional along a line between the center of the core and the field point. An angle of obliquity was measured between this line and the normal to the pressure vessel wall. The attenuation of radiation by the reactor vessel and the steel skirt was determined from the use of exponential kernels and Peebles's buildup factors (Reference 17).

Dose rates from core fission products were computed at the surface of the shield skirt as a function of lead shielding thickness for various times after shutdown. Detailed calculations on the dose rates from fuel in the temporary storage racks were not made. It was estimated that the dose rates from these sources would, at a maximum, equal those from core sources. The shield thickness required to reduce the radiation level to 12.5 mrem/hr is shown in Figure 5-24 as a function

of shutdown time. Since it is feasible to use steel rather than lead as a shield material, an equivalent required thickness of steel was determined from a ratio of the linear absorption coefficients.

Figure 5-1a. Primary Gamma Dose Rates Along Core Radial Centerline

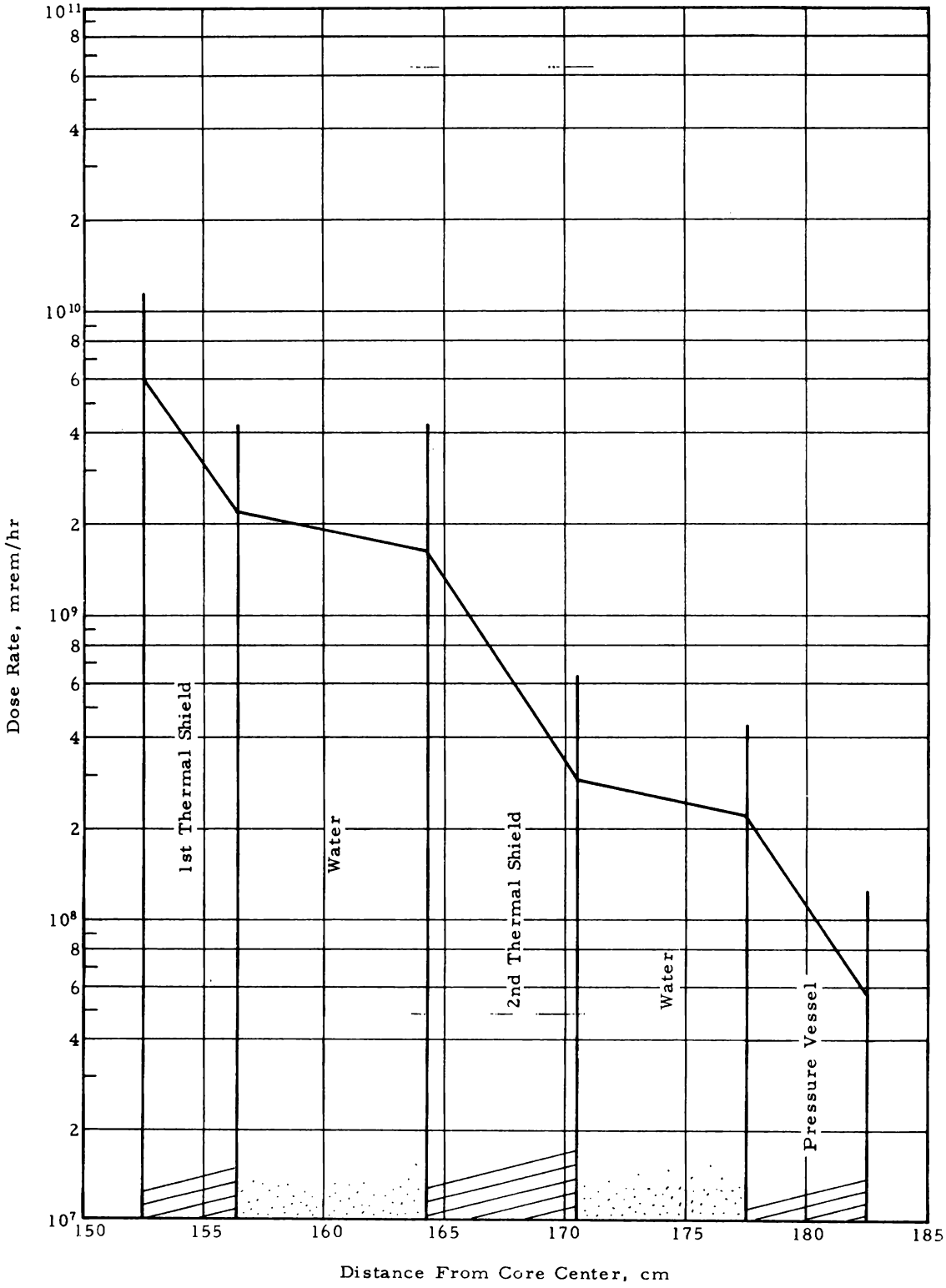

Figure 5-1b. Primary Gamma Dose Rates Along Core Radial Centerline

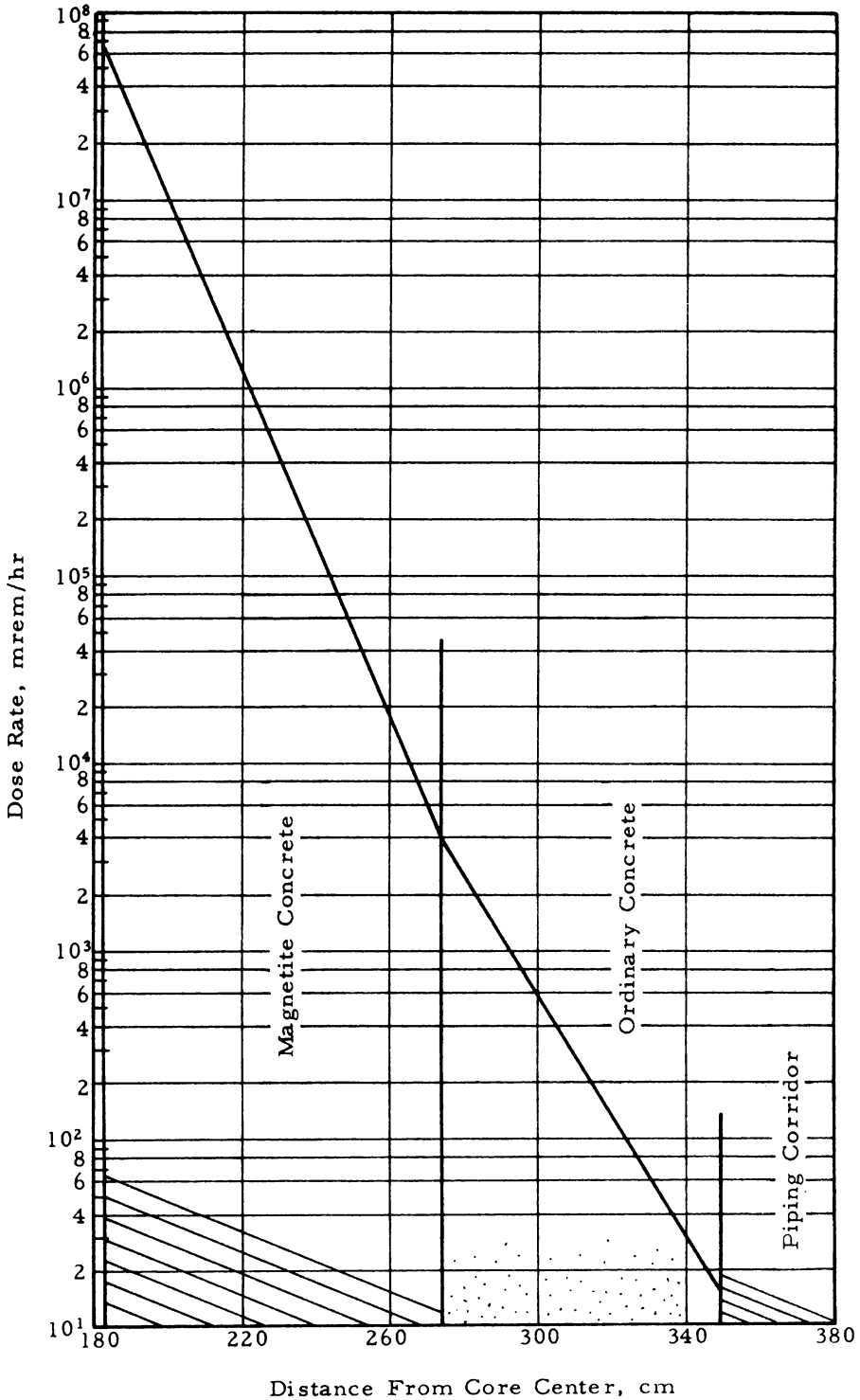

Figure 5-2a. Fast and Thermal Neutron Fluxes Along Core Radial Centerline

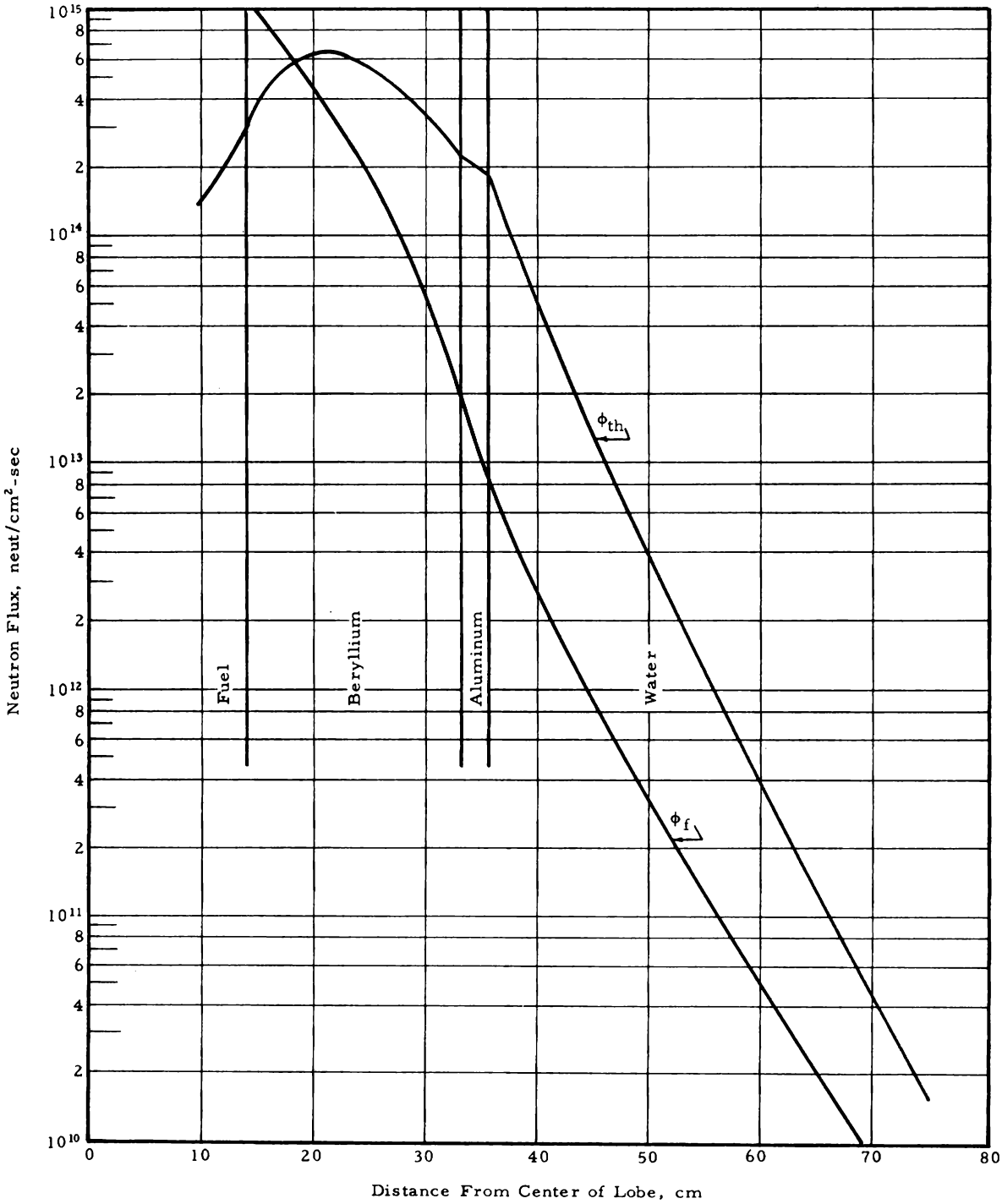

Figure 5-2b. Fast and Thermal Neutron Fluxes Along Core Radial Centerline

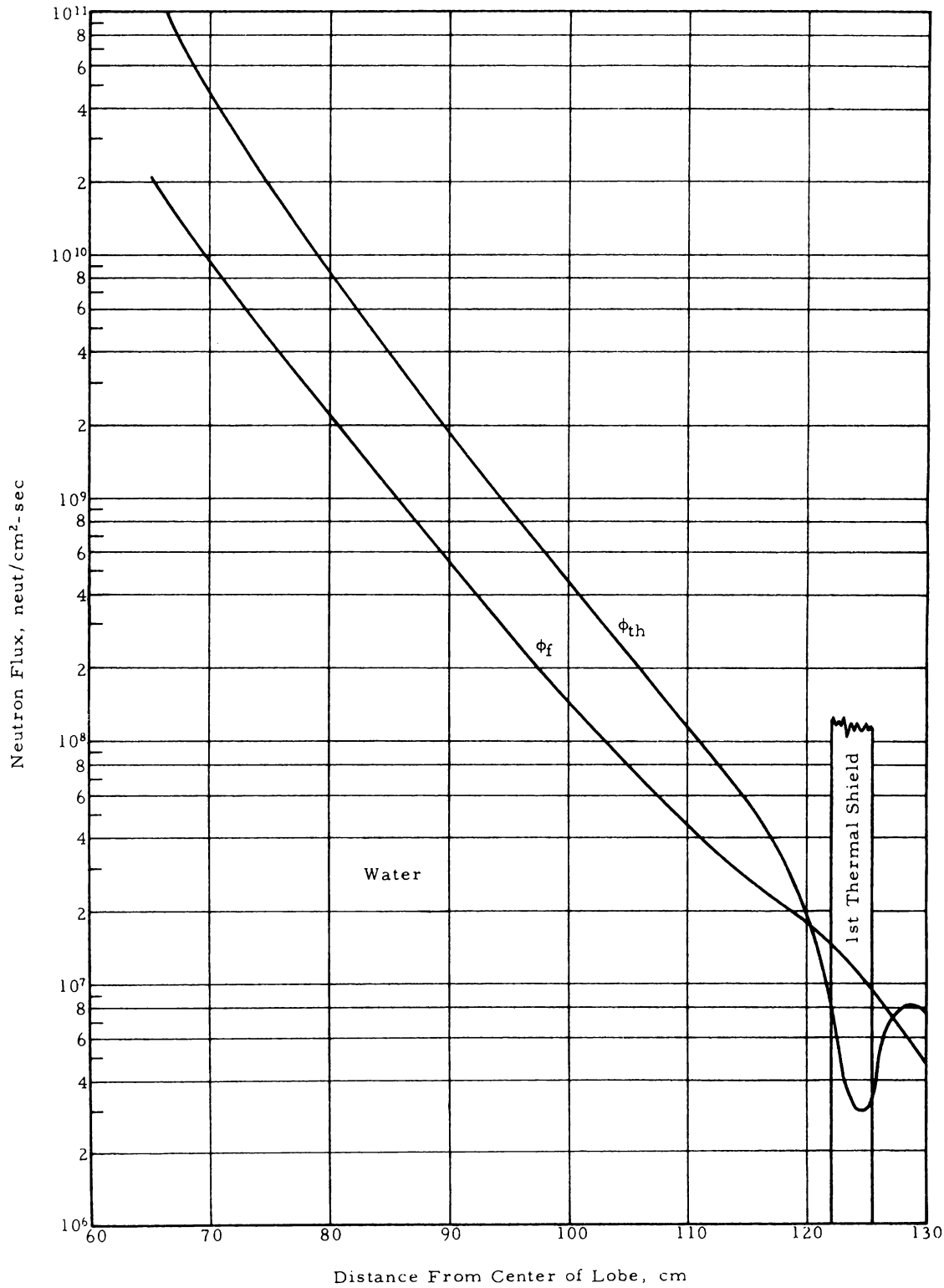

Figure 5-2c. Fast and Thermal Neutron Fluxes Along Core Radial Centerline

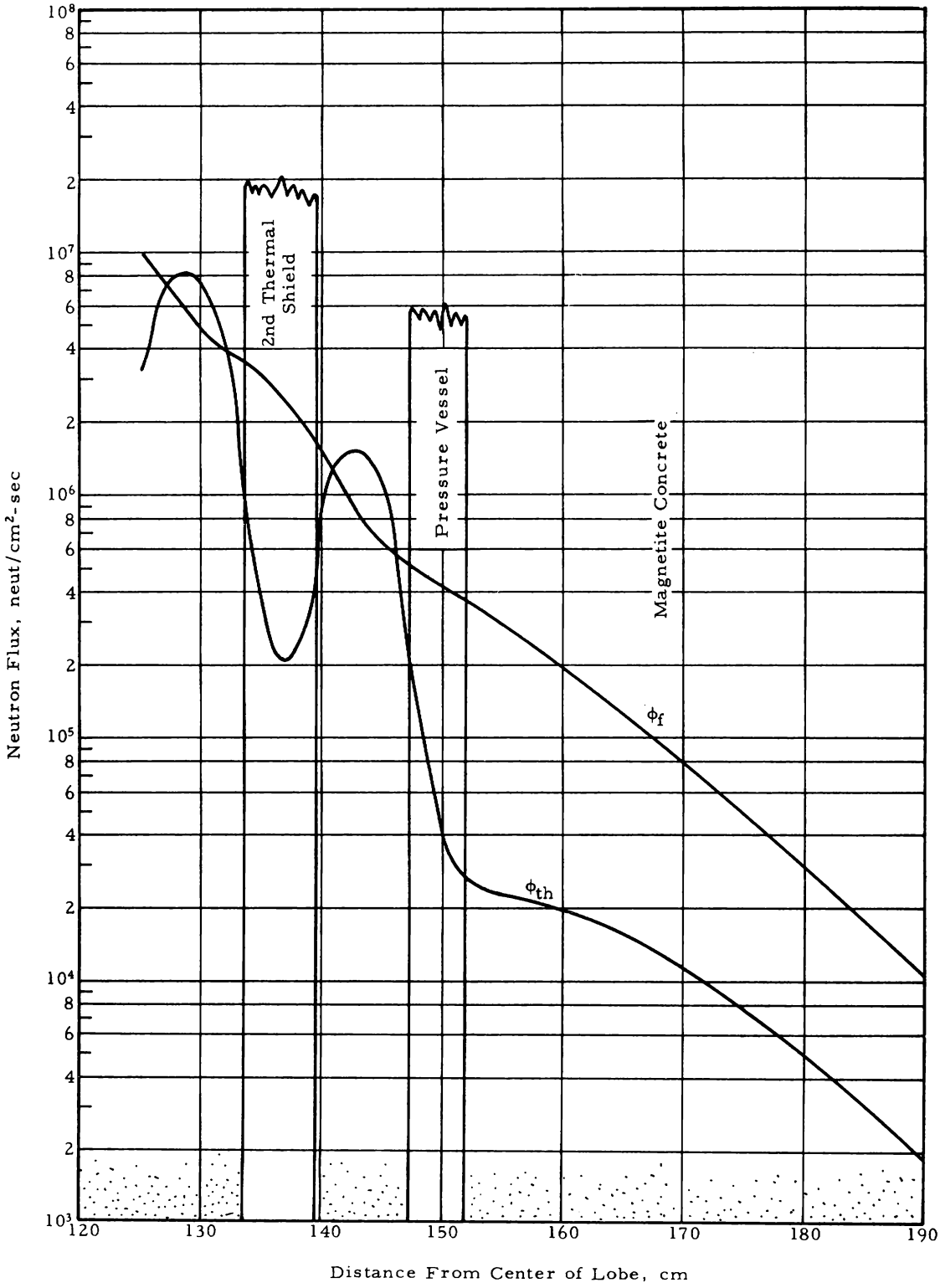

Figure 5-2 d. Fast and Thermal Neutron Fluxes Along Core Radial Centerline

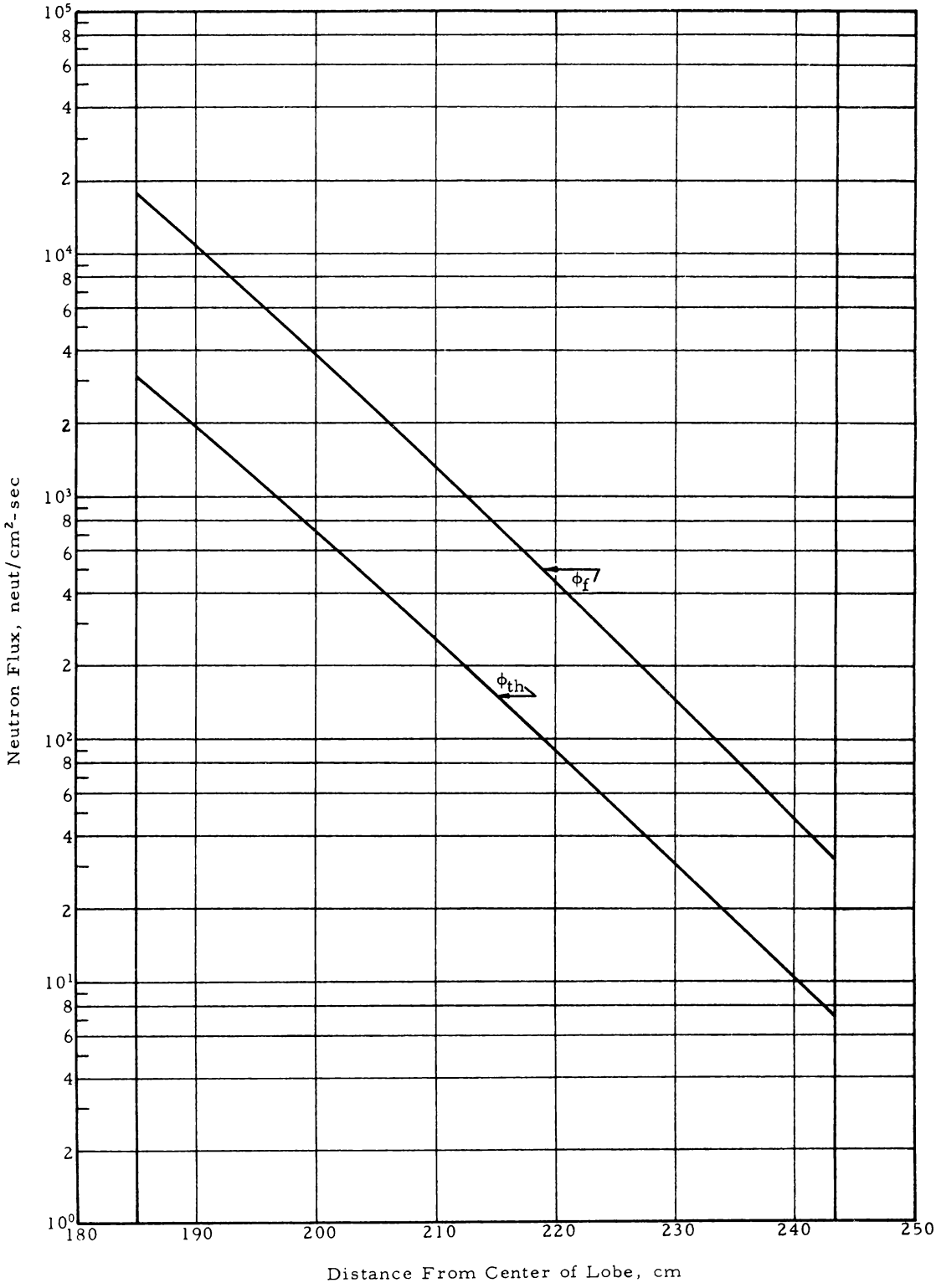

Figure 5-3a. Secondary Gamma Dose Rates Along Core Radial Centerline

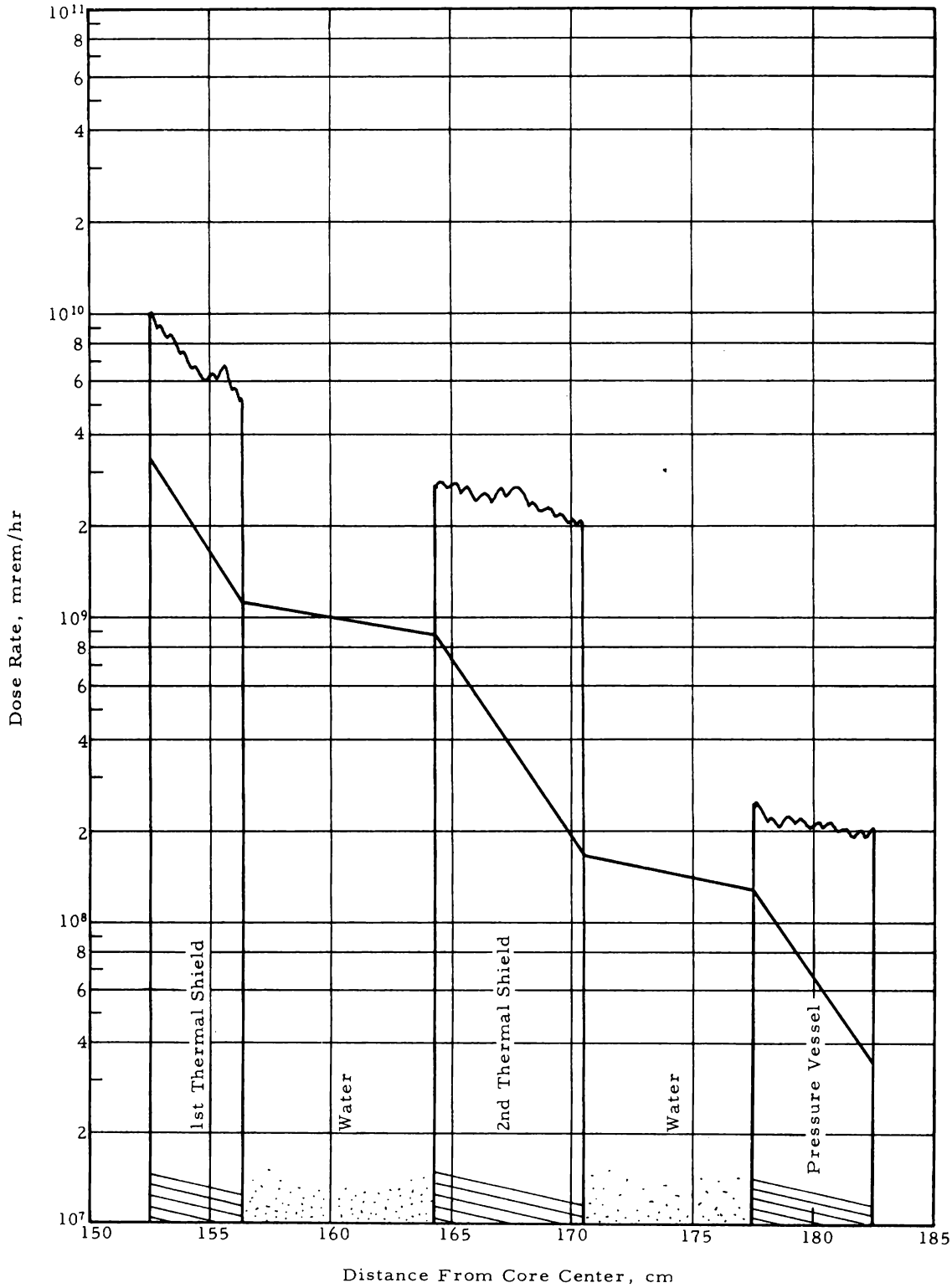

Figure 5-3b. Secondary Gamma Dose Rates Along Core Radial Centerline

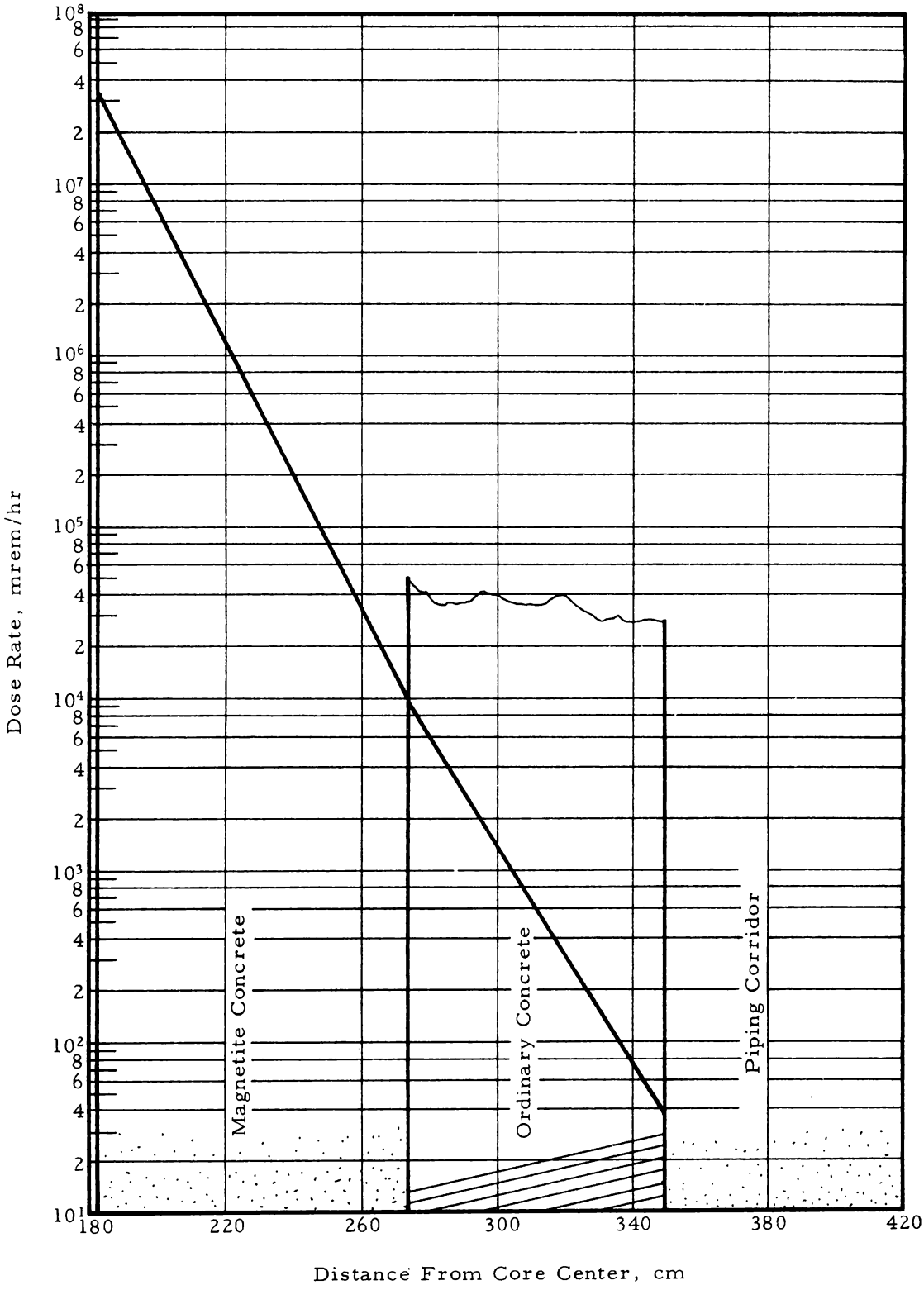

Figure 5-4. Dose Rates at Outer Surface of Piping Corridor Shield From Single Infinite-Length Primary Pipe

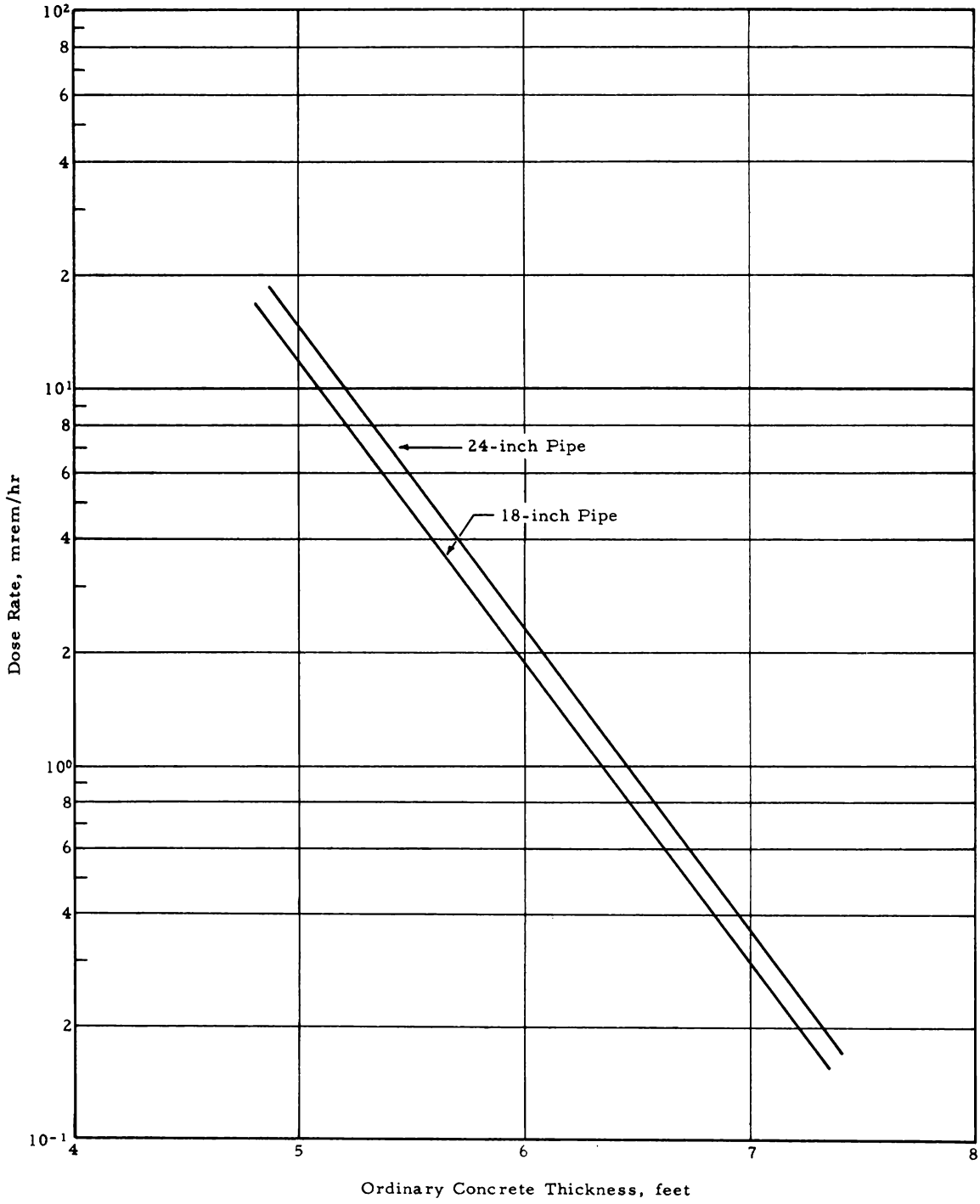

Figure 5-5. Dose Rate From an 800-kw Test Element Through Ordinary Concrete After 1 Hour Shutdown (1 Foot of Water Between Element and Concrete)

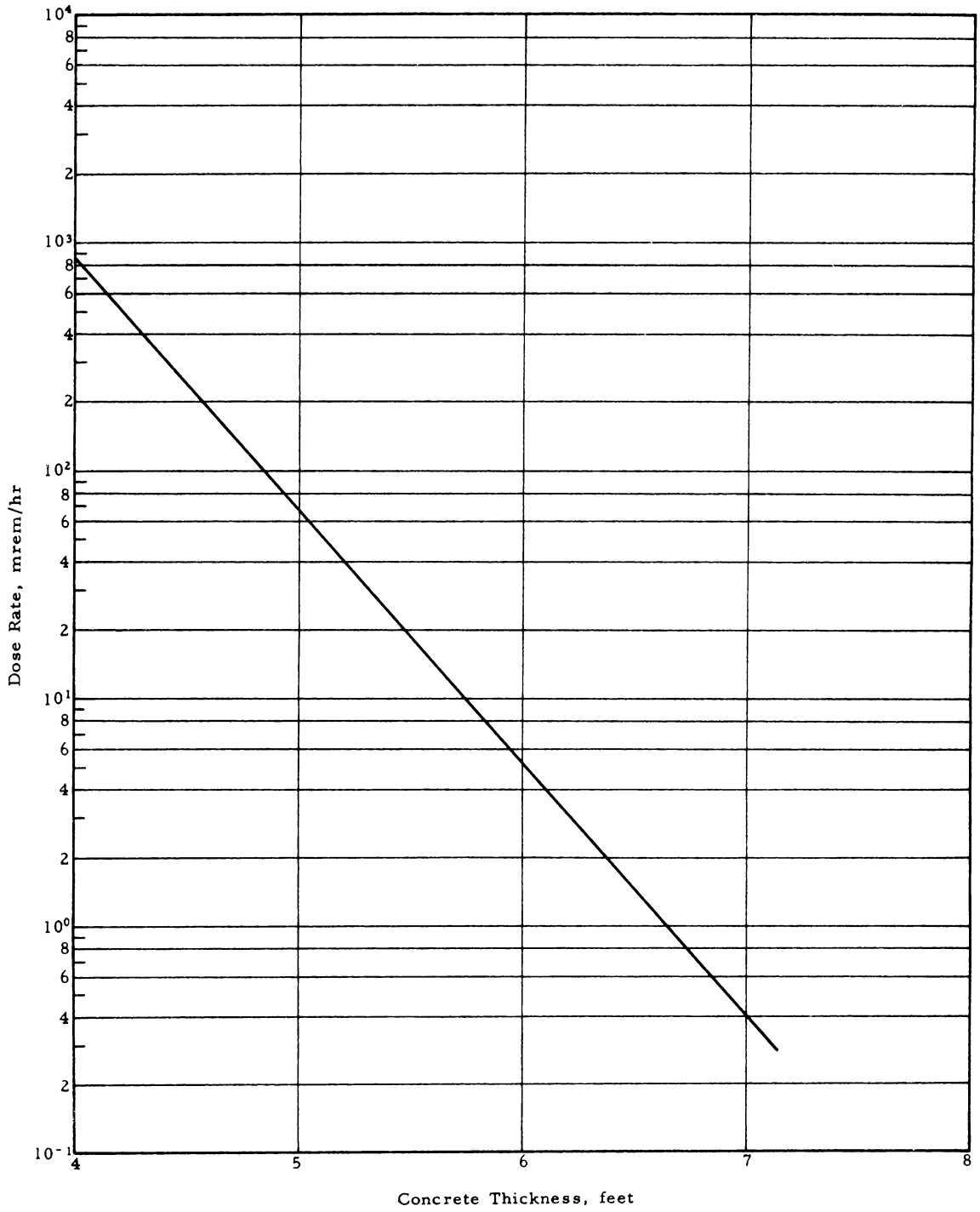

Figure 5-6. Dose Rate Outside the Subpile Room Door (N-16 in a Single Loop Operating at 20 gpm)

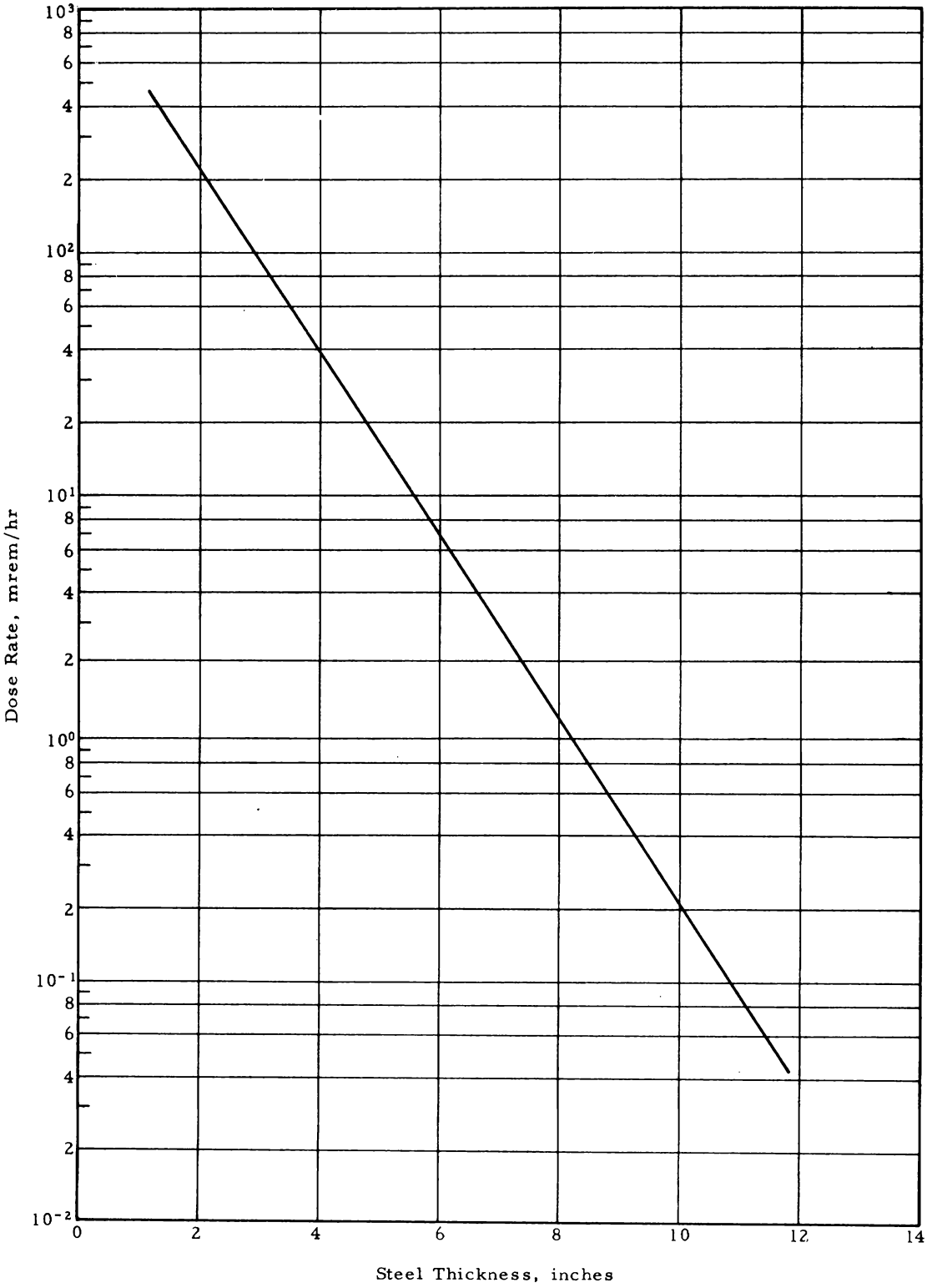

Figure 5-7. Dose Rate Through Lead From N-16 Activity in a Single Loop Operating at 20 gpm, 4-Inch Steel and 6-Inch Polyethylene Shields Included, Dose Point 6-Inches Below Shield

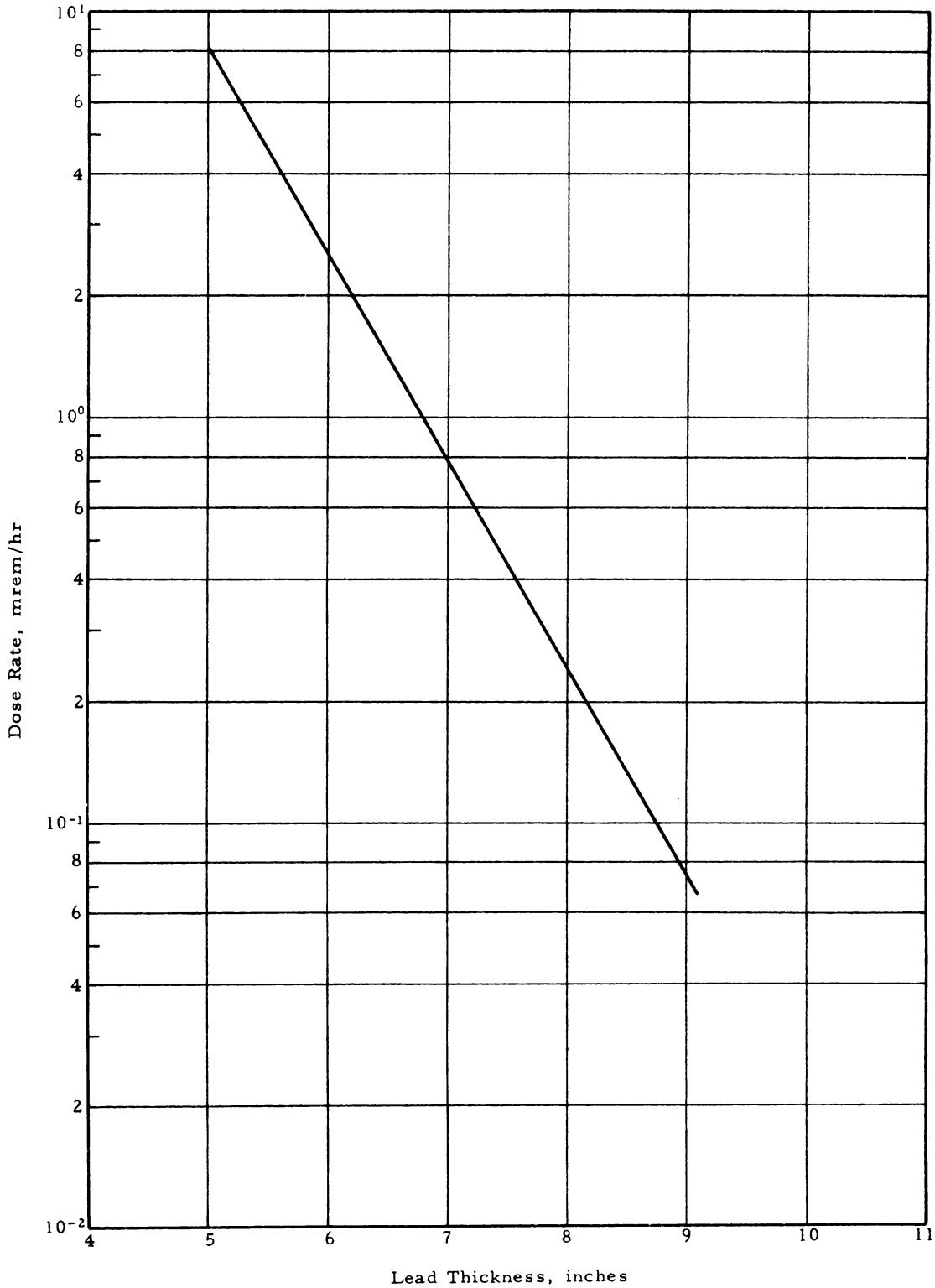

Figure 5-8. Dose Rates From Fission Products in Loop Trap Through Lead, Dose Point 1 Foot From Shield, 4-Inch Steel and 6-Inch Polyethylene Shields Included

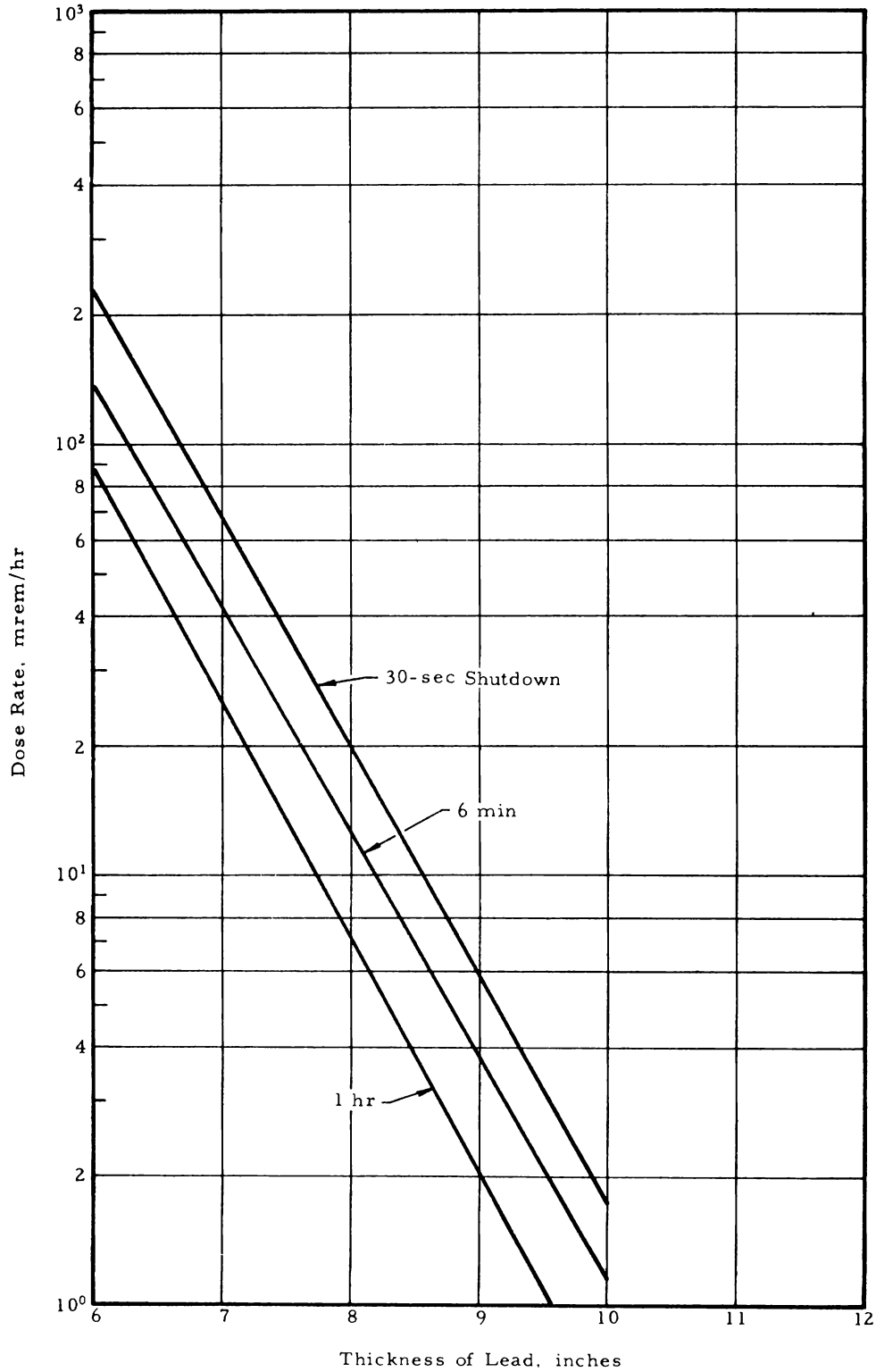

Figure 5-9. Water Required Above a Single Average Fuel Element to Maintain a 50-mrem/hr Surface Dose Rate (Element Vertical)

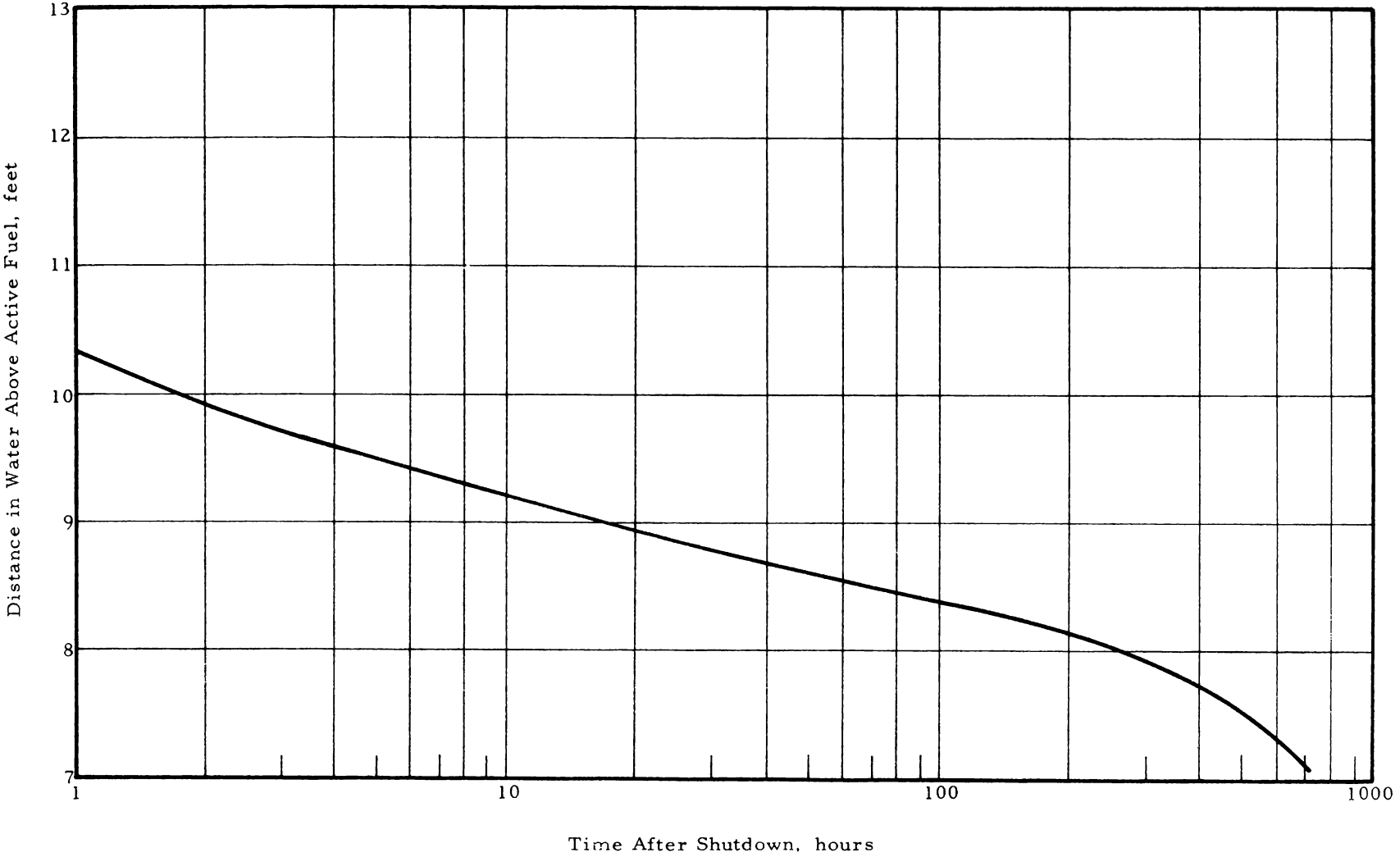

Figure 5-10. Dose Rate Through Canal Wall From a Row of Fuel Elements Along the Mid-Plane of the Elements (15 Days Shutdown, 6 Inches Water Between Elements and Wall)

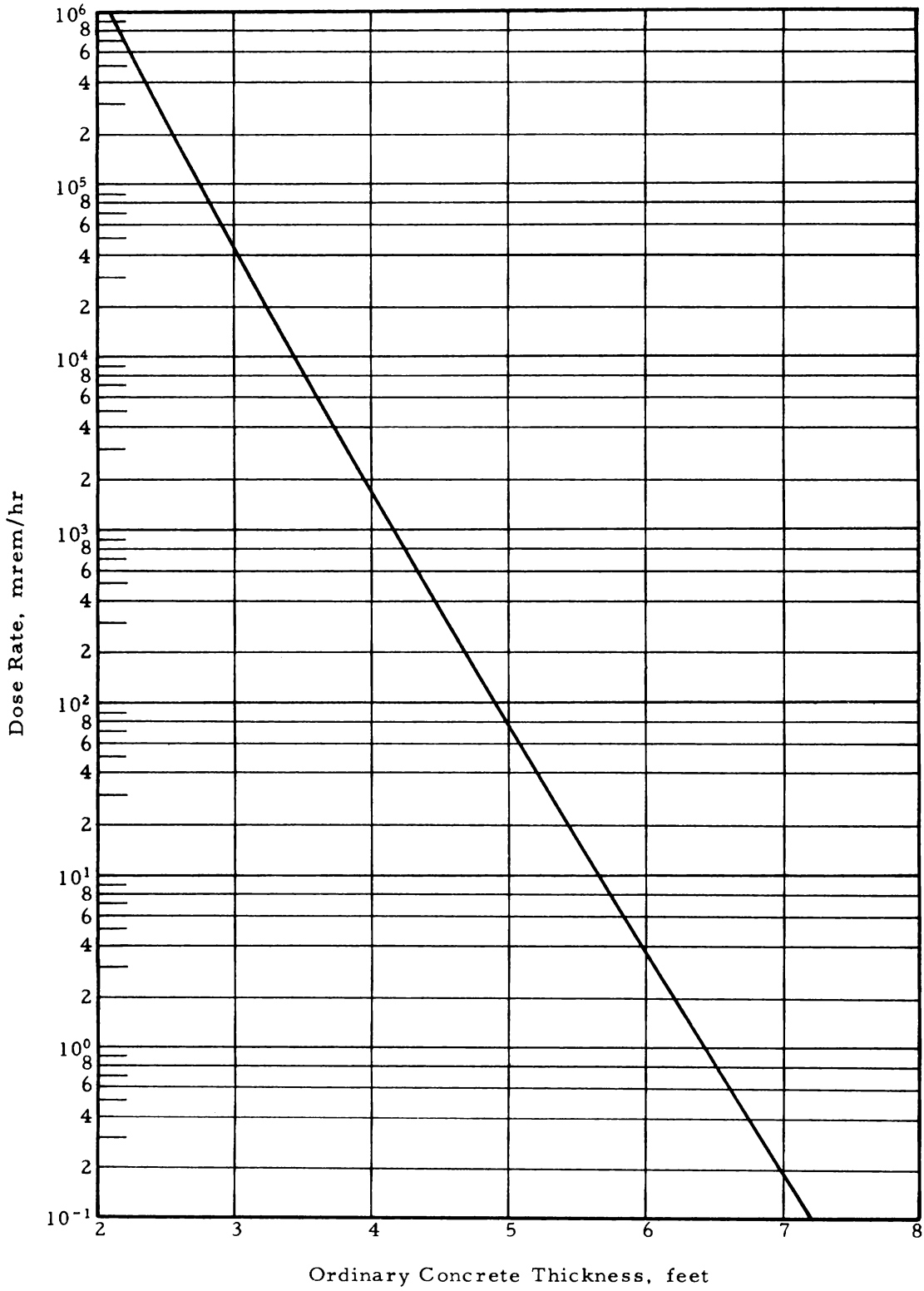

Figure 5-11. Dose Rate From Row of Spent Elements Through Canal Floor (15 Days Shutdown, 6 Inches Water Between Fuel and Floor)

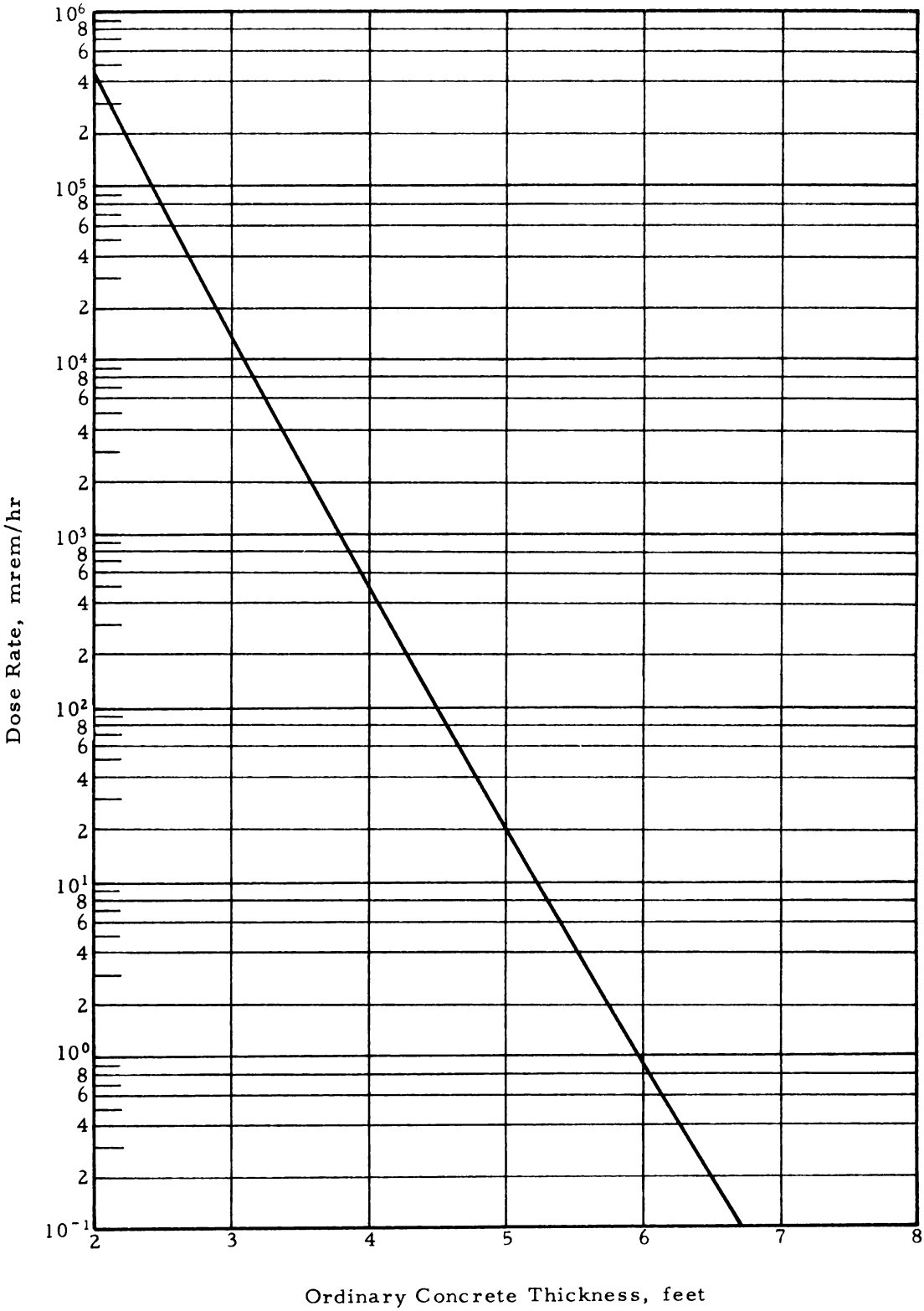

Figure 5-12. Dose Rate in Water Above the ATRC at 5 kw

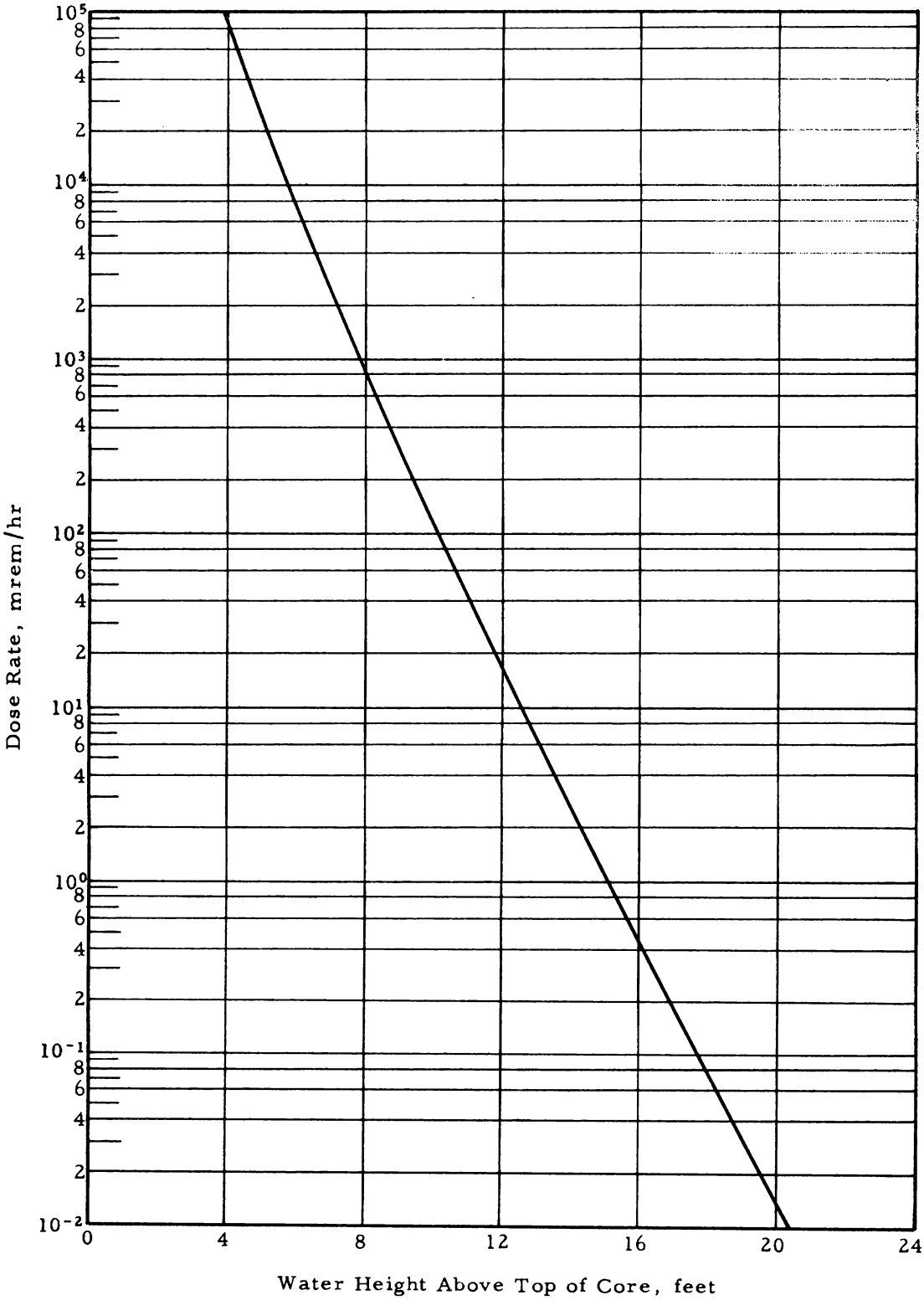

Figure 5-13. Dose Rate Along the Radial Centerline of the ATRC at 5 kw (5 Feet of Water Between Core Center and Pool Wall)

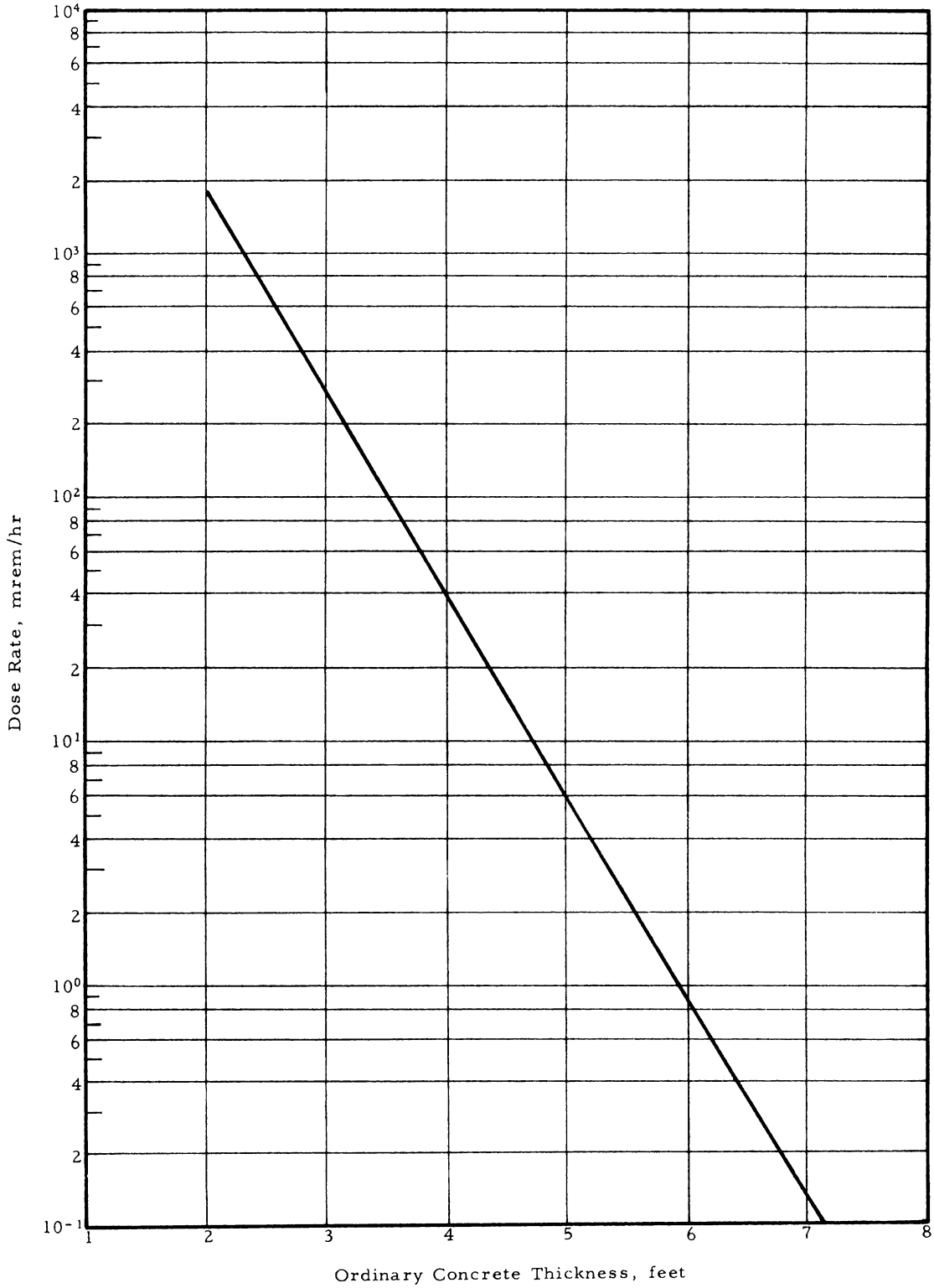

Figure 5-14. Dose Rate From ATRC at 5 kw Through Bottom of Pool (5 Feet of Water Between Core and Pool Floor)

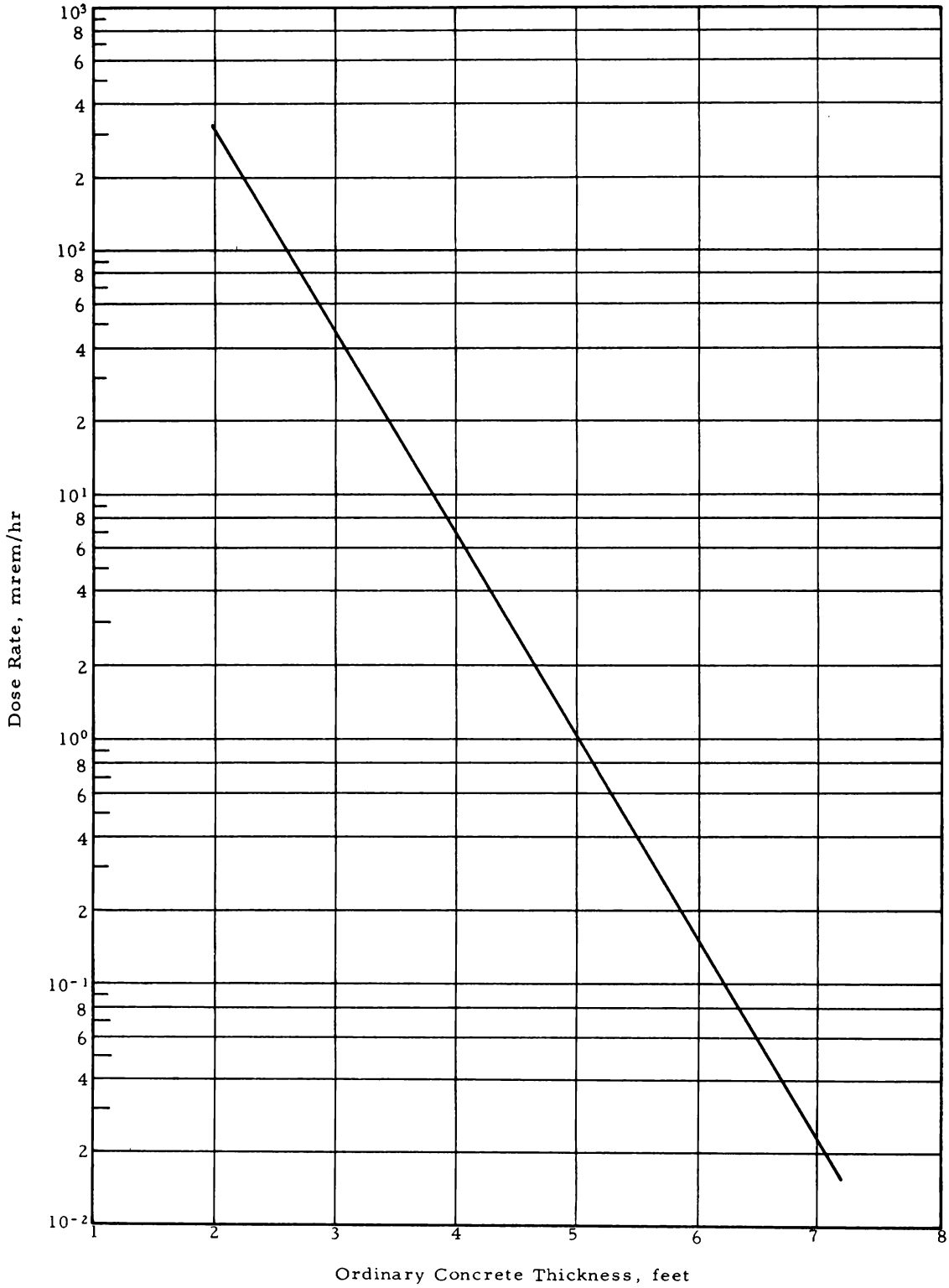

Figure 5-15. Dose Rate Through Canal Wall From a Single Fuel Element Along the Mid-Plane of the Element (12 Hours Shutdown, 6 Inches Water Between Element and Wall)

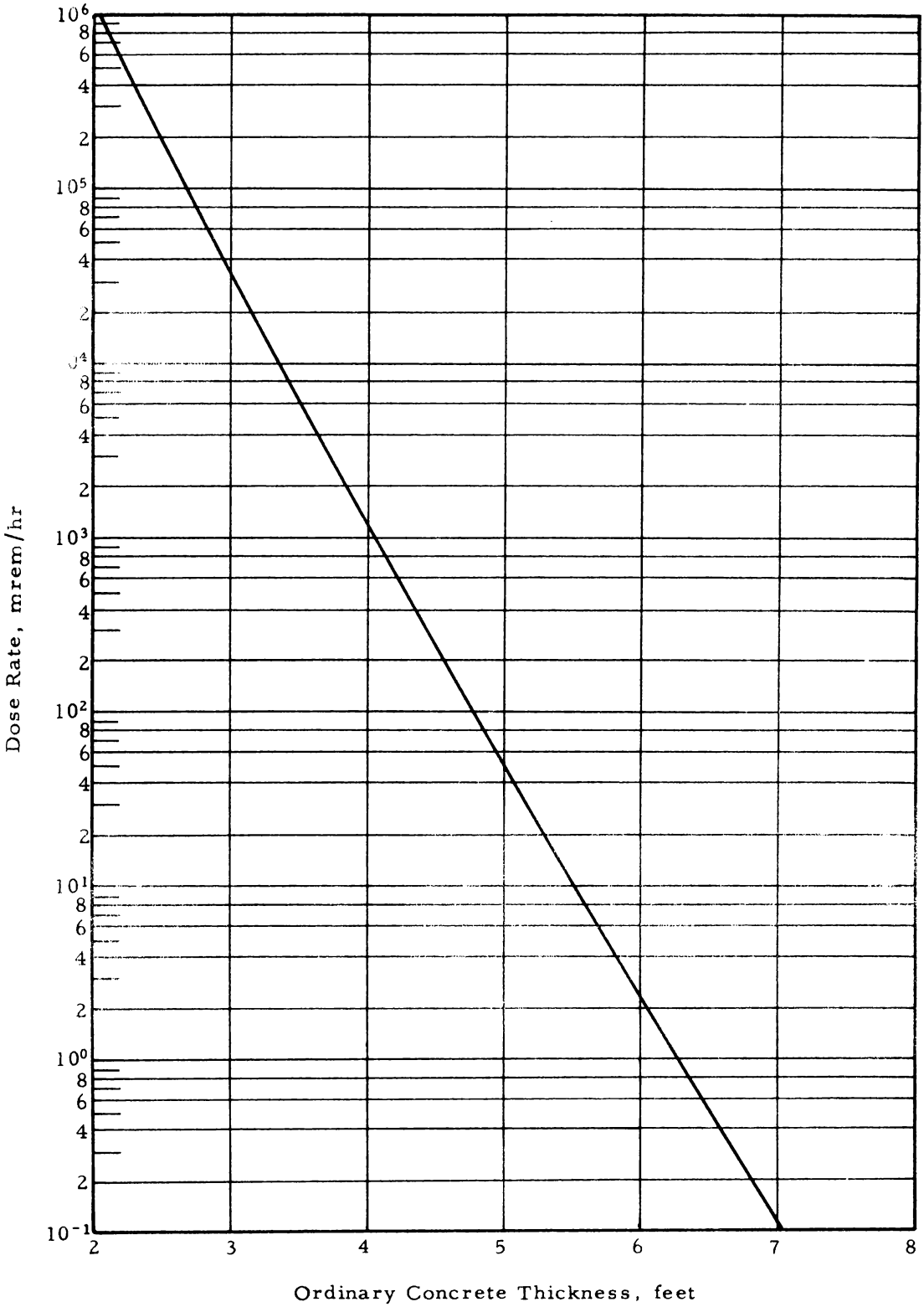

Figure 5-16. Dose Rates From Primary Pipes Through the Pipe Tunnel Walls

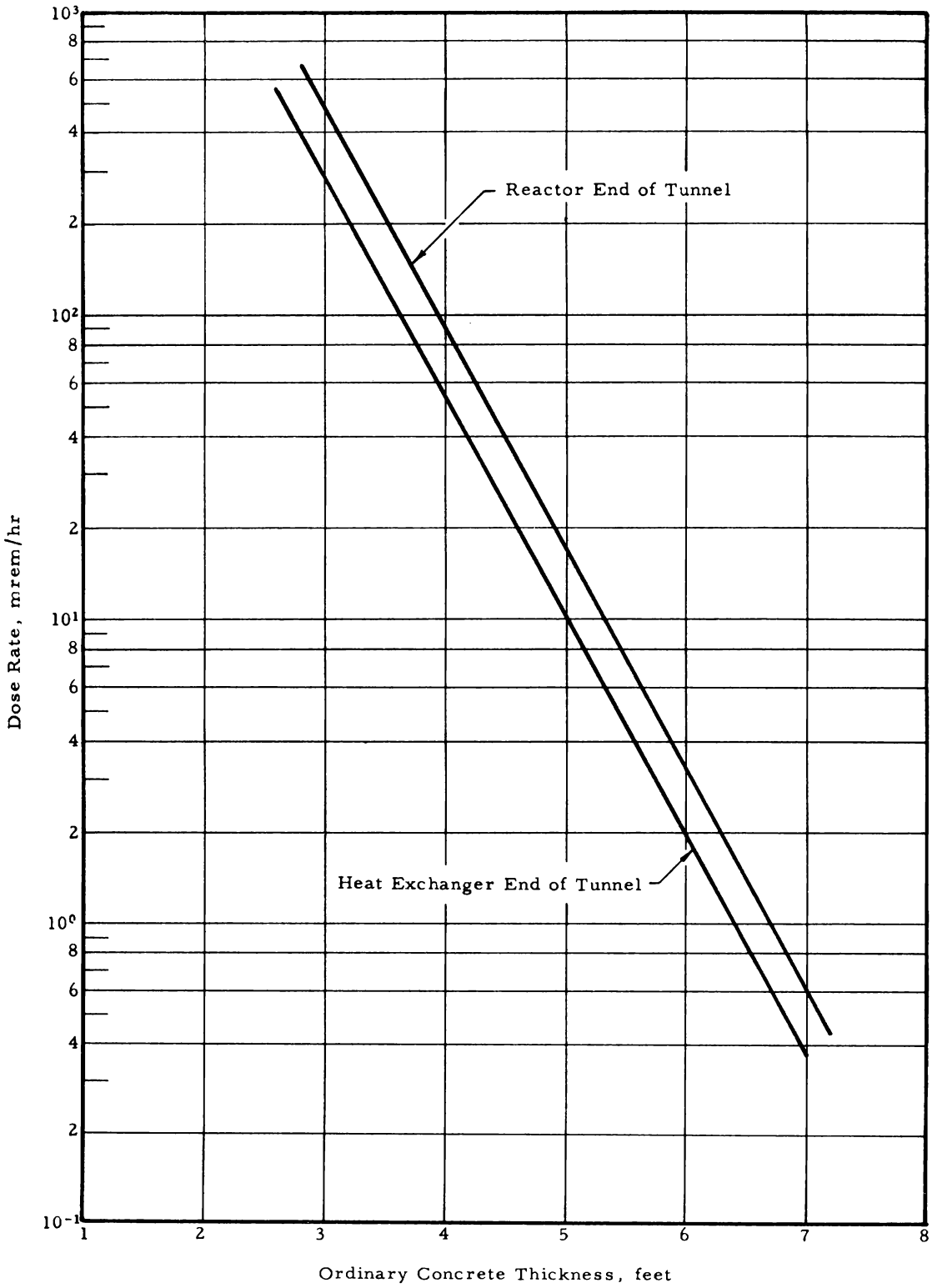

Figure 5-17. Dose Rates Through a Concrete Shield Wall From All Heat Exchangers

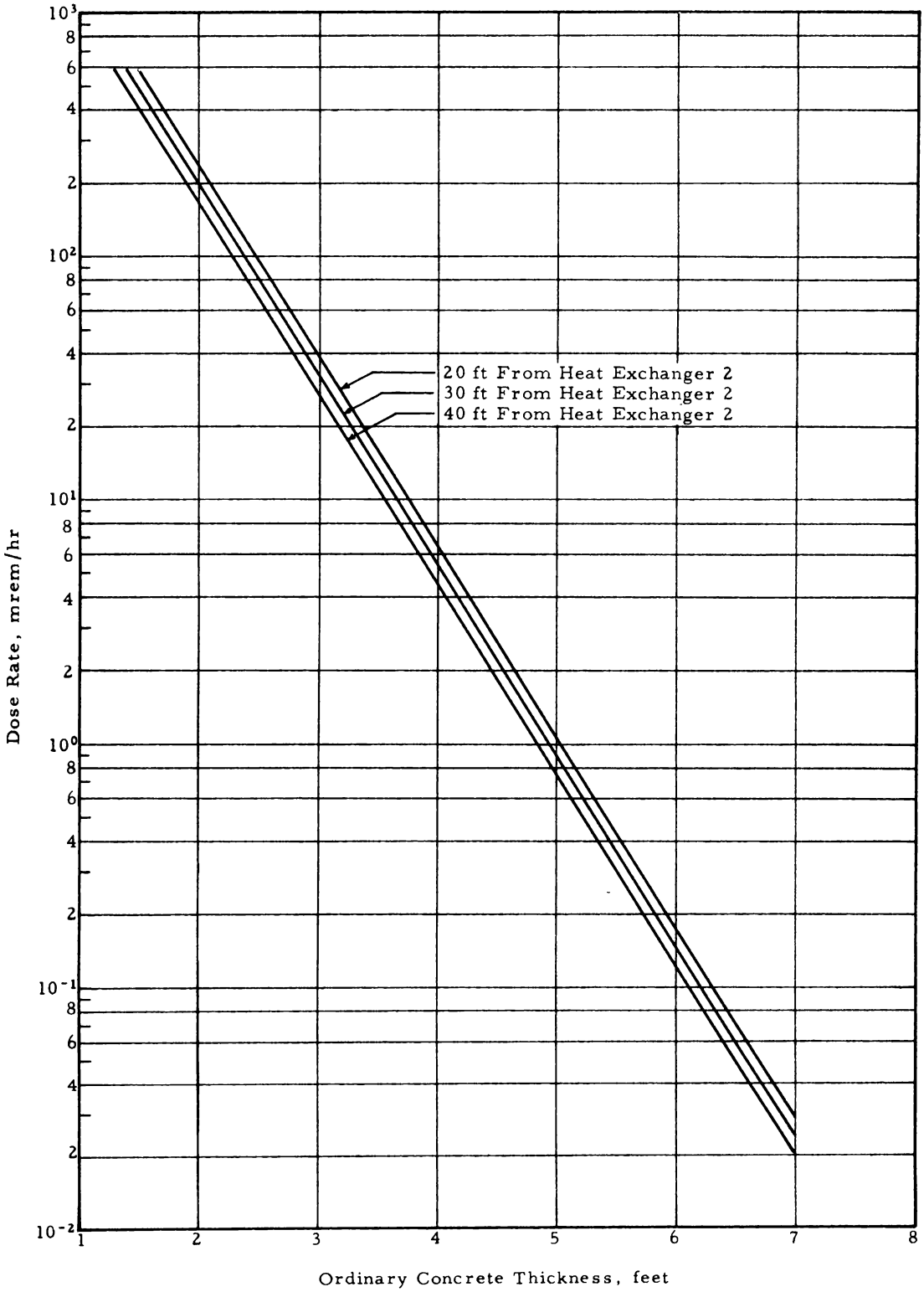

Figure 5-18. Dose Rates From All Pipes in Heat Exchanger Room Through Concrete Shield Wall

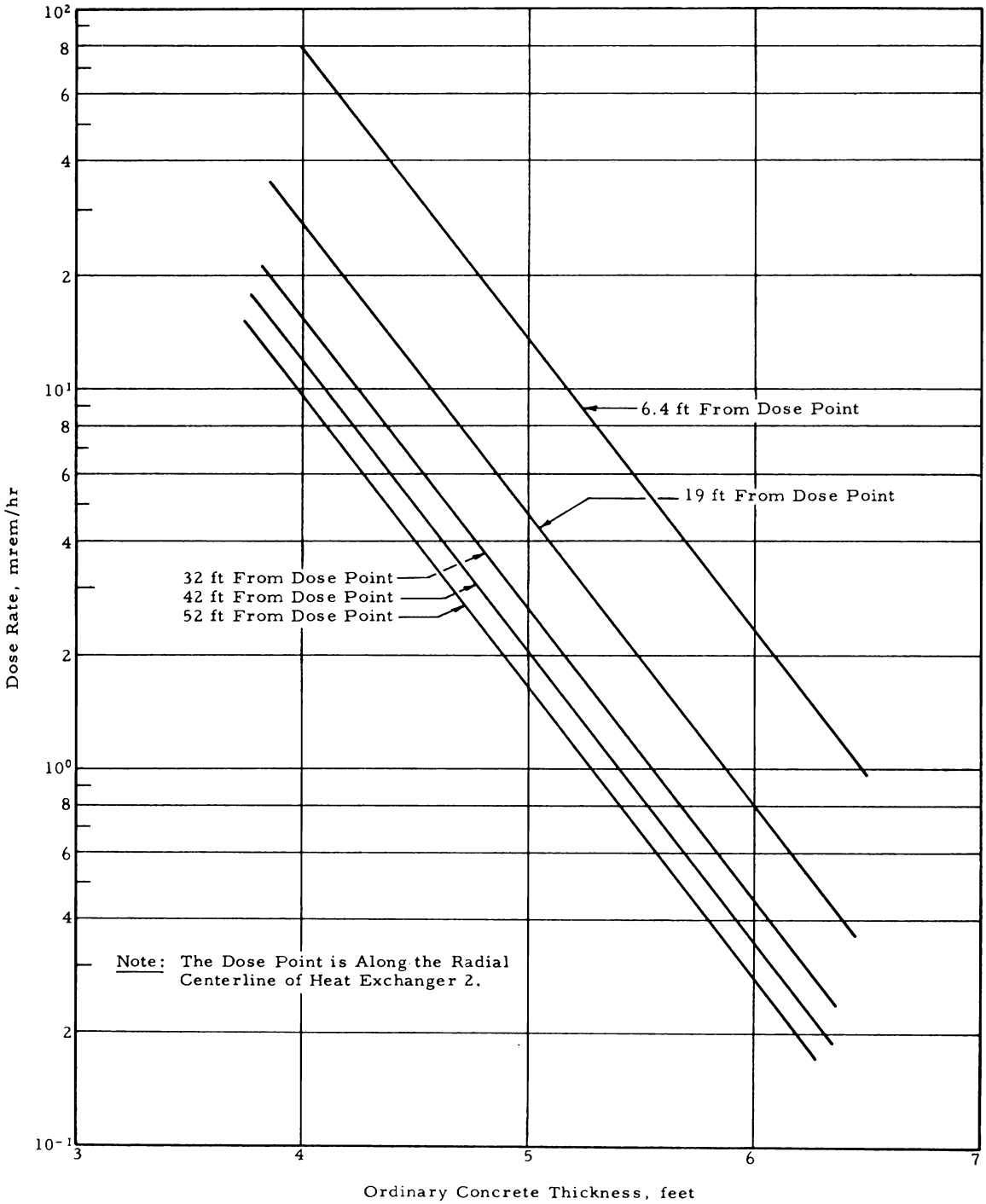

Figure 5-19. Dose Rate From a Primary Pump Through Concrete Shield Wall

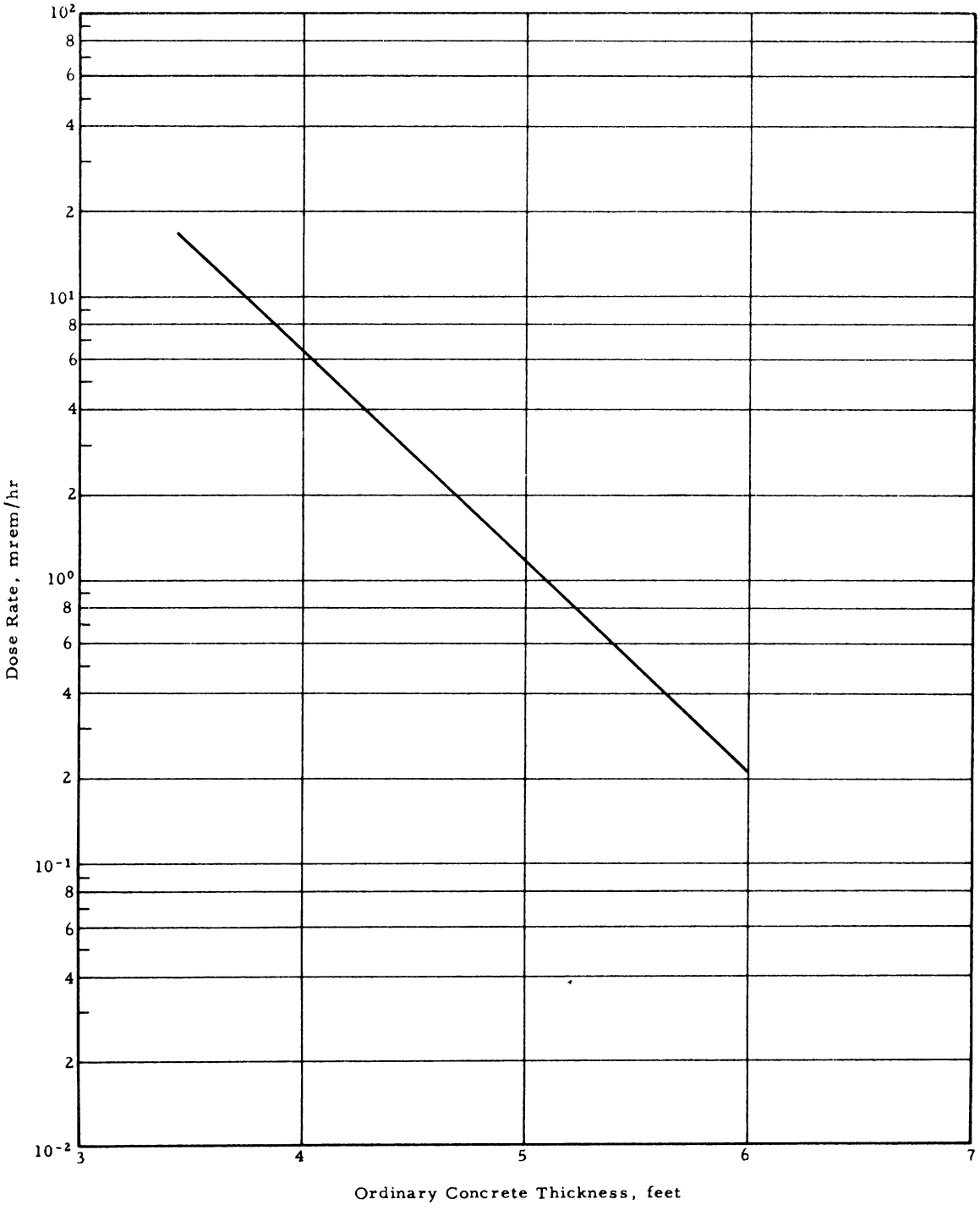

Figure 5-20. Dose Rate in Pump Room 2 From Heat Exchangers and Piping (Dose Rate From Adjacent Pumps Not Included)

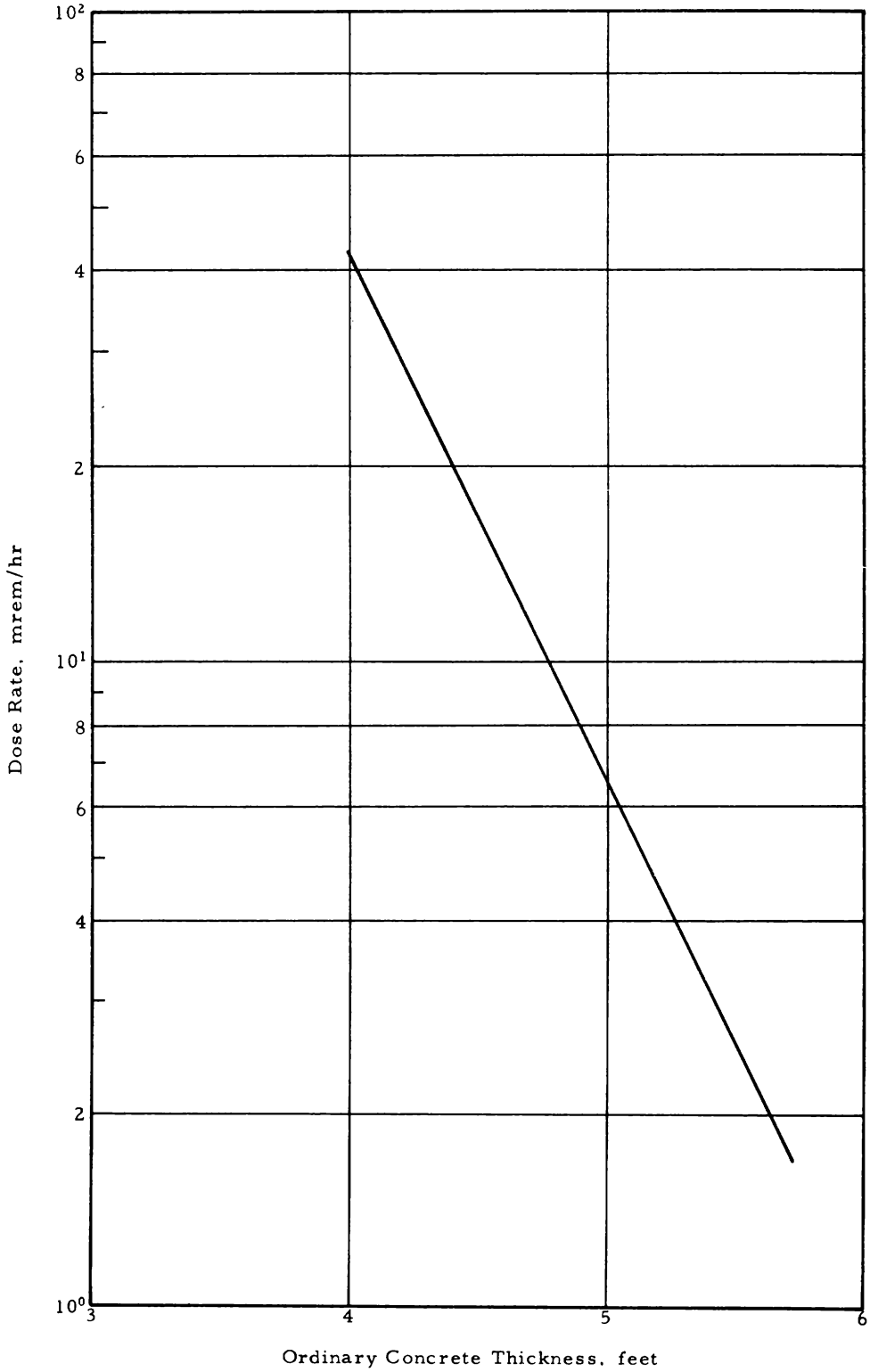

Figure 5-21. Total Dose Rate Through the Ceiling of Heat Exchanger Room at a Point Above Heat Exchanger 2

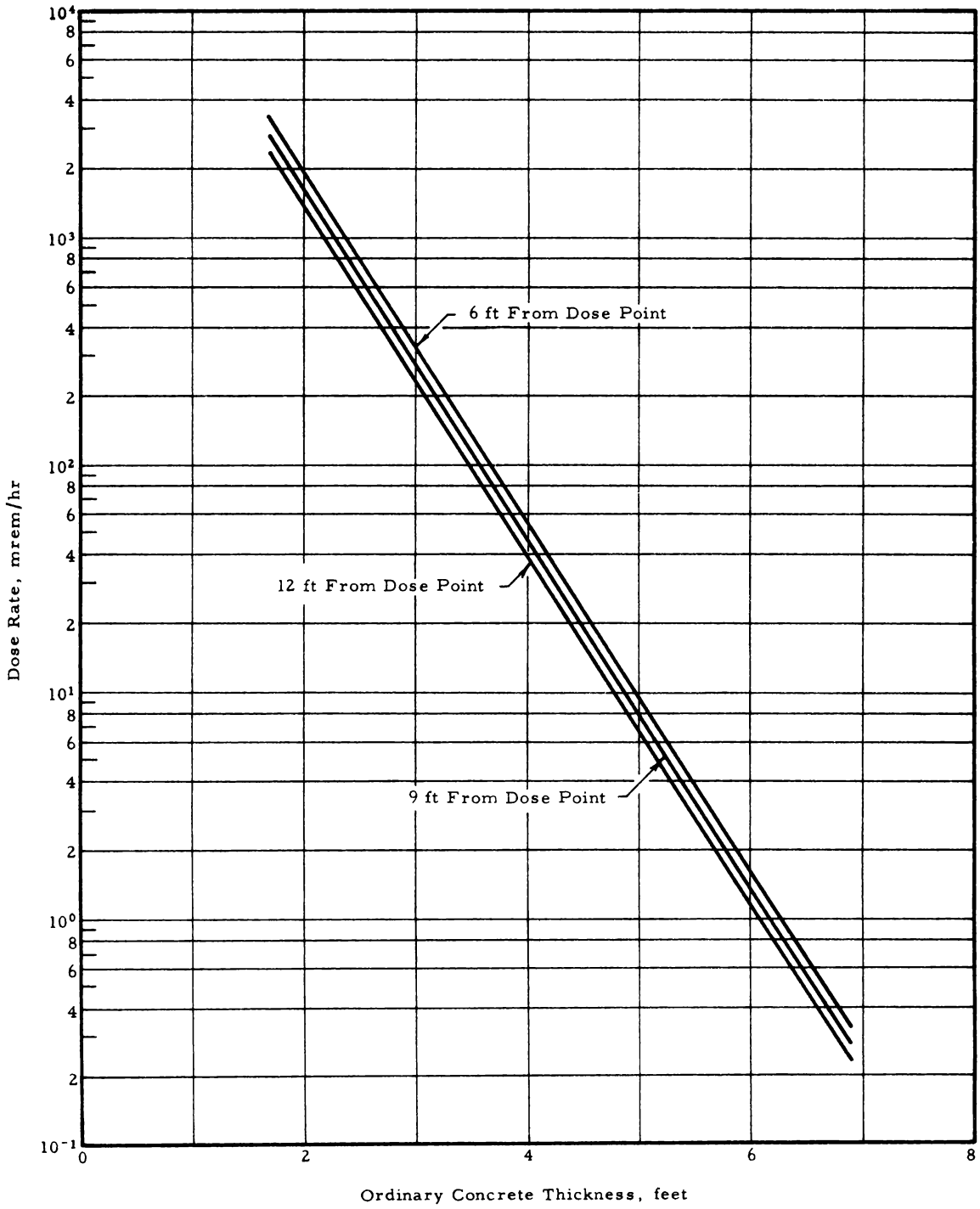

Figure 5-22. Thickness of Magnetite Concrete Required for a Dose Rate of 2.5 mrem/hr From Two Test Loop Pipes Containing N-16

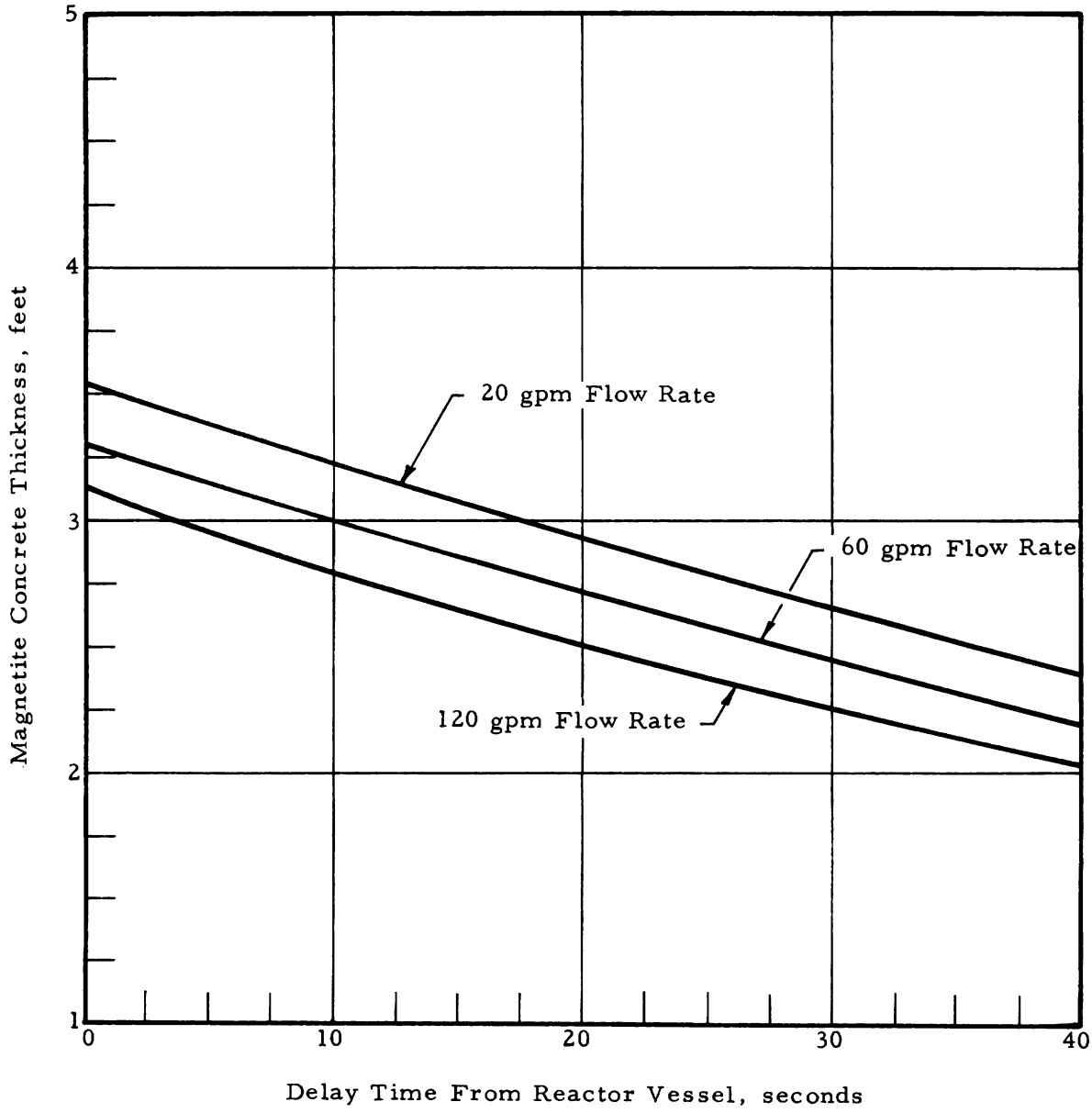

Figure 5-23. Dose Rate From Fission Products Uniformly Dispersed in Test Loop Through 3 Feet of Magnetite Concrete

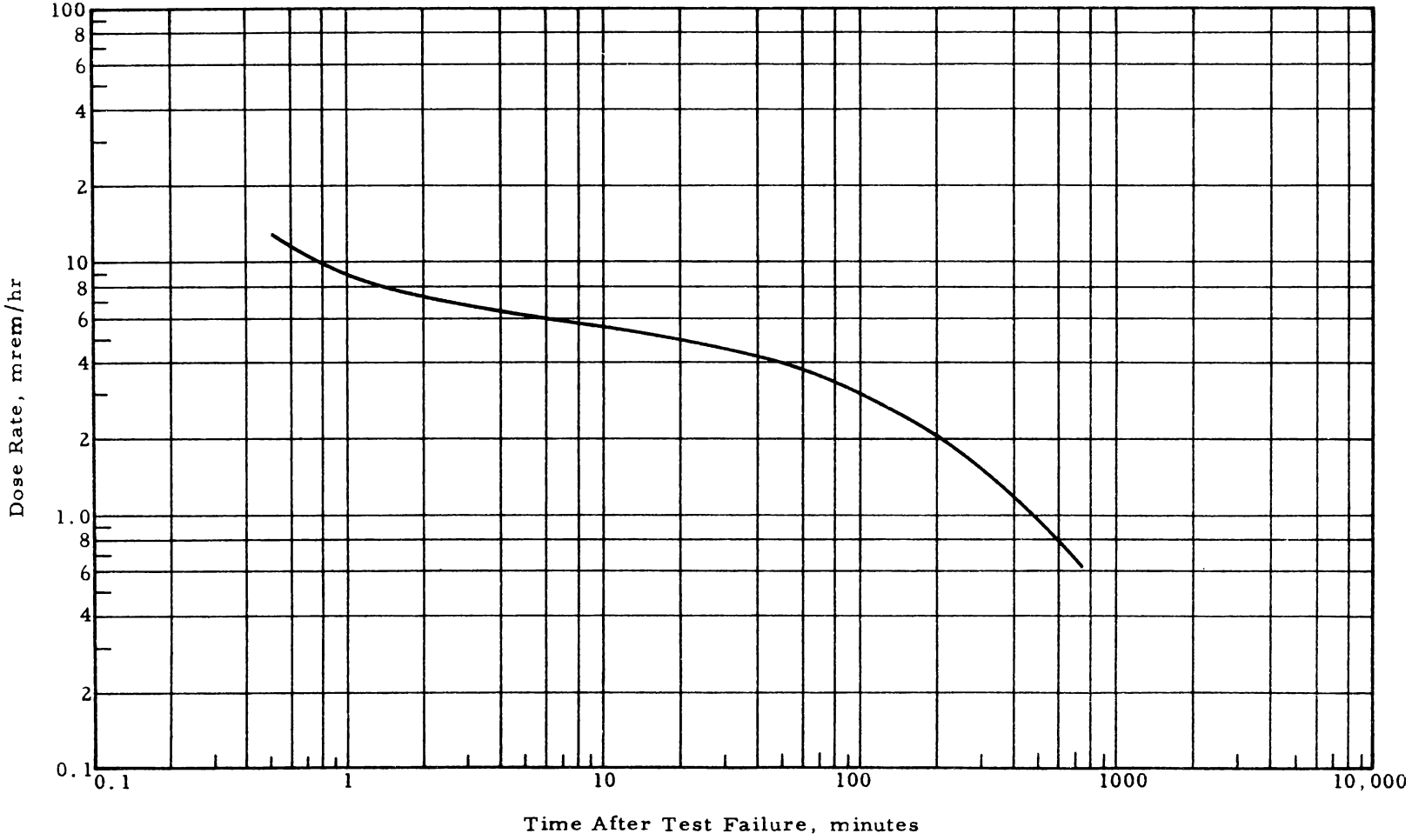

Figure 5-24. Thickness of Lead Shielding Required Around Reactor Vessel for a 12.5-mrem/hr Dose Rate in Capsule Trench From Spent Fuel in Core and Storage Rack Vs Shutdown Time

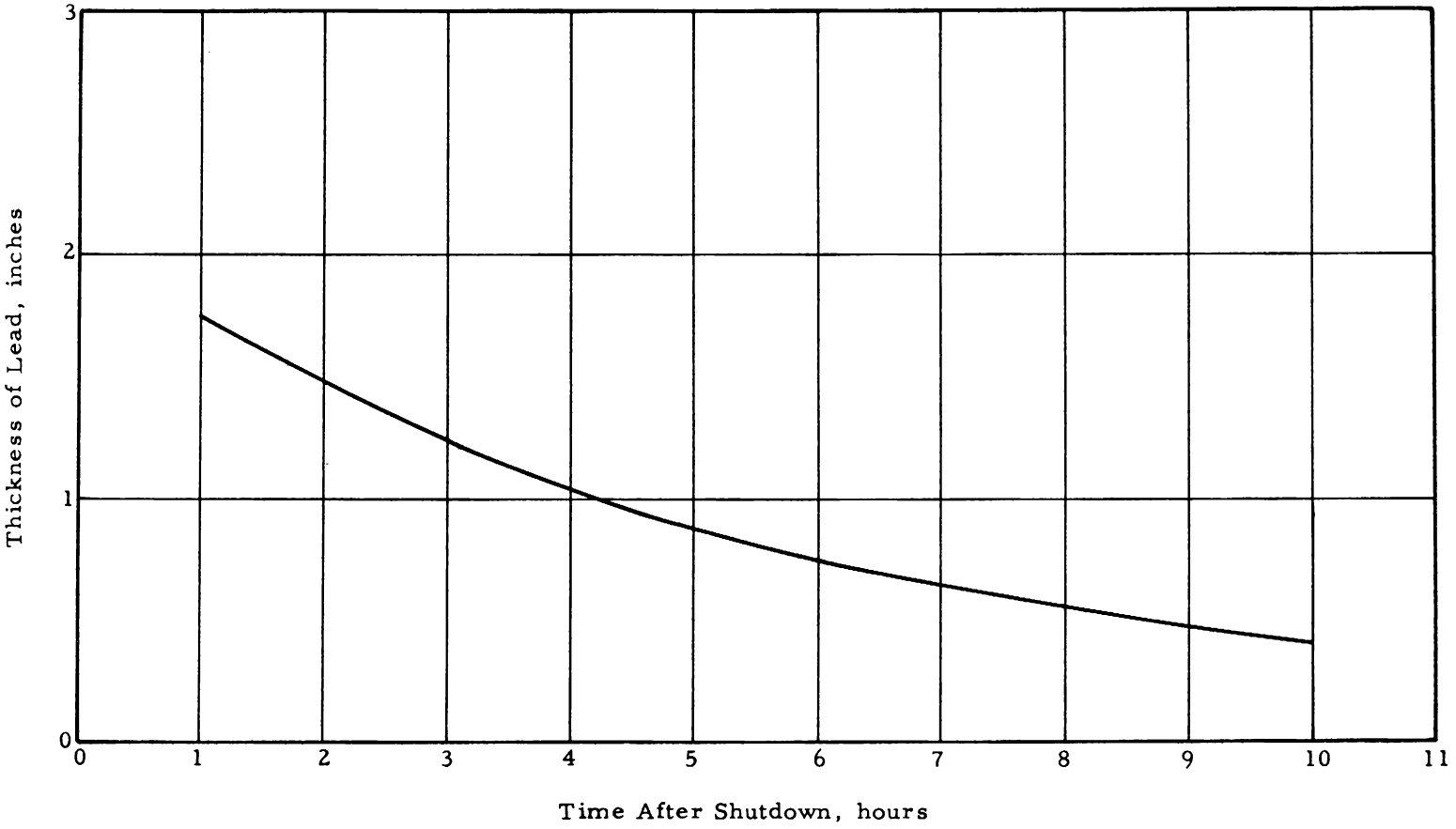

6. MATERIALS ACTIVATION

The calculations of dose rates from activated core components and internals were accomplished by both manual and computer methods. The computer programs utilized were DER-013 and DER-074. A discussion of the methods of these two programs is found in the Appendixes.

6.1. Outer Aluminum Reflector Blocks

The outer aluminum reflector blocks are composed of segments 4 inches square and 4 feet long. They are made of 6061-T6 aluminum, which has the following composition:

Element	Analysis, wt %
Si	0.4 - 0.8
Fe	0.7
Cu	0.15 - 0.4
Mn	0.15
Mg	0.8 - 1.2
Cr	0.15 - 0.35
Zn	0.25
Ti	0.15
Al	Remainder

Since the reflector block removal will be accomplished by removing individual segments through the drop-tube, the dose rates were calculated through water for a single activated segment of the aluminum reflector block. The volumetric activity of the aluminum for each of the above elements was calculated for three shutdown times. The source strength due to an activated element is:

$$S_v = \phi \frac{\rho N \sigma}{A} (W_f) (I_f) Y(E) (1 - e^{-\lambda t_1}) e^{-\lambda t_2}$$

where

ϕ = thermal neutron flux, n/cm^2-sec

ρ = density of element, gm/cm^3

N = Avogadro's number (6.03×10^{23})

σ = microscopic cross section, cm^2

A = atomic weight

W_f = weight fraction of the element in the material

I_f = isotopic fraction of parent element

Y = gamma yield per disintegration

λ = disintegration constant, cm^{-1}

At shutdown the majority of the activity of the reflector block is due to Mn-56 activation and to Na-24 produced by the fast reaction Al-27 (n, α) Na-24. Mn-56 has a half-life of 2.5 hr and disintegration energies of 2.98, 2.13, 2.65, 1.81, and 0.845 mev. Na-24, however, has a 15.1-hr half-life and 2.75- and 1.37-mev gamma energies. Hence, after about 12 hours shutdown the Na-24 activity dominates. Using these activities as source inputs in DER-013, the dose rate from a 4-inch-square, 4-foot-long reflector block segment was calculated. A cosine distribution was applied to the source strengths in the axial direction, and the thermal neutron flux shape was applied in the radial direction. The exponential dose buildup of water was used. In the calculations it was assumed that the core had been operated at 250 MW and that the reflector blocks had remained in position for 2 years or more.

The dose rates from a single segment of the reflector block are shown in Figure 6-1 as a function of shield water thickness for four shutdown times.

6.2. Beryllium Reflector Blocks

The beryllium reflector is composed of the following elements in the weight percentages indicated:

Element	Analysis, wt %
Be	98.4
C	0.13
Fe	0.16

Element	Analysis, wt %
Al	0.05
Si	0.05
Mg	0.08
B	1.2×10^{-4}
Cd	1×10^{-4}
Li	5×10^{-5}
Other	0.04

Fe-58 was found to be the element of primary importance in the beryllium activation, since the other elements either activate weakly or decay rapidly. The Fe-58 activates by neutron absorption to Fe-59, which has a half-life of 45 days and emits gamma radiation of about 1.3-mev energy. Hence, the Fe-59 activation problem cannot be reasonably handled by increasing the time between core shutdown and reflector removal. However, the anticipated 2-day shutdown will be more than adequate to permit the decay of the shorter half-life elements such as aluminum and magnesium, which activate highly. The beryllium reflector blocks will be removed from the vessel through the top head, and shielding will be necessary. Dose rates from an activated reflector block were computed as a function of lead thickness around the reflector. Computer program DER-013 was employed in the calculation, utilizing a quarter of a hollow cylinder as the geometrical model. The outer radius of the hollow cylinder was 64 cm, and an inner radius of 36 cm was calculated to represent an average of the nonuniform inner radius. The volumetric source strength of the Fe-59 in the beryllium at the core mid-plane was found to be 3.4×10^8 photons/cc-sec near the outer edge of the reflector. A cosine distribution was applied to the source strengths in the axial direction, and the thermal neutron flux shape predicted by the multigroup program was used in the radial direction. The dose buildup factors for lead were used in the program.

Figure 6-2 shows the dose rate in air as a function of lead thickness at a distance of 20 feet from a 90° segment after 2 years of core operation at 250 MW.

6.3. Neck Shim Rods and Regulating Rods

The neck shim rods and regulating rods are made of hafnium. The cross section data on individual hafnium isotopes for neutrons above the thermal energy group is incomplete, but from available information it was estimated that these epithermal neutrons do not contribute significantly to the hafnium activation. The hafnium activation was considered mainly due to the following interactions:

Reaction	Energy, mev	Product half-life	Gamma photon yield
Hf-174 (n, γ) Hf-175	0.430	70 days	0.015 0.975
Hf-179 (n, γ) Hf-180	0.444 0.333 0.216	5.5 hr	0.80 0.20 0.20
Hf-180 (n, γ) Hg-181	0.482 0.346	44.6 days	0.89 0.132

The activation calculations were made for the worst case, i.e., the active rod fully inserted in the core. It was assumed that the rods had been in the operating core for 6 months or longer. The volumetric activities were computed by the method discussed in Section 6.1. The dose rates from these components were then calculated as a function of shield water thickness and shutdown time using program DER-013. The geometry employed was that of a cylinder 4 feet long and 0.70 inch in diameter. The buildup factors for water were used. Figure 6-3 shows the results of the calculations.

6.4. Outer Shim Control Cylinder

Figure 6-4 shows the dose rate from an activated outer shim control cylinder as a function of shield water thickness for several shutdown times. In the calculations it was assumed that the core was operated at 250 MW and that the outer shim control cylinder had been in the operating reactor for 6 months or longer. The control cylinder is beryllium and has a radius of 3.75 inches except on the segment containing the hafnium, where the radius is 3.5 inches. The hafnium is 0.25 inch thick. The method of calculating the activity and dose rate from the beryllium drum

is the same as that discussed for the beryllium reflector blocks. The hafnium was represented geometrically as a segment of a cylindrical shell. The significant reactions leading to hafnium activation were discussed in the preceding section.

6.5. Flux Trap Fillers and Flux Trap Baffles

The dose rates from the flux trap filler and the flux trap baffle are shown in Figures 6-5 and 6-6, as functions of time after shutdown and shield water thickness. It was assumed in the calculations that the core had been operated at 250 MW and that the baffle and filler had remained in the core for 1 year or longer before being removed. Both of these components are manufactured using 6061-T6 aluminum and were assumed to have been in an average thermal flux of 3.6×10^{14} n/cm^2-sec. The dose rates were calculated as before using DER-013. Volumetric gamma source strengths were obtained from the formula given in Section 6.1. The flux trap filler was represented by an activated aluminum cylinder with a radius of 3.6 cm and a height of 4 feet. The flux trap baffle was treated as a hollow cylindrical source with an inner radius of 6.67 cm, an outer radius of 7.46 cm, and a height of 4 feet. Dose buildup factors of water were used in the program.

6.6. Neck Shim Housing Rod Sleeve

Dose rates from the activated neck shim housing rod sleeve through water for various reactor shutdown times are shown in the following three figures. Figure 6-7 shows the dose rate from an aluminum (6061-T6) rod sleeve which has been in the operating core for 1 year or longer. Figure 6-8 shows the dose rate from an Inconel-X rod sleeve which has been in the core for 1 year, and Figure 6-9 gives the dose rate for an Inconel-X rod sleeve which has been in the operating core for 10 years. The composition of the Inconel-X by weight per cent is as follows:

Element	Weight percent
Ni	70 min
Cr	14 - 16
Ti	2.25 - 2.75
Cb	0.7 - 1.2

Element	Weight percent
Al	0.4 - 1.0
Fe	5 - 9
Mn	0.3 - 1.0
Si	0.5 max
Cu	0.2 max
C	0.8 max
S	0.01 max
Co	0.2

The core power was 250 MW having a cosine axial and a uniform radial distribution. The rod sleeve was assumed to be subjected to an average thermal neutron flux of 3.3×10^{14} neut/cm^2-sec over the periods indicated above. The volumetric source strengths of this activated component were calculated by the methods given in Section 7.1. These were then converted to line source strengths by multiplying by the cross-sectional area of the sleeve. The dose rates from the rod sleeve were obtained by treating the sleeve as a 4-foot-long line source. Dose buildup factors for water were used.

6.7. Neck Shim Housing

Since it is necessary to remove the neck shim housing through the reactor vessel head, the dose rates from this activated component were calculated for varying thicknesses of lead shielding. There are five elements of concern in the 6061-T6 aluminum of the neck shim housing. These elements, their half-lives, and their volumetric source strengths at shutdown, after 5 years of reactor operation, are listed below.

Element	Half-life	Source strengths, photons/cc-sec
Cu-64	12.8 hr	3.32×10^{11}
Fe-59	45 days	4.86×10^{8}
Mn-56	2.6 hr	5.05×10^{11}
Cr-51	27 days	6.76×10^{10}
Zn-65	250 days	1.36×10^{10}

Figure 6-10 shows the dose rate at a distance of 20 feet in air from an activated neck shim housing as a function of lead shielding thickness and shutdown time. Although a 5-year operating time was assumed, the results are not significantly different if the operating time is as short as 1 year, since equilibrium activity is reached in all but one of the elements in this period of time. In this case the source was treated as a small segment of a large hollow cylindrical source with a 4-foot length. Calculations were performed using program DER-013. The average thermal neutron flux over the operating time was assumed in the calculation to be 3.3×10^{14} neut/cm^2-sec.

Figure 6-1. Dose Rate Through Water Along the Radial, Centerline of an Activated Outer Reflector Block

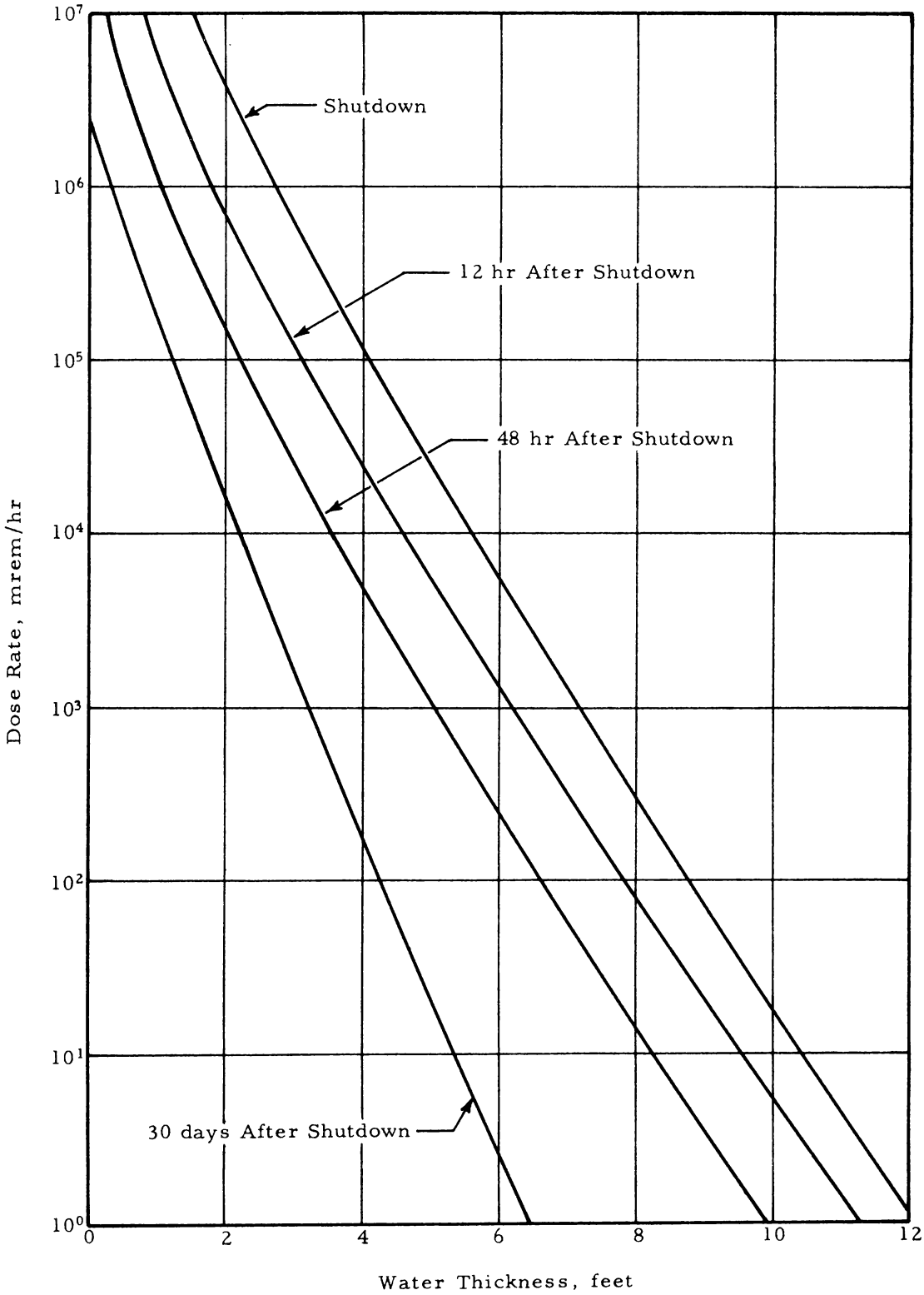

Figure 6-2. Dose Rate (Fe-59 Activity) at 20 Feet in Air From 1/4 of ATR Reflector After 2-Year Operation and 2-Day Shutdown

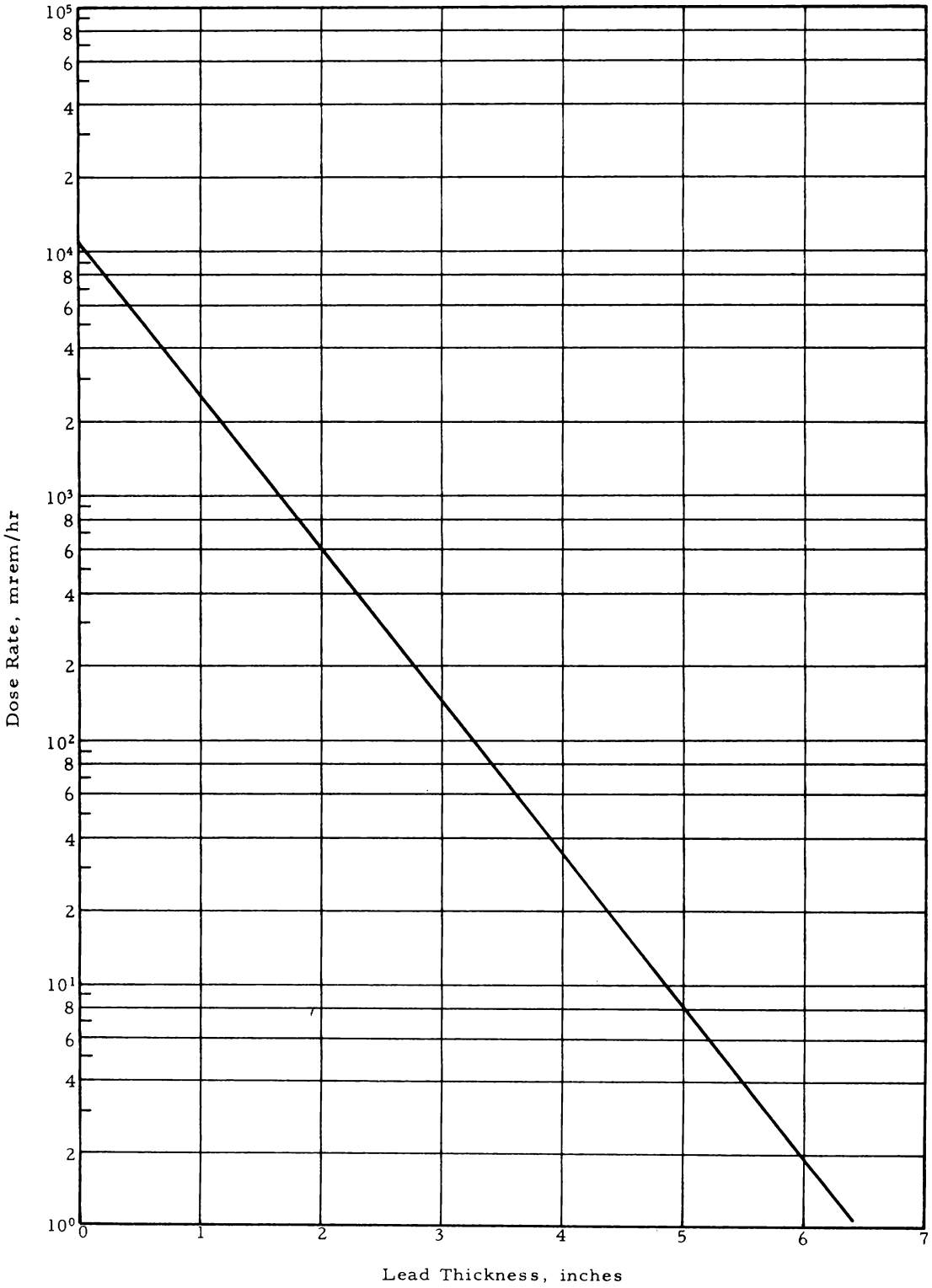

Figure 6-3. Dose Rate Through Water Along the Radial Centerline of an Activated Neck Shim Rod or Activated Regulating Rod

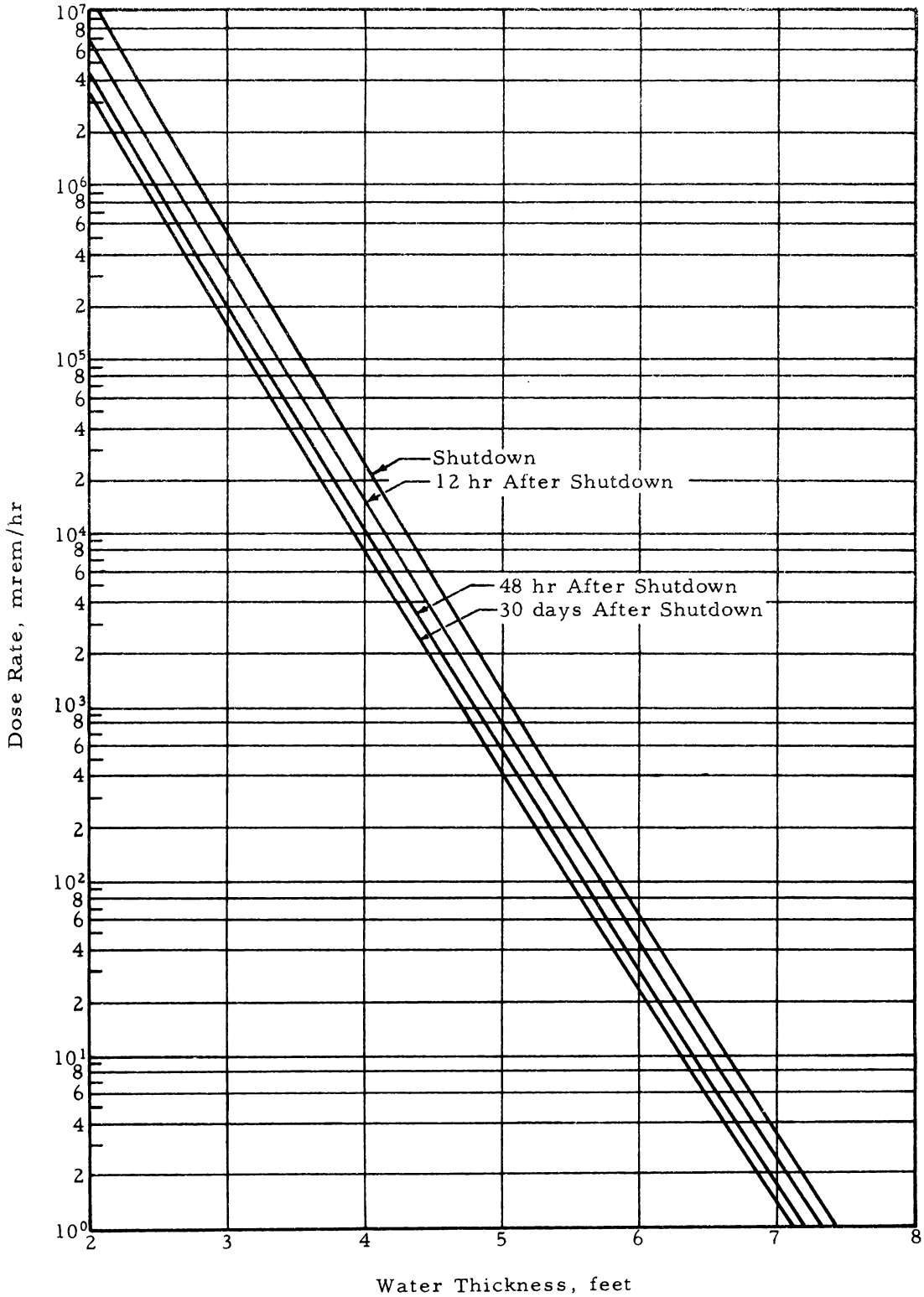

Figure 6-4. Dose Rate Through Water Along the Radial Centerline of an Activated Outer Shim Control Cylinder

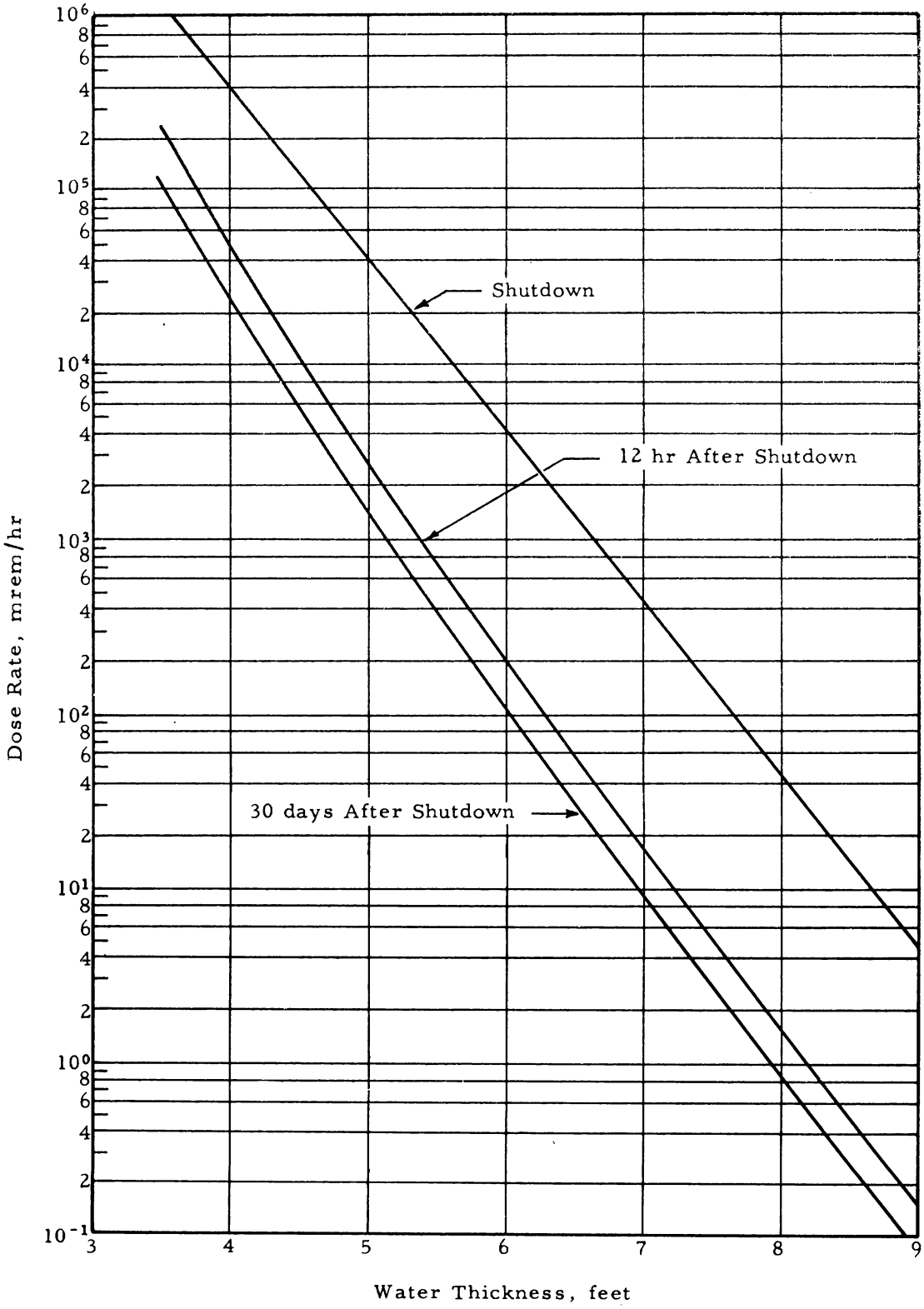

Figure 6-5. Dose Rate Through Water Along the Radial Centerline of an Activated Flux Trap Filler

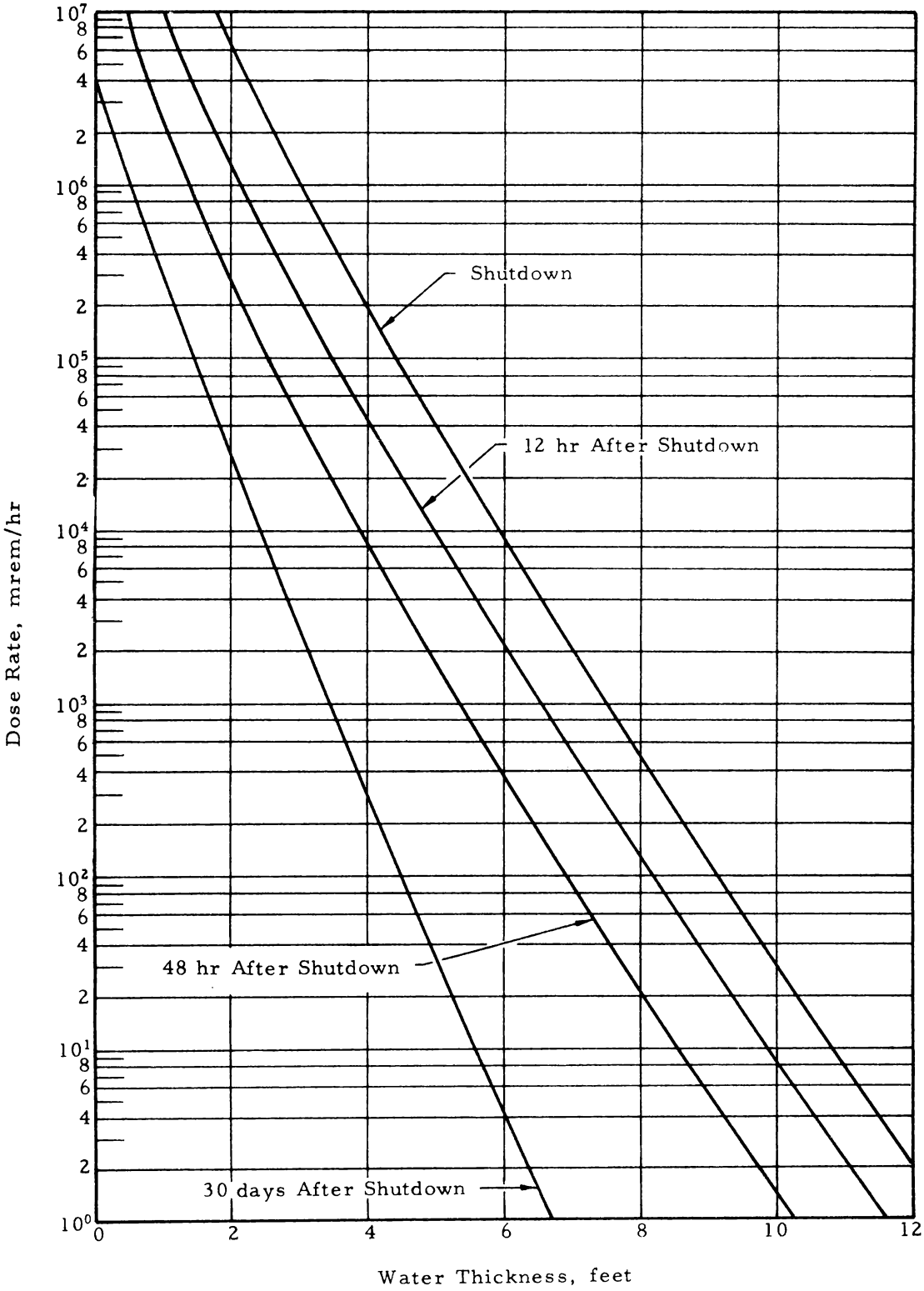

Figure 6-6. Dose Rate Through Water Along the Radial Centerline of an Activated Flux Trap Baffle

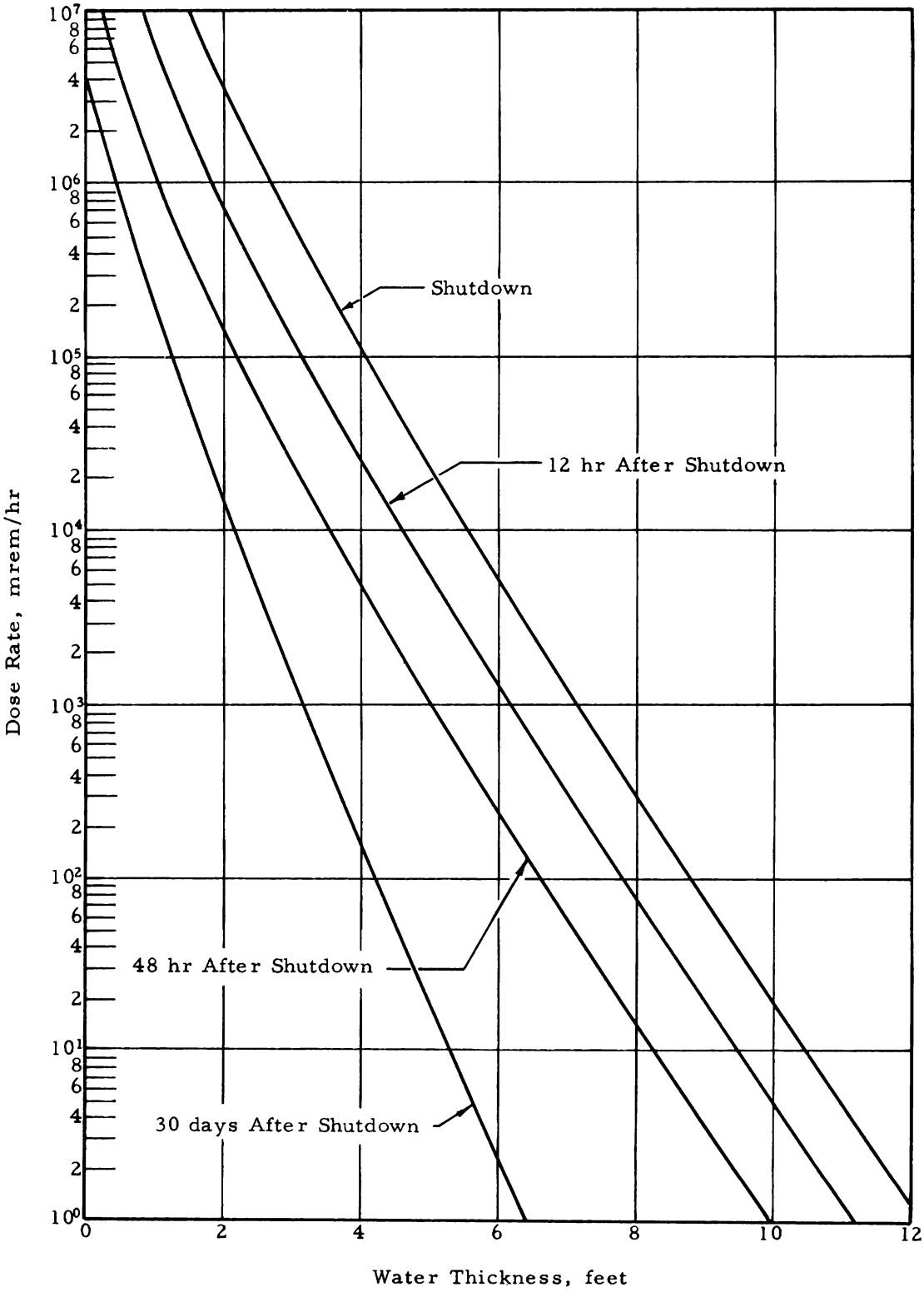

Figure 6-7. Dose Rate Through Water Along the Radial Centerline of an Activated Neck Shim Housing Rod Sleeve (Aluminum) After 1 or More Years Irradiation Time

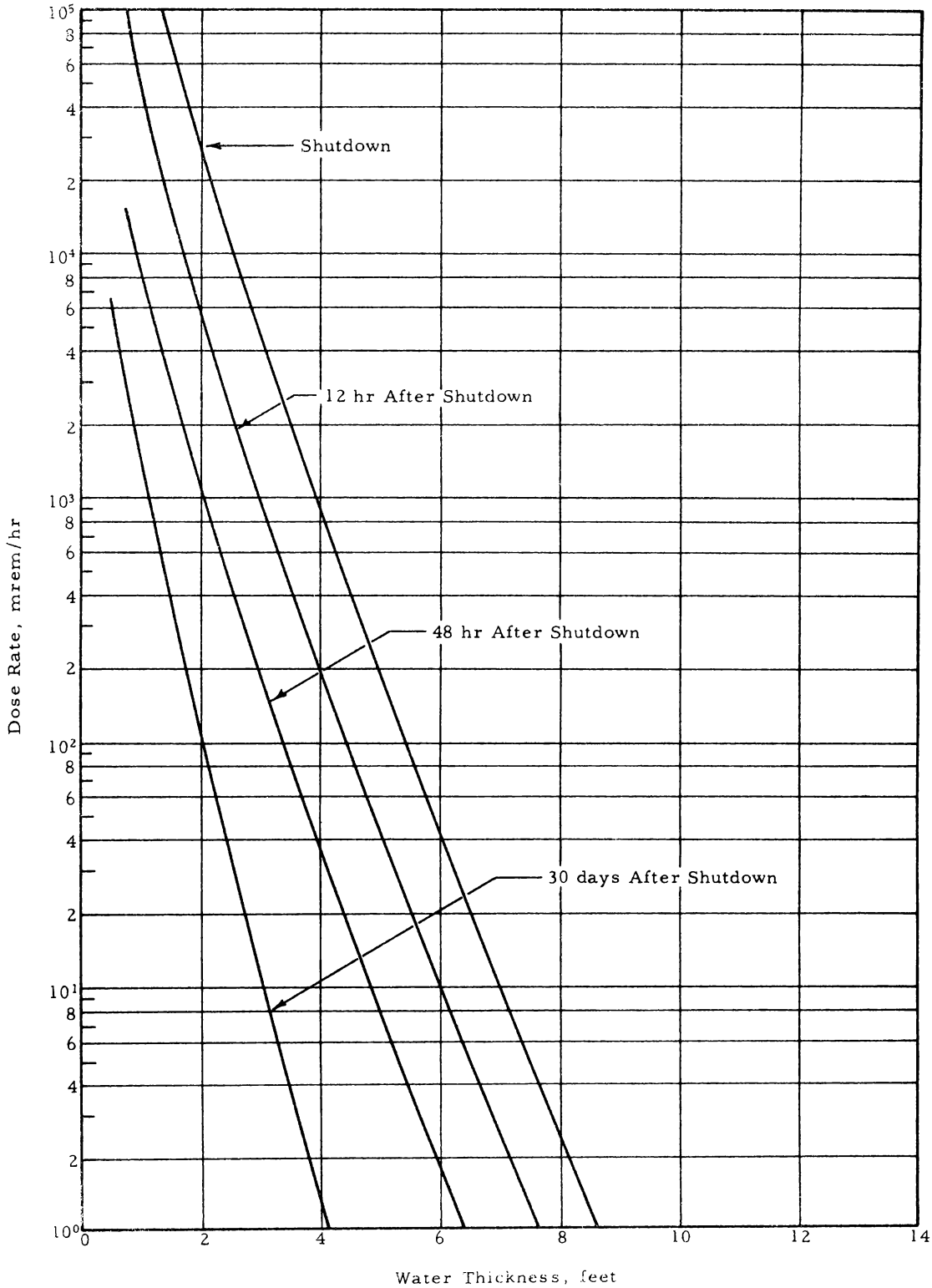

Figure 6-8. Dose Rate Through Water Along the Radial Centerline of an Activated Neck Shim Housing Rod Sleeve (Inconel-X) After 1 Year Irradiation Time

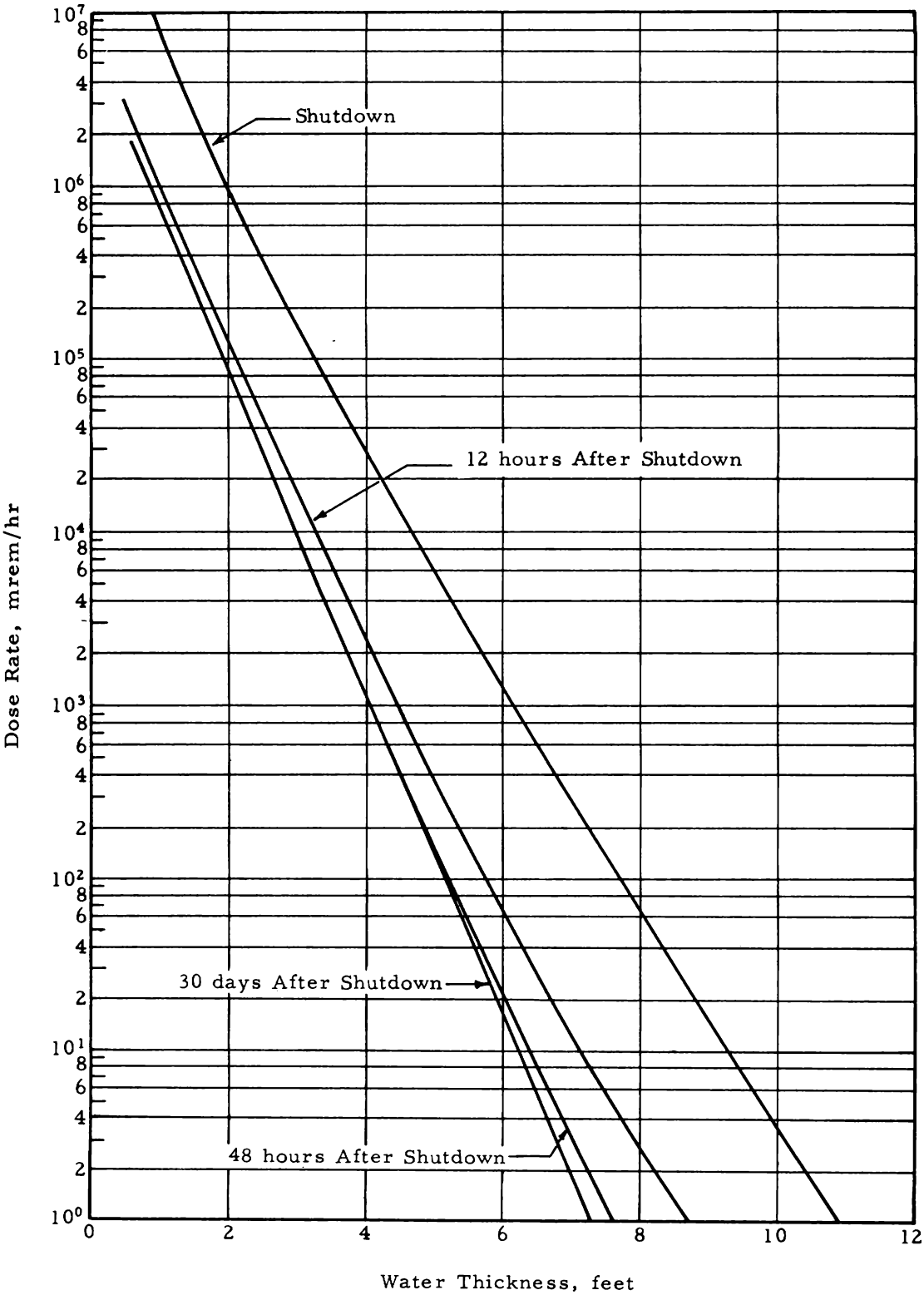

Figure 6-9. Dose Rate Through Water Along the Radial Centerline of an Activated Neck Shim Housing Rod Sleeve (Inconel-X) After 10 Years Irradiation Time

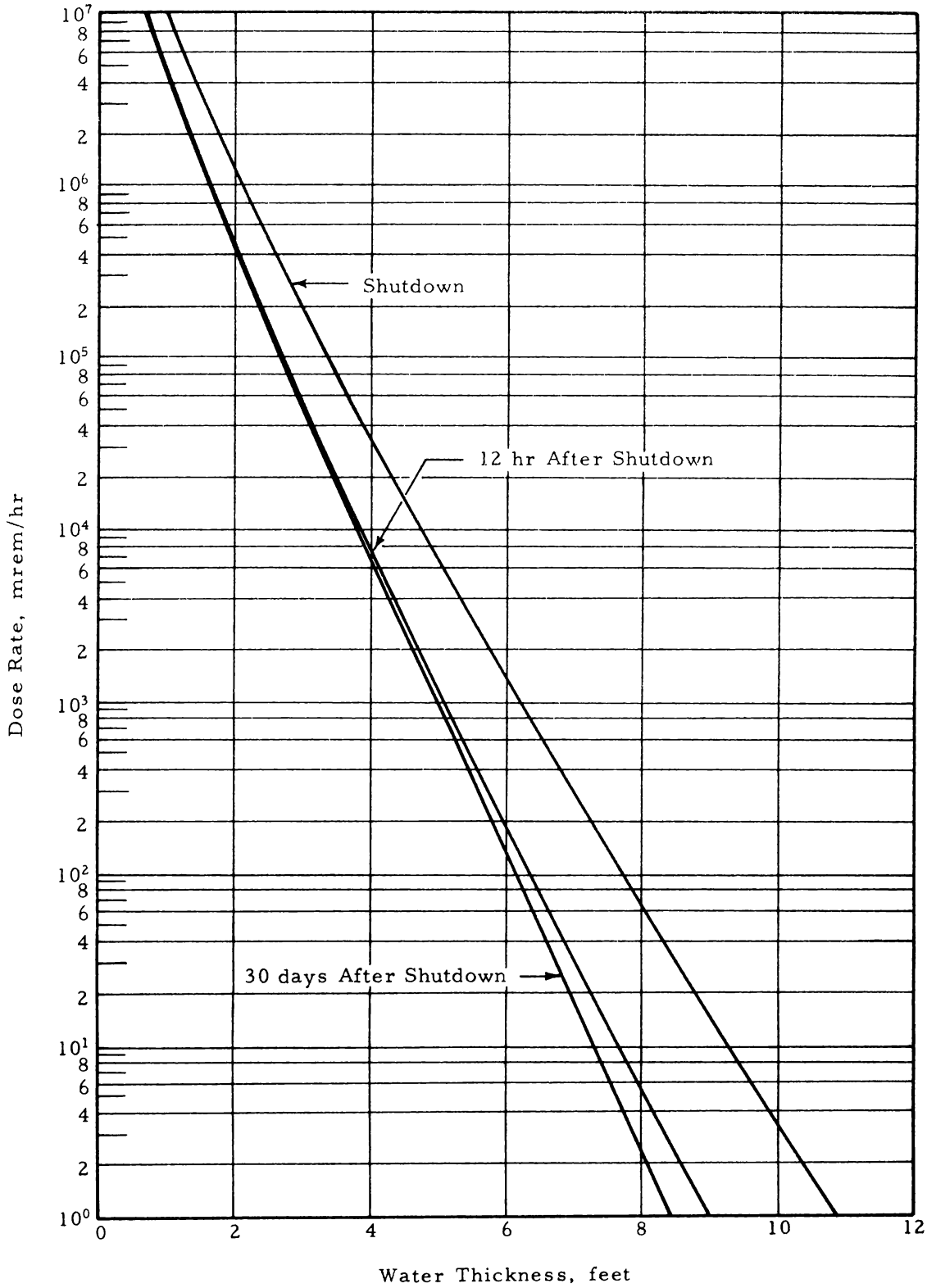

Figure 6-10. Dose Rate 20 Feet Away in Air Along the Radial Centerline of an Activated Neck Shim Housing After 5 Years Irradiation Time

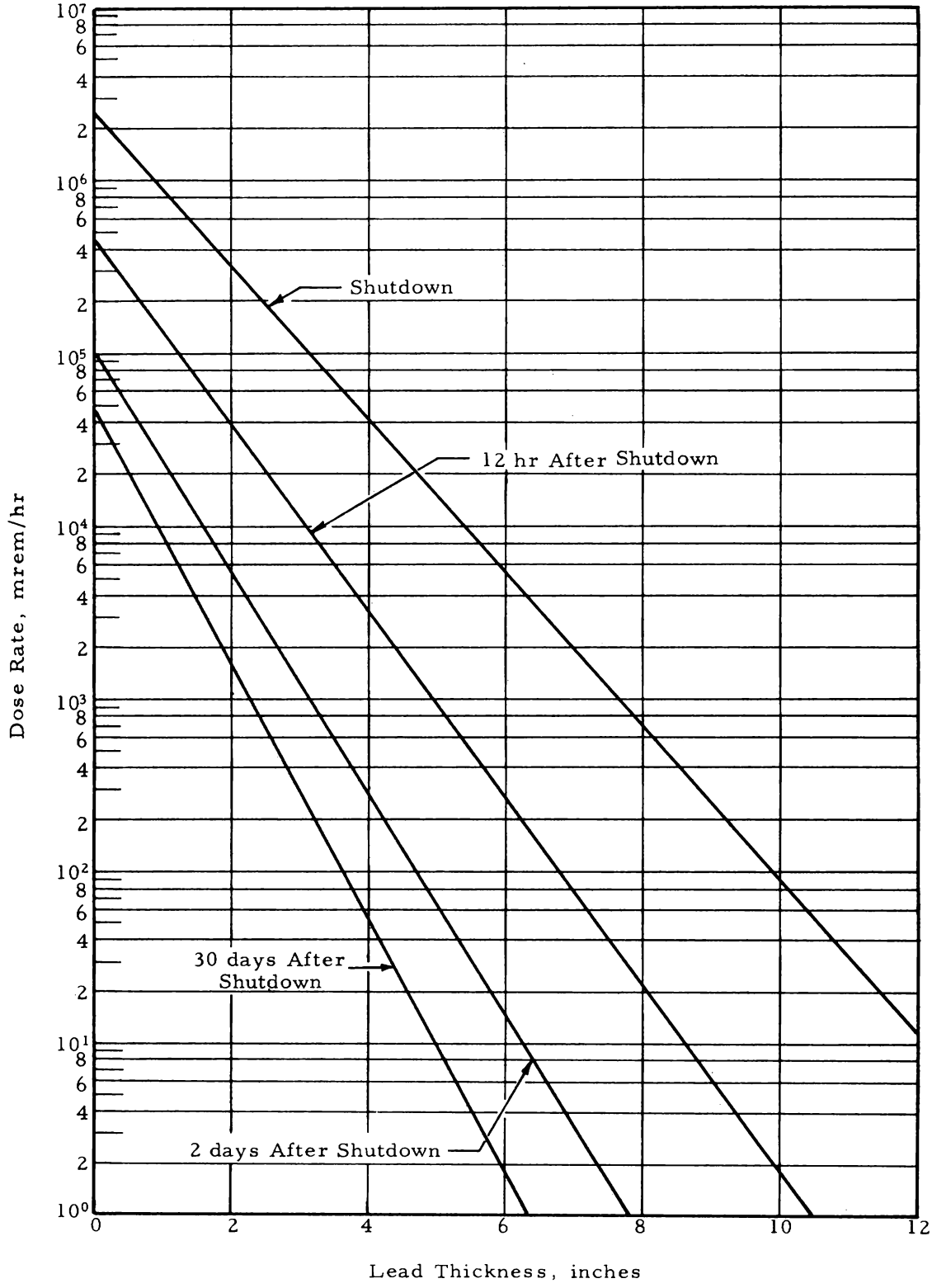

7. FUEL ELEMENT TRANSFER

7.1. Top Head Shielding

The arrangement of the top head shield assembly is shown in Figure 7-1. A discussion of the methods of calculating shield thicknesses in the various areas is given below.

7.1.1. Working Platform

The working platform is designed to restrict the dose rate at its upper surface to 1 mrem/hr or less from the operating core and from the N-16 in the primary coolant. The core was treated as a homogenized cylindrical source with a mean radius of 36 cm and a height of 122 cm. The core power was assumed to be 250 MW and to have a cosine distribution ranging from 1.4 max/avg at the core midplane to 0.40 min/avg at the top and bottom of the core. A uniform radial power distribution was assumed. Program DER-013 was used to calculate the dose rates at the top of the platform from the operating core as a function of platform thickness. Dose buildup factors for iron were used in the program. Figure 7-2 shows the results of the calculation. This figure also shows the dose rate at the same location from the fission products of an 800-kw test specimen which has been elevated to within 2 feet of the bottom closure plate. This is the specimen location that produces the maximum dose rate on the working platform, since the closure plate shields some portion of the specimen at higher elevations. The test specimen was treated as a cylindrical source with a radius of 2.22 cm and a height of 122 cm. The fission products were assumed to be axially distributed with the same cosine shape assigned to the core. The average values of the volumetric source strengths due to fission products in an 800-kw test specimen after infinite operation and 1 hour shutdown are listed below for 1-mev energy groups.

Energy	S_v, photons/cc-sec
0.5	2.03×10^{13}
1.5	4.28×10^{12}
2.5	4.06×10^{11}
3.5	7.51×10^{9}
4.5	1.51×10^{9}

These values were derived from the integral gamma ray spectrum of U-235 fission products given by Scoles[14]. The calculation was accomplished by use of the point source integration program, DER-013, with the use of steel buildup factors. The coolant level in both calculations was assumed to be 6 inches above the lower edge of the closure plate.

The source that determined the thickness of the platform was the N-16 of the primary coolant in the upper portion of the pressure vessel. The transit time required for the primary coolant to reach the pool at the top of the pressure vessel after core transit is calculated to be approximately 41 seconds. Since the core exit equilibrium activity of the coolant is 1.8×10^7 photons/cc-sec, the volumetric source strength in the pool at this time is about 3.8×10^5 photons/cc-sec. DER-013 was used to calculate the dose rate on the upper surface of the working platform using dose buildup factors for steel. The water level was again considered to be at 6 inches above the lower edge of the closure plate. The geometry of the source was that of a half-cylinder. Slant penetrations and shadow shielding reduce the influence of the far half of the cylinder sufficiently so that it can be neglected. The radius of the source was 5.25 feet, and the height was taken to be 2.5 feet. It was not considered necessary to extend the source height beyond 2.5 feet, since self-absorption reduces the flux from lower regions to relative unimportance. Figure 7-3 shows the dose rate on top of the working platform due to the N-16 of the coolant as a function of steel thickness. This thickness is in addition to the 4-inch-thick top head. As may be seen, a thickness of about 12 inches of steel is required to reduce the dose rate to the design level.

7.1.2. Loop Transfer Shield Plate

The transfer plate, which is located atop the shield cylinder, was designed for a dose rate of 1 rem/hr at its outer surface during test specimen transfer. The source strengths of the fission products in an 800-kw test specimen after infinite operation and 1 hour shutdown, as well as their treatment in the machine program DER-013, are discussed in the preceding paragraphs on the working platform. It was assumed that the test specimen was raised into the removal sleeve so that the upper end of the specimen was at the level of the bottom edge of the loop transfer shield plate. Figure 7-4 shows the results of the calculations of dose rate as a function of plate thickness. From this figure it can be seen that a thickness of 14.75 inches of steel is required to meet design requirements for the transient dose rate.

7.1.3. Shield Cylinder

The shield cylinder was sized to restrict the transient dose rate at its outer surface to 1 rem/hr or less during test specimen transfer. Program DER-013 was used to calculate dose rates as a function of shield thickness. The geometry and source strength due to the fission products in the test element are the same as those discussed in Section 7.1.1 concerning the working platform. It was assumed that the test specimen was entirely within the removal sleeve. Figure 7-5 shows the dose rates predicted by the calculations. The required thickness of steel to meet the design specifications is 17 inches. To reduce the bulk in this region, a bimetallic cylinder with a thickness of 3 inches of steel and 9 inches of lead was used as an equivalent substitute.

7.1.4. Instrument Lead Duct

The five instrument lead ducts, carrying neutron detectors for startup instrumentation, extend from the removal sleeve in the top head shield cylinder out under the working platform. Although these ducts have some curvature, they are oriented so that it is possible for both direct radiation from a transient test specimen in the removal sleeve and scattered radiation from the N-16 of the primary coolant in the pressure vessel to stream to the ducts under the working platform. A preliminary calculation showed that adequate shielding for the transient test specimen would also be adequate for any scattered radiation

from the N-16 at the mouth of the instrument lead duct. Figure 7-6 shows dose rates as functions of lead shield thickness over the end of the duct from the direct line-of-sight radiation of an 800-kw test specimen in the removal sleeve. To limit the transient dose rate emerging from the duct to the design level of 1 rem/hr, a thickness of 6.5 inches of lead for a 2-hour-shutdown specimen or 6.8 inches of lead for a 1-hour-shutdown specimen is required. This lead slab extends about 8 inches on each side of the duct centerline so that radiation emerging at an angle from the duct cannot circumvent it. Computer program DER-013 was used in the direct radiation calculations. The test specimen was represented as a cylindrical source 2.22 cm in radius and 10 cm in height. This is the maximum height of the source that can influence the dose rates at the other end of the duct, since the source is shielded sufficiently at higher and lower levels. The method of determining the volumetric source strengths for the test specimen and the source strengths for each energy group are given in Section 7.1.1.

Scattering from the face of the shield at the end of the duct was also found to contribute to the dose rates in the adjacent areas. Hence, it was recommended that two shields be located on each side of the end shield. Since the radiation reaching the region of concern must scatter through a rather large angle, the radiation is degraded to a relatively low energy. Consequently, the thickness of the side shields was determined to be only 1.5 inches of lead or 2.5 inches of steel. A thicker shield is required on top of this configuration (in the plane of the working platform), since the region above is subjected to some direct radiation from the N-16 in the primary coolant during operation. As mentioned previously, the coolant was found to have a volumetric source strength of about 3.8×10^5 gammas/cc-sec. The level of the coolant water was assumed to be 6 inches above the lower edge of the closure plate. Using buildup factors of steel in DER-013 and treating the source as a half cylinder with a radius of 5.25 feet and a height of 2.5 feet, a shield thickness of 5 inches of lead was calculated for a dose rate of 1 mrem/hr at the shield surface during normal core operation.

7.2. Cask Transfer Station

A shielding study was made of the various suggested designs for the cask transfer station. The design chosen was one which afforded optimum shielding against both scattered and direct radiation during the transfer of a test element. The design is for a T-shaped channel in a lead base. This channel accommodates a test element in either of the two arms. The transfer station extends 1 foot above the water level of the storage canal. To limit the transient dose rates from a test element to 1 rem/hr or less over the canal, a hinged shielding door is used to cover the mouth of the cask channel. To prevent radiation leakage through any cracks or spaces around the door fitting, the door is made of lead and shaped to protrude into the channel of the transfer station. The required door thickness, as measured through the protrusion, was calculated to be 6 inches (see Figure 7-7). In addition, the door was made 22 inches wide, thus overlapping the 6-inch wide channel by 8 inches on each side. This thickness applies from the top of the door down to 2 inches beneath the water surface. However, starting at 2 inches below the water surface, the door was constantly tapered to a zero thickness at 18 inches below the water surface. The door thickness was determined by the direct radiation from the fission products of a test specimen in one arm of the platform channel rather than by the scattered radiation from the specimen. Calculations of the flux and energy of the scattered radiation showed this to be valid, since the scattering angle degrades the energy of the radiation much below that of the direct radiation. The dose rate through the lead shielding door from scattered radiation is shown in Figure 7-8.

The direct radiation from the test specimen in an arm of the transfer station is required to penetrate a thickness of from 2 to 4 inches of steel and lead to reach the leg of the T-shaped channel. The test specimen was treated as an 800-kw cylindrical source with a radius of 2.22 cm and a height of 122 cm. The fission products were assumed to be distributed in the test specimen in an axial cosine distribution ranging from 1.4 max/avg at mid-plane to 0.40 min/avg at the top and bottom of the element. The specimen volumetric source strengths due to fission products after infinite operation and 1 hour shutdown are listed as a function of energy in Section 7.7.1. Figure 7-7 shows the results of the

calculations of the shielding door thickness employing program DER-013. The overlap thicknesses and the width of the overlap were determined by making the slant penetrations equivalent to the lead thickness at normal incidence. The taper on the door was determined by reducing the door thickness by the lead equivalence of the slant penetration through water.

Figure 7-9 shows the dose rate as a function of the thickness of the transfer station for the top 12-inch segment. As may be seen, about 9.5 inches of lead or the equivalent are required around the test element except on the side which has the hinged shielding door. Because of the problems in shielding the air-filled upper extension, 13 inches of lead (not including the hinged shielding door) are required on the side near this extension. Since there is increasing water shielding with increasing depth, the station was reduced in size in the underwater portion. The reduction begins at 2 inches beneath the water surface and continues to a zero thickness at 5.5 feet below the water surface. This design restricts the transient dose rate at the canal water surface to 1 rem/hr or less during the transfer of an 800-kw test specimen. The source, geometry, and methods for calculating the station size were the same as those used in determining the thickness of the hinged shielding door.

7.3. Spent Fuel Element Transfer Cask

Normal fuel transfer procedures involving the fuel transfer cask consist of the removal of nine spent fuel elements, which have decayed for 90 days following 17 days operation at 250 MW. The cask shielding is designed to limit the radiation levels to those included in the proposed rule for spent fuel shipment, 10 CFR 72, i.e., 200 mrem/hr at the shield surface and 10 mrem/hr 3 meters from the surface in air during normal spent fuel removal.

In computing dose rates, the fuel elements were represented by a homogeneous cylindrical source. Since the configuration and metal-to-water ratio of elements in the cask are similar to those of the core fuel region, self-absorption coefficients and gamma sources for the fuel region, as shown in Table 3-2, were used. The average volumetric gamma source strengths for the core at 90 days shutdown are shown below for average energies in 1-mev energy intervals.

Energy, mev	Gamma ray source strength, photons/cc-sec-mev
0.5	4.4×10^{11}
1.5	4.54×10^{10}
2.5	3.06×10^{8}

Dose rates were computed along the radial centerline of the cask using the cylindrical case in program DER-074 and along the axial centerline using the truncated core case. To account for the various power-peaking factors, the calculations are based on "hottest" elements whose average power density is twice the average core power density. Figure 7-10 shows the dose rates, axially and radially, as functions of lead thickness. The curves show the dose rates 3 meters from the cask surface, since the shield thicknesses are governed by the "10 mrem/hr at 3 meters" criterion.

The transfer cask has an ID of 13.75 inches, with 10.5 inches of lead and 5/8 inch of steel on the sides, 9.5 inches of lead and 3/4 inch of steel on the bottom, and a top plug consisting of 11 inches of lead and 1 inch of steel. As may be seen from Figure 7-10, these thicknesses are sufficient to satisfy the design dose rate criteria during normal fuel element transfer.

Dose rates were also computed for a special case of transferring a single fuel element after a shutdown period of one day. The element was approximated by a 4-foot line source with the following gamma source strengths per 1-mev energy interval.

Energy, mev	Gamma ray source strength S_L, photons/cm-sec-mev
0.5	1.6×10^{14}
1.5	1.7×10^{13}
2.5	2.4×10^{12}
3.5	3.6×10^{11}

As in the previous case, power-peaking factors are taken into account by using an element with a power density of twice the average core power density. Dose rates were obtained from the line source case

of DER-074 and are shown in Figure 7-11, both axially and radially, as functions of lead shielding thickness. Attenuation by water within the cask was neglected.

7.4. NR Loop Handling Cask

The loop handling cask is designed for the wet transfer of test specimens to and from the NR loop pressure tubes and for the dry transfer of irradiated pressure tubes and flow tubes. The cask consists of three major sections: a base, a lower body, and an upper body (see Figures 7-12, 7-13, and 7-14).

The base section houses the bottom closure door and provides an enlarged diameter for shielding around the closure door cavity. The cylindrical section of the base has a 54-inch OD and a nominal thickness of about 20 inches. Except for the bottom closure door, all shielding in the base section is steel. The closure door seals the bottom of the cask cavity by translation at a right angle to the cavity axis. The door consists of a steel box structure filled with lead and provides a minimum shield thickness equivalent to 9 inches of lead.

The lower body is a cylindrical shielding section, which extends upward approximately 7 feet from a flanged connection with the cask base. This section provides the primary shielding during transfer of test specimens and irradiated components. It consists of a lead-filled annulus between two steel shells and a cooling coil contained in a third inner shell. The ID of the inner shell is 6.75 inches, and the total shield thickness (lead and steel) is equivalent to 11.25 inches of lead for gamma energies of 2.5 mev.

The upper body section is bolted to the lower body and provides a tubular cavity about 20 feet long with a 7-inch ID for the purpose of maintaining a water environment during specimen transfer. The lower 5 feet of the section consists of a shield, equivalent to 8 inches of lead at the base and tapering to 1 inch at its upper point.

The shielding for the transfer cask is sized to restrict the radiation levels from a test specimen situated in the cask to those specified in 10 CFR 72. The calculations were based on a 4-foot long specimen which had operated at 800 kw for an infinite time. It was assumed there was a 2-hour decay period between reactor shutdown and specimen

removal. The specimen was represented by a line source of uniform strength located on the axial centerline of the cask. The unit energy gamma source strengths per centimeter of specimen length, after 2 hours shutdown, are shown below.

Energy, mev	Gamma ray source strength S_L, photons/cm-sec-mev
1.5	5.1×10^{13}
2.5	4.0×10^{12}
3.5	6.6×10^{10}
4.5	2.3×10^{10}

Dose rates were computed along the radial centerline of the specimen for various thicknesses of lead using the line source case in program DER-074. The source was assumed to be located along the axial centerline of the cask with 3.25 inches of water between the source and the cask ID. Figure 7-15 shows the dose rate 3 meters in air from the cask surface versus thickness of lead shielding. Approximately 11.25 inches of lead, or the equivalent, is needed to reduce the radiation level to 10 mrem/hr. For this thickness, the dose rates are governed by the 2.5-mev gamma energy group. To account for shielding afforded by the structural steel, lead was replaced by steel according to the ratio of their linear absorption coefficients at 2.5 mev.

The dose rate requirements for the base section are less stringent than those for the main body of the cask, since the radiation levels that occur during specimen transfer are of a transient nature. The minimum shield thicknesses were determined on the basis of an integrated dose of 15 mrem at the shield surface during specimen transfer. It was assumed that 1 minute would be required for the specimen to pass through the base section. On this basis, a transient dose rate of 1 rem/hr is allowable. The cylindrical portion of the base has a thickness of 20 inches, which is sufficient to reduce the transient dose rates to well below the 1 rem/hr limit. Shielding was added to the flange areas to provide, along any line of sight to any portion of the specimen, a minimum of 15 inches of steel. This was calculated as being sufficient to insure that the dose rate would not exceed 1 rem/hr.

The shield thickness for the bottom closure plug was computed with the test specimen represented by a line source located along the axial centerline of the cask with 19.5 inches of water between the lower end of the specimen and the closure door. Dose rates were calculated 3 meters from the shield surface as a function of lead thickness by a point kernel integration along the length of the source. Self-absorption by the source was assumed to be that of water. The results showed that a shield thickness equivalent to 8 inches of lead is required to conform to the proposed shipping regulations.

During loop component removal, the upper 1-foot section of the inpile portion of the loop will be situated in the upper body section of the cask. The shielding for the upper body is sized to restrict the dose rates from the activated loop components to 10 mrem/hr 3 meters from the shield surface. The 1-foot loop section was assumed to have been exposed to a thermal flux of 1.5×10^{14} n/cm^2-sec for a period of 2 years. The activated loop components (flow tube, pressure tube, and insulating tube) are made of stainless steel 347. Isotope activation was computed on the basis of the following elemental weight percentages:

Element	Wt %
Cr	18
Ni	12
Fe	70
Ta	0.1
Co	0.04

The activated loop was approximated by a 1-foot line source of uniform strength, and dose rates were calculated as a function of lead shielding thickness. The dose rate at the surface of an 8-inch lead shield is 150 mrem/hr. The dose rates are constant for shutdown times of several days, since the gamma rays from the longer-lived isotopes in the activated steel dominate.

An estimate was made to determine the dose rates in the vicinity of the top head shield during loop removal as a result of radiation streaming through the bottom of the cask and scattering on the top head

shield. It was assumed that the center of a 4-foot activated loop section was located in the cask 6.5 feet from the bottom opening and that the bottom of the cask was 5 feet from the top head shield plate. The loop was represented by a line source, and the gamma energy flux incident on the shield plate was computed by point source summation along the length of the activated loop section. It was assumed that the flux was incident on a circular area of the shield plate formed by the angle between the cask axial centerline and a line extending from the bottom of the 4-foot line source to the lower inside edge of the cask. A 6.5-inch cask ID was used. The area subtended is 670 cm^2. The calculations were performed for gamma energy groups of 0.31, 0.81, and 1.25 mev. Scattering from the steel surface was computed by using the total energy albedos for gamma rays perpendicularly incident on a steel slab of infinite thickness. The values used are shown below:

Gamma energy, mev	Total energy albedo
0.31	6.3×10^{-2}
0.81	3.8×10^{-2}
1.25	2.7×10^{-2}

It was assumed that the reflected energy flux was independent of the angle of reflection, and the subtended area of 670 cm^2 was treated as a point source located at the intersection of the cask centerline with the shield plate. The dose rate 10 feet from this point was computed to be 2 rem/hr. Since the removal of a test loop section is an infrequent operation, radiation exposure should be limited through administrative control rather than additional shielding.

7.5. Dose Rates During Refueling

The original design criterion for transferring spent fuel elements from the core through the discharge chute was a dose rate of 25 mrem/hr at the surface of the water from a raised fuel element 1 hour after shutdown following 17 days operation at full power. Dose rates were calculated above a vertical element as a function of water over the element. The element was represented by a line source of uniform strength. The power density of an average element was used. This representation is

considered to be as effective as designing for the "hottest" element and accounting for end effects. Absorption coefficients along the length of the element were assumed to be those of water, and dose buildup factors for water were used. The resulting dose rate is shown in Figure 7-16 as a function of water depth above the active fuel region. About 11 feet of water are required for a 25-mrem/hr dose rate.

The depth of water over the active core during spent fuel transfer is 18 feet. The length of the active fuel element is 4 feet, and about 2 feet are needed for clearance over the drop tube shield. This leaves a working margin of 1 foot. The above numbers are probably conservative, since it is unlikely that fuel will be transferred sooner than 3 hours after shutdown.

Figure 7-1. Reactor Top Head Shielding General Arrangement (Dwg. No. 670-MS-115)

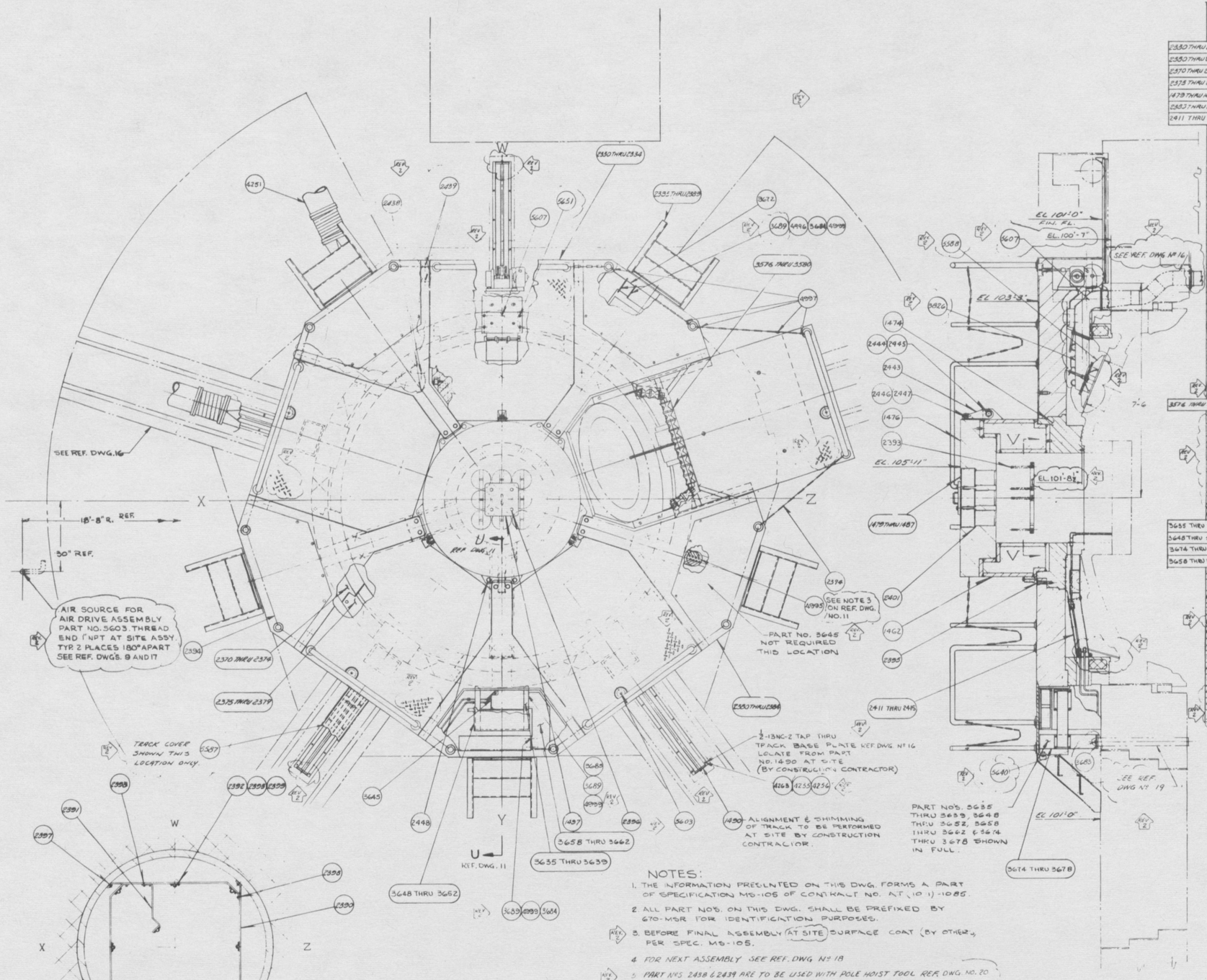

G70 MSR PART NO.	QUAN	ATR-1075-MTR- DWG. NO.	NAME	DESCRIPTION	MAT'L SPEC.
2400	—	G70-MS-115	REACTOR TOP HEAD SHIELDING SEAL ASSY.		—
2330 THRU 2334	1 EACH	G70-MS-164	SHIELD DOOR ASS'Y.		AS NOTED
2350 THRU 2354	1 EACH	G70-MS-117	SHIELD BLOCK ASS'Y.		AS NOTED
2370 THRU 2374	1 EACH	G70-MS-116	58.6° SHIELD RING ASS'Y.		AS NOTED
2375 THRU 2379	1 EACH	G70-MS-117	58.8° SHIELD RING ASS'Y.		AS NOTED
1479 THRU 1487	1 EACH	G70-MS-165	TRANSITION PLATE PLUG		AS NOTED
2383 THRU 2389	1 EACH	G70-MS-168	SHIELD		AS NOTED
2411 THRU 2415	1 EACH	G70-MS-170	INSTRUMENTATION SERVICES CONDUIT "A"		AS NOTED
2443	3	G70-MS-175	CLEVIS		AS NOTED
1462	1	G70-MS-118	SHIELD CYL. ASS'Y.		AS NOTED
1474	1	G70-MS-165	INNER SUPPORT RING ASS'Y.		AS NOTED
1490	5	G70-MS-118	TRACK ASS'Y.		AS NOTED
1497	1	G70-MS-118	PLUG RETAINER ASS'Y.		AS NOTED
1476	1	G70-MS-165	TRANSITION PLATE ASS'Y.		AS NOTED
2390	4	G70-MS-175	CABLE SUPPORT		AS NOTED
2391	1	G70-MS-175	BRACKET		AS NOTED
2392	5	G70-MS-175	CLAMP		AS NOTED
2393	5	G70-MS-175	SPRING		AS NOTED
2394	60 FT	G70-MS-115	CHAIN	AMERICAN CHAIN & CABLE CO. 1/2" PITCH NO. 51 BRASS CHAIN	CARBON STEEL COMP.
2396	10	G70-MS-115	SOC. HD. CAP SCR.	1-8NC-2 x 3/4 LG.	CARBON STL. COMP.
2396	4	G70-MS-115	HEX. HD. CAP SCR.	5/8-11NC-2 x 2 1/2 LG.	CARBON STL. COMP.
2397	4	G70-MS-115	HEX. HD. CAP SCR.	1/2-13NC-2 x 1 LG.	CARBON STL. COMP.
2398	10	G70-MS-115	SOC. HD. CAP SCR.	3/8-16NC-2 x 1/2 LG.	CARBON STL. COMP.
2399	18	G70-MS-115	SOC. H.D. CAP SCR.	10-32NC-2 x 3/8 LG.	CARBON STL. COMP.
2401	5	G70-MS-118	O-RING	PARKER SEAL CO. "PARKER NO. 2-260-DR" 2700-DR COMPD.	N-70 S. SILICONE COMP.
2444	3	G70-MS-115	HEX. HD. BOLT	2-4 1/2 NC-2 x 5 3/4 LG.	CARBON STL. COMP.
2445	3	G70-MS-115	HEX. NUT	2-4 1/2 NC-2	CARBON STL. COMP.
2446	3	G70-MS-115	HEX. HD. BOLT	1-8NC-2 x 3 1/4 LG.	CARBON STL. COMP.
2447	3	G70-MS-115	HEX. NUT	1-8NC-2	CARBON STL. COMP.
2448	10	G70-MS-115	HEX. HD. BOLT	1-8NC-2 x 6 1/2 LG.	CARBON STL. COMP.
5603	1	670-MS-185	AIR DRIVE ASS'Y.		AS NOTED SEE NOTE 6
3576 THRU 3580	5 EACH	670-MS-177	SHIELD PLUG ASS'Y.		AS NOTED
3635	5	G70-MS-186	GASKET "A"		AS NOTED
3640	10	G70-MS-115	HEX. HD. BOLT	1/2-13 NC-2 x 1 3/4 LG.	CARBON STL. COMP.
2438	4	G70-MS-115	HEX. HD. BOLT	3/8-11NC-2 x 2 1/2 LG. (SEE NOTE 5)	CARBON STL. COMP.
2439	4	G70-MS-115	HEX HD. BOLT	3/10 NC-2 x 2 1/2 LG. (SEE NOTE 5)	CARBON STL. COMP.
5607	5	G70-MS-198	EXHAUST DUCT		AS NOTED
5588	3	G70-MS-197	HELIPACTIC LOWER SHIELD ASS'Y.		AS NOTED
3626	3	G70-MS-204	EXHAUST DUCT ASS'Y.		AS NOTED
5651	20	G70-MS-115	SOC. HD. CAP SCREW	5/8-11NC-2 x 3 1/2 LG.	CARBON STL. COMP.
4263	50	670-MS-118	HEX HD BOLT	5/8-11NC-2 x 1 1/2 LG.	CARBON STL. COMP.
3655 THRU 3659	1 EACH	670-MS-186	SHIELD BLOCK ASSEMBLY		AS NOTED
3648 THRU 3652	1 EACH	670-MS-186	SHIELD BLOCK COVER ASSY.		AS NOTED
3674 THRU 3678	1 EACH	670-MS-186	JUNCTION BOX ASSEMBLY		AS NOTED
3658 THRU 3662	1 EACH	670-MS-186	DUCT		AS NOTED
4251	1	670-MS-190	VENT DUCT ASS'MT.		AS NOTED
3672	1	670-MS-186	DUCT EXTENSION		AS NOTED
4995	1	670-MS-195	PRES. SEALWATER LINES ASS'MT.		AS NOTED
3684	6	670-MS-186	GASKET "B"		AS NOTED
3689	8 4	670-MS-115	HEX HD. BOLT	5/8-16NC-2 x 1/2 LONG	CARBON STL. COMP.
4996	4	670-MS-115	HEX NUT	5/8-16NC-2	CARBON STL. COMP.
4999	4 8	670-MS-115	WASHER	5/8 I.D. x 1 1/16 O.D. x 1/16 THK.	CARBON STL. COMP.
3685	5	670-MS-186	GASKET "C"		AS NOTED
4997	4 0	670-MS-115	SWIVEL SNAP	= 5/8 OPEN EYE-AMERICAN CHAIN & CABLE CO. OR EQUIV.	CARBON STL. COMP.
3645	4	670-MS-186	PLATE WELDMT.		AS NOTED
4253	50	670-MS-115	WASHER	1/32 I.D. x 1 1/16 O.D. x 3/32 THK.	CARBON STL. COMP.
4254	50	670-MS-115	LOCK WASHER	5/8 MED. SPRING	CARBON STL. COMP.
3587	5	670-MS-192	TRACK COVER		AS NOTED

NO	DATE	REVISIONS	BY	APPD
2	0-8-63	REVISED NOTE AT 3 (ADDED NOTE AT H-11)		
		AIR DRIVE & AIR DRIVE ASSY. WAS CONTROLLING PART - 15		
		PART NO. 3687 W AS 4996		
		ADDED "SEE REF. DWG. NO. 16"		
		ADDED "SEE REF. DWG. NO. 19"		
		REVISED PICTURE		
		PER DETAILS		
		REVISED PT. NO. 4263 NOTE 6 WAS 5		
		ADDED EL. 101'-8½", EL. 100'-7"		
		DELETED REF. DWG. 12, PT. NOS. 4215		
		4216, 4217, 4218, 4219, 4266		
		4261 & 4262 & DETAIL A - A		
		ADDED PART NOS. 3587, 3686, 5588		
		3607, 3681, 3640, 2438, 2439		
		3651; REF. DWGS. 19620		
		REV. NOTES 3 & 5 ADDED NOTE 6		
		PART NOS. 2330 THRU 2334 & 5603		
		½-13 NC-2 TAP NOTE - CHANGED		
		PART NOS. 4261 & 4262 TO 4235		
		4254 & PART NO. 2450 TO 2403		
1	10-4-62	REVISED TO AGREE WITH AS BUILT		

NO	DRAWING TITLE	DWG. NO.
1	REACTOR TOP HEAD SHIELDING DETAILS SHT. 1	670-MS-116
3	REACTOR TOP HEAD SHIELDING DETAILS SHT. 3	670-MS-118
4	REACTOR TOP HEAD SHIELDING DETAILS SHT. 4	670-MS-123
5	REACTOR TOP HEAD SHIELDING DETAILS SHT. 5	670-MS-124
6	REACTOR TOP HEAD SHIELDING DETAILS SHT. 6	670-MS-125
7	REACTOR TOP HEAD SHIELDING DETAILS SHT. 7	670-MS-126
8	REACTOR TOP HEAD SHIELDING DETAILS SHT. 8	670-MS-127
9	REACTOR TOP HEAD SHIELDING DETAILS SHT. 9	670-MS-128

	DRAWN	BY	DATE
	CHECKED		
	APPROVED B & W		
	APPROVED B & W		
	APPROVED EBASCO		
	APPROVED EBASCO		
	APPROVED		
	APPROVED PPCO		
	APPROVED AEC		
	SCALE	3/4"-1'-0"	
	DATE	APRIL 24 63	

ATR

REACTOR TOP HEAD SHIELDING GENERAL ARRANGEMENT

THE BABCOCK & WILCOX CO.
ATOMIC ENERGY DIVISION
LYNCHBURG, VA.

FOR

EBASCO SERVICES INCORPORATED
TWO RECTOR STREET, NEW YORK, N.Y.

FOR

ARCHITECT – ENGINEER

U.S. ATOMIC ENERGY COMMISSION
IDAHO OPERATIONS OFFICE
IDAHO FALLS, IDAHO

DWG. NO. ATR-1075-MTR-GRO-MS-115 REV. (2)

NOTES:

1. THE INFORMATION PRESENTED ON THIS DWG. FORMS A PART OF SPECIFICATION MS-105 OF CONTRACT NO. AT(10-1)-1085.
2. ALL PART NOS. ON THIS DWG. SHALL BE PREFIXED BY 670-MSR FOR IDENTIFICATION PURPOSES.
3. BEFORE FINAL ASSEMBLY AT SITE SURFACE COAT (BY OTHERS) PER SPEC. MS-105.
4. FOR NEXT ASSEMBLY SEE REF. DWG. NO. 18
5. PART NOS. 2438 & 2439 ARE TO BE USED WITH POLE HOIST TOOL REF. DWG. NO. 20
6. AIR PRESSURE FOR PART NO. 5603 TO BE SET AT 40 PSI MAX.

Figure 7-2. Dose Rate at Surface of Working Platform Vs Platform Thickness

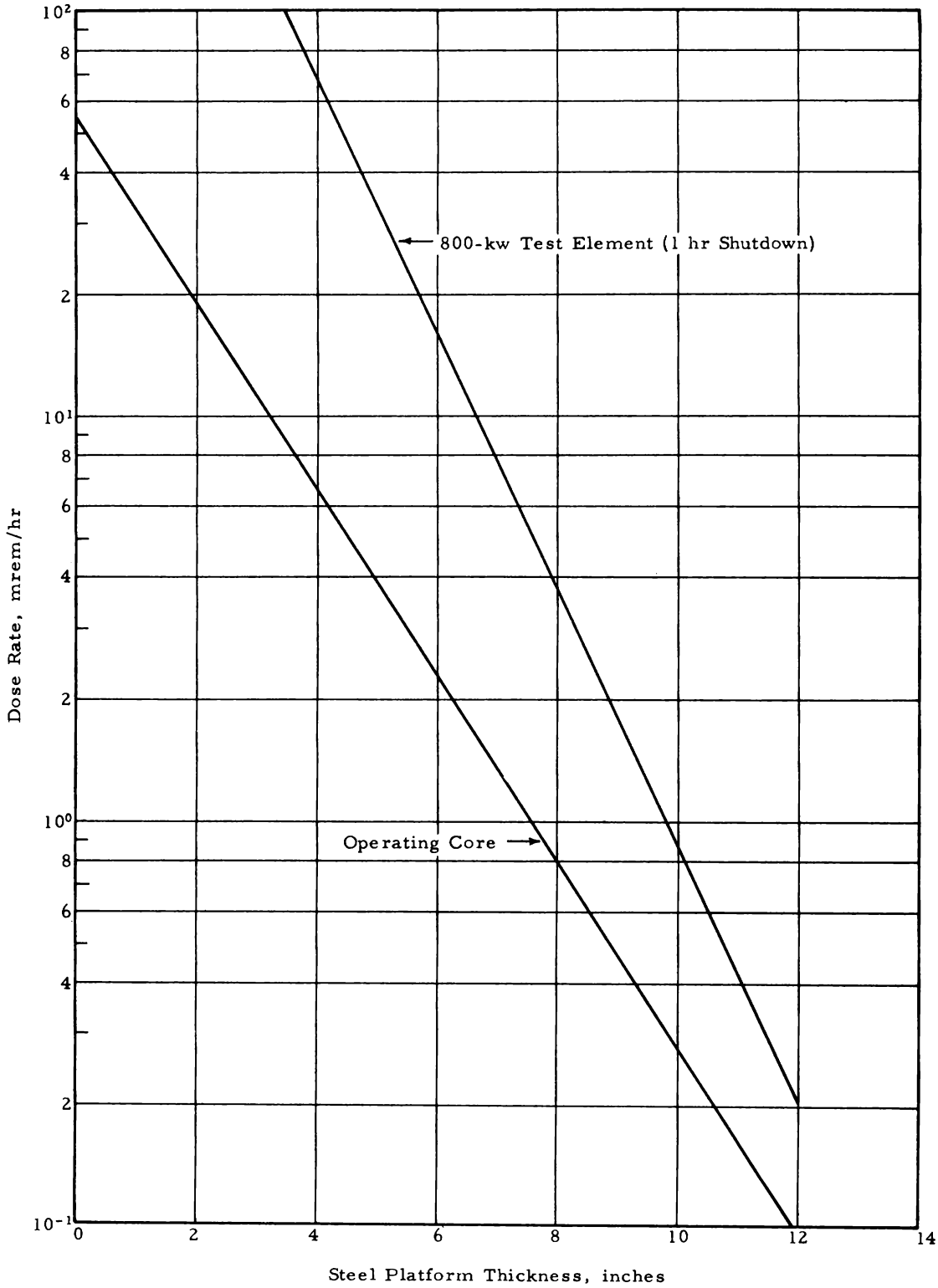

Figure 7-3. Dose Rate at the Top Surface of the Working Platform From N-16 Activity Vs Platform Thickness

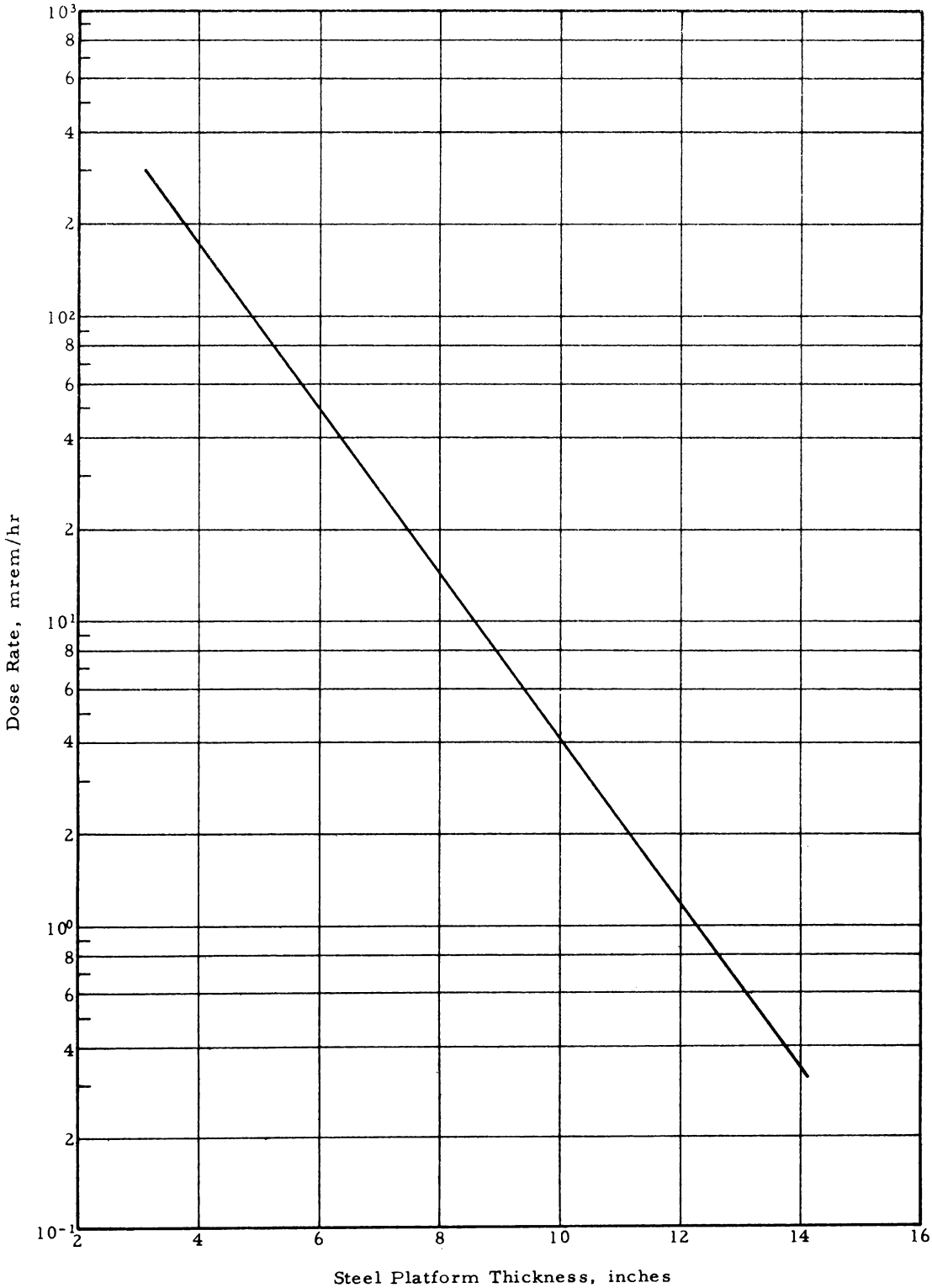

Figure 7-4. Dose Rate at Surface of the Transfer Plate From an 800-kw Test Specimen in the Removal Sleeve With Infinite Irradiation Time and 1-Hour Decay Time

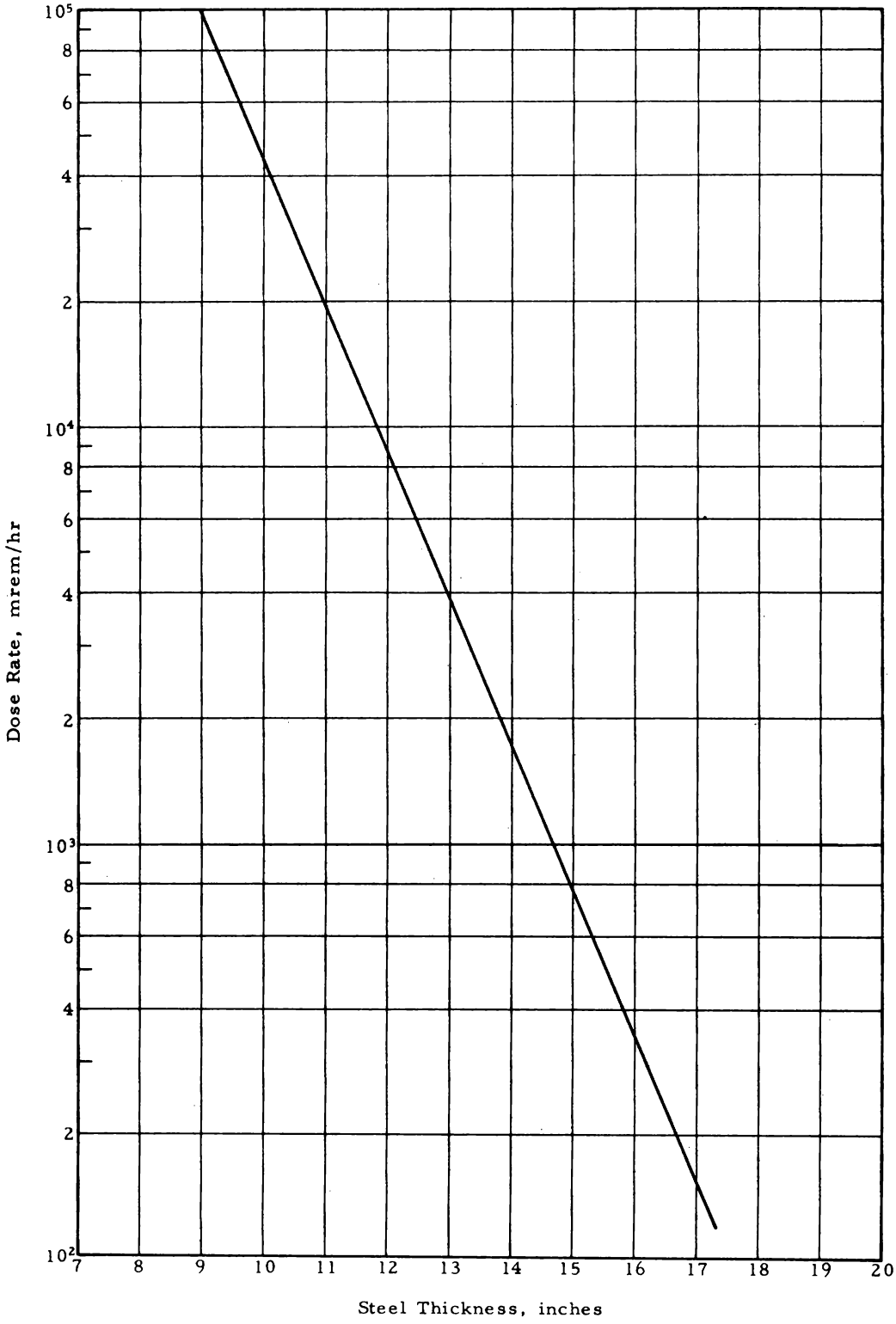

Figure 7-5. Dose Rate at Surface of Shield Cylinder From an 800-kw Test Specimen in the Removal Sleeve With Infinite Irradiation Time and 1-Hour Decay Time

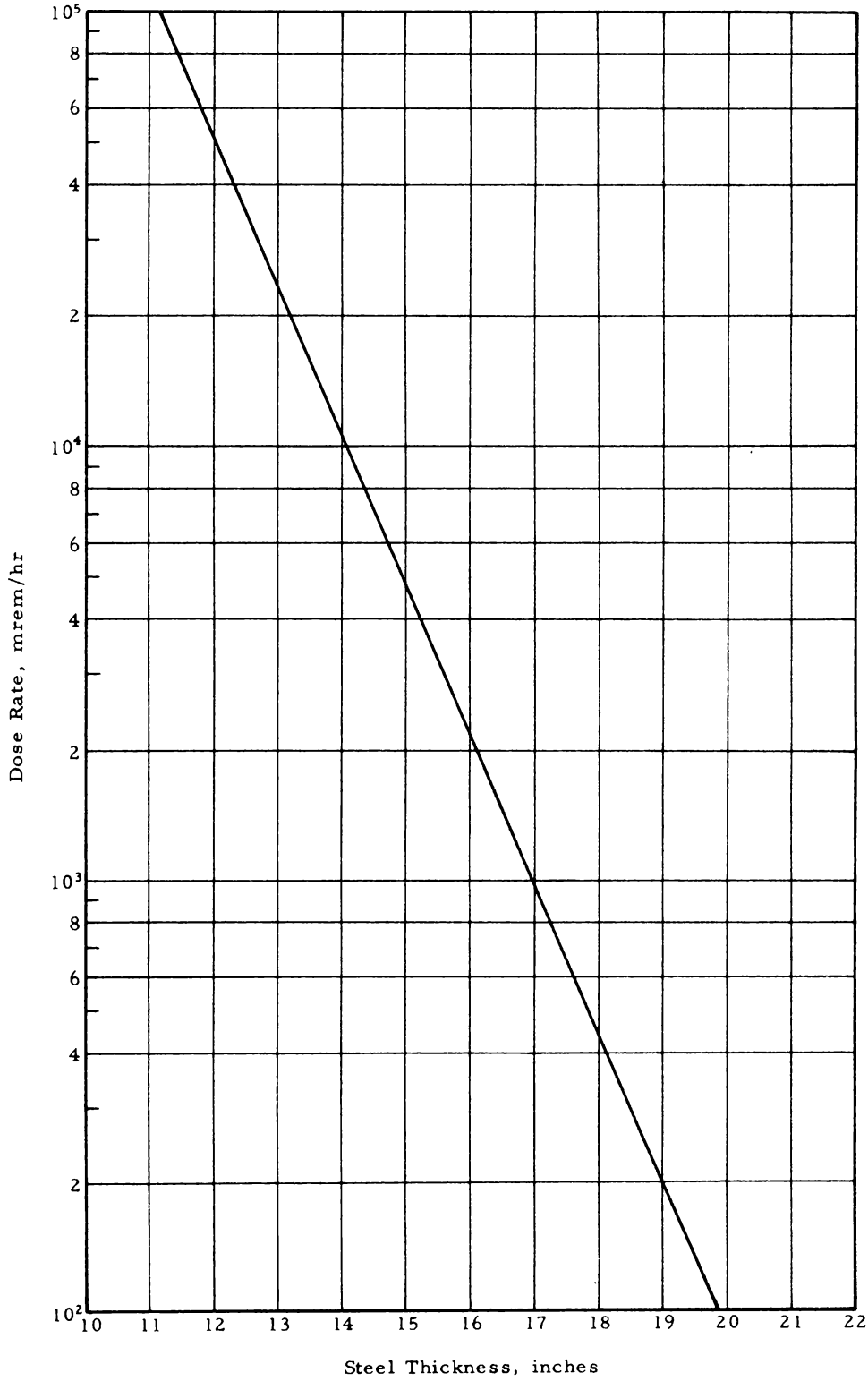

Figure 7-6. Dose Rate Vs Lead Thickness on Instrument Duct During Removal of an 800-kw Test Specimen

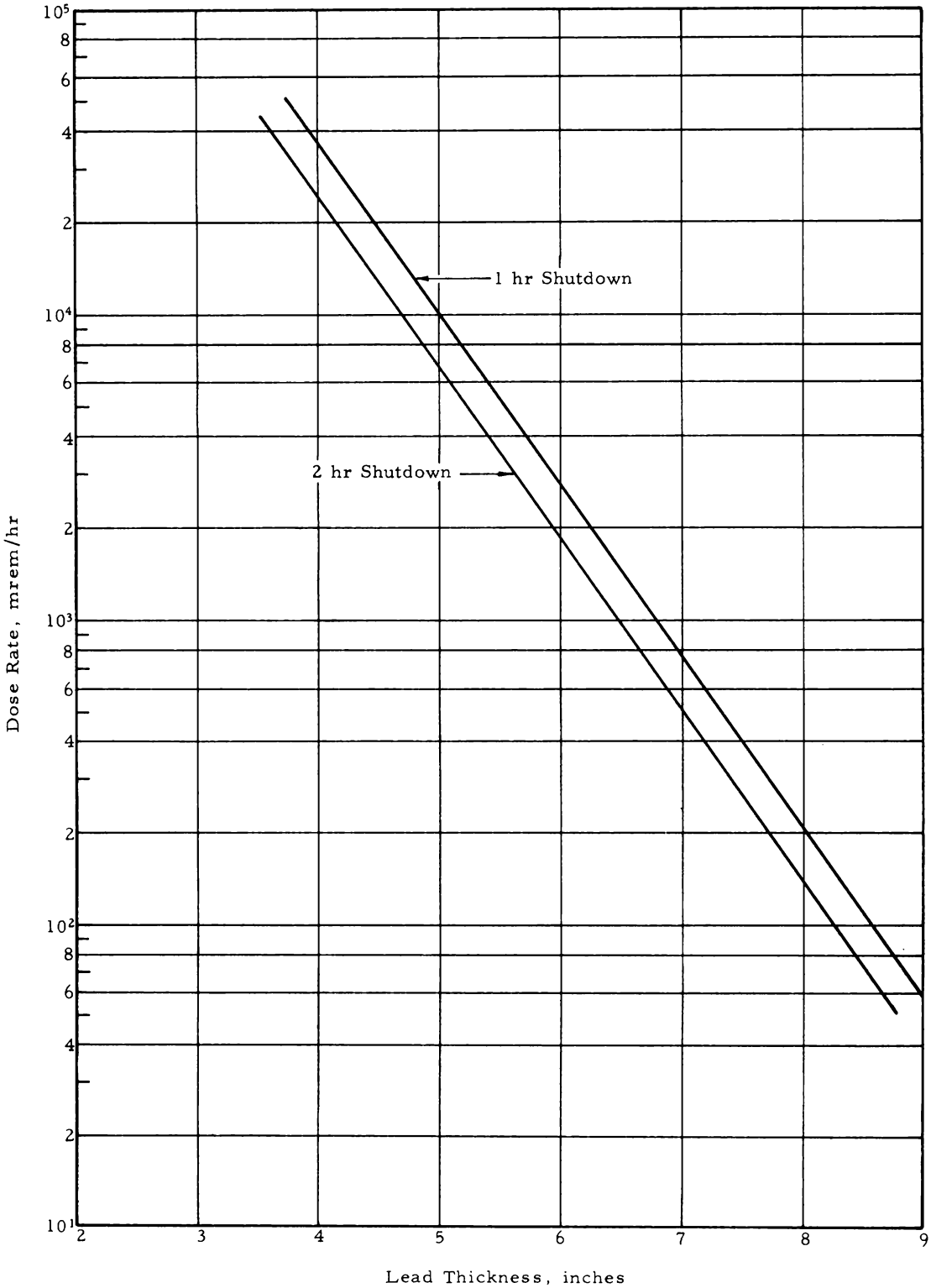

Figure 7-7. Direct Radiation Dose Rate as a Function of Lead Shielding Door Thickness From an 800-kw Test Specimen With Infinite Irradiation Time and 1-Hour Decay Time

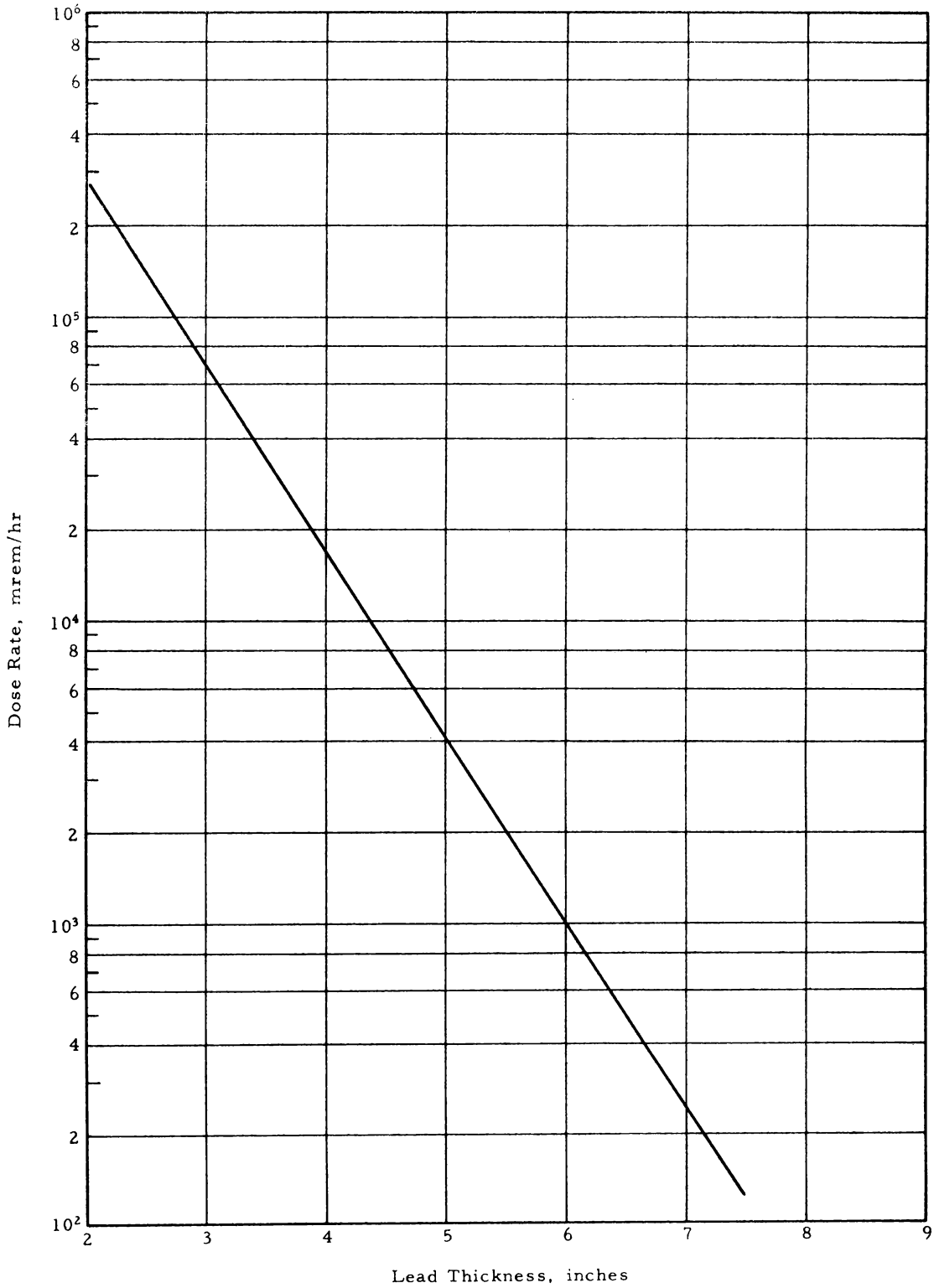

Figure 7-8. Scattered Radiation Dose Rate as a Function of Lead Shielding Door Thickness From an 800-kw Test Specimen With Infinite Irradiation Time and 1-Hour Decay Time

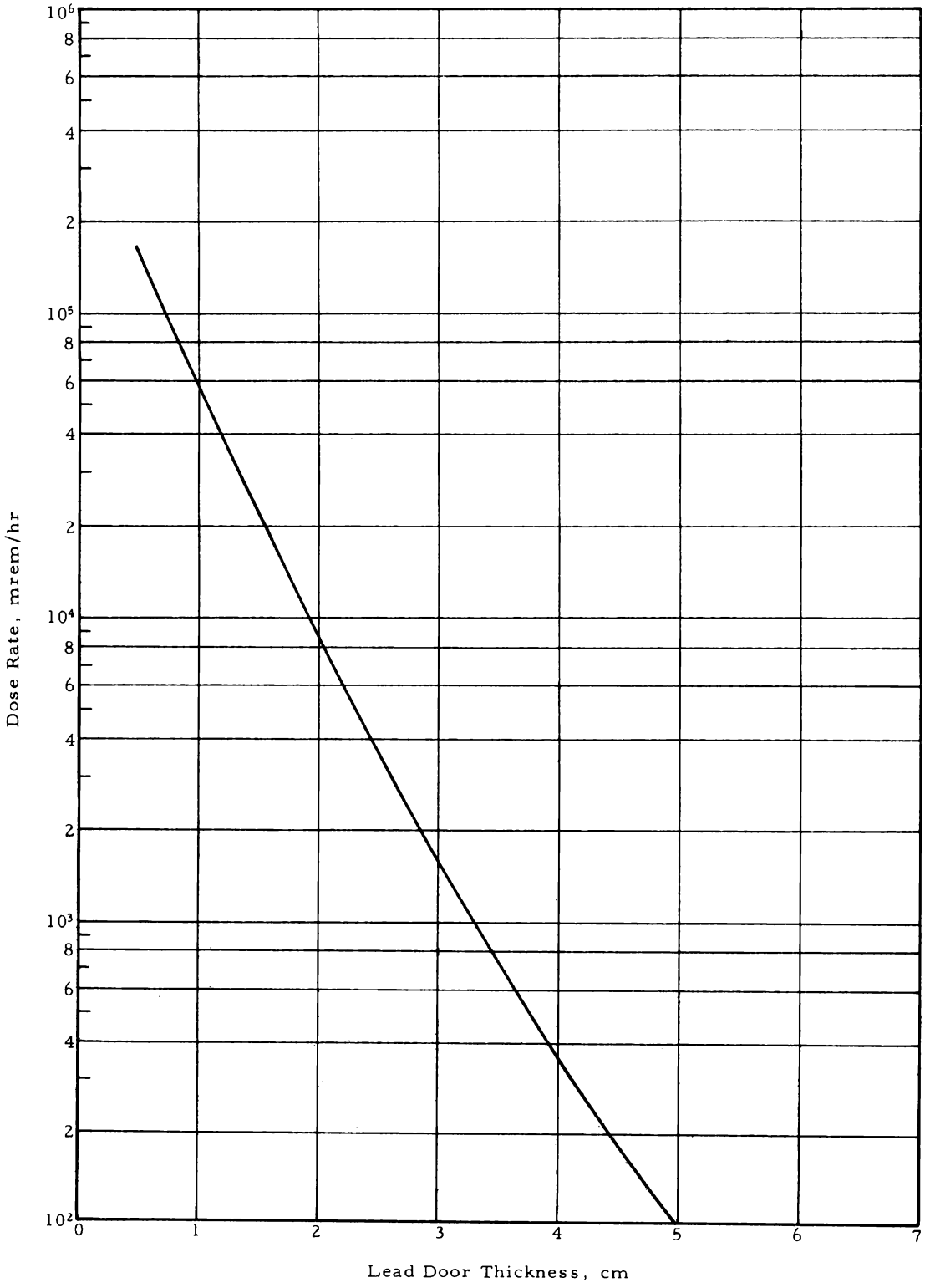

Figure 7-9. Dose Rate Through Lead From an 800-kw Test Specimen in the Upper Extension of the Cask Transfer Station With Infinite Irradiation Time and 1-Hour Decay Time

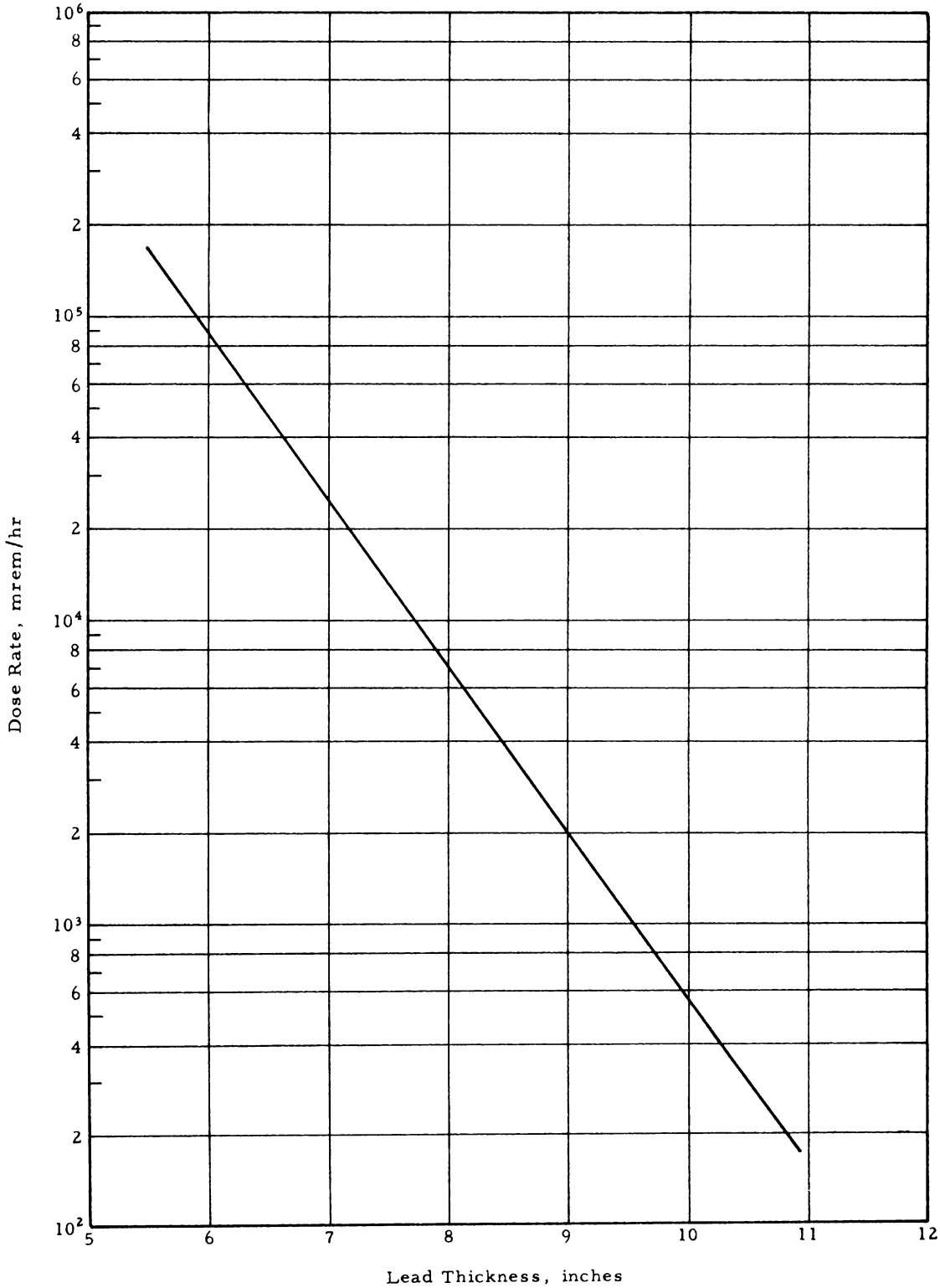

Figure 7-10. Dose Rate 3 Meters From Surface of Spent Fuel Transfer Cask (Nine Elements at 90 Days)

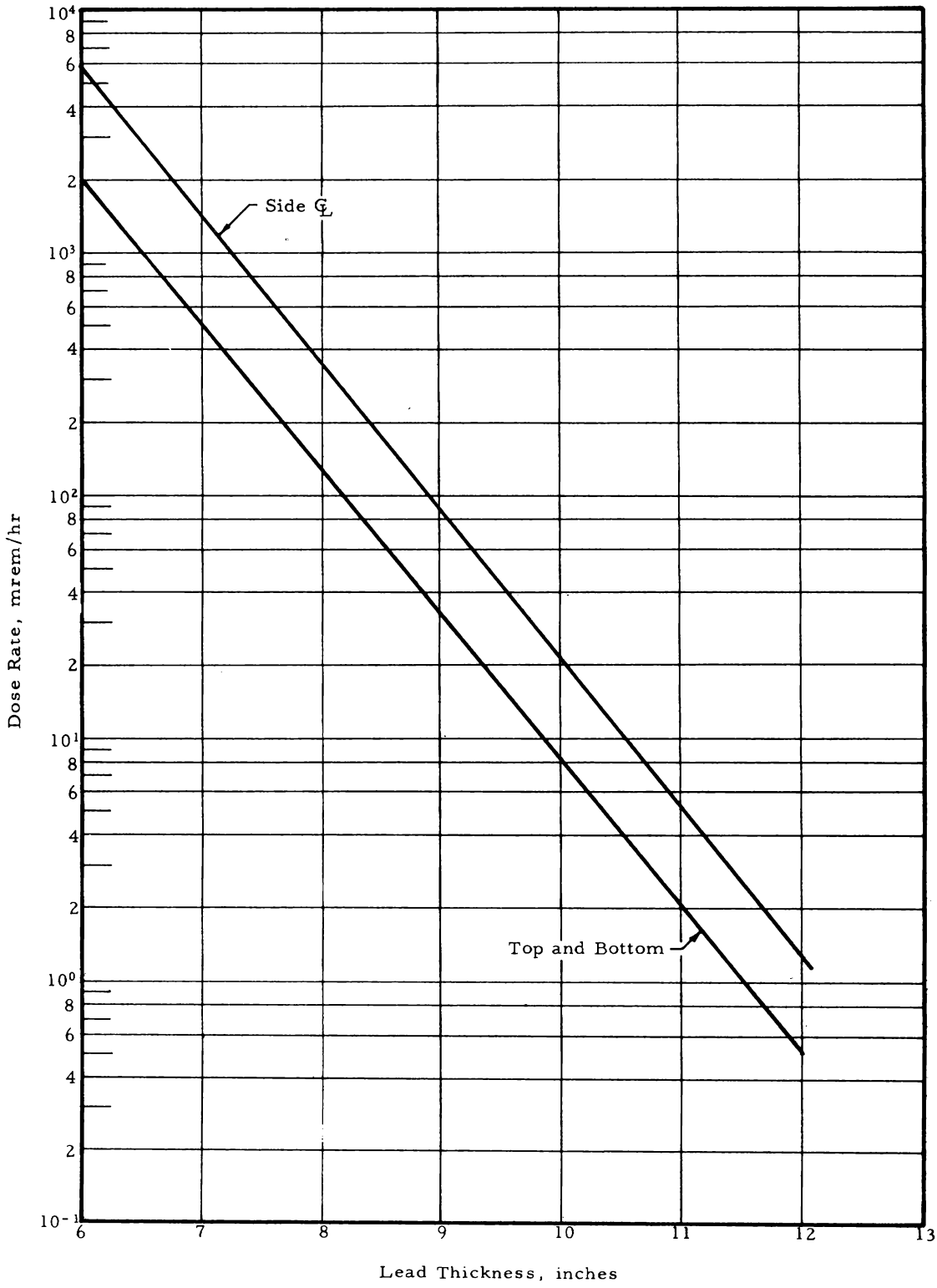

Figure 7-11. Dose Rate 3 Meters From Surface of Spent Fuel Transfer Cask (One Element at 1 Day)

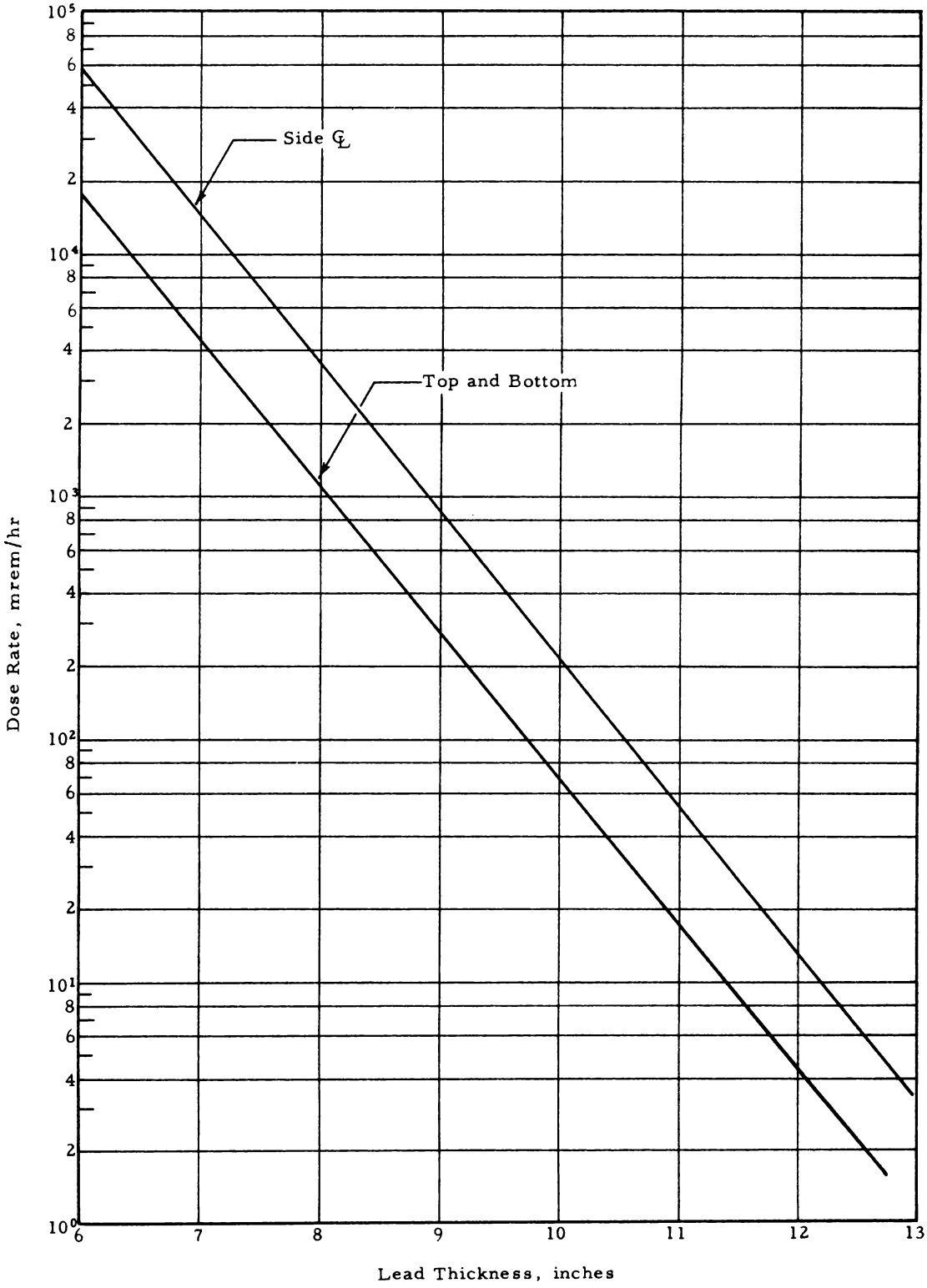

Figure 7-12. N. R. Loop Handling
Cask Arrangement
(Dwg. No. 670-MS-101)

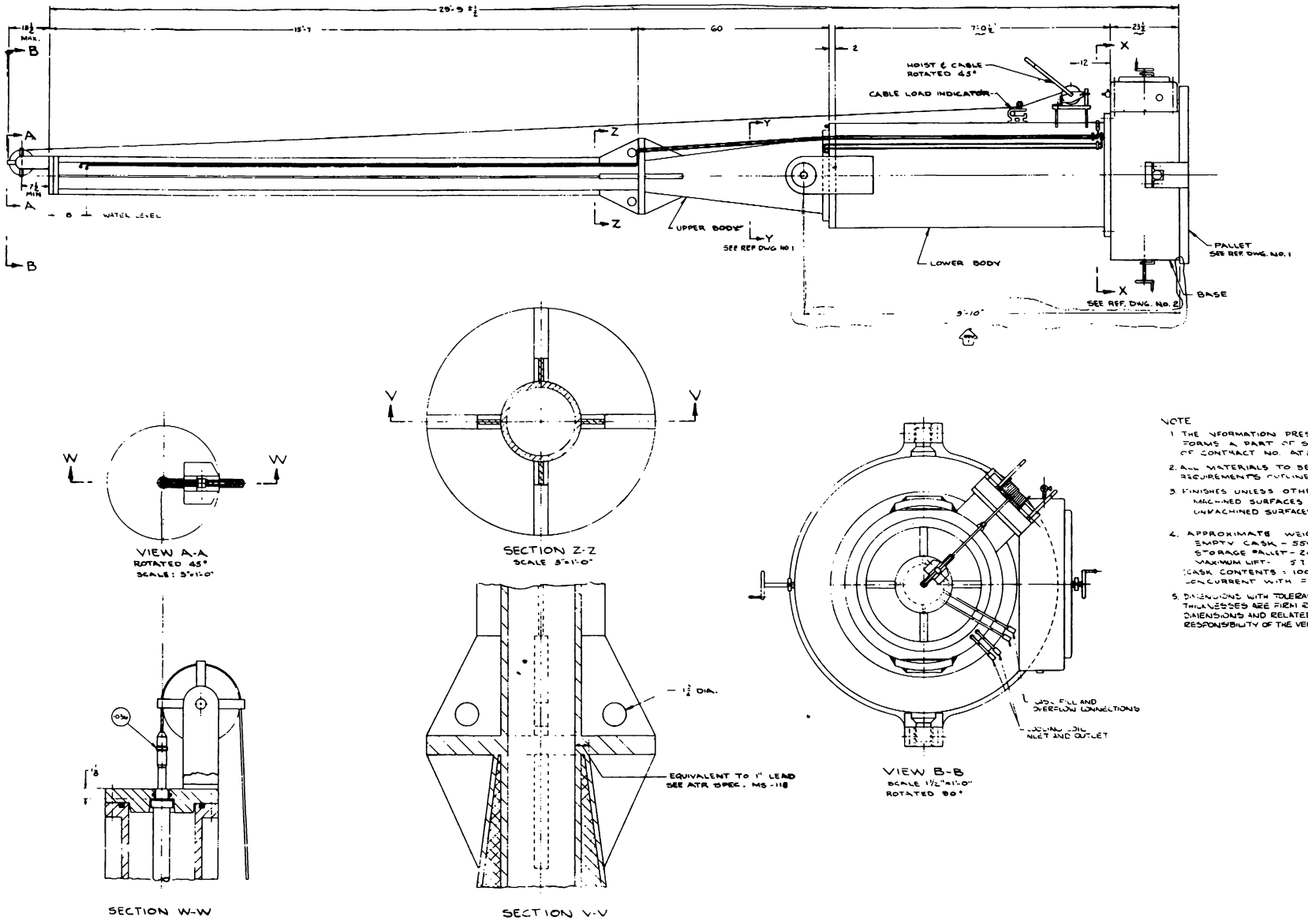

Figure 7-13. N. R. Loop Handling Cask
Sections and Details
(Dwg. No. 670-MS-102)

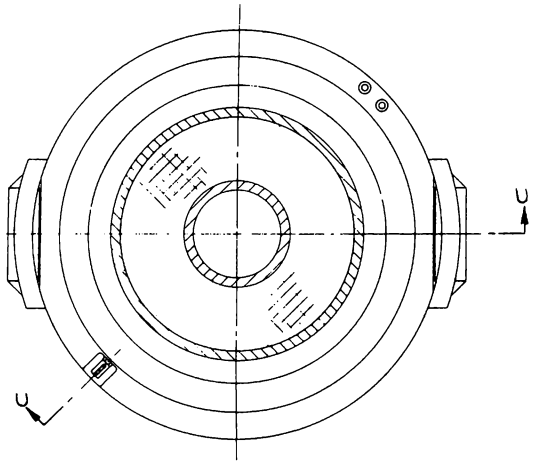

SECTION Y-Y
SCALE: 3"=1'-0"

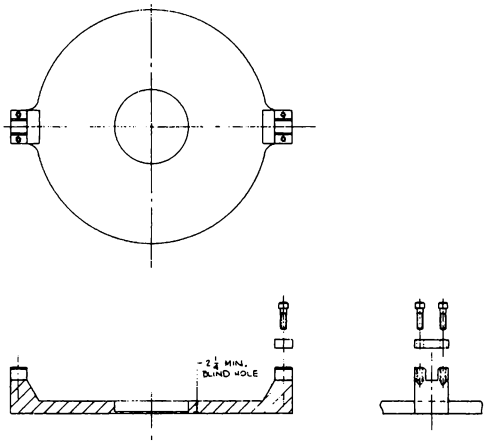

CASK STORAGE PALLET
(MAY BE A WELDMENT)
SCALE 1"=1'-0"

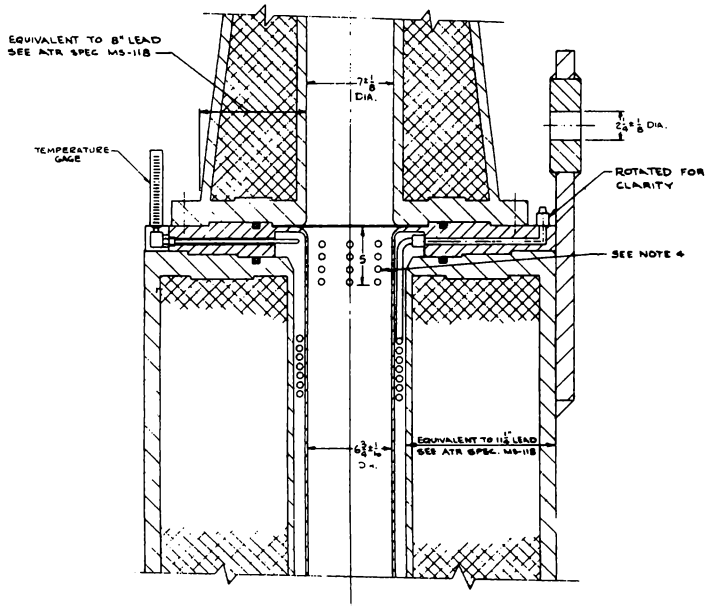

SECTION U-U

NOTES

1. THE INFORMATION PRESENTED ON THIS DRAWING FORMS A PART OF SPECIFICATION NO. MS-118 OF CONTRACT NO. AT(10-1)-1085.
2. ALL MATERIAL TO BE IN ACCORDANCE WITH REQUIREMENTS OUTLINED IN ATR SPECIFICATION MS-118.
3. DIMENSIONS WITH TOLERANCES AND SHIELDING THICKNESSES ARE FIRM REQUIREMENTS. OTHER DIMENSIONS AND RELATED TOLERANCES ARE THE RESPONSIBILITY OF THE VENDOR.
4. HOLES REQUIRED FOR DIMENSION SHOWN. HOLES PROVIDED SHALL BE SIZED, FINISHED & LOCATED TO AVOID ANY INTERFERENCE WITH LOAD WHEN IT IS LIFTED OR LOWERED.

Figure 7-14. N. R. Loop Handling Cask Base (Dwg. No. 670-MS-103)

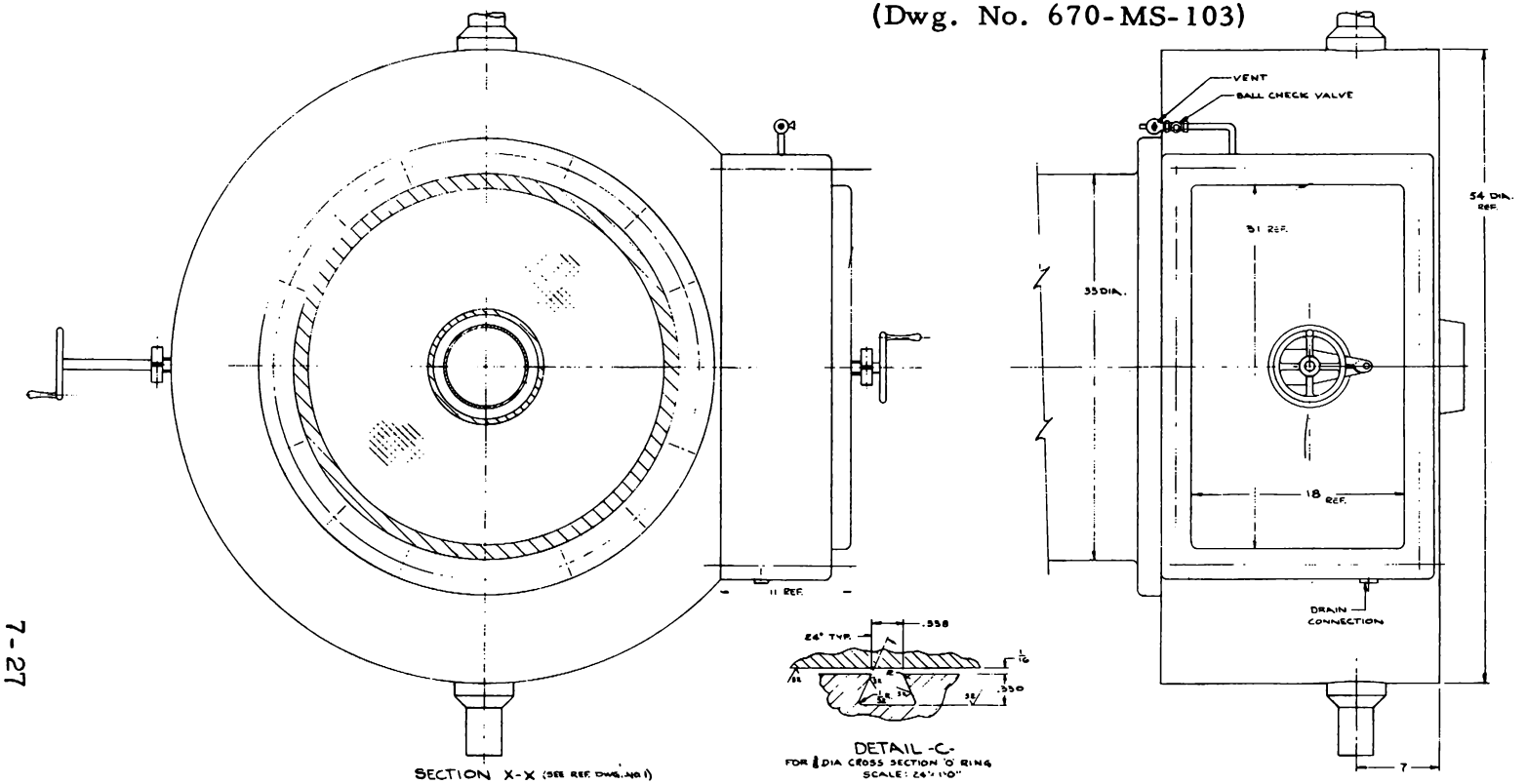

DETAIL -C-
FOR ⅛ DIA CROSS SECTION 'O' RING
SCALE: 24"=1'0"

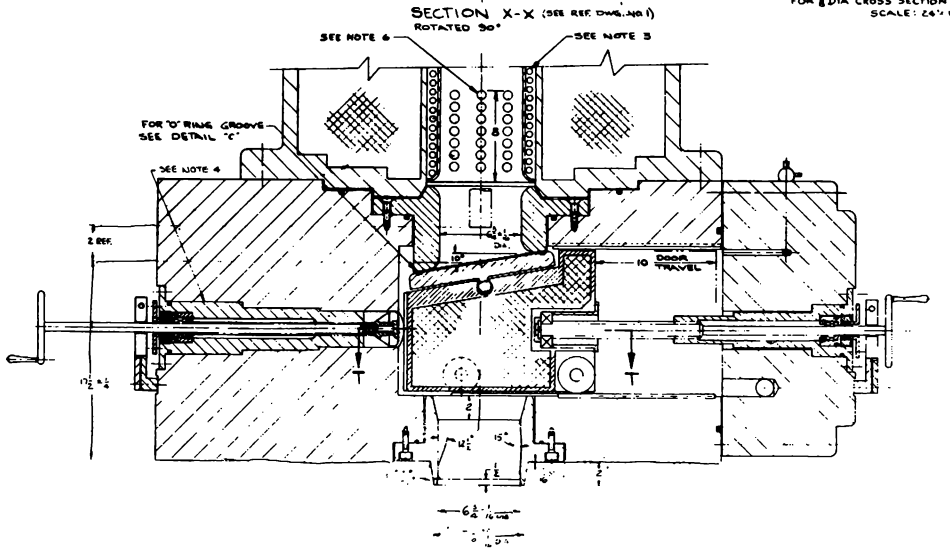

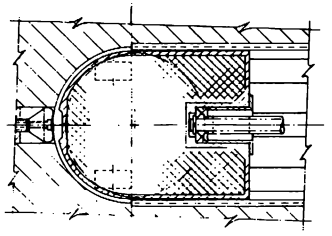

SECTION T-T

NOTES

1. THE INFORMATION PRESENTED ON THIS DRAWING FORMS A PART OF SPECIFICATION NO. MS-118 OF CONTRACT NO. AT(10-1)-1085.
2. ALL MATERIAL TO BE IN ACCORDANCE WITH REQUIREMENTS OUTLINED IN ATR SPECIFICATION MS-118.
3. DOUBLE WOUND COOLING COIL- UNIFORM PITCH- MEAN DIA. OF COIL 8" APPROX. TUBING ½ OD. x .035 WALL. TOTAL COILS-100 JOINED AT BOTTOM FOR RETURN LOOP.
4. SOLID SHIELDING PLUG FOR THIS CAVITY SHALL ALSO BE FURNISHED BY THE VENDOR.
5. DIMENSIONS WITH TOLERANCES AND SHIELDING THICKNESSES ARE FIRM REQUIREMENTS. OTHER DIMENSIONS AND RELATED TOLERANCES ARE THE RESPONSIBILITY OF THE VENDOR.
6. HOLES REQUIRED FOR DIMENSION SHOWN. HOLES PROVIDED SHALL BE SIZED, FINISHED, AND LOCATED TO AVOID ANY INTERFERENCE WITH LOAD WHEN IT IS LIFTED OR LOWERED.

Figure 7-15. Dose Rate From 800-kw Test Element Through the Radial Centerline of the Loop Handling Cask (2 Hours Shutdown, 3 Meters From Cask Surface in Air)

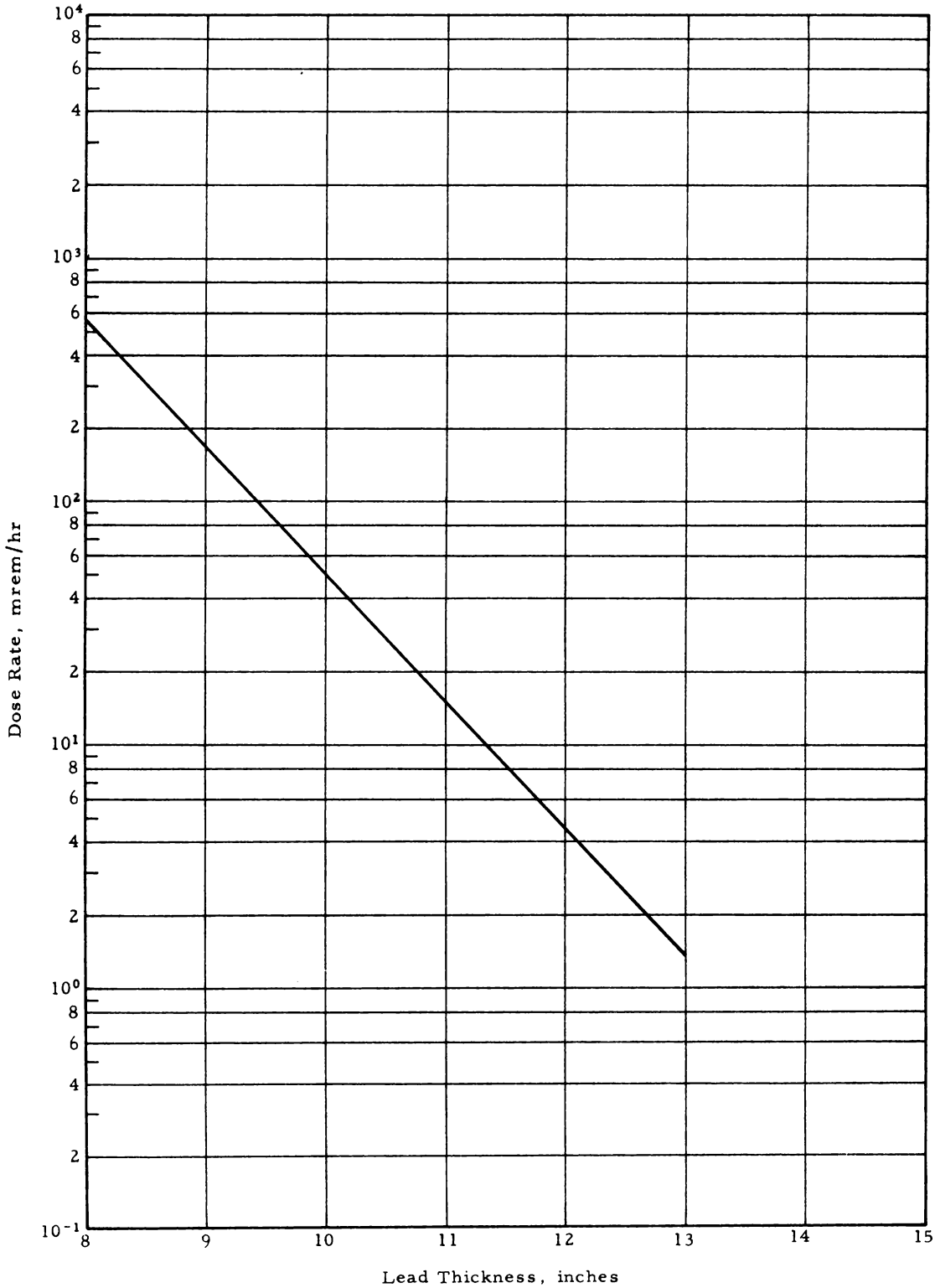

Figure 7-16. Dose Rate in Water Above a Single Spent ATR Fuel Element After 1 Hour Shutdown

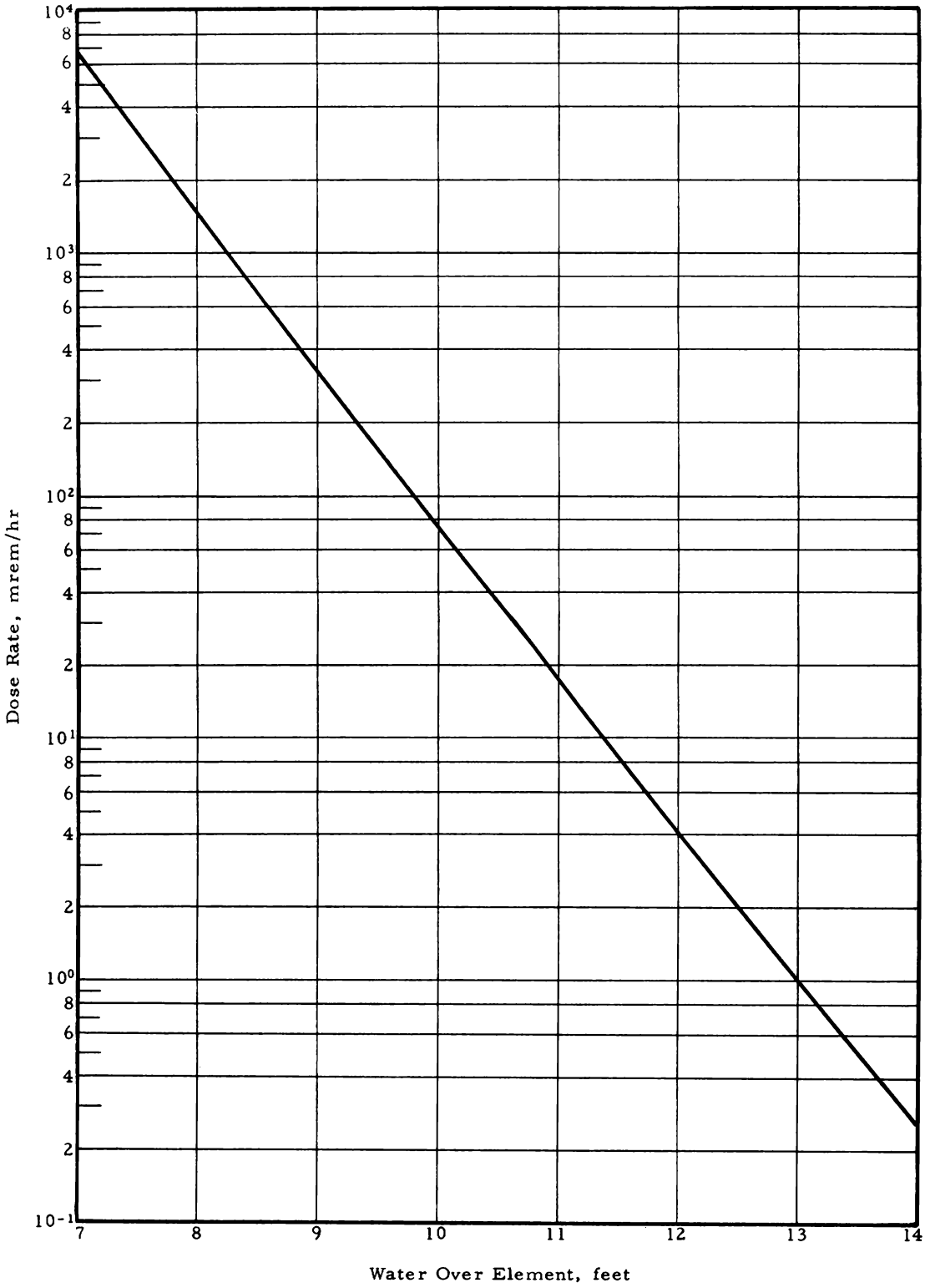

APPENDIX A

DER-029, Secondary Gamma Code

The computation of the secondary gamma ray flux generated by thermal neutron capture in a shield array is of prime importance in shield analysis. The equation defining the uncollided secondary gamma ray flux at the plane surface of a single infinite slab shield is

$$\phi = \Sigma_a \phi_o \int_0^L e^{\sigma z} dz \int_0^\infty \frac{e^{-\mu r}}{4\Pi r^2} 2\Pi\rho d\rho \qquad \text{(A-1)}$$

where

ϕ = uncollided gamma ray flux at the source slab surface

Σ_a = macroscopic radiative capture cross section for the production of gamma rays from thermal neutrons

ϕ_o = existing thermal neutron flux in source slab

σ = slope of thermal neutron flux through source slab

μ = linear absorption coefficient of gamma rays for source slab

z = variable for distance into a slab of thickness L

ρ = variable for vertical distance in the shield slab

$r(z, \rho)$ = distance from differential volume element of integration to point of measurement

The solution of this equation is

$$\phi = \frac{\Sigma_a \phi_o}{2\sigma} \left[e^{\sigma L} E_1(\mu L) - E_1(\mu L - \sigma L) + \mathrm{Ln}\left|\frac{\mu}{\mu - \sigma}\right| \right] \qquad \text{(A-2)}$$

With the substitution of $\sigma^* = \frac{\sigma}{\mu_1}$ and $b = \mu z$ into the equation to convert the equation to μz space, the equation becomes

$$\phi = \frac{\Sigma_a \phi_o}{2\sigma} \left[e^{\sigma^* b} E_1(b) - E_1(b - \sigma^* b) + \mathrm{Ln}\left|\frac{b}{b - \sigma^* b}\right| \right] \qquad \text{(A-3)}$$

This equation is derived for either side of an infinite, single-medium, source slab where the thermal flux through the slab is represented by a simple exponential:

$$\phi = \phi_o e^{\sigma z} \tag{A-4}$$

Equation A-3 for a single, homogeneous slab may be further modified to permit the calculation of the gamma flux from any source slab in a shield array at any interface in the array. This is accomplished by calculating the flux from each slab independently assuming the entire shield array has a thermal neutron flux slope corresponding to and normalized to that of the source slab being considered. The contribution from the entire shield array at any interface is then corrected by subtracting the gamma flux contributions from all portions except the source slab being considered. Using this difference method the following equation is deduced for the uncollided flux:

$$\phi = \frac{\Sigma_a \phi_o^*}{2\sigma} \left\{ e^{\sigma^* B} E_1(B) - e^{\sigma^* b} E_1(b) - E_1\left[(1-\sigma^*)B\right] + E_1\left[(1-\sigma^*)b\right] \right\} \tag{A-5}$$

where

$b = \mu x$ of shield slab between source slab and dose point

$B = b + \mu x$ of source slab

$\phi^* = \phi_o e^{-\sigma^* b}$

Equation A-5 was modified to account for photon yield in a given unit energy interval per thermal neutron capture by substituting $\overline{\Sigma}_a(E)$ for Σ_a in Equation A-5 where:

$$\overline{\Sigma}_a(E) = Y(E)\Sigma_a \tag{A-6}$$

and $Y(E)$ = photon yield per capture per mev.

A further modification was made in the equation to include gamma ray buildup of the form:

$$\text{Buildup} = A_1 e^{-a_1 B} + (1 - A_1) e^{-a_2 B} \tag{A-7}$$

The modified equation was incorporated into computer program DER-029 to calculate the total flux at each interface from all source slabs in each gamma energy interval.

APPENDIX B

DER-074, Basic Geometry Code

DER-074 is a general purpose digital computer program designed to calculate the heat generation rates and dose rates in and through laminated shield slabs for five idealized geometries.

The geometries and equations used in solving for the attenuation of gamma rays from each of the five geometries are as follows:

Type	Geometry
Point	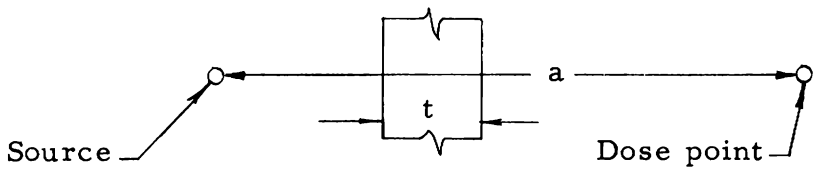
Line	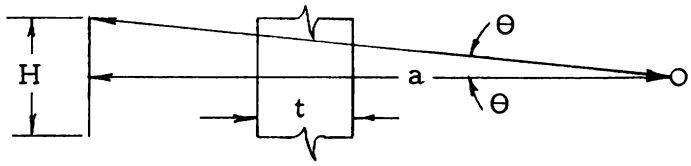
Disk	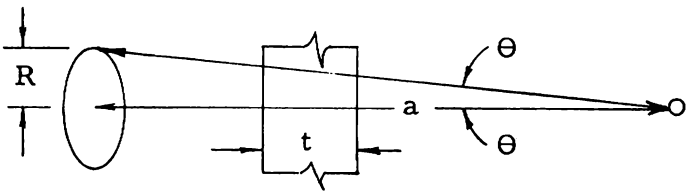
Truncated cone	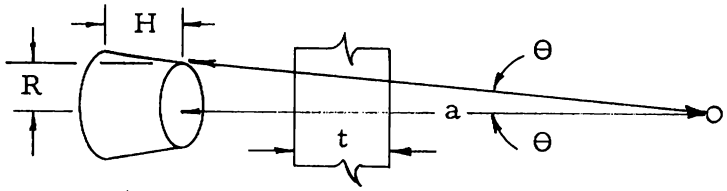
Cylinder	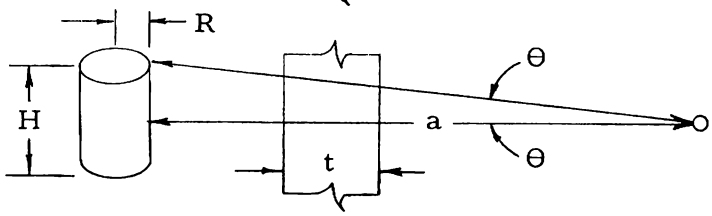

Geometry	Equation
Point	$\phi = \frac{BS}{4\Pi a^2} e^{-b}$
Line	$\phi = \frac{BS_\ell}{2\Pi a} [F(\Theta, b)]$
Disk	$\phi = \frac{BS_a}{2} [E_1(b) - E_1(b \sec \Theta)]$
Truncated cone	$\phi = \frac{BS_v}{2\mu_s} \left[E_2(b) - E_2(b_1) + \frac{E_2(b_1 \sec \Theta)}{\sec \Theta} - \frac{E_2(b \sec \Theta)}{\sec \Theta} \right]$
Cylinder	$\phi = \frac{BS_v}{2\mu_s} \left[E_2(b) \frac{F(\beta, b)}{F(\Pi/2, b)} - E_2(b_1) \frac{F(\beta, b)}{F(\Pi/2, b)} \right] \frac{F(\Theta, b)}{F(\Pi/2, b)}$

where

B = buildup factor

S = gamma source, photons/sec

$b = \sum_i \mu_i t_i$

μ_i = linear absorption coefficient of shield i, cm^{-1}

t_i = thickness of shield i, cm

S_ℓ = line source strength, photons/cm-sec

$F(\Theta, b) = \int_0^\Theta e^{-b \sec \Theta'} d\Theta'$

S_a = disk source strength, photons/cm^2-sec

S_v = volumetric source strength, photons/cc-sec

μ_s = absorption coefficient of source material, cm^{-1}

$$E_1(b) = \int_b^\infty \frac{e^{-t}}{t} dt$$

$$E_2(b) = b \int_b^\infty \frac{e^{-t}}{t^2} dt$$

$$b_1 = \mu_s H + \sum_i \mu_i t_i$$

$$\beta = \tan^{-1} R/a$$

The equations used are as derived by Rockwell[2] with the exception of the equation for the cylindrical source. The semi-empirical equation which is used for this solution substitutes a finite truncated slab source of equal area for the cylindrical source. The agreement of this solution with the numerical solution of the exact geometry is shown in Table B-1.

Table B-1. Percent Error Between Numerical Solution and Semi-Empirical Fit

b	a = 50 R	a = 20 R	a = 10 R	a = 2 R
		$\mu_s a = 1$		
1	-4.35	- -	-1.08	-4.19
3	-21.3	- -	-4.62	-1.84
10	-10.4	- -	-8.99	-11.54
25	-4.13	- -	-3.04	-8.95
		$\mu_s a = 3$		
1	-1.05	- -	-0.2	-3.23
3	-14.65	- -	-0.81	+0.36
10	-9.54	- -	-8.38	-6.15
25	-3.8	- -	-2.38	+0.38
		$\mu_s a = 5$		
1	-0.88	- -	+1.27	-9.3
3	-5.69	- -	+11.4	-6.13
10	-9.8	- -	-7.54	-11.1
25	-3.9	- -	-1.67	-4.82
		$\mu_s a = 20$		
1	0.0	+16.9	+1.59	-10.6
3	-1.1	+25.3	+2.36	-7.38
10	-8.3	-11.95	-8.48	-12.9

It can be seen that the error in the use of this semi-empirical equation for the cylindrical source is well within the limits of the error of the calculation.

The program is designed for a minimum of input preparation for any given problem. The tape dictionary includes shielding constants for the materials shown below. The constants are stored as functions of energy, and therefore straight line interpolation for the desired energy constants is used.

Water	Heavy water
Iron	Graphite
Lead	Polyethylene
Ordinary concrete	Aluminum
Barytes concrete	Uranium
Ilmenite concrete	

The limitation on the program is the number of energy groups that can be solved for any one group of input. This is limited to 10 energy groups. The number of shield slabs which can be solved is unlimited in that the program sums the relaxation lengths of the preceding slabs automatically.

Buildup is included in the program by use of a sum-of-exponentials fit,

$$B(\mu x) = A_1 e^{-\alpha_1 \mu x} + (1 - A_1) e^{-\alpha_2 \mu x}$$

where $B(\mu x)$ = buildup factor for relaxation lengths μx

A_1, α_1, α_2 = material and energy dependent constants

μx = relaxation lengths

The buildup factor for any material at any given point in a shield array can be chosen by use of input data.

APPENDIX C

DER-006A, Fission Product Buildup and Decay Code

The digital computer program, DER-006A, is a solution of coupled time dependent equations describing fission product buildup and decay in a reactor core. The program solution computes the concentration in a reactor core of any isotope in a specified fission product chain. The program limitations are five or less isotopes in the chain, six fission product buildup times, and six decay times after shutdown.

Data concerning the gamma emitters among the fission products are sketchy and incomplete and would in many cases lead to an underdesign. For this reason a literature survey was performed to obtain data on the gamma emitters. A set of important radioactive fission products to be expected from fission and the number and energies of expected gamma rays from each emitter were tabulated. Although there are probably many more fission products present than are known, the great majority of these have extremely short half-lives and have only small effects on radiation levels and shielding studies, since the integrated dose from these emitters is extremely small. They will, however, contribute greatly to any studies on the decay heat from fission products.

A list of isotopes and their associated gammas are included in this appendix. Many of the values are based on a plausible decay scheme and a total disintegration energy and represent a "best guess".

The program has provisions for the calculation of fission product buildup and decay for one or two fissionable isotopes in the reactor core. In the case of two fissionable isotopes, two assumptions were made:

1. A linear growth of converted material and a linear decrease in U-235 fission rate.
2. An operating time of t_1 for the core lifetime.

If attention is restricted to a core with U-233 and U-235 fissions, the fission rate or power in U-235 is given by:

$$P = P_0 - \left(\frac{1 - a}{t_1}\right) P_0 t$$

and in U-233 by

$$P = P_0 \left(\frac{1 - a}{t_1}\right) t$$

where a = fraction of power in U-235 at lifetime t_1. A general equation can be written as

$$P = \delta P_0 - a P_0 t$$

where for U-235: $\delta = 1$, a is +

for U-233: $\delta = 0$, a is -

By defining

N_i = ith element in chain

y_i = independent yield of ith isotope, atoms/fission

i = fraction of the (i - 1) isotope decaying to the ith isotope

the concentration of the ith isotope is

$$\frac{dN_i}{dt} + \lambda_i N_i = \delta y_i P_0 K - y_i K P_0 \text{ at} + \beta_{i-1} \lambda_{i-1} N_{i-1}$$

or for the first isotope in the chain

$$\frac{dN_1}{dt} + \lambda_1 N_1 = \delta y_1 P_0 K - y_1 K P_0 \text{ at}$$

and the second isotope in the chain

$$\frac{dN_2}{dt} + \lambda_2 N_2 = \delta y_2 P_0 K - y_2 K P_0 \text{ at} + \beta_1 \lambda_1 N_1$$

A review of the various chains shows that a maximum of five isotopes would adequately describe all chains with the exception of a few short-lived isotopes. The concentrations of those omitted can be found by a ratio of yields, since they are essentially in equilibrium at all times.

All decay chains are not completely described, especially where they branch in the middle of the chain. A choice must be made of the branching desired, and corrections must be made later. Once again the fairly short half-lives and slowly varying fission rates allow correction of answers later on. A chain may also be broken into several parts using the correct branching factors.

The solution of the five equations is tedious but straightforward and is given below for $KP_0 = A$ and $\psi_i = \lambda_i \beta_i$

$$N_1 = a_1 e^{-\lambda_1 t} + a_2 t + a_3$$

where

$$a_1 = -a_3$$

$$a_2 = -\frac{y_1 A_a}{\lambda_1}$$

$$a_3 = \frac{\delta y_1 A}{\lambda_1} - \frac{a_2}{\lambda_1}$$

$$N_2 = B_1 e^{-\lambda_1 t} + B_2 e^{-\lambda_2 t} + B_3 t + B_4$$

where

$$B_1 = \frac{\psi_1 a_1}{\lambda_2 - \lambda_1}$$

$$B_2 = - B_4 - B_1$$

$$B_3 = \frac{1}{\lambda_2} [\psi_1 a_2 - y_2 A_a]$$

$$B_4 = \frac{\delta y_2 A}{\lambda_2} - \frac{B_3}{\lambda_2} + \frac{\psi_1 a_3}{\lambda_2}$$

$$N_3 = \gamma_1 e^{-\lambda_1 t} + \gamma_2 e^{-\lambda_2 t} + \gamma_3 e^{-\lambda_3 t} + \gamma_4 t + \gamma_5$$

where

$$\gamma_1 = \frac{\psi_2 B_1}{\lambda_3 - \lambda_1}$$

$$\gamma_2 = \frac{\psi_2 B_2}{\lambda_3 - \lambda_2}$$

$$\gamma_3 = - \gamma_5 - \gamma_1 - \gamma_2$$

$$\gamma_4 = \frac{1}{\lambda_3} [- y_3 A_a + \psi_2 B_3]$$

$$\gamma_5 = \frac{\delta y_3 A + \psi_2 B_4}{\lambda_3} - \frac{\gamma_4}{\lambda_3}$$

$$N_4 = \Delta_1 e^{-\lambda_1 t} + \Delta_2 e^{-\lambda_2 t} + \Delta_3 e^{-\lambda_3 t} + \Delta_4 e^{-\lambda_4 t} + \Delta_5 t + \Delta_6$$

where

$$\Delta_1 = \frac{\psi_3 \gamma_1}{\lambda_4 - \lambda_1}$$

$$\Delta_2 = \frac{\psi_3 \gamma_2}{\lambda_4 - \lambda_2}$$

$$\Delta_3 = \frac{\psi_3 \gamma_3}{\lambda_4 - \lambda_3}$$

$$\Delta_4 = -\Delta_6 - \Delta_1 - \Delta_2 - \Delta_3$$

$$\Delta_5 = -\frac{y_4 A_a + \psi_3 \gamma_4}{\lambda_4}$$

$$\Delta_6 = \frac{\delta y_4 A + \psi_3 \gamma_5}{\lambda_4} - \frac{\Delta_5}{\lambda_4}$$

$$N_5 = E_1 e^{-\lambda_1 t} + E_2 e^{-\lambda_2 t} + E_3 e^{-\lambda_3 t} + E_4 e^{-\lambda_4 t} + E_5 e^{-\lambda_5 t} + E_6 t + E_7$$

where

$$E_1 = \frac{\psi_4 \Delta_1}{\lambda_5 - \lambda_1}$$

$$E_2 = \frac{\psi_4 \Delta_2}{\lambda_5 - \lambda_2}$$

$$E_3 = \frac{\psi_4 \Delta_3}{\lambda_5 - \lambda_3}$$

$$E_4 = \frac{\psi_4 \Delta_4}{\lambda_5 - \lambda_4}$$

$$E_5 = -E_7 - E_1 - E_2 - E_3 - E_4$$

$$E_6 = \frac{1}{\lambda_5}(-y_5 A_a + \psi_4 \Delta_5)$$

$$E_7 = \frac{1}{\lambda_5}(y_5 A \delta + \psi_4 \Delta_6) - \frac{E_6}{\lambda_5}$$

These equations can be used for a nonconverter core by letting $\delta = 1$ and $a = 0$. For short times after $t = 0$, an error is made, since a linear approximation is used and U-233 and Pu-239 do not grow immediately. However, the values predicted by the equation are slight for times over 50 days.

Examination of the differential equations shows that they will describe the decay of the fission products after shutdown if KP_0 or A is set equal to zero. DER-006A will calculate the growth at several operating times and for the decay after shutdown.

Table C-1. Fission Product Constants Used in DER-006A

i	Isotope	$T_{1/2}$	λ, sec^{-1}	β_i	U-235 y_i	U-233 y_i	Pu-239 y_i
1	I-137	22s	3.15×10^{-2}	0.94	0.049	0.072	0.048
2	Xe-137	3.9m	2.962×10^{-3}	1	0.010	0	0.0044
3	Cs-137	27y	8.17×10^{-10}	0.92	0	0	0
4	Ba-137m	2.6m	4.442×10^{-3}	1	0	0	0
1	I-138	5.9s	1.175×10^{-1}	1	0.034	0.071	0.031
2	Xe-138	17m	6.794×10^{-4}	1	0.021	0	0.021
3	Cs-138	32.9m	3.510×10^{-4}	1	0.003	0	0.002
1	I-139	2.7s	2.567×10^{-1}	1	0.018	0.071	0.020
2	Xe-139	41s	1.69×10^{-2}	1	0.029	0	0.024
3	Cs-139	9.5m	1.216×10^{-3}	1	0.012	0	0.012
4	Ba-139	85m	1.358×10^{-4}	1	0.001	0	0.001
1	Xe-140	16s	4.331×10^{-2}	1	0.037	0.069	0.0338
2	Cs-140	66s	1.05×10^{-2}	1	0.023	0	0.020
3	Ba-140	12.8d	6.266×10^{-7}	1	0.003	0	0.003
4	La-140	40.5h	4.753×10^{-6}	1	0	0	0
1	Xe-141	1.7s	4.076×10^{-1}	1	0.018	0.062	0.020
2	Cs-141	Sh	1.000×10^{0}	1	0.029	0	0.021
3	Ba-141	18m	6.416×10^{-4}	1	0.012	0	0.010
4	La-141	3.7h	5.203×10^{-5}	1	0.001	0	0.001
5	Ce-141	32.8d	2.445×10^{-7}	1	0	0	0
1	Cs-142	1m	1.155×10^{-2}	1	0.034	0.055	0.0509
2	Ba-142	6m	1.925×10^{-3}	1	0.022	0	0.014
3	La-142	74m	1.56×10^{-4}	1	0.003	0	0.002
1	Ba-143	30s	2.31×10^{-2}	1	0.049	0.046	0.0531
2	La-143	19m	6.078×10^{-4}	1	0.013	0	0.010
3	Ce-143	33h	5.833×10^{-6}	1	0	0	0
4	Pr-143	13.7d	5.855×10^{-7}	1	0	0	0
1	Ce-144	290d	2.765×10^{-8}	1	0.061	0.046	0.0529
2	Pr-144	17.5m	6.6×10^{-4}	1	0	0	0
1	Ce-145	3.0m	3.85×10^{-3}	1	0.042	0.027	0.0424
2	Pr-145	5.95h	3.235×10^{-5}	1	0	0	0
1	Ce-146	13.9m	8.309×10^{-4}	1	0.032	0.020	0.0343
2	Pr-146	24.4m	4.733×10^{-4}	1	0.001	0	0.001
1	Nd-147	11.3d	7.098×10^{-7}	1	0.026	0.014	0.0292
2	Pm-147	2.6y	8.48×10^{-9}	1	0	0	0
1	Nd-149	2h	9.625×10^{-5}	1	0.013	0.007	0.0189
2	Pm-149	54h	3.564×10^{-6}	1	0	0	0
1	Nd-151	15m	7.70×10^{-4}	1	0.0048	0.0026	0.0117
2	Pm-151	27.5h	7.00×10^{-6}	1	0.0002	0	0
3	Sm-151	73y	3.02×10^{-10}	1	0	0	0
1	Sn-128	57m	2.026×10^{-4}	1	0.005	0.0057	0.008
2	Sb-128	10.3m	1.121×10^{-3}	1	0	0	0

Table C-1. (Cont'd)

i	Isotope	$T_{1/2}$	λ sec^{-1}	β_i	U-235 y_i	U-233 y_i	Pu-239 y_i
1	Sb-129	4.6h	4.185×10^{-5}	0.24	0.010	0.0114	0.013
2	Te-129m	33.5d	2.394×10^{-7}	1	0	0	0
3	Te-129	74m	1.56×10^{-4}	1	0	0	0
1	Sb-129	4.6h	4.185×10^{-5}	0.76	0.010	0.0114	0.013
2	Te-129	74m	1.56×10^{-4}	1	0	0	0
1	Sn-130	2.6m	4.442×10^{-3}	1	0.020	0	0.020
2	Sb-130	12m	9.625×10^{-4}	1	0	0.025	0
1	Sb-131	23.1m	5.00×10^{-4}	0.15	0.029	0.048	0.0287
2	Te-131m	30h	6.416×10^{-6}	1	0	0	0
3	Te-131	25m	4.620×10^{-4}	1	0	0.041	0
4	I-131	8d	1.003×10^{-6}	0.01	0	0	0
5	Xe-131m	12d	6.684×10^{-7}	1	0	0	0
1	Sb-131	23.1m	5.00×10^{-4}	0.85	0.029	0.048	0.0287
2	Te-131	25m	4.62×10^{-4}	1	0	0	0
3	I-131	8d	1.003×10^{-6}	0.01	0	0	0
4	Xe-131m	12d	6.684×10^{-7}	1	0	0	0
1	Sn-132	2.2m	5.25×10^{-3}	1	0.034	0	0.039
2	Sb-132	2m	5.775×10^{-3}	1	0	0.062	0
3	Te-132	77h	2.50×10^{-6}	1	0.010	0	0.0012
4	I-132	2.4h	8.021×10^{-5}	1	0	0	0
1	Te-133m	63m	1.833×10^{-4}	1	0.046	0.066	0.0397
2	Te-133	2m	5.775×10^{-3}	1	0.014	0	0.009
3	I-133	20.5h	9.39×10^{-6}	0.024	0.005	0	0.004
4	Xe-133m	2.3d	3.487×10^{-6}	1	0	0	0
5	Xe-133	5.27d	1.522×10^{-6}	1	0	0	0
1	Te-133m	63m	1.833×10^{-4}	1	0.046	0.064	0.0397
2	Te-133	2m	5.775×10^{-3}	1	0.014	0	0.009
3	I-133	20.5h	9.39×10^{-6}	0.976	0.005	0	0.004
4	Xe-133	5.27d	1.522×10^{-6}	1	0	0	0
1	Sb-134	50s	1.386×10^{-2}	1	0.030	0.071	0.0269
2	Te-134	44m	2.625×10^{-4}	1	0.037	0	0.025
3	I-134	52.5m	2.20×10^{-4}	1	0.009	0	0.005
1	Te-135	2m	5.775×10^{-3}	1	0.042	0.071	0.039
2	I-135	6.68h	2.882×10^{-5}	0.3	0.017	0	0.016
3	Xe-135m	15.6m	7.403×10^{-4}	1	0	0	0
4	Xe-135	9.2h	2.092×10^{-5}	1	0.003	0	0.003
1	Te-135	2m	5.775×10^{-3}	1	0.042	0.071	0.039
2	I-135	6.68h	2.882×10^{-5}	0.7	0.017	0	0.016
3	Xe-135	9.2h	2.092×10^{-5}	1	0.003	0	0.003
1	I-136	86s	8.058×10^{-3}	0	0.063	0.072	0.021
2	Cs-136	12.9d	6.218×10^{-7}	1	0.000062	0	0.0296

Table C-1. (Cont'd)

i	Isotope	$T_{1/2}$	λ sec^{-1}	β_i	U-235 y_i	U-233 y_i	Pu-239 y_i
1	Pd-111	22m	5.25×10^{-4}	1	0.00018	0.0003	0.0027
2	Ag-111	7.5d	1.069×10^{-6}	1	0	0	0
1	Pd-112	21h	9.166×10^{-6}	1	0.00011	0.00020	0.0010
2	Ag-112	3.2h	6.016×10^{-5}	1	0	0	0
1	Ag-113	5.3h	3.632×10^{-5}	0.005	0.0001	0.0002	0.00065
2	Cd-113m	5.1y	4.327×10^{-9}	1	0	0	0
1	Ag-114	2m	5.775×10^{-3}	1	0.0001	0.00018	0.00049
1	Ag-115	20m	5.775×10^{-4}	0.91	0.00011	0.00017	0.00041
2	Cd-115	53h	3.632×10^{-6}	1	0	0	0
3	In-115m	4.5h	4.278×10^{-5}	1	0	0	0
1	Ag-115	20m	5.775×10^{-4}	0.09	0.00011	0.00017	0.00041
2	Cd-115	43d	1.865×10^{-7}	1	0	0	0
1	Cd-117m	3.0h	6.417×10^{-5}	1	0.0001	0.00017	0.00039
2	Cd-117	50m	2.31×10^{-4}	1	0	0	0
3	In-117m	2.3h	8.37×10^{-5}	0.28	0	0	0
4	In-117	1.1h	1.75×10^{-4}	0.01	0	0	0
5	Sn-117m	14d	5.729×10^{-7}	1	0	0	0
1	Cd-118	50m	2.31×10^{-4}	1	0.0001	0	0.00039
2	In-118	4.5m	2.567×10^{-3}	1	0	0	0
1	In-119	17.5m	6.6×10^{-4}	1	0.0001	0	0.00039
2	Sn-119m	250d	3.208×10^{-8}	1	0	0	0
1	Sn-121	27.5h	7.00×10^{-6}	1	0.00014	0.00019	0.00044
1	Sn-123	39.5m	2.924×10^{-4}	0	0.00015	0.00014	0.00065
2	Sn-123	136d	5.897×10^{-8}	1	0.000012	0	0.00005
1	Sn-125m	9.8m	1.179×10^{-3}	0	0.00011	0	0.00072
2	Sn-125	9.4d	8.532×10^{-7}	1	0.00012	0.0006	0.00072
3	Sb-125	2.0y	1.103×10^{-8}	0.18	0.00011	0	0
4	Te-125m	58d	1.383×10^{-7}	1	0	0	0
1	Sn-126	50m	2.31×10^{-4}	1	0.001	0.009	0.0022
2	Sb-126	9h	2.139×10^{-5}	1	0	0	0
1	Sn-127	1.5h	1.283×10^{-4}	1	0.0024	0.0018	0.0039
2	Sb-127	93h	2.069×10^{-6}	0.16	0.0001	0	0
3	Te-127m	105d	7.638×10^{-8}	1	0	0	0
4	Te-127	9.3h	2.069×10^{-5}	1	0	0	0
1	Sn-127	1.5h	1.283×10^{-4}	1	0.0024	0.0018	0.0039
2	Sb-127	93h	2.069×10^{-6}	0.84	0.0001	0	0
3	Te-127	9.3h	2.069×10^{-5}	1	0	0	0
1	Kr-94	1.4s	4.95×10^{-1}	1	0.006	0.068	0.005
2	Rb-94	Sh	1.00×10^{0}	1	0.023	0	0.018
3	Sr-94	2m	5.775×10^{-3}	1	0.029	0	0.022
4	Y-94	16.5m	7.00×10^{-4}	1	0.007	0	0.005

Table C-1. (Cont'd)

i	Isotope	$T_{1/2}$	λ sec^{-1}	β_i	U-235 y_i	U-233 y_i	Pu-239 y_i
1	Y-95	10.5m	1.1×10^{-3}	1	0.064	0.066	0.059
2	Zr-95	65d	1.234×10^{-7}	0.014	0	0	0
3	Nb-95m	90h	2.138×10^{-6}	1	0	0	0
4	Nb-95	35d	2.292×10^{-7}	1	0	0	0
1	Y-95	10.5m	1.10×10^{-3}	1	0.064	0.066	0.059
2	Zr-95	65d	1.234×10^{-7}	0.986	0	0	0
3	Nb-95	35d	2.292×10^{-7}	1	0	0	0
1	Zr-97	17h	1.132×10^{-5}	0.95	0.062	0.059	0.059
2	Nb-97m	60s	1.155×10^{-2}	1	0	0	0
3	Nb-97	72.1m	1.601×10^{-4}	1	0	0	0
1	Zr-97	17h	1.132×10^{-5}	0.05	0.062	0.059	0.059
2	Nb-97	72.1m	1.601×10^{-4}	1	0	0	0
1	Nb-99	3.8m	3.039×10^{-3}	1	0.061	0.048	0.059
2	Mo-99	68h	2.83×10^{-6}	0.1	0	0	0
3	Tc-99m	6.04h	3.187×10^{-5}	1	0	0	0
1	Mo-101	14.6m	7.91×10^{-4}	1	0.050	0.026	0.059
2	Tc-101	14.0m	8.25×10^{-4}	1	0	0	0
1	Mo-102	12m	9.625×10^{-4}	1	0.042	0.024	0.058
2	Tc-102	25s	2.772×10^{-2}	1	0	0	0
1	Ru-103	39.8d	2.015×10^{-7}	0.95	0.029	0.0088	0.057
2	Rh-103m	57m	2.026×10^{-4}	1	0	0	0.001
1	Mo-105	5m	2.31×10^{-3}	1	0.006	0.0046	0.025
2	Tc-105	Sh	1.00×10^{0}	1	0.003	0	0.012
3	Ru-105	4.5h	4.278×10^{-5}	1	0	0	0
4	Rh-105m	45s	1.54×10^{-2}	1	0	0	0
5	Rh-105	36.5h	5.273×10^{-6}	1	0	0	0
1	Ru-106	1y	2.207×10^{-8}	1	0.0038	0.0033	0.050
2	Rh-106	30s	2.31×10^{-2}	1	0	0	0
1	Tc-107	1.5m	7.7×10^{-3}	1	0.0016	0.0022	0.032
2	Ru-107	4m	2.888×10^{-3}	1	0.0004	0	0.008
3	Rh-107	26m	4.442×10^{-4}	1	0	0	0
1	Ru-108	4m	2.887×10^{-3}	1	0.0008	0	0.020
2	Rh-108	18s	3.85×10^{-2}	1	0	0	0
1	Rh-109	1h	1.925×10^{-4}	1	0.00028	0.0009	0.015
2	Pd-109	13.6h	1.415×10^{-5}	1	0	0	0
3	Ag-109m	40s	1.733×10^{-2}	1	0	0	0
1	Se-83m	67s	1.034×10^{-2}	0.1	0.003	0.008	0.00050
2	Se-83	25m	4.62×10^{-4}	1	0.0018	0	0.00035
3	Br-83	2.3h	8.37×10^{-5}	1	0	0	0
4	Kr-83m	114m	1.013×10^{-4}	1	0	0	0

Table C-1. (Cont'd)

i	Isotope	$T_{1/2}$	λ sec^{-1}	β_i	U-235 y_i	U-233 y_i	Pu-239 y_i
1	Se-83m	67s	1.034×10^{-2}	0.9	0.003	0.008	0.00050
2	Br-83	2.3h	8.37×10^{-5}	1	0	0	0
3	Kr-83m	114m	1.013×10^{-4}	1	0	0	0
1	Se-84	2m	5.775×10^{-3}	1	0.011	0.015	0.001
2	Br-84	30m	3.85×10^{-4}	1	0	0	0
1	Br-85	3m	3.85×10^{-3}	1	0.015	0.025	0.0020
2	Kr-85m	4.36h	4.415×10^{-5}	0.2	0	0	0
3	Kr-85	10.57y	2.087×10^{-9}	1	0	0	0
1	Br-87	55s	1.26×10^{-2}	1	0.027	0.046	0.0082
2	Kr-87	78m	1.48×10^{-4}	1	0	0	0
1	Br-88	15.5s	4.471×10^{-2}	1	0.029	0.054	0.010
2	Kr-88	2.77h	6.949×10^{-5}	1	0.008	0	0.002
3	Rb-88	17.8m	6.488×10^{-4}	1	0	0	0
1	Br-89	4.51s	1.537×10^{-1}	1	0.046	0.051	0.018
2	Kr-89	3.18m	3.632×10^{-3}	1	0	0	0
3	Rb-89	15.4m	7.5×10^{-4}	1	0.002	0	0.001
4	Sr-89	53d	1.513×10^{-7}	1	0	0	0
1	Kr-90	33s	2.1×10^{-2}	1	0.052	0.064	0.022
2	Rb-90	2.74m	4.215×10^{-3}	1	0.007	0	0.003
3	Sr-90	28y	7.88×10^{-10}	1	0	0	0
4	Y-90	64.8h	2.971×10^{-6}	1	0	0	0
1	Kr-91	9.8s	7.071×10^{-2}	1	0.037	0.066	0.020
2	Rb-91	14m	8.25×10^{-4}	1	0.020	0	0.009
3	Sr-91	9.7h	1.985×10^{-5}	0.4	0.002	0	0.001
4	Y-91m	51m	2.264×10^{-4}	1	0	0	0
5	Y-91	58.3d	1.376×10^{-7}	1	0	0	0
1	Kr-91	9.8s	7.071×10^{-2}	1	0.037	0.066	0.020
2	Rb-91	14m	8.25×10^{-4}	1	0.020	0	0.009
3	Sr-91	9.7h	1.985×10^{-5}	0.6	0.002	0	0.001
4	Y-91	58.3d	1.376×10^{-7}	1	0	0	0
1	Kr-92	3s	2.31×10^{-1}	1	0.027	0.068	0.018
2	Rb-92	80s	8.663×10^{-3}	1	0.028	0	0.017
3	Sr-92	2.6h	7.404×10^{-5}	1	0.006	0	0.002
4	Y-92	3.6h	5.347×10^{-5}	1	0	0	0
1	Kr-93	2s	3.465×10^{-1}	1	0.013	0.068	0.005
2	Rb-93	Sh	1.00×10^{0}	1	0.031	0	0.023
3	Sr-93	7m	1.65×10^{-3}	1	0.020	0	0.014
4	Y-93	10h	1.925×10^{-5}	1	0.001	0	0
1	Sm-153	47h	4.095×10^{-6}	1	0.0015	0.0009	0.0041
1	Sm-155	23.5m	4.914×10^{-4}	1	0.00031	0.0003	0.0022
2	Eu-155	1.7y	1.298×10^{-8}	1	0	0	0
1	Sm-156	10h	1.925×10^{-5}	1	0.00013	0.0002	0.0012
2	Eu-156	14d	5.729×10^{-7}	1	0	0	0

APPENDIX D

DER-013, Point Source Summation Code

DER-013 is designed to calculate the dose rate, heating rate, or flux due to primary or secondary gamma radiation. Several geometries are utilized by the program; however, the basic source geometry from which the program operates is the cylinder. Variations of this geometry are accomplished by applying the appropriate input data. These variations include a cylindrical shell source, a rectangular source, and a disk source. The program has provisions for 15 shields arranged either axially or radially about the source. The axial shields are represented as slabs, and the radial shields assume the same geometry as the source. The source and shields may be located in a specified shielding medium. Flux, dose rate, or heating rate points may be located at any position either outside the source, within the source material, inside the exclusion volume of the hollow cylinder, or in the medium. The program accommodates 10 energy groups of photons and provides for radial and/or axial variations in source strength.

For the calculations the program divides a cylindrical source into a number of volumetric sources (mesh volumes), which are then treated as point sources located at the center of each volume (see Figure D-1). The size, shape, and number of mesh volumes calculated by the program depend on the input data. The initial division of the source is accomplished by separating it into cylindrical shells starting at its outer radius and ending at the radius of the exclusion volume or the center of the source, as the case may be. Axially, mesh volumes are begun at the bottom of the shell. The normal or slant penetration and flux through all of the shields for each energy group from a given mesh volume are calculated and stored before the routine moves to the next mesh volume. The program solves the equation for the intercept of the line $[(y - y_1)(x_2 - x_1) = (y_2 - y_1)(x - x_1)]$ between the source point and the dose point

with each of the shield interfaces [$x^2 + y^2 = r^2$ for a cylindrical shield or Z = a for a plane shield] in the x – y plane. From these intercepts the distances in the x – y plane are calculated:

$$\overline{P_1 P_2} = \sqrt{(x_2 - x_1)^2 + (y_2 - y_1)^2}.$$

The slant penetration distances in each shield in three dimensions is then calculated for each column of mesh volumes by a ratio of the total plane distance to the total three-dimensional distance. The flux from each source point is

$$\phi = B \frac{S_o}{4\Pi a^2} e^{-b}$$

where

S_o = point source strength, γ/sec

a = distance from source point to flux point, cm

$$b = \sum_{1}^{n} \mu_i \, t_i$$

i = number of shield

μ = linear absorption coefficient

t = thickness of shield

$B = A_1 e^{-\alpha_1 b} + A_2 e^{-\alpha_2 b}$ = buildup factor

The equation then becomes:

$$\phi = \frac{S_o}{4\Pi a^2} \left[A_1 e^{-(1+\alpha_1)b} + A_2 e^{-(1+\alpha_2)b} \right]$$

Fluxes from the volumetric sources are calculated in the axial direction before a radial angular change is initiated to calculate a new column of mesh volumes. With the appropriate input the program applies a self-calculated axial distribution to the source points. If this is not desirable, however, there are provisions for inserting a distribution in source strengths, both axially and/or radially.

When the entire source has been divided and analyzed, the machine prints out the total builtup flux, dose rate, or heating rate from each energy group.

Figure D-1. Point Source Summation Program Method

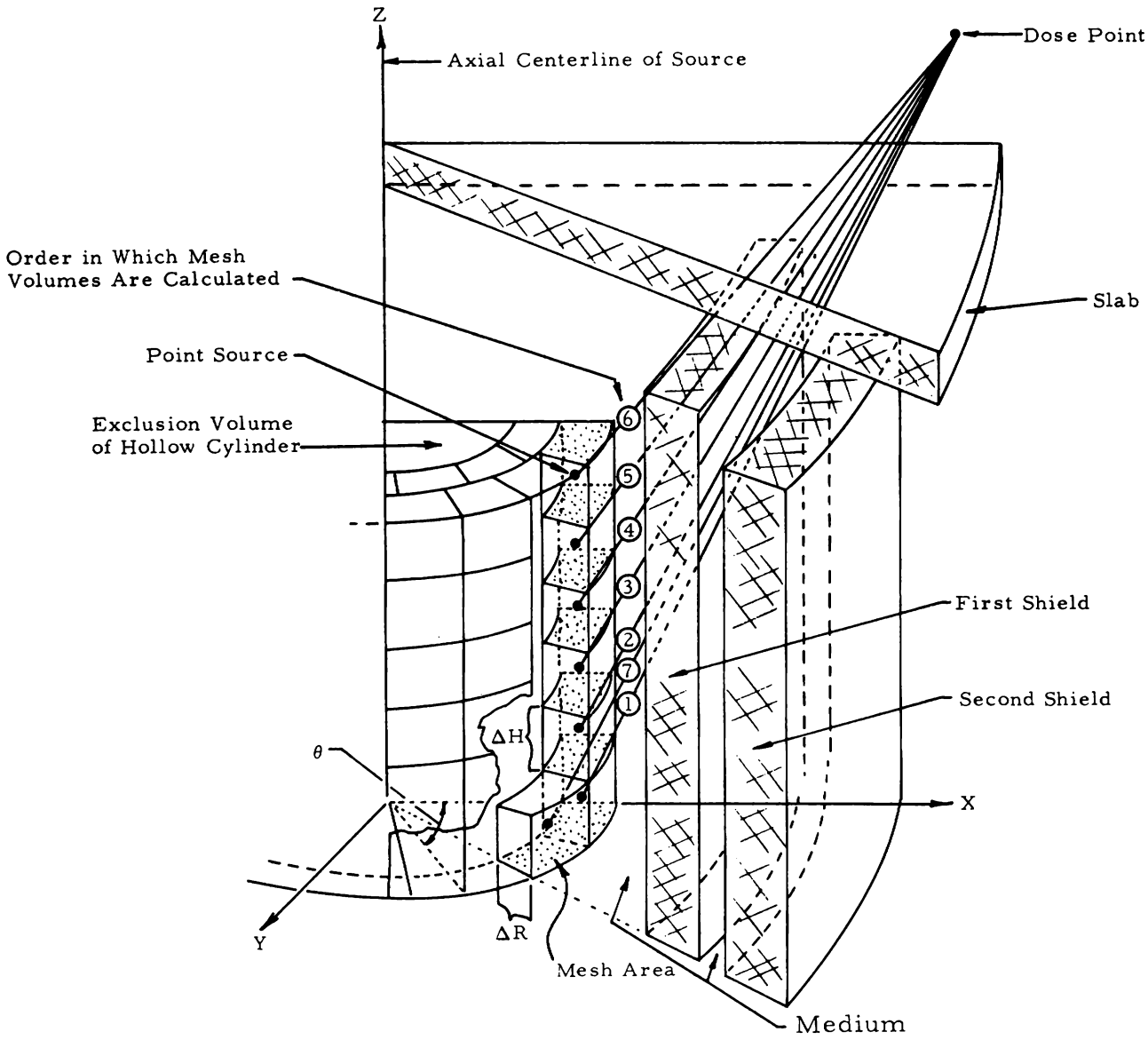

REFERENCES

1 Sievert, R., Acta Radiologica 1, 89 (1921).

2 Rockwell, T., III, Ed., Reactor Shielding Design Manual, TID-7004, March 1956.

3 Etherington, H., Ed., Nuclear Engineering Handbook, McGraw-Hill Book Co., Inc., 1958.

4 Foderaro, A. and Obenshain, F., Fluxes from Regular Geometric Sources, WAPD-TN-508, June 1955.

5 Mangum, Y. P., Jr., Flux From Homogeneous Cylinders Containing Uniform Source Distributions, NNSD-R-7-4/1, November 1956.

6 Goldstein, H. and Wilkins, J. E., Jr., Calculations of the Penetration of Gamma Rays, NYO-3075, June 1954.

7 Goldstein, H., Fundamental Aspects of Reactor Shielding, Addison-Wesley Publishing Co., Inc., 1959.

8 Maienschein, F. C., et al, Gamma Rays Associated With Fission, A/Conf. 15/P/670, June 1958.

9 Deloume, F. E., Gamma Ray Energy Spectra from Thermal Neutron Capture, APEX-407, August 1958.

10 Perkins, J. F. and King, R. W., "Energy Release From the Decay of Fission Products", Nuclear Science and Engineering 3, 1958.

11 Smith, W. R. and Turner, M. A., Nuclear Merchant Ship Reactor Shield Design Summary Report, The Babcock & Wilcox Company, BAW-1144-1, Lynchburg, Virginia, August 1959.

12 Martin, H. C., Physical Review 93, 498, 1954.

13 Shure, K., The O^{16} (n,ρ) N^{16} Reaction Cross Section, WAPD-BT-25, May 1962.

[14] Scoles, J. F., Calculated Gamma-Ray Spectra from U^{235} Fission Products, NARF-58-37T (FZK-9-132), August 1958.

[15] Roy, J. C. and Hawton, J. J., Table of Estimated Cross-Sections for (n, α) (n,ρ), and (n, 2n) Reactions in a Fission Neutron Spectrum, AECL-1181, December 1960.

[16] Bayhurst, B. P. and Prestwood, R. J., (n, 2n), (n, α), and (n,ρ) Excitation Functions of Several Nuclei from 7.0 to 19.8 Mev, La-2493, December 1960.

[17] Peebles, G. H., Gamma Ray Transmission Through Finite Slabs, Rand Report R-240, 1952.